Combining Pharmacology and Mutational Dynamics to Understand and Combat Drug Resistance in HIV

A dissertation
submitted for the degree of
Doctor of Philosophy

by

Max von Kleist, B.Sc., M.Sc.

Supervisor: Dr. Wilhelm Huisinga

Hamilton Institute
National University of Ireland, Maynooth
Ollscoil na hÉireann, Má Nuad

December 14, 2009

Contents

Summary

After 25 years of research the cure for HIV remains to be found. The use of combination therapy has led to a dramatic decline in morbidity associated with the infection. However, the virus develops drug resistance, thereby eliminating treatment options and putting the patient in risk of death.

Up to now, the mechanisms of resistance development are poorly understood. Drug resistance can only develop, if the virus is replicating. However, drug treatment strongly inhibits viral replication.

In this thesis, we develop a novel mathematical model of the HIV life cycle, that can incorporate the effects of all approved anti-HIV drugs mechanistically. The model includes possible mutation events, that allow the virus to develop resistance and escape from drug pressure. Based on this model, we analyze the drug-class specific impact of antiviral treatment on the reproduction of HIV and subsequently on resistance development. We find that some novel inhibitors, despite superior performance in terms of viral load decay, poorly inhibit the emergence of drug resistance. Furthermore, we develop the mathematical foundation of a treatment scheduling routine, which minimizes the probability that resistance emerges during therapy. The method suggests that more frequent treatment change could reduce the risk of resistance development.

In the second part of the thesis, we focus on the pharmacology of anti-HIV compounds. Poor drug exposure, both in time and space, can be a major cause of insufficient virus suppression and resistance development. We give a detailed description of pharmacokinetic- and pharmacodynamic models and suggest a modelling pipeline. Finally, we model the pharmacokinetics and pharmacodynamics of the nucleoside reverse transcriptase inhibitor (NRTI) zidovudine, and validate our model with *in vitro* and *in vivo* data. For zidovudine we found that less frequent dosing can create windows of poor viral suppression.

Introduction

Almost 25 years after the discovery of the human immunodeficiency virus (HIV) as the cause of Acquired Immunodeficiency Syndrome (AIDS), AIDS continues to be a globally spreading, life-threatening infectious disease [1]. In the first world, AIDS can be treated with a cocktail of antivirals, that prolong life-expectancy, but fail to eradicate the virus [2]. The main causes of this failure are not entirely understood, but one key element is the development of drug resistance [3], resulting from the versatile nature of HIV [4]. In the context of HIV therapy, drug resistance leads to the relapse of virus [5], re-emergence of AIDS-related symptoms and eliminates further treatment options [6].

The mechanism underlying the development of drug resistance under therapy are only partly understood. HIV can only evolve while it is replicating. However, replication is strongly inhibited by drug treatment. This contradiction requires to study three major aspects of HIV adaptation in parallel, as they appear *in vivo*: (i) The pharmacology of anti-HIV drugs and (ii) the mutational- and (iii) replicative dynamics of HIV. However, in most scientific publications, these aspects are treated individually.

Mathematical analysis of drug resistance data has revealed many insights into evolutionary escape-pathways from drug treatment [7–10] and mathematical modelling of HIV dynamics has offered many insights into the time scales and mechanisms of viral replication (e.g. [11–14]). However, these models often lack the link to pharmacology. Subsequent extensions of the initial models have analyzed the general impact of temporally varying drug concentrations on virus dynamics after treatment [15–19] and recent work has established the entire link from intra-patient pharmacology to viral dynamics [20, 21]. However, the fields of pharmacology and HIV dynamics are separately addressed in most cases and there is substantial room for improvement.

Purpose of the Study. The purpose of this project is to build the link between pharmacology and HIV replicative- and mutational dynamics in order to study resistance development under drug treatment. This requires the development of mathematical models of HIV replication- and evolution that can incorporate the effects of all approved anti-HIV compounds. Furthermore, it requires mathematical models that can accurately describe the pharmacokinetics (concentration-time course) and pharmacodynamics (effect-concentration) of antivirals.

Outline. In the first part of the thesis (chapters 1–3) the reader is introduced to the pertinent biological background. Chapter 1 introduces the reader to the clinical aspects of HIV and AIDS, in terms of the methodologies used to determine the state of infection, disease progression and drug resistance, as well as the general treatment approaches. In chapter 2 we will give a detailed description of the viral life cycle, providing the background for understanding current pharmaceutical approaches against HIV. In Chapter 3 we will give a detailed overview of currently approved anti-HIV drug treatments and provide an outlook on future developments.

The second part of the thesis introduces a novel model of viral dynamics and evolution, that allows to accurately incorporate the mechanism of action of all approved anti-HIV drugs, providing the link

between pharmacology and clinical endpoints (e.g. plasma HIV RNA). The introduction of novel inhibitors required the development of a novel measure of drug efficacy, the reproductive capacity, that will be introduced in chapter 4. Finally, we utilize the novel model and the novel measure of drug efficacy to propose and test an optimal treatment sequencing protocol.

In the third part of the thesis (chapter 5–7), we introduce the reader to pharmacokinetic and pharmacodynamic modelling with application to antiviral drugs. The reader is introduced to the general concepts of pharmacokinetics in chapter 5, with special emphasis on establishing the link between measurable drug concentrations in the blood-plasma and drug concentrations at the effect site (which are mostly not available). In chapter 6, pharmacodynamic concepts are introduced and the pharmacodynamics of nucleoside reverse transcriptase inhibitors are exemplified. In chapter 7, we will exemplify the pharmacokinetic-pharmacodynamic relationship for a specific drug (zidovudine).

Part I

Biological Background

Chapter 1

AIDS, HIV & Clinical Practice

In 1981, reports of a new disease, (mainly) infecting homosexual men and injection drug users, emerged in the USA. This unknown disease caused tumors, such as Kaposi's sarcoma and other opportunistic infections originating from immunologic abnormalities [22]. Subsequently, the new disease was named 'acquired immunodeficiency syndrome' (AIDS) based on the signs, symptoms, infections, and cancers associated with the deficiency of the immune system. In 1983, Barré-Sinoussi and Montagnier isolated a new human T-cell leukemia viruses (HTLV) from a patient with AIDS [23]. They showed that the virus was able to infect lymphocytic cells and may thus be the cause of AIDS. Roughly at the same time an identical virus was isolated by Gallo and colleges [24]. The newly discovered virus was initially termed HTLV-III or LAV (lymphoadenopathic virus), which was later changed to HIV (human immunodeficiency virus). In the sequel it became clear that this new virus is the cause of AIDS [25]. In 2008, Barré-Sinoussi and Montagnier received the nobel prize in medicine for their work on the discovery of HIV.

1.1 Pathology & Epidemiology

The number of cells expressing the CD4 (cluster of differentiation 4) receptor ($CD4^+$- cell count) is the main marker associated with the pathology of HIV-infection (see fig. 1.1). A $CD4^+$ T-cell count below 200 per μL of blood has been established as a clinical marker for the definition of AIDS [26].
HIV infection can be divided into an acute, a chronic and a final phase, which is typically associated with AIDS (see e.g. [27]). The length of time from primary infection to the development of AIDS can vary widely between individuals. The majority of people infected with HIV, if not treated, develop signs of HIV-related illness within 5-10 years, but the time between infection with HIV and being diagnosed with AIDS can be 10–15 years or even longer [1].
Acute phase. Following infection, infected cells cannot be detected for 1–3 days. The first infected cells, that become detectable are resting memory $CD4^+$ T cells that express chemokine (C-C motif) receptor 5 (CCR5), the virus co-receptor [28]. Over the following 3 days, the number of infected cells increases. At $\sim$ 1 week, virus becomes detectable in local lymph nodes; Langerhans cells or dendritic cells are involved in carrying virus to these sites [29, 30]. Around day 7, virus begins hematogenous spread (spread by the blood) and is seeded to other sites, particularly to the gut-associated lymphoid tissue (GALT) where large numbers of $CD4^+$ $CCR5^+$ memory T cells reside [31]. This seeding to other sites results in an exponential expansion of the infection, with up to 20% of gut-associated CD4 T cells infected and $\sim$80% destroyed [32, 33]. Virus appears in the blood, with viremia peaking at around day 21, often $> 10^7$ virus particles per ml of plasma (see fig 1.1). Then the level of HIV-1 starts to fall, either because of saturation of the main target cell population (memory $CD4^+$ $CCR5^+$ T cells) [34] or because of the appearance of specific immune responses, or both [35, 36]. Without therapeutic intervention, virus levels fall 10- to 100-fold and level out to a relatively stable set point (with $\approx 10^5$ virus per mL) between 2 and 6 months after infection.
Chronic phase. After the acute phase, blood $CD4^+$ T cell levels, which dip in acute infection, usually recover as the viral set point is reached, but then gradually decline. However, this gradual

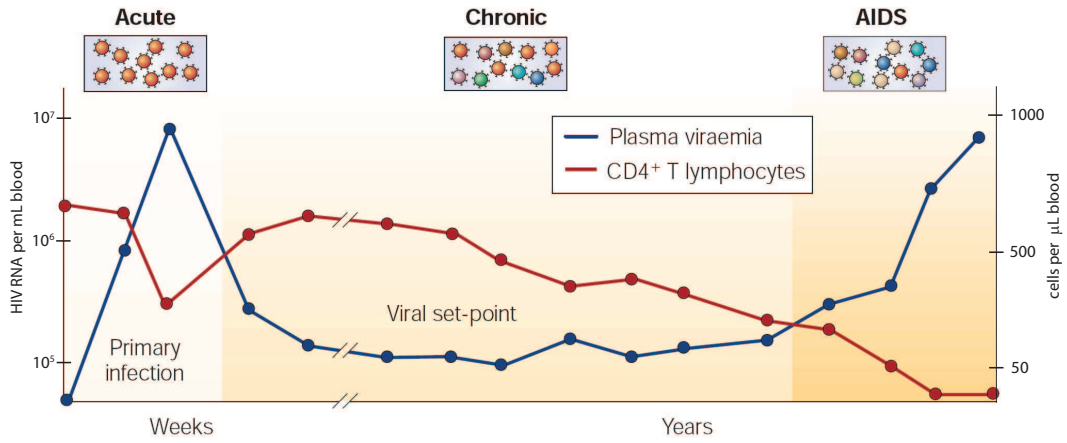

Figure 1.1: Time course of HIV infection. Picture modified from [27]

decline masks what is really happening in the whole CD4$^+$ T cell population [28]. The virus levels generally stay around the set point for many months or years.

Final phase. The final phase is characterized by a loss of immune function and the occurrence of

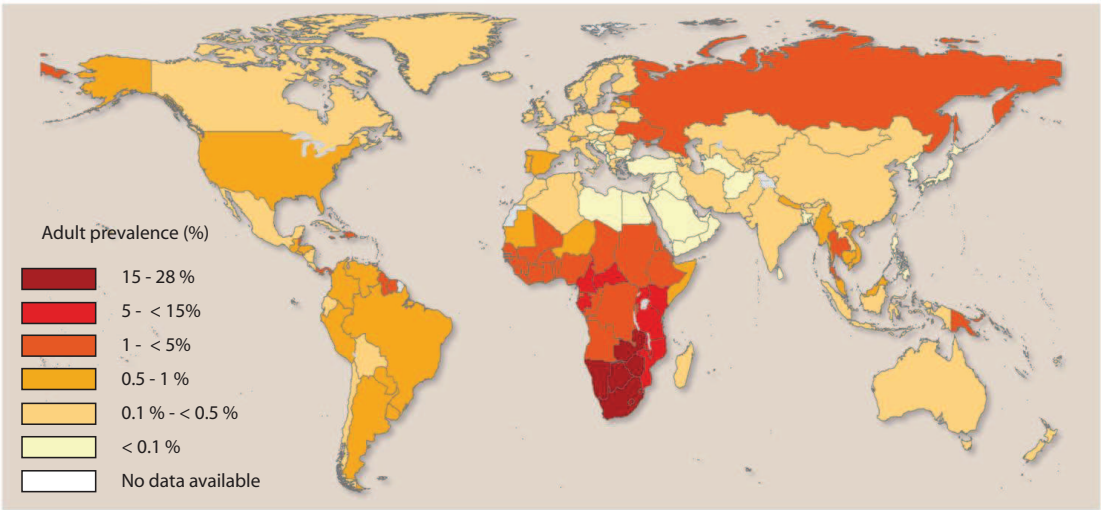

Figure 1.2: Global View on HIV infection 2008. Picture modified from [1]

opportunistic infections. To date it is unclear how HIV causes AIDS. Although simple depletion of the major target of HIV infection, the CD4$^+$ T cell, can explain much of the observed immunosuppression, other factors seem to be involved.

A major cause of CD4$^+$ T cell loss appears to result from their increased susceptibility to apoptosis when the immune system remains activated [37]. Persistent immune activation might be a direct result from HIV-infection or indirectly caused by the loss of mucosal defence [38], which leads to microbial translocation [39]. Although new T cells are continuously produced by the thymus to replace the ones lost, the regenerative capacity of the thymus is slowly destroyed by direct infection of its thymocytes by HIV [40, 41]. Eventually, the minimal number of CD4$^+$ T cells necessary to maintain a sufficient immune response is lost, leading to AIDS.

The United Nations AIDS (UNAIDS) committee has estimated the number of HIV-infected people to 33 millions (range: 30-36 millions) for 2007 [1]. The number of HIV-infected people has leveled off since 2001, however it is still increasing. Sub-Saharan Africa remains the region most heavily affected

by HIV, accounting for 67% of all people living with HIV and for 75% of AIDS deaths in 2007 (see 1.2). Some of the most worrisome increases in new infections are now occurring in populous countries in other regions, such as Indonesia, the Russian Federation, and various high-income countries. In 2007 there were 2.7 million new HIV infections and 2 million HIV-related deaths. Young people aged 15–24 account for an estimated 45% of new HIV infections worldwide.

1.1.1 Target Cells

Essential for HIV target cell infection is the presence of CD4 receptors [42, 43] and co-receptors, either CCR5 or CXCR4 (CXC receptor 4, also called fusin) [44–49]. Studies of disease progression in humans [50, 51] and in nonhuman primates [52] have established that the tropism of viral isolates for CXCR4 or CCR5 clearly defines the cellular targets for HIV *in vivo*. Although a greater number of potential target cells express the CXCR4 receptor [53], CCR5 co-receptor usage is favored in early infection [54], implying that reproduction in CCR5-tropic cells (e.g. activated T-cells of the gut-associated lymphoid tissue) is more efficient. In later stages of disease a 'co-receptor switch' from CCR5 to CXCR4 occurs [55], which might be partitially due to the depletion of target $CD4^+$ $CCR5^+$ cells.

The virus, entering through which ever route, acts primarily on the following cells [56, 57]:

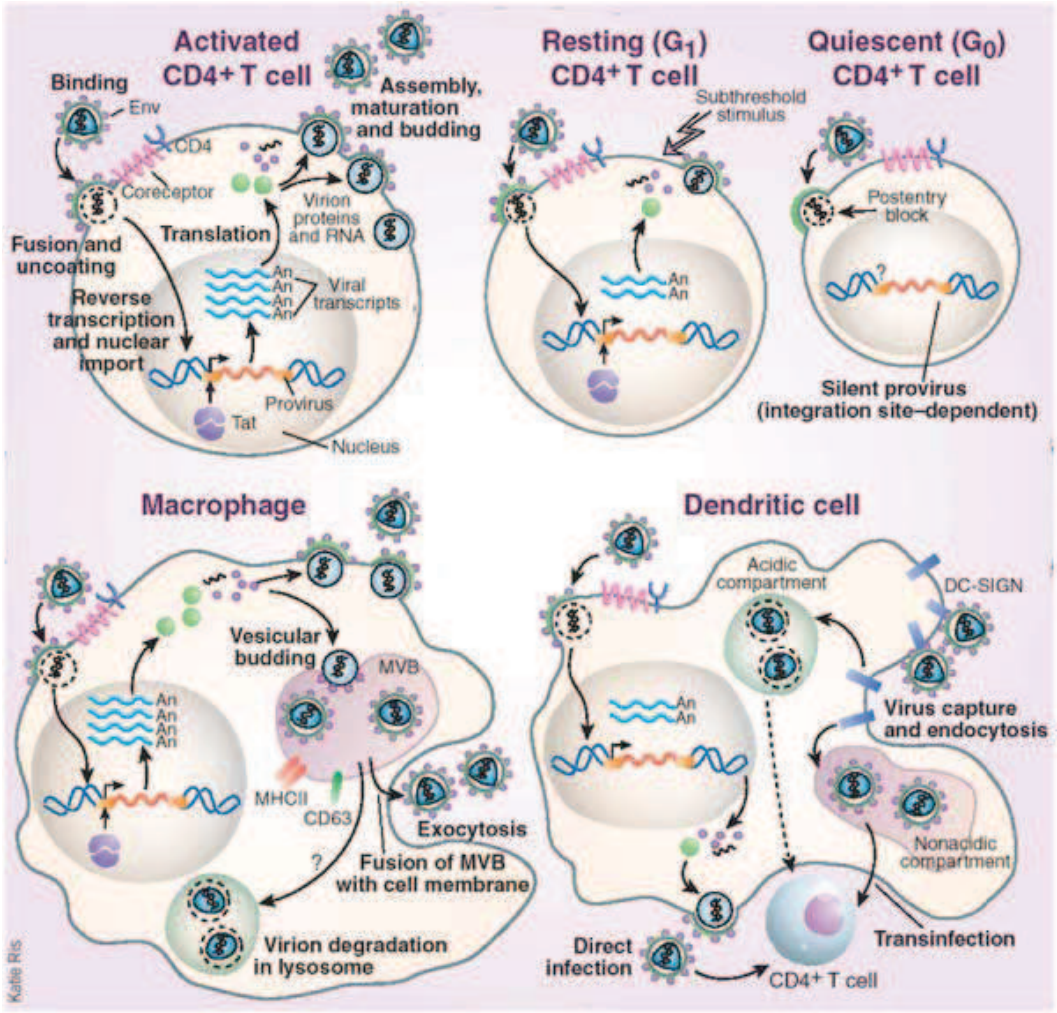

Figure 1.3: Major cell types involved in HIV infection. Picture taken from [56].

- **CD4$^+$ T-helper cells** [58, 59]
- **CD4$^+$ macrophages** [60, 61]
- dendric cells (e.g. langerhans) [62–64]
- natural killer cells/natural killer T-cells [65, 66]
- Other: CNS: microglia and macrophages [67–71]

This broad cell tropism of HIV and the distribution of target cells into partially pharmacologically or immunologically restricted areas, such as the brain, poses an enormous challenge for the design of effective anti-HIV treatments. The life cycle of HIV in important target cells is schematically illustrated in figure 1.3.

1.1.2 HIV Subtypes and Diversity

HIV is a retrovirus belonging to the genus lentiviridae [72]. The genome of HIV consists of a linear, positive-sense, single stranded RNA. As with all other retroviruses, the single stranded RNA needs to be reversely transcribed into double stranded DNA by the viral enzyme reverse transcriptase (RT) and then inserted into the genome of the host cell. We will detail the various steps in the life cycle of HIV in chapter 2. Five groups of lentiviruses can be clustered on the basis of the hosts they infect (primates, sheep and goats, horses, cats, and cattle). Within the primate lentivirus group, simian immunodeficiency virus (SIV) and the two human viruses, HIV-1 and HIV-2 are distinguished. HIV-1 and HIV-2 sequences diverge by more than 50%. Furthermore, HIV-2 contains the vpx gene that is absent in HIV-1. HIV-1 RNA consists of ∼9200 (9181) nucleotides (`NC_001802`) [73–75] in contrast to HIV-2 (10359 nucleotide bases; `NC_001722`). Most drugs are developed against HIV-1. Because of this high divergence between HIV-1 and HIV-2, only a minority of drugs is also effective against HIV-2. The genomic structure of HIV and the constituents will be detailed in chapter 2. HIV exhibits an enormous diversity [76]. HIV-1 consists of several groups, which are distinguished based on sequence diversity. Of these groups, group M is the globally spread form.

1.2 Host Defence Mechanisms

The infected host can defend itself against HIV mainly through production of (neutralizing) antibodies and through cytotoxic T lymphocytes (CTL) response.

1.2.1 Antibody Responses.

Anti-HIV directed neutralizing antibodies are produced by B-cells through previous interaction with T-helper cells, the primary target of HIV. Antibody responses are directed against the surface of HIV viruses, more specifically against the envelope protein (Env) that is necessary for viral entry into host cells. However, the accessible parts of the Env protein are very variable [77, 78] and the conserved parts of Env are poorly accessible [79–82], making it very difficult for the immune system to build up an effective defense against HIV based on antibodies.

1.2.2 CTL Responses.

Cytotoxic T lymphocytes responses are elicited by virus-specific CD8$^+$ cells after previous interaction with T-helper cells. Multiple mechanisms have been associated with the antiviral effect. CTL can lyse HIV-1-infected cells *in vitro* and block propagation of the infection [83]. These cells also produce soluble factors that can mediate this effect [84, 85]. CTL responses kill infected cells through lysis, or induction of apoptosis, or they block intracellular replication through the excretion of soluble factors, such as interferons (IFN). However, CD8$^+$ T lymphocyte responses have a tendency to be

highly focused on a limited number of epitopes and are thus limited by the propensity of the virus to accumulate mutations in T lymphocyte epitopes and to evade cellular immune control [86–88]. Early studies showed that virus-specific $CD8^+$ T lymphocyte responses emerge during acute infection coincident with initial control of primary viremia [35, 89, 90]. CTL responses seem to be the most effective immunological control mechanism against HIV *in vivo* [91]. However, one significant limitation of cellular immune responses is that they can probably not protect against acquisition of HIV-1 infection. Given the time required for $CD8^+$ T lymphocyte responses to expand after infection, it may be difficult for e.g. vaccine-elicited T lymphocytes to prevent early immunopathologic events completely [92].

1.2.3 Intracellular Defense Mechanisms.

A number of host cellular proteins can interfere with the intracellular replication of HIV. The protein APOBEC3G for example can cause hyper-mutations in the viral genome [93], thus providing an intracellular protection against HIV. Also, siRNA and miRNA can suppress and silence viral mRNA [94,95]. The host cell proteasome has been reported to account for the degradation of $\approx 50\%$ of the viral proteins, prior to integration [96]. Some of these intracellular modulators require an extracellular input, like IFN, which is excreted by CTLs. For an overview of some intracellular factors refer to e.g. [97].

1.3 Treatment

Current treatment options for HIV include vaccines [98] and synthetic drugs [99]. The use of synthetic compounds has been very successful, allowing to control viremia and reduce morbidity [100]. However, synthetic compounds cannot cure HIV and lead to a live-long dependency on these drugs. Vaccine efforts have been less successful. There is currently no effective anti-HIV vaccine.

1.3.1 Vaccines & the STEP Study

Vaccine efforts are based on boosting the host-defense mechanisms, such as antibody and CTL responses. Therefore, they face the same problems that are associated with the host-defense mechanisms. However, a continuous presentation of antigens by vaccines can elicit a strong and persistent immunological response [101, 102].
The extensive subtype diversity and mutagenicity of HIV pose enormous challenges upon the design of effective vaccines. To overcome the diversity and mutagenicity of HIV, vaccines have to induce broadly neutralizing activity against conserved regions of HIV.

The STEP study. The STEP study was a huge multi-center clinical study of Merck's CTL-based vaccine. The study consisted of of 3,000 subjects in America, the Caribbean and Australia and 3,000 subjects in South Africa. Merck's recombinant Adenovirus 5 (rAd5) vectors expressed HIV-1 clade B genes Gag, Pol and Nef. Responses to this vaccine were partially suppressed in individuals with pre-existing neutralizing antibodies against the vaccine vector [103–106]. On 21 September 2007, the STEP study was unexpectedly terminated at the first planned interim analysis, when the Data and Safety Monitoring Board declared futility in the study achieving its primary end points [107]. Moreover, in subjects with pre-existing Ad5-specific neutralizing antibodies, a greater number of HIV-1 infections occurred in vaccinees than in placebo recipients. It is currently unclear whether the lack of efficacy in the STEP study simply represents the failure of the Merck rAd5 vaccine product or whether this might mean the failure of the T-cell vaccine concept overall [98].
The failure of the STEP study had a large impact on the community. Most vaccine trials have been halted and a return to basic science was employed in order to understand the principal mechanisms of HIV immunology.

1.3.2 Antiviral Drugs

Although vaccines have helped to control several of the most important viral pathogens, there is currently little prospect of an effective vaccine for the human immunodeficiency virus [99] and with $\sim$ 33 millon people infected worldwide an urgent need for antiviral treatment. There are currently 25 synthetic anti-HIV drugs on the market [108], which as combination therapy, known as highly active anti-retroviral therapy (HAART), have transformed what used to be a rapid and lethal infection into a chronic condition that can be controlled for many years. Antivirals can help to control HIV, in such a way, that AIDS does not develop, they, however, do not eradicate HIV, but lead to a life-long dependence on medication with all its toxicities [109, 110].

However, in HIV-infected individuals under antiviral treatment it is a matter of time until drug resistance emerges and drug treatment becomes ineffective. It is still unclear how drug resistance develops under effective treatment.

There are two major theories trying to explain the failure of HAART: (i) The latency-theory [111] states, that there are some latently infected cells with a half-life of month to years, that, after discontinuation of HAART, become activated and release virus. (ii) The 'sanctuary-theory' [112] assumes that replication is ongoing, despite HAART, and that in the course of this ongoing replication mutant strains are formed, that can resist drug therapy and therefore lead to a rebound of virus.

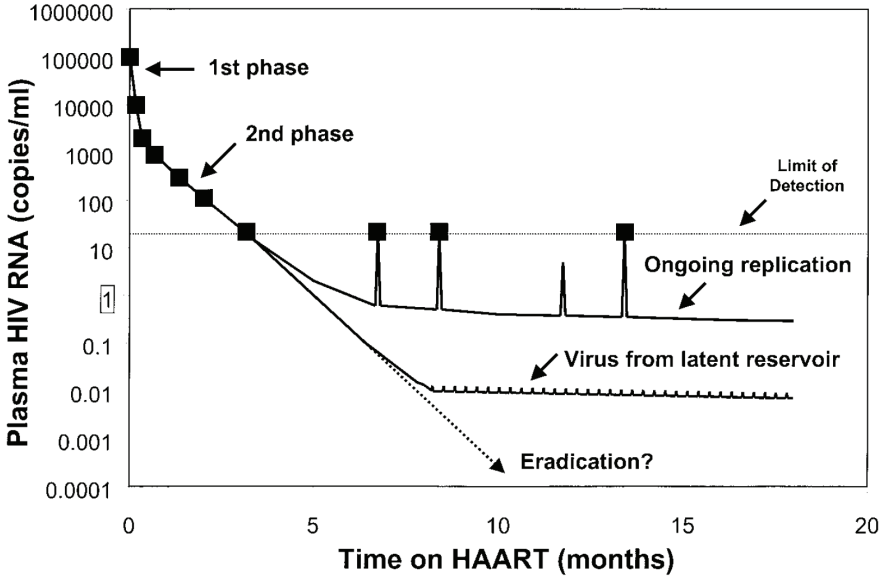

Figure 1.4: Hypothetical decay curve for plasma virus levels in a patient treated with highly active antiretroviral therapy (HAART). Illustration from [113].

The latency-theory coincides with the unability to detect virus after successful HAART. There is experimental evidence for the existence of this reservoir [114]. The latent reservoir has been experimentally quantified in [115]. The potentially very slow decay of this reservoir might make the eradication of HIV impossible (see figure 1.4). However, this theory alone cannot explain the emergence of drug resistance during therapy, since the viral genome contained in this reservoir cannot evolve in the absence of replication [114].

It is known that HIV infects pharmacokinetically restricted anatomical compartments (e.g. brain, genital tract) [57]. The sanctuary-theory explains the unability to detect plasma virus as a result of compartmentalization of HIV infection [116–120]. Furthermore, the detection of viral 'blips' (see

figure 1.4) could indicate ongoing replication in certain sanctuaries, that are insufficiently represented by plasma viral loads.

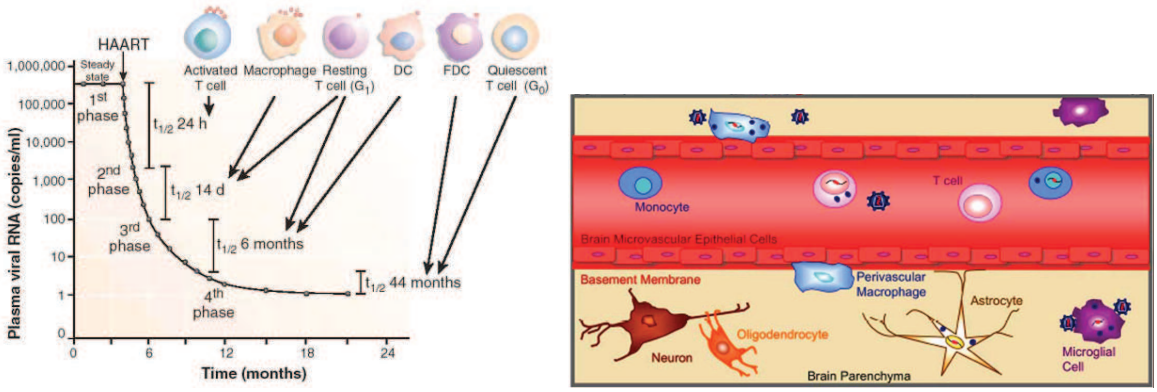

Figure 1.5: Left: The live span of the major cell types involved in HIV infection. Picture taken from [56]. Right: Cellular HIV-1 reservoirs in the CNS. Perivascular macrophages and microglia are the major HIV-1 producing cells in the CNS. HIV-1 infection of astrocytes is considered to be non-productive. Picture taken from [121].

1.4 Clinical Data Acquisition

1.4.1 Quantifying HIV Infection.

The standard for monitoring the status of the viral infection is to take blood samples and determine the viral load. The blood is not the main target tissue of HIV [57], however it represents the amount of circulating virus and is therefore a good indicator of the exchange of viral particles between local sites. The limit of detection of the standard assays is 50 HIV RNA copies/ml [122–124].

1.4.2 Quantifying Drug-related Resistance.

There are two types of HIV resistance testing: genotypic and phenotypic [125]. Phenotypic assays test the susceptibility of patient-derived virus towards a drug. Genotypic assays sequence patient-derived virus.

Standard sequencing technologies in genotypic assays can only pick up mutant populations if they are present in the 20–50% range at best [126]. Codon-specific, hybridization methods in genotypic assays are usually more sensitive than sequencing technologies in detecting minority species. They can pick up mutant populations if they are present in the 2–5% range [127,128]. Recent improvements in sequencing technologies [129] allow the detection of sequences, that are present in 1% of the population. Generally, the results of genotypic assays can be reported within 1–2 weeks of sample collection.

Standard phenotypic assays amplify a patient-derived segment of the *Gag/Pol* gene that incorporates protease, reverse transcriptase and some of *Gag*. Replication of virus at different drug concentrations is monitored by expression of a reporter gene and is compared with the replication of a reference HIV strain. The drug concentration that inhibits 50% of viral replication (i.e., the median inhibitory concentration IC_{50}) is calculated, and the ratio of the IC_{50} of test- and reference viruses is reported as the fold increase in IC_{50} (i.e., fold resistance). For most drugs, phenotypic change will be detected if at least 20% of the viral population is resistant. One obvious potential limitation of these assays is that their utility is restricted to reverse transcriptase inhibitors and protease inhibitors. However, these assays have recently been extended and can now be used for novel inhibitors as well [130, 131]. Results are usually available in 2–3 weeks.

Since the genotype accounts for the phenotype, they must correlate. Multiple mutations are usually needed to generate high-level resistance, and there are very complex interactions which can be additive or suppressive in complex ways [125]. Important contributions in understanding the multiple pathways of resistance development have been made (e.g. [132]), and there are various tools available to predict drug resistance (phenotype) from sequence data. A summary of algorithms that help interpreting genotypic assays is given in [133]. A compilation of relevant drug resistance mutations is e.g. available though the International AIDS Society [134].

1.5 Summary

HIV load (HIV RNA per mL blood) is the most important clinical marker to quantify the state of infection, whereas the CD4 count is the most important marker for the progression of the disease. HIV infection is typically divided into 3 stages. The acute phase is occurs at the time-scale of weeks (see fig. 1.1) and coincides with the spread of HIV into most physiological compartments. The acute phase is followed by the chronic phase, in which the viral load declines to a stable set point and the CD4 count partly recovers. In the final phase, viral load continuously increases, while the CD4 count is gradually declining. The drop of CD4 cells coincides with symptoms of immunodeficiency. A CD4 count below 200 cells/mL blood is defined as AIDS.

Currently, there is no effective vaccine against HIV. However, HIV can be treated with a combination of antiviral drugs, known as highly active antiviral therapy (HAART). HAART cannot eradicate the virus, however, it can slow the progression of the disease and reduce AIDS-related morbidity. Current treatment goals are to suppress AIDS and prolong survival. The Food and Drug Administration (FDA) defines treatment success based on the suppression of plasma viremia, a stable $CD4^+$ count and no AIDS-related symptoms [2]. After acquisition of HIV, the current optimistic prospects of the infected are a life with HIV, under constant drug treatment. However, these prospects are challenged by the emergence of drug resistance mutations, that render the therapy inefficient, and therefore eliminate therapeutic options.

There are two main theories which try to explain the failure of HAART to eradicate HIV: (i) The 'latency-theory' states that HIV replication is sufficiently inhibited by antivirals, but that eradication cannot be achieved due to the extremely long life-span of some HIV-infected cells (see fig. 1.5). This theory, however, cannot explain the emergence of drug resistance. (ii) The 'sanctuary-theory' is based on the fact that antiviral drugs might insufficiently suppress the virus either in certain HIV infected cells or pharmacologically restricted anatomical compartments, like e.g. the brain and genital tract (see fig. 1.3).

1.6 Glossary: HIV/AIDS Medical Terms

CD4: Cluster of differentiation 4: Surface receptor of HIV susceptible cells.
CCR5: C-C-motif receptor 5: Most important co-receptor for HIV.
CXCR4: CXC-motif receptor 4: Important co-receptor for HIV. Typically utilized at later stages of disease.
epitope: Localized region on the surface of an antigen, capable of inducing an immune response
viremia: Presence of virus in the blood stream.
latent infection: Pathology in a dormant or hidden stage.
viral blip: An isolated appearance of virus above the limit of detection (> 50 copies of viral RNA per mL)
viral load: concentration of virus per mL of blood. Determined indirectly by most methods through quantification of viral RNA levels.

Chapter 2

HIV Life Cycle

HIV comprises 15 proteins and an RNA (see fig 2.1). The RNA encodes for nine genes (Gag, Pol, Env, Tat, Rev, Nef, Vif, Vpr and Vpu). The HIV proteins can be clustered on the basis of their functionality:

1. Protease (PR), reverse transcriptase (RT) and integrase (IN) are viral enzymes. They are encoded in the Pol gene. After translation of the Pol gene, the enzymes are produced through proteolytic cleavage by PR (PR has an autocatalytic function).

2. The structural proteins are nucleocapsid (NC, p7), capsid (CA, p24), matrix (MA, p17) and two envelope glycoproteins: transmembrane- (TM, gp41) and surface protein (SU, gp120). The structural proteins originate from the Gag-gene with the exception of the envelope glycoproteins, which originate from the Env gene. The final proteins are formed after proteolytic cleavage of their precursors by PR (in the case of Gag) and host proteases (in the case of Env). NC associates with the genomic RNA and protects it from digestion. CA forms the capsid/core that encloses the genomic RNA and some proteins that are necessary for the infection of a host cell, such as IN and RT. A matrix surrounds the capsid, ensuring the integrity of the virion particle. The outer membrane of the virus is derived from the host cell and includes the envelope glycoproteins gp41 and gp120.

3. The regulatory proteins Tat (p16, transcriptional transactivator protein) and Rev (p19, "regulator of expression of viral proteins") interact with host enzymes and are essential for the successful replication of HIV. The regulatory proteins are produced after multiple splicing of transcribed RNA.

4. The accessory proteins Vif (p23, viral infectivity factor), Vpu (p16, virus protein U), Vpr (p12, viral protein R) and Nef (p27, "negative replication factor") interact with host cellular pathways, improving the intracellular replication of HIV. These accessory proteins are produced through partial splicing of proviral RNA transcripts. The C-terminal Gag protein p6 is also termed accessory protein. It is important for the release of viral particles and for attracting Vpr to the viral core.

In this chapter we will detail the life cycle of HIV and the functions of the various viral proteins within the life cycle. This will be important in order to understand and accurately model drug interference with the viral life cycle.

2.1 Binding and Fusion.

The HIV envelope consists of a gp41 and gp120 (see table 2.1). They form the outer sphere of the virus, with gp41 serving as an anchor and gp120 being entirely exposed to the solute. The first steps in the infection of a target cell by mature HIV-1 particles are mediated by binding of gp120 to the CD4 receptor of the host cell (see fig. 2.2). This induces a conformational change in gp120 that exposes

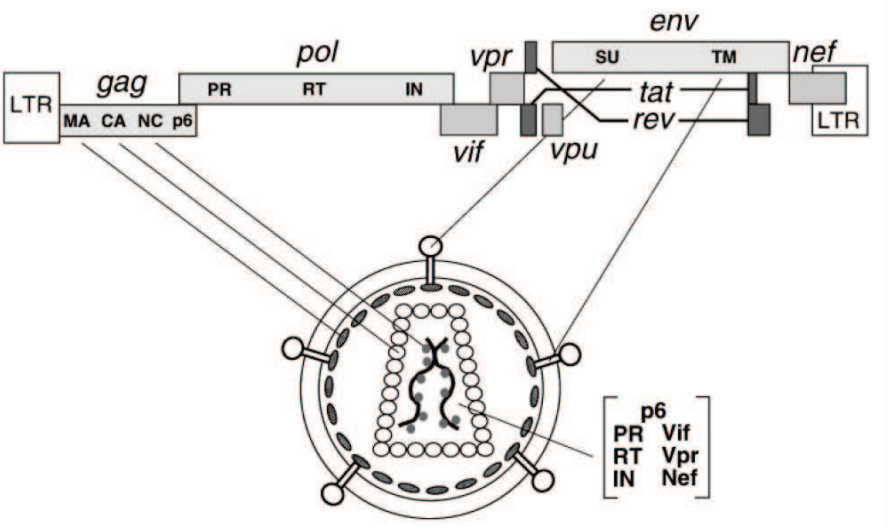

Figure 2.1: Organization of the HIV proviral genome and assembly. Illustration from [135].

the co-receptor binding site (see fig. 2.2). Exposure of the co-receptor binding site permits binding of gp120 to the co-receptor (either CCR5 or CXCR4). Co-receptor binding induces a conformational changes in gp41, which leads to the insertion of the fusion peptide into the host cell membrane [136]. Interactions between the gp41 sub-domains HR1 and HR2 finally pull the viral- and the host cell membrane in close proximity, allowing them to fuse.

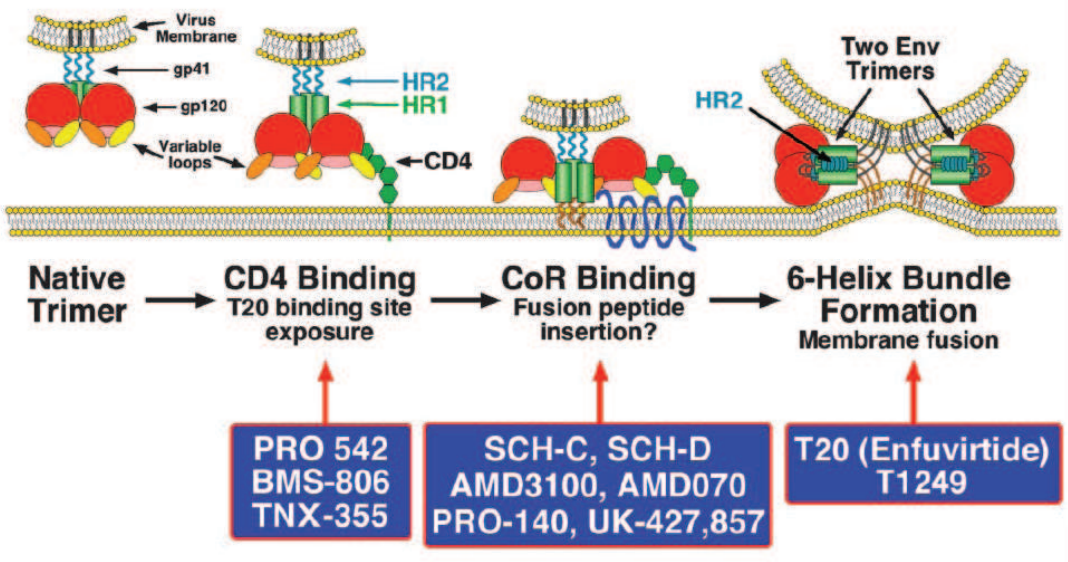

Figure 2.2: HIV fusion with a host cell. Illustration from [99].

2.2 Reverse Transcription and Integration.

Following virus entry, the viral core is released into the cytoplasm of the target cell [137]. Reverse transcription of the viral RNA takes place in the cytoplasm [138–141]. It is generally believed that

the reverse transcription process is already initiated in virus particles [142,143] and is then completed in the cystosol of the target cell, after viral entry (see e.g. [144]). Reverse transcription is a chain reaction in which ≈10000 RNA bases (genomic RNA) are degraded and a double stranded DNA of ≈20000 DNA bases is generated simultaneously by RT. Reverse transcription is a particularly interesting process for drug targeting: (i) It is absolutely essential for successful HIV infection and (ii) the nature of the chain reaction offers many opportunities to interfere (e.g. [145]). The majority of anti-HIV drugs inhibit this enzyme by various mechanisms.

The process of reverse transcription is highlighted in fig. 2.3. Reverse transcriptions is initiated by tRNA binding to the primer binding (PB) site of the viral RNA. Several viral factors (including Tat, Nef, Vif, Vpr, IN and NC) and some host cellular proteins form a large RNA-tRNA complex [146]. This

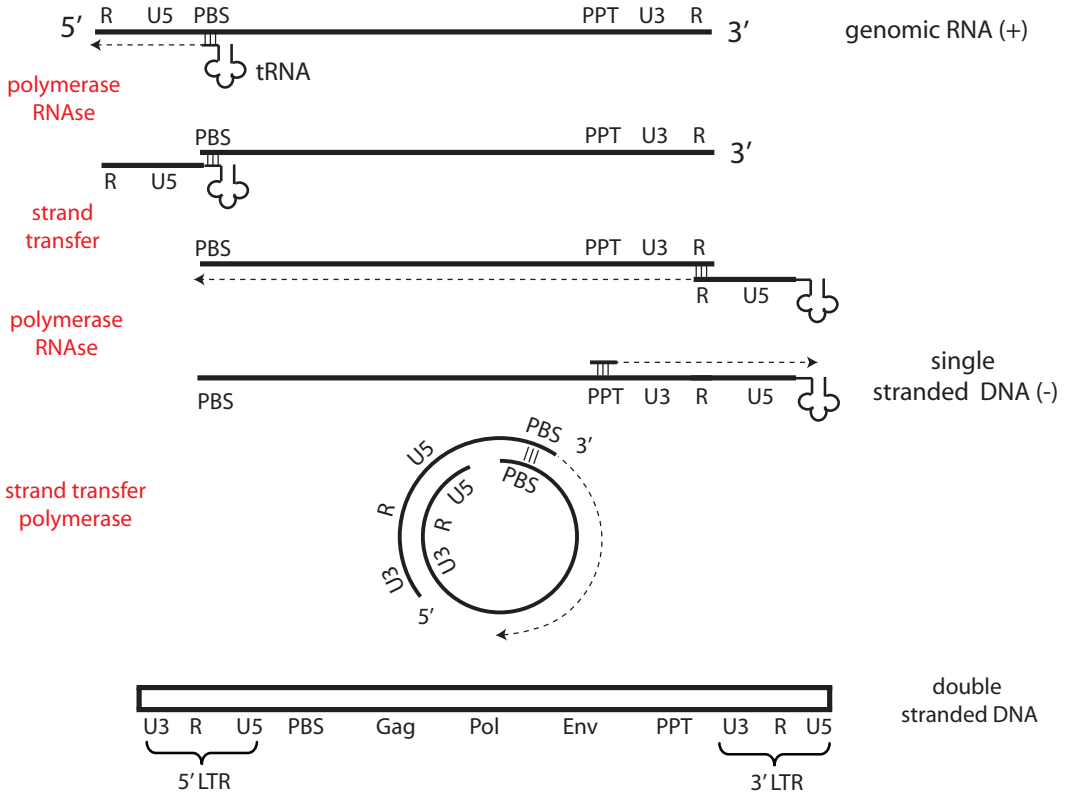

Figure 2.3: Illustration of the process of reverse transcription

complex is specifically recognized by RT [147]. Binding of the cellular tRNA to the PB site of the viral RNA has provided a hydroxyl-group for the initiation of reverse transcription. The RNA-dependent DNA polymerase (reverse transcription) is initiated, after some initial modifications at the 5'-end of the viral RNA, which ensure the correct order of the long terminal repeats (LTRs) in the nascent DNA. After reverse transcription (RNA → DNA), the complementary single stranded RNA (except for its polypurine (PP) site) is degraded by the RNase function of RT. The first elongation- and RNase steps have produced a negative-sense single stranded DNA, that is bound to the PP remainder of the viral RNA. The PP site is now used for the initiation of the second elongation step, which produces the 5' end of the future positive-sense DNA strand. The nascent DNA strands now hybridize at their PB sites allowing the completion of the positive-sense DNA strand by the polymerase function of RT (DNA → DNA). Finally, the missing 3' end of the negative-sense DNA is completed. Compared to the single stranded genomic RNA, this complicated process ensures that both double stranded DNAs have a U3-R-U5 sequence at their ends (see fig. 2.3), that serves as a transcription promoter.

Upon completion of reverse transcription, newly formed viral DNA associates with viral- (MA, IN

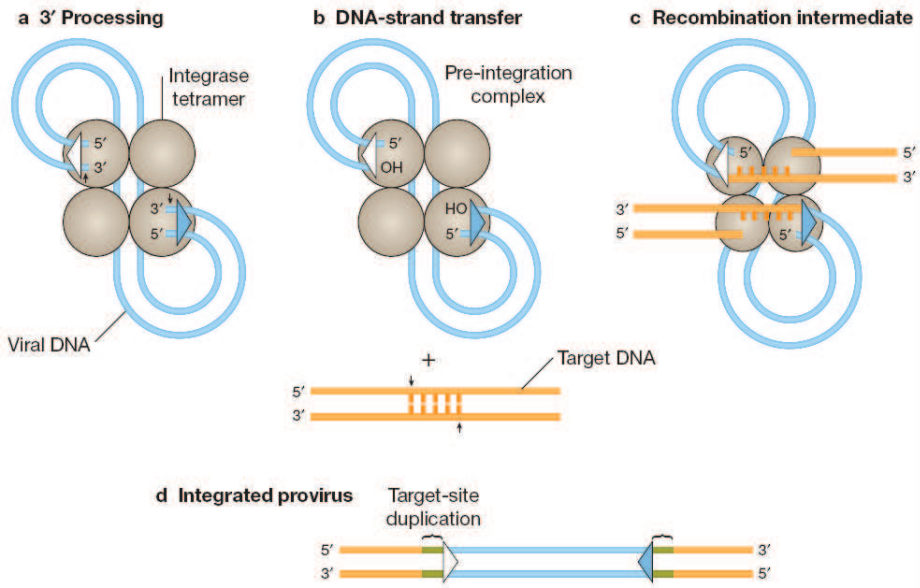

Figure 2.4: HIV-1 Integration. Illustration from [148].

and Vpr) and host cell proteins into the so-called pre-integration complex (PIC). The PIC is transported into the nucleus via an active mechanism 4–6 h after infection [149]. HIV PICs were shown to traffic along microtubuli towards the nucleus with MA inducing interaction with host cell actins [150]. Vpr has been reported to enhance the transport of the viral DNA into the nucleus (in particular in nondividing cells [151]), by promoting direct or indirect interactions with the cellular machinery regulating the nucleo-cytoplasmic shuttling [152].

Integration of double-stranded viral DNA occurs in three steps [153, 154]: (i) 3' processing, (ii) strand transfer; and (iii) DNA repair (see fig. 2.4). During the 3' processing, IN removes a "pGT" dinucleotide at each 3' end of the viral long terminal repeats (LTRs), adjacent to a highly conserved "CA" dinucleotide. This reaction takes place in the cytoplasm within the preintegration complex (PIC). The subsequent strand transfer occurs in the nucleus following the nuclear import of the PIC. In the nucleus, the viral IN cleaves phosphodiester bridges located on either side of the major groove in the target DNA. Next, the processed CA-3'-OH viral DNA ends are ligated to the 5'-O-phosphate ends of the target DNA. The integration process is completed by cleavage of the unpaired dinucleotides from the 5' ends of the viral DNA and repair of the single stranded gaps created between the viral and target DNA. This repair is probably accomplished by host-cell DNA repair enzymes.

HIV integrations sites are evenly spread over the human genome, with preferences within genes. Wang et al. [155] have mapped $\approx$ 40000 unique integration sites within the human genome.

2.2.1 Pre-integration Latency

Zhou at al. [96] have calculated that intracellular viral genomes decay with a half-life of $\approx$2 days in resting $CD4^+$ cells. Koelsch et al. have shown in [156] that the unintegrated viral DNA decays rapidly with an *in vitro* halflife of 1-4.8 days, in agreement with earlier studies [96]. They conclude that the decay of total viral DNA after initiation of HAART is disproportionately over represented by the loss of unintegrated HIV DNA, suggesting that the levels of total HIV DNA after prolonged therapy largely represent integrated HIV genomes. This indicates that latently infected cells seem to originate from infected cells with integrated HIV DNA and not from cells with unintegrated DNA.

2.3 Amplification of Viral Proteins.

Following integration into the host chromosome, the integrated provirus serves as the template for the synthesis of viral RNAs that ultimately encode the full repertoire of structural, regulatory and accessory proteins. The HIV long terminal repeat (LTR) and the two viral regulatory proteins Tat and Rev are essential for the effective transcription of viral RNA. Once RNA is transcribed, it is eventually spliced in the nucleus to produce partially spliced mRNAs, which encode the Env, Vif, Vpu, and Vpr proteins, and small, multiply spliced mRNAs, which are translated into Rev, Tat, and Nef. Unspliced RNAs function as mRNAs for the Gag and Gag-Pol polyprotein precursors, or are packaged into progeny virions as genomic RNA (see fig. 2.5). The mRNA is transported from the nucleus to the cytoplasm by Rev, where it is translated into proteins or packaged. The Env mRNA is translated at the endoplasmic reticulum. The Gag and Gag-Pol polyproteins become localized to the cell membrane.

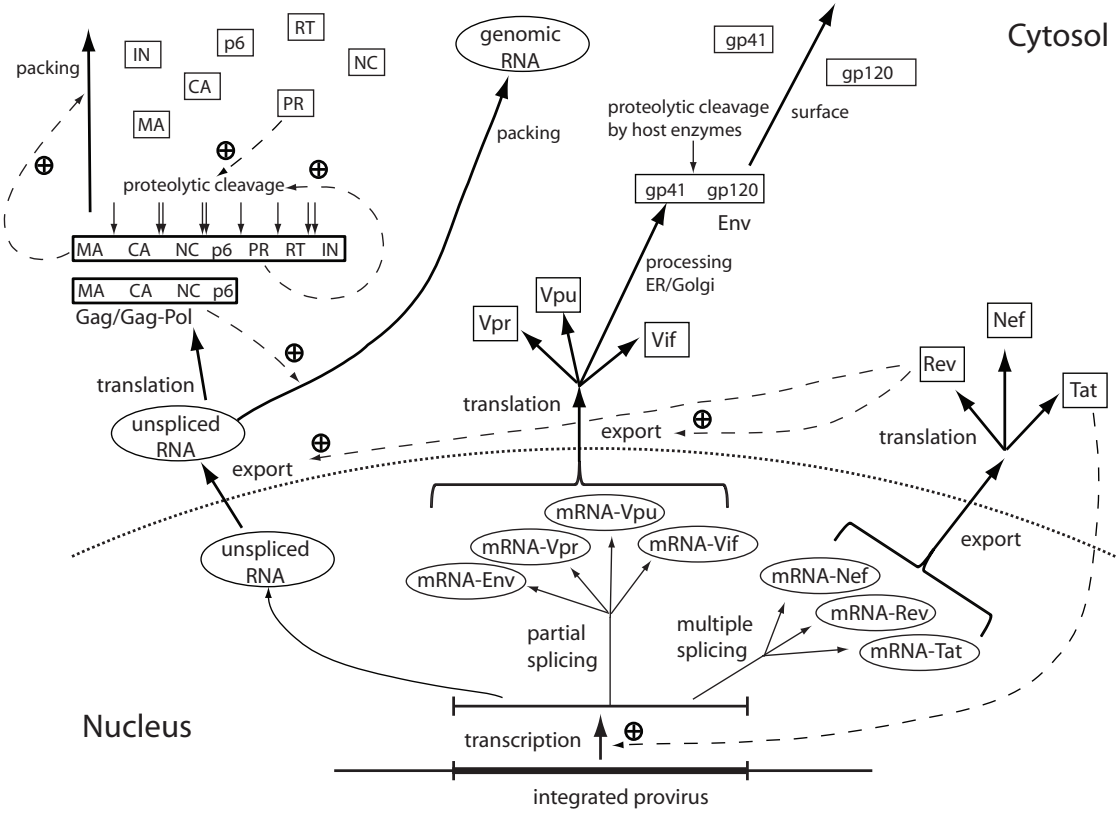

Figure 2.5: Post-integration events.

The HIV-1 long terminal repeat (LTR) acts as an inducible promoter [157]. The basal transcriptional activity from the HIV LTR is very low. It was very soon realized that RNA synthesis is greatly increased (by more than two logs) when Tat is present [158, 159]. Tat recruits elongations factors to the nascent viral transcript and thereby greatly improves transcription of HIV RNA [160]. Thus, Tat constitutes a positive feedback for the expression of viral RNA [161] (see also fig. 2.5). The Tat protein, although being nuclear in localization, is also released from infected cells and acts on uninfected cells. Extracellular Tat seems to play an important role in AIDS pathogenesis since, when taken up by uninfected cells, it can deregulate gene expression [162, 163].

The protein Rev functions as an important switch in the expression of HIV proteins. With low concentrations of Rev (which are abundant initially after integration) nuclear export of viral RNA is inefficient. Viral RNA that resides in the nucleus is multiply spliced, encoding for the regulatory

proteins Tat, Rev and Nef [135]. Rev aims at overcoming this default pathway by actively shuttling viral RNA from the nucleus to the cytoplasm [164]. Thus, when sufficient amounts of Rev are achieved, more partially spliced or unspliced RNA is produced, encoding for Env, Vif, Vpu, Vpr and Gag/Gag-Pol (see fig. 2.5). The Gag-Pol polyprotein mRNA is generated through a frameshift which leads to overreading of the Gag stop-codon.

The protein Nef enhances the infectivity and the reproduction of HIV through two mechanisms [165]: (i) It induces down-regulation and degradation of CD4 receptors [166]. This way Nef prevents aggregation of Env proteins with host-cell CD4 (ii) Nef inhibits apoptosis in the infected host cell by interfering with the apoptotic pathway [167,168] and by downregulation of MHC receptors for immune recognition (by e.g. CTLs) [169]. The protein Nef has also been connected with the deleterious effects of HIV infection: It induces an "exhaustive" phenotype [170, 171] in uninfected, HIV-specific T-cells, which increases apoptosis [172]. The net effect of Nef is a reduced clearance of virus/infected cells resulting in high viral loads and the pathological potential *in vivo* [173].

The host cell protein APOBEC3G is an RNA-editing primate enzyme that plays an important role in intracellular anti-viral immunity [93]. Upon incorporation into virions it de-aminates cytosine bases in the positive strand viral RNA genome (C $\rightarrow$ U), which leads to hypermutations (G $\rightarrow$ A) in the proviral complementary DNA, destabilizing the viral genome. The HIV protein Vif counteracts APOBEC3G by inducing a rapid (halflife of 1-2 min) degradation of APOBEC3G [174].

Several reports describe Vpr as a protein that arrests cells in the G2 phase of the cell cycle [175–178]. *In vitro* studies suggest that the viral promoter LTR is highly active in the G2 phase of the cell cycle [179, 180]. Therefore, G2 arrest may promote optimal transcription from the LTR, which in turn promotes an increase in viral output. Vpr has also been shown to contribute to the cytopathicity of HIV in infected cells by inducing cell death [181, 182].
Vpu is the smallest of all accessory proteins in HIV with the highest degree of variability [183]. It is a transmembrane protein that is not packed in the virus particle [184]. It is found only in HIV-1 and simian immunodeficiency viruses from chimpanzees [183]. Not much is known about Vpu activity activity *in vivo*. During viral protein amplification, Vpu has been shown *in vitro* to interact with the CD4 molecule in the rough endoplasmic reticulum (RER), resulting in its degradation via the proteasome pathway [185].

2.3.1 Post-integration Latency

HIV-1 transcription is tightly regulated: silent in long-term latency and highly active in acutely-infected cells. In computational studies [186], post-integration latency has been explained on the basis of Tat-expression. In a recent study [187], it has been shown that the regulatory protein Rev also plays a crucial role, since it translocates genomic-length and partially spliced RNAs from the nucleus to the cytoplasm, where it is translated. In another study [188] it has been shown that domains within HIV LTR interact with host cell proteins, such as NF–κB, relaxing the restricting chromatin structure and thus enabling transcription of HIV RNA. Thus, there are at least three mechanisms by which post-integration latency can be explained [189]: (i) A restricting chromatin structure, which renders the provirus inaccessible [190]. (ii) Dysfunctioning of Rev, which leads to nuclear retention of HIV transcripts [187] and (iii) silencing or dysfunctioning of Tat, which leads to insufficient transcriptional activity [186]. Current pharmacological interventions that aim at driving HIV out of latency focuss mostly on relaxing the chromatin structure [191, 192].

2.4 Virus Release and Maturation.

Retroviruses can leave the cell in a single step directly from the plasma membrane or, alternatively, can bud directly into multivesicular bodies and then exit cells via the exosome pathway. Remarkably, virus release from both the plasma membrane and multivesicular bodies can occur directionally into

specialized sites of cell-to-cell contact called virological synapses [193].

During amplification, Rev causes a switch in the production of proteins, inducing the production of proteins that originate from unspliced RNA, such as Env, Gag, Pol and Gag-Pol. As a result, Env output is continuously increased. Env glycoproteins are processed (glucosylated) in the endoplasmatic reticulum and Golgi apparatus, cleaved into gp41 and gp120 by host cell proteases [194] and then expressed at the cell surface. Gag proteins are synthesized in the cytoplasm of the infected cell and assemble into virus particles that typically bud from the plasma membrane. While the Env glycoproteins and the Pol-encoded enzymes are required for the production of infectious progeny virions, expression of Gag proteins alone is generally sufficient for the assembly and release of non-infectious, virus-like particles [195, 196]. Approximately 2000 to 5000 Gag polypeptides are required to form a single spherical, immature HIV-1 particle [197]. Gag proteins contain four conserved regions that perform distinct functions during viral assembly: the N-myristilated (fatty acid attached) MA domain targets the protein to cellular membranes, CA makes important protein-protein interactions during particle assembly and NC captures the viral RNA genome and couples RNA binding and assembly. The C-terminal p6 domain of Gag encodes a function that is crucial for the release of virions (see fig. 2.1).

MA is the N-terminal component of the Gag polyprotein (see fig. 2.1 and fig. 2.6). MA is post-translationally myristilated at the N-terminus. MA harbors three transport signals (membrane- when myristilated, nuclear localization- without myristilation and nuclear export- [198]) and is regarded as a shuttling protein in infected cells [199]. Two discrete features are involved in membrane targeting: (i) an N-terminal myrisate group and basic residues located in the first 50 amino acids. The myrisate groups are inserted into the lipid bilayer and the basic residues interacts with the phospholipid head groups of the host cellular plasma membrane. MA also associates with the gp41 cytoplasmic tail during assembly and is responsible for incorporation of Env into virus particle [200].

The nuclear export signal is important for Gag intracellular localization: Mutations that block nuclear export result in the aberrant accumulation of Gag and viral genomic RNA in the nucleus and in the production of RNA–deficient virions [201]. A mechanism consistent with these two nuclear signals is proposed in which the nuclear location signal targets Gag to the nucleus for genome binding while the nuclear export signal subsequently targets the Gag–RNA complex to the cytosol.

The CA domain of Gag promotes oligomerization of the Gag molecules at the plasma membrane and thus enhances the assembly of virus particles [202–204].

The NC domain of Gag directs genome packaging by discriminating between spliced and unspliced viral RNAs. Selection is mediated by interactions between the NC domains of the assembling viral Gag polyproteins and segments of the viral genome, called Ψ-sites, which are located $\approx$120 nucleotides upstream of the Gag start codon within the viral RNA transcript [205]. This region contains the major splice-donor site and is destroyed upon splicing, indicating a possible mechanism for discriminating between spliced and unspliced viral mRNAs [206].

The HIV packaging signal within the RNA overlaps with elements that promote RNA dimerization and there is considerable evidence that genome dimerization and packaging are intimately coupled [207]. A total of about 1500 NC molecules [208] coat the genomic RNA in the form of NC oligomers [209]. NC controls the formation of dense core structures, where reverse transcription is prevented [210–212]. Thus, the NC would exert a control on the timing of the viral DNA synthesis by the active RT enzyme, delaying the start phase in virus producer cells [213].

HIV uses the host cell machinery for budding from the cell membrane. The C-terminal p6 domain of Gag (see fig. 2.1) encodes a function that is crucial for the release, or pinching-off, of assembled virions from the host-cell plasma membrane [215]. HIV p6 stimulates viral egress from the plasma membrane by co-opting the cellular machinery that is usually responsible for the inward vesiculation in late endosomes that generates multivesicular bodies [216].

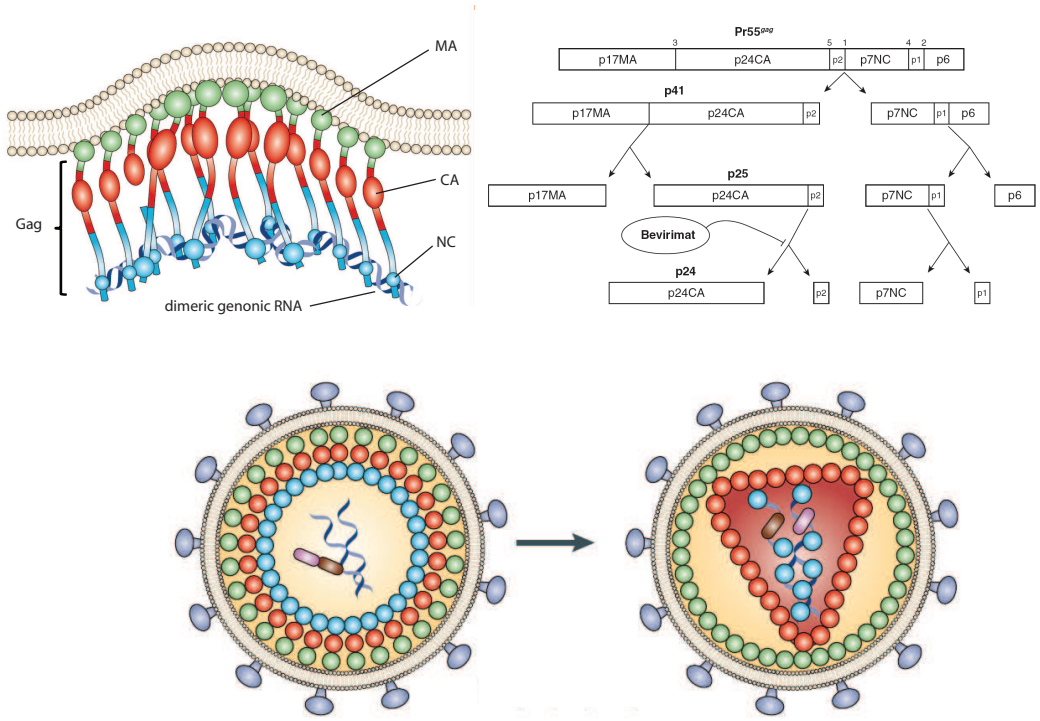

Figure 2.6: Assembly and maturation of viral particles. Illustrations from [195] and [214].

Vpu has been shown *in vitro* to mediate enhancement of viral particle release [217, 218] through the formation of ionconductive channels at the cell surface which might lead to a global modification of the cellular environment [219, 220].

HIV assembly is a two-stage process involving an intermediate immature virus particle that, upon budding from the plasma membrane, undergoes a morphologically dramatic maturation step to yield the infectious particle (see fig. 2.6). This transformation is mediated by the viral protease PR. During-, or following budding, the activated PR cleaves the polyprotein precursors, Gag and Gag-Pol, into their constituent domains [214]. These matured proteins are then free to reassemble to form the structures of the infectious virion. Maturation of the precursor proteins begins by cleavage of Gag-Pol [221] and continues by a process of ordered cleavages governed by differences in the processing rates at each cleavage site (see fig. 2.6) [222,223]. The ordered processing suggests that a regulated cleavage cascade is necessary for proper virion maturation and, therefore, infectivity [214]. Indeed, mutations that either abrogate or alter the rate of cleavage of HIV Gag lead to the formation of aberrant, noninfectious particles [224].

Timing of Protease activity Proteases are enzymes which cleave proteins between specific aminoacids. HIV protease is known to cleave the HIV proteins Gag and Pol. The timing of protease activity is important because intracellular (immature) processing of Gag compromises particle assembly [225]. Pol cleavage, on the other hand, provides an intracellular supply of retroviral enzymes IN, PR and RT, which facilitates multiple integration of provirus into the host cell, given the continually increasing abundance of viral building blocks. Thus, PR could provide a switch between (i) virus production and (ii) manifestation of infection/diversity within a host cell.

For all retroviruses, the completion of the viral budding process correlates with the activation of

the viral protease by an unknown mechanism, and, as the structural (Gag) polyproteins are cleaved by the viral protease, maturation of the immature virus-like particle into an infectious virion [226]. It is generally believed that processing of precursor polyproteins is ordinarily delayed until after virus release. One model for PR activation suggests that aggregation of the precursors at budding sites promotes PR dimerization, which in turn, activates PR [225]. Therefore, a mechanism that delays dimerization until nascent virion particles are separated from their host cell might control the activity of PR. Davis et al. [227] showed that dimerization is enabled by oxidating (acidic) pH conditions. The findings have been confirmed by Szeltner et al. and Louis et al. [228,229], who determined the catalytic optimum of PR at a pH value of ≈ 5. Thus, the activity of the viral protease *in vitro* depends on pH, with an increase in catalytic rates at acidic and neutral pH. The virus could potentially create this optimal milieu through Vpu, which can form ionconductive channels at the cell surface in proximity to the virus budding site, leading to a local modification of the cellular environment [219, 220].

However, there is some evidence for proteolytic activity of PR within the cell: intracellularly cleaved MA [230] is packed into the cores of viral particles and is necessary for the initial steps of infection [199]. As discussed earlier, Pol cleavage might facilitate multiple provirus integration. Thus, moderate intracellular activity of PR might increase the infectivity of virions and lead to a minifestation/latency in long-lived cells, that are fairly resistant to the cytopathic effects [231, 232] of HIV, like macrophages.

2.5 Summary

HIV consists of 9 genes and 15 proteins. Due to the limited number of proteins that HIV provides, it is still possible to comprehend most of their functions. Therefore, we have provided a detailed overview of the roles of the various HIV proteins within the viral replication cycle.

The problem of latent infection, which is one major obstacle for the eradication of HIV (see section 1.3.2), originates in the life cycle of HIV. We have discussed the molecular reasons for pre- and post-integration latency in section 2.2.1 and 2.3.1 and discussed experimental data on the stability of these types of latency. The majority of experimental evidence suggests, that pre-integration latency is determined by the half life of intracellular viral RNA and DNA (section 2.2.1), which was found to be relatively short. Post-integration latency on the other hand is determined by the life-time of the host cell, which can be many month (see fig. 1.5). Thus, it can be inferred that post-integration latency is the main source for latent infection of cells by HIV.

As many novel viral targets are being explored, it is particularly important to understand the role of the targeted proteins in the replication cycle. Not all viral proteins are suitable for pharmaceutical targeting. Inhibiting the function of the viral protein Tat, for example, might lead to latency (see section 2.3.1), which is currently believed to be one of the major bottlenecks to HIV eradication (see section 1.3.2). Some viral proteins are more important than others. The three enzymes (RT, PR and In) for example are absolutely essential. However, different mechanisms of inhibition can lead to different drug-target stoichiometries: Inhibiting the substrate of protease, Gag, for example, requires $\approx$ 5000 drug molecules in order to prevent viral maturation (drug-target stoichiometry: 5000:1), whereas inhibiting the enzymatic center requires one drug molecule (drug-target stoichiometry: 1:1). In the next section, we will discuss antiviral approaches against HIV. We will thus build on the information given in this section, which provides the reader a good background on the molecular targets in antiviral treatment.

Enzymes		
PR	protease	processes immature HIV proteins
IN	integrase	integrates viral cDNA into host cell DNA
RT	reverse transcriptase	converts viral genomic RNA into cDNA
Structural Proteins		
NC	nucleocapsid	encapsulates & protects genomic RNA
CA	capsid	forms viral capsid
MA	matrix protein	forms viral matrix
TM/gp41	transmembrane protein	HIV receptor protein attached to viral membrane
SU/gp120	surface protein	exposed HIV receptor protein
Accessory & Regulatory Proteins		
Nef	negative replication factor	down-regulates CD4, prevents apoptosis
Vif	viral infectivity factor	counteracts APOBEC3G
Vpu	viral protein U	down-regulates CD4, activates PR
Vpr	viral protein R	arrests cell in G2 phase
Tat	transcr. transactivator prot.	up-regulates HIV transcription
Rev	regulator of expr. of viral prot.	shuttles viral mRNA out of nucleus
p1–p66	-alternative notation-	viral proteins /protein subunits denoted by molecular weight (kD)

Table 2.1: HIV proteins.

Chapter 3

HIV-treatment

3.1 A Brief History of HIV Treatment

Since the isolation of the HI-Virus in 1983, drug discovery and development have transformed what used to be a lethal disease in to a treatable, chronic infectious disease [233].

While drug therapy consisted of a single nucleoside reverse transcriptase inhibitor (NRTI) in 1987, which lead to the rapid emergence of drug resistance [234, 235], in the following years the repertoire of NRTIs had been constantly growing (see table 3.1 on page 32). However, the prospects until late 1995 were a delay of disease progression for month, possibly a few years. By the end of 1995 a novel drug class entered the stage: protease inhibitors (PIs). This innovation paved the way for highly successful drug combinations, known as highly active antiretroviral therapy (HAART) [236, 237]. HAART is a combination treatment, in which usually 2–4 drugs from different drug classes are given together. HAART revolutionized AIDS treatment: Virus rapidly decayed to undetectable levels and significant reductions in AIDS-related mortality were reported [238, 239]. In the early era, HAART consisted of two NRTIs and one PI. However, first generation PIs had unfavourable pharmacokinetics, resulting in a high pill burden and complicating treatment adherence. In the following, three major improvements were made: (i) PIs were combined with a low dose of the PI ritonavir, which inhibits their metabolic degradation, thus lowering the pill burden. (ii) The novel class of fully synthetic non-nucleoside reverse transcriptase inhibitors (NNRTIs) with very long halflifes entered the repertoire of antivirals. (iii) Combinations of drugs were marketed, further reducing the pill burden.

By 2002, eradication of HIV was attempted [240, 241], but failed due to the persistence of virus in latently infected cells or anatomical reservoirs [242].

In 2003, the drug enfurvirtide, belonging to the novel class of fusion inhibitors (FI), was released. It was followed in 2007 by compounds of the novel classes of CCR5 antagonists and integrase inhibitors (InI). Currently there are 25 anti-HIV drugs available, belonging to 6 different classes (summarized in table 3.1).

Many novel compounds are in late clinical development (see table 3.2), including the class of maturation inhibitors (MI). A complete list of drugs in clinical trials can be assessed through [243]. Some emerging targets in HIV treatment are reviewed in [244].

3.2 Antiviral Drug Resistance.

HAART has led to a dramatic decline in the morbidity and mortality associated with HIV infection. In spite of this, many HIV-infected patients receiving HAART are unable to achieve sustained levels of plasma HIV RNA below limits of detection. Only approximately 50% of patients who received HAART therapy in a non-clinical trial setting were reported to achieve the goal of viral suppression [245–248].

Response rates with subsequent regimens after initial failure of primary HAART (salvage regimen) are considerably lower [249]. Drug treatment failure is mainly associated with accumulation and evolution of drug resistance [250]. Accumulation of drug resistance can lead to cross-resistance within a drug class or even multi-antiretroviral class failure, leaving limited options for future therapy [251]. Furthermore, re–application of the same or similarly selective antiretroviral agents can lead to virological failure as a result of emergence of resistance derived from previously archived resistant virus [252]. It was demonstrated that drug resistant HIV-1 species are present not only as minor constituents of circulating virus populations, but also in the latent resting $CD4^+$ reservoir long after resistance is no longer detectable in the plasma [253].

Drug resistance can occur in various patterns: (i) One point Mutation: In some cases (e.g lamivudine-resistance), a single amino acid substitution confers absolute resistance. (ii) Accumulative resistance: HIV protease accumulates high-level resistance to protease inhibitors through multiple mutations (e.g. Tipranavir). (iii) Fitness valleys: For zidovudine it is believed that initial mutations confer resistance and that subsequent mutations compensate for the functional losses of the enzyme. However, the exact mechanisms are not well understood. A good overview over relevant drug resistance mutations is available through the International AIDS Society [134].

The emergence, transmission and archiving of drug-, or drug class resistance drives the need for new innovative drugs, without cross-resistance to existing antivirals. Therefore, many novel strategies are pursued in drug discovery and development, with the aim of keeping up with the viral evolutionary dynamics.

3.3 Current Guidelines for the Use of HAART

The term HAART encompasses a variety of combinations of the available 25 drugs, depending on the patient's situation. Usually (e.g. in first-line therapy) HAART consists of two NRTIs and either an NNRTI, or (ritonavir-boosted) PI. The recommended NRTI backbone consists of the drugs tenofovir (TDF) and emtricitabine (FTC), the recommended NNRTI is efavirenz (EFV) and the recommended first-line PIs are either ritonavir-boosted atazanavir (ATV/RTV), ritonavir-boosted darunavir (TMC114/RTV) or ritonavir-boosted lopinavir (LPV/RTV). Some untypical combinations include Mega-HAART (involving ≥ 5 antiretroviral drugs), double-boosted PIs (containing three PIs) and triple-Nukes (containing three NRTIs) [2].

Currently, HAART does not aim at the eradication of HIV [2], which is primarily due to the belief that the pool of latently infected $CD4^+$ cells leads to a life-long persistence of HIV infection [254–257]. However, the latency theory might not be the only explanation for the persistence of HIV, as ongoing evolution, despite HAART, challenges the underlying assumption of complete suppression (e.g. [258]). Based on the assumption that HIV can not currently be eradicated by HAART, the department of health and human services (DHHS) panel on antiretroviral guidelines for adults and adolescents [2] formulates the following treatment goals: (i) reduce HIV-related morbidity and prolong survival, (ii) improve quality of life, (iii) restore immunologic function, (iv) maximally suppress viral load.

Since the aim of the current treatment strategy is the long-lasting suppression of AIDS, the current consensus is to initiate treatment as late as possible, thereby using up as little treatment options as possible and reserving alternative treatment options for the time when drug resistance has developed.

Definition: therapy success. Plasma viremia is the primary clinical marker of therapy success [2]. Plasma viremia should fall below the levels of detection (≈ 50 HIV RNA/mL) within the 3–4 month (not later than 6 month) after initiation of therapy. Within the first 4 weeks plasma viremia should decay by at least 2 log [HIV RNA/ml blood]. With ongoing therapy plasma viremia should remain suppressed (below detection limit).

Definition: therapy failure. Therapeutic failure is best understood in the context of virologic

success, that is, virologic failure is defined as the inability to achieve and maintain suppression of plasma viremia. Furthermore, two consecutive HIV RNA > 400 copies/mL after 24 weeks or detectable levels (> 50 copies/mL) by 48 weeks in a treatment-naive patient, who is initiating therapy, are defined as incomplete virologic response. After virologic suppression, repeated detection of HIV RNA ("blips") is defined as virologic rebound.

In the case of therapy failure the DHHS recommends to change therapy. However, there is no consensus whether therapy should be changed upon detection of viral blips, or after detection of viral rebound at higher levels ($\geq$ 1000 copies/mL). Upon recognition of treatment failure, resistance is assessed and the information is combined with prior resistance history. Follow-up regimen are selected based on the resistance history of the infected patient. Follow-up regimen should contain at least two "active" (no cross-resistance) drugs.

Theory: When does HAART work?
The currently applied HAART does not eradicate HIV, however, it suppresses plasma viremia and prevents the disease progression. A very similar scenario can be observed with (elite) long-term non-progressors [259], which are HIV infected patients with low plasma viremia that, in the absence of treatment, do not develop the symptoms of immunodeficiency. In HIV non-progressors, HIV is effectively controlled by the immune system [260].

One theory how HAART pushes a patient into this labile balance between virus replication and immune control might be that in the presence of HAART, the viral reproduction, and therefore the rate of adaptation is decreased to a point where the virus- and the immune adaptation level each other. A similar scenario can be observed in the asymptomatic stage, with the exception that the immune system is usually less compromised in the early stages of infection, than during the later stages and thus able to handle a greater extent of viral adaptation.

3.4 Principles of Targeting HIV

Antiviral strategies can generally be divided into two groups: (i) Strategies that enhance the removal of pathogens and therefore decrease their expected lifetime and (ii) strategies that reduce the expected number of offspring within the pathogen's lifetime (productivity). While vaccine efforts aim at reducing the lifetime of the virus, by increasing its removal by the immune system, most synthetic compounds do not target the virus itself, but rather reduce the productivity of the virus.

Although it might seem un-intuitive, it is more effective to target the pathogen itself. This process is usually self-sufficient for eradicating the pathogen. The expected lifetime of a pathogen can be indefinite, since pathogens do not die on their own. Thus, decreasing the productivity of the pathogen in the absence of pathogen removal will not lead to the eradication of the virus. In terms of HIV, even the most potent regimens might fail, if the immune system is severely compromised (e.g. by the disease itself) and viral removal is insufficient.

3.4.1 Viral and Host Targets

The paradigm of antiviral drugs has been to target enzymes of the virus, thus achieving a maximal effect at low host cell toxicity, because there is little cross–inhibition of host cell proteins. This paradigm has been used to develop almost all current antiviral therapies, and it will continue to be an important drug-development strategy in the future [99, 261]. However, the versatile nature of HIV [262], driven by the huge reservoir of replicating virus ($\approx 10^7$ infected cells), creates an ensemble of viral targets, that can possibly confer (part-) resistance against any antiretroviral agent.

In the case of viruses, the interaction with host enzymes is obligatory, as viruses require the host cell environment to replicate (e.g. [263]). Therefore, it has been proposed to target host enzymes, which

perform essential interactions with the virus, instead of viral proteins that exists only in a mutant ensemble within the viral population [264]. Approaches targeting host proteins could be less prone to select for drug resistance, because the drug target itself is not subject to evolutionary optimization. However, host enzymes usually perform essential functions. Therefore, targeting a host factor might require very elaborated modes of action of the inhibitor [265] (discussed in the next subsection), that selectively block the virus-host factor interaction/-or response, but allow the host protein to perform essential host-related functions. Although both viral and cellular factors can be targeted, viral factors should optimally be 'knocked-out', while, if a host protein is targeted, a detailed knowledge about the various protein functions is required in order to circumvent toxicity [266]. The mode of action of a drug that targets a host protein would optimally be selective for the specific interaction that is required by the virus.

Antivirals that target the host receptors CCR5 and CXCR4 are good examples, in which specific interactions of the virus with the host are inhibited through modulation of the host protein.

Viral Enzymatic Targets. Most of the currently licensed drugs for HIV target enzymatic reactions. These compounds inhibit viral enzymes in two ways: The first group of inhibitors (InIs, PIs and NNRTIs) target the enzymatic activity by various mechanisms. The second group of inhibitors (NRTIs and maturation inhibitors MI) compete with/or inhibit the substrate of the enzymatic reactions.
While inhibition of the enzyme activity has an effect on all enzymatic reactions carried out by the enzyme, competing with/or inhibiting the substrate only disables a specific reaction that is carried out by the enzyme. However, inhibition/competetition of the substrate can be more bottlenecking in terms of resistance development for HIV, if there is no alternative for the substrate (e.g. in the case of NRTIs). In this case, resistance mutations can permanently impair the fitness of the virus.

The mechanism of action of anti-HIV drugs will be discussed in more detail in the next section.

Other Viral Targets. All currently approved anti-HIV drugs target Pol (enzymes) and Env (surface protein) encoded proteins. While the enzymes were initially targeted by antivirals (due to their inalienability for the replication of HIV) accessory proteins (Nef, Vif, Vpu and Vpr) and regulatory proteins (Tat and Rev) have drawn little attention as potential targets so far. Due to the rapid emergence and possible archiving of drug mutations with potential cross-resistance, it has been realized that widening the molecular targets of HIV therapy by targeting regulatory/accessory proteins may expand treatment options, resulting in high impact effective new therapy. However, targeting accessory/regulatory proteins might not be as successful as targeting enzymes for two reasons: (i) Mechanistically, the targeted processes (protein–protein or protein–nucleic acid interactions) involve large interaction surfaces, which are difficult to potently inhibit. (ii) Accessory proteins might exist to maximize the efficacy of viral replication, but they are not essential for the replication of the virus [267].

HIV-1 regulatory proteins, Tat and Rev, are required for HIV-1 replication and therefore represent two important viral targets for drug development [268]. Because Tat is responsible for the transactivation of HIV transcription, inhibition of Tat might lead to latency [186] and is thus a rather unattractive target. However, it might be more attractive to target some of the other Tat-mediated interactions, e.g. in the reverse transcription process [269]. A review of the pharmacological approaches to inhibit Tat is given in [270]. So far, clinical trials of Tat inhibitors have been unsuccessful [271].

Rev is responsible for shuttling mRNA out of the nucleus, thus preventing splicing. In [187] it was shown, that inhibition of Rev might lead to latency through retention of viral RNA in the nucleus. This type of latency might significantly differ from the one that would be observed when Tat is inhibited: In the case of Rev, the virus production might be inhibited, however, Env proteins might still be expressed to the cell surface, triggering immune response, since Env proteins are shuttled by a Rev-independent mechanism. One promising target has been the interaction of Rev with cellular co-factor DDX3 of the nuclear shuttling complex [272]. Some of the efforts in controlling Rev activity are reviewed in [273].

Accessory proteins (Nef, Vif, Vpu and Vpr) were reported to improve viral growth, without being absolutely essential. However, their importance as virulence factors is being more and more appreciated: they can dramatically alter the course and severity of viral infection, replication and disease progression. None of the HIV accessory proteins display enzymatic activity: they rather act by altering cellular pathways via multiple protein-protein interactions with a number of host cell factors. Therefore, most of the current attempts focusses on targeting specific HIV protein/host cell partner interactions that are important in the HIV life cycle. A review of the current pharmacological efforts is given in [274].

3.4.2 Molecular Mode of Inhibition

An orthosteric inhibition describes the effect of a ligand through steric hindrance. Orthosteric inhibitors occupy and block the site on the targeted enzyme that is required for the reaction. Therefore, binding of an inhibitor precludes the binding of a ligand, because they require the same binding site. Orthosteric inhibitors are, therefore, 'non-permissive' (see fig. 3.1, left).

Allosteric inhibition denotes the effect of an inhibitor on a protein through interaction with a site on the protein that is distinct from the natural binding locus on the protein. Through binding, allosteric inhibitors modulate the protein itself and therefore modulate the response of the protein to a ligand. Therefore, inhibition of a reaction by an allosteric modulator occurs through the protein and not through steric interaction [265]. Allosteric inhibitors can be 'permissive' (see fig. 3.1, right), allowing an endogenous- or residual response while they are bound to the protein.

Examples of allosteric inhibitors for HIV treatment are: Maraviroc (CCR5-antagonist), all currently licensed NNRTIs and the upcoming class of maturation inhibitors (see table 3.1). All other anti-HIV compounds (NRTIs, PIs, InI, FIs) can be considered as orthosteric inhibitors (see table 3.1).

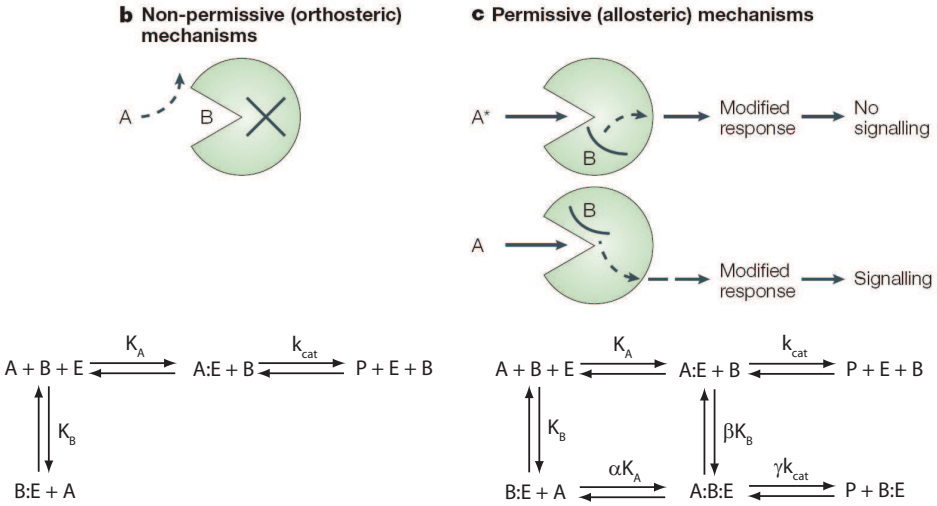

Figure 3.1: Upper panel: A) An orthosteric mechanism of inhibition. The inhibitor **B** binds to the active center/substrate binding site of the target protein. Therefore, with the inhibitor in place, the (viral- or host-) substrate **A** cannot bind and elicit effects. B) An allosteric inhibition. The inhibitor binds the protein at a different site than the substrate binding site. Through binding, the inhibitor modulates the protein. This modification might lead to a modulation (**A**), or a termination (**A***) of the substrate response, depending if the allosteric inhibition is permissive or not. Reaction graphs: left: non-permissive inhibition, right: permissive inhibition. Upper illustration taken from [265].

name	trade name	company	launched	mode
Nucleoside/Nucleotide reverse transcriptase inhibitors (NRTI/NtRTI)				
Zidovudine (AZT/ZDV)	Retrovir	GlaxoSmithKline/generic	1987	ortho
Didanosine (DDI)	Videx	Bristol-Meyers Squibb/generic	1991	ortho
Zalcitabine (DDC)	HIVID	Roche	1992	ortho
Stavudine (D4T)	Zerit	Bristol-Meyers Squibb/generic	1995	ortho
Lamivudine (3TC)	Epivir	GlaxoSmithKline, Shire Pharmaceuticals	1998	ortho
Abacavir (ABC)	Ziagen	GlaxoSmithKline	1999	ortho
Tenofovir disoproxil fumarate (TDF)	Viread	Gilead	2001	ortho
Emtricitabine (FTC)	Emtriva	Gilead	2003	ortho
Non-nucleoside reverse transcriptase inhibitors (NNRTI)				
Nevirapine (NVP)	Viramune	Boehringer Ingelheim	1996	allo
Efavirenz (EFV)	Sustiva, Stocrin	Bristol-Meyers Squibb, Merck	1998	allo
Delavirdine (DLV)	Rescriptor	Pharmacia & Upjohn, Agouron, Pfizer	1999	allo
Etravirine (TMC-125)	Intelence	Tibotec	2008	allo
Protease Inhibitors (PI)				
Saquinavir (SQV)	Invirase	Hoffmann-La Roche	1995	ortho
Indinavir (IDV)	Crixivan	Merck	1996	ortho
Ritonavir (RTV)	Norvir	Abbott, GlaxoSmithKline	1996	ortho
Nelfinavir (NFV)	Viracept	Agouron, Pfizer	1997	ortho
Amprenavir (APV)	Agenerase,Prozei	Vertex	1999	ortho
Lopinavir + ritonavir (LPV/RTV)	Kaletra,Aluvia	Abbott	2000	ortho
Atazanavir (ATV)	Reyataz,Zrivada	Bristol-Meyers Squibb, Novartis	2003	ortho
Fosamprenavir (FOS-APV)	Lexiva,Telzir	Vertex, GlaxoSmithKLine	2003	ortho
Tipranavir (TPV)	Aptivus	Boehringer Ingelheim	2005	ortho
Darunavir (TMC114)	Prezista	Tibotec	2006	ortho
Entry Inhibitors (CCR5/FI)				
Enfuvirtide	Fuzeon	Timeris, Roche	2003	ortho
Maraviroc	Celsentri, Selzentry	Pfizer	2007	allo
Integrase Inhibitors (InI)				
Raltegravir	Isentress	Merck	2007	ortho

Table 3.1: Currently approved antiviral for the treatment of HIV infection

name	class	company
Elvitegravir	InI	Japan Tobacco, Gilead
Vicriviroc	CCR5	Schering-Plough
Bevirimat	MI	Panacos Pharmaceuticals
Amdoxovir	NRTI	RFS Pharma
Apricitabine	NRTI	Avexa
Racivir	NRTI	Pharmasset
Rilpivirine	NNRTI	Tibotec

Table 3.2: Novel anti-HIV drugs in late clinical trials [243].

3.5 Antivirals

3.5.1 Entry Inhibitors: CCR5-antagonists and FI

Entry inhibitors exert their action at the reversible steps before cell fusion (see fig. 3.2). They block the infection of susceptible cells and do not contribute to the clearance of free virus directly.

From a pharmacokinetic point of view, entry inhibitors have the advantage that their target site is extracellular. Therefore, entry inhibitors face (at least) one pharmacokinetic hurdle less than all other anti-HIV compounds (the cellular membrane). Not having to worry about cell penetration allows greater flexibility in the design of drugs as exploited in the case of enfuvirtide. Furthermore, in many cases, target site concentrations are directly related to (unbound) plasma concentrations, which simplifies exploring the pharmacokinetic-pharmacodynamic relation for these compounds, because patient plasma concentrations can be measured directly. However, penetration into some target sites might still be restricted due to vascular barriers (barriers from the plasma to the interstitial space). The most important vascular barriers in HIV infection are blood-brain-barrier (BBB) and blood-testis-barrier (BTB).

CCR5-Antagonists.

A decade ago, researchers found that a deletion in the CCR5 gene confers resistance to HIV-infection in 1–2% of humans who are homozygous for this mutation [275–277]. Individuals who have a 32 base pair deletion in the CCR5 coding region fail to express CCR5 on the cell surface. Individuals with this deletion appear to be immunocompetent with no other obvious abnormalities. This suggested that blocking the function of CCR5 may not be detrimental and thus indicated a great potential for CCR5 antagonists in the treatment of HIV infection. Since these discoveries, the development of antiretroviral therapy utilizing CCR5 antagonism has been of particular interest [278, 279].

In HIV infection, CCR5 is the main co-receptor. Typically, CCR5-tropic virus is dominating in the early- and asymptomatic stages of the disease, while the CXCR4-tropic form can dominate in later stages of disease (in $\approx 50\%$ of all cases). CCR5 antagonists inhibit CCR5-tropic HIV, but are not active against either CXCR4, or dual CCR5/CXCR4-tropic HIV strains.

In August 2007 Pfizer's Selzentry (maraviroc) [280] gained approval as the first small-molecule CCR5 antagonist for the treatment of HIV. Maraviroc binds to transmembrane domains of the CCR5 coreceptor, inducing a conformational shift that renders the HIV-binding domain less accessible [281]. Maraviroc is an allosteric inhibitor of the virus-host cell attachment [21]. Once bound, it dissociates only very slowly *in vitro* (dissociation half-life of 15.95 hours [280]). Pharmacokinetic fluctuations in the maraviroc concentration are expected to have little consequences if the *in vitro* observed slow dissociation from the receptor holds *in vivo*. Maraviroc displays additive or synergistic inhibition to all currently licensed drugs *in vitro* [282]. Jacqmin et al. [21] have modelled the effect of maraviroc and explained the discrepancy between the *in vitro* potent binding of maraviroc to the CCR5 receptor (K_D = 0.089 ng/ml) and the observed *in vivo* effect (IC_{50} = 8 ng/ml) [283] based on the assumption that only 1.2% of free activated receptors are utilized to elicit 50% of the maximum in-

fection rate. This excess of available receptors implies that in the presence of maraviroc, dispensable receptors need to be blocked first, before any marked decrease in the infection rate, and consequently in the viral load, can be detected (see fig. 3.2, right). However, the calculations in [21] did not take into account that the allosteric mode of action of maraviroc might be permissive, as suggested by [284].

HIV can become resistant to maraviroc by switching to CXCR4 usage instead of CCR5 [285]. In one example, HIV can become resistant to the CCR5 antagonist maraviroc by modifying its envelope glycoprotein gp160 so that it can bind to the host CCR5 receptor even with inhibitor in place [284]. This observation might support the notion of 'permissiveness' in the allosteric mode of action of maraviroc.

Maraviroc, which is a substrate of the efflux transporter P-glycoprotein, shows limited distribution to the central nervous system as evidenced by cerebrospinal fluid concentrations that were 10% of the free plasma concentration following intravenous infusion in rats, but is well distributed into the testes [286].

In a Phase III study that compared maraviroc with efavirenz (both given together with zidovudine and lamivudine), maraviroc failed to meet the non-inferiority threshold.

About a dozen co-receptors mediate HIV-1 entry *in vitro* [287]. Among these coreceptors, however, probably only CCR5 and CXCR4 are important as front-line pharmacological targets, because they are the main co-receptors used by HIV-1 to enter $CD4^+$ T cells and macrophages [288–290].

Escape mutants against co-receptor antagonists can utilize the following mechanisms: (i) they may continue to use the same coreceptor in an inhibitor-insensitive manner if the inhibitor is allosteric; (ii) coreceptor switching may occur; (iii) an entirely different co-receptor may be used by the escape mutant. For the only approved coreceptor antagonist, maraviroc (CCR5), coreceptor switching to CXCR4 or inhibitor-insensitivity to in the CCR5 using strains has been observed [285].

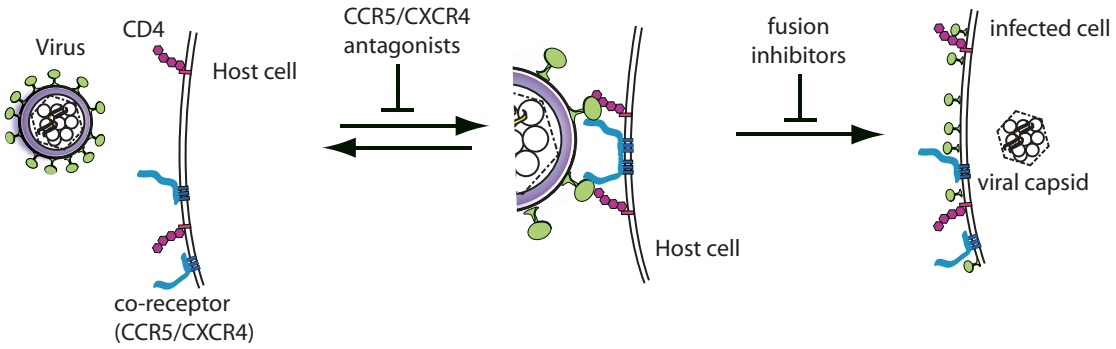

Figure 3.2: Illustration of the action of entry inhibitors within the viral life cycle.

Fusion Inhibitors: FI

Following the interaction between the gp120–CD4 complex and the chemokine receptor CCR5 or CXCR4, additional conformational changes take place in the viral envelope that cause a shift from a non-fusogenic to a fusogenic state of the HIV gp41, which ultimately drive the fusion process. The N-terminal domain of gp41 is exposed and inserted through the fusion peptide into the host cellular membrane. The HR1 and HR2 sub-domains of gp41 condense through formation a six-helix bundle structure (3xHR1 and 3xHR2), that brings the viral- and cellular membrane in close proximity, allowing them to fuse (see fig. 2.2) [291].

Enfuvirtide is a synthetic peptide of 36 amino acids that mimics an HR2 fragment of gp41 [292]. Its binding to the HR1 region blocks the formation of the six-helix bundle structure, which is critical for the fusion process [281].

The primary target of enfuvirtide, the HR2 sub-domain of gp41 is only transiently exposed during viral entry. Sensitivity to enfuvirtide was reduced 2–fold when intercellular adhesion molecule type 1, which accelerates the cell-cell fusion process, was present in the host cell [293]. In a recent study [294], it was shown that a large proportion of HIV particles fuse with the cell after endocytosis. The endosome is not in exchange with the cell surrounding medium, in which enfuvirtide is mainly distributed. Therefore, when the HR2 domain (enfuvirtide's target) is exposed within the endosome, the drug might not be present [295].

Enfuvirtide resistance involves the selection of a broad spectrum of changes in the HR1 region of gp41. Overall, enfuvirtide should be considered as a drug with a low genetic barrier for resistance. Cross-resistance to enfuvirtide is not conferred to other antiretroviral agents.

Enfuvirtide is specific for HIV-1 and is similarly active against various HIV-1 clade isolates and CXCR4 (X4; associated with disease progression), CCR5 (R5; usually involved in HIV transmission) or dual tropic strains. The enfuvirtide concentration required for inhibition of HIV-2 was 10^3- to 10^4-fold greater than that required for HIV-1 inhibition [296].

Enfuvirtide is synergistic in combination with various individual antiretroviral agents [297]. Enfuvirtide in conjunction with other anti-retroviral therapy is approved in the US, Europe and countries worldwide for use in the treatment of HIV infection in treatment-experienced patients. Enfuvirtide is not recommended for use in antiretroviral-naive patients.

3.5.2 Reverse Transcriptase Inhibitors: NRTI and NNRTI

The reverse transcriptase (RT) is a retrovirus-specific enzyme. It uses the viral genomic RNA as a template to produce a double-stranded DNA transcript, that can be inserted into the host-cell genome. In order to complete this process, the reverse transcriptase performs two enzymatic reactions (see fig. 3.3): (i) an (RNA- and DNA dependent) polymerase function and (ii) an RNAse function. The anticipated overall process of reverse transcription is illustrated in fig. 2.3. During each step of DNA chain prolongation, the two processes of chain prolongation and the reverse reaction (excision) are competing with one another (see fig. 3.3, upper panel and fig. 3.5, right panel). The excision process has been discovered in the context of resistance development to some NRTIs.

Reverse transcriptase inhibitors exert their effect intracellular, where reverse transcription takes place. The overall process of reverse transcription (RNA $\rightarrow$ DNA) is irreversible, since the genomic RNA is consumed during the process. Within the viral life cycle, reverse transcriptase inhibitors apply their effect after the irreversible step of cell fusion (see fig. 3.2). Inhibition of reverse transcription can lead to the degradation of essential components of the pre-integration complex (PIC), including the viral genome, and thus fend-off infection. Therefore, reverse transcriptase inhibitors directly contribute to the clearance of virus, like all other drugs that exert their effect after virus-cell fusion and before the irreversible step of viral genome integration.

Nucleoside/Nucleotide reverse transcriptase inhibitors (NRTI)

The first NRTI, zidovudine (AZT), was initially intended as an anticancer drug. In 1985, shortly after it was established that HIV is the cause of AIDS, a team from Burroughs Wellcome (now GlaxoSmithKline) showed that AZT was efficient against HIV [298, 299]. In 1987 AZT became the first approved agent for the treatment of HIV. Successive discovery of NRTIs was based on the principle mechanism of action of AZT.

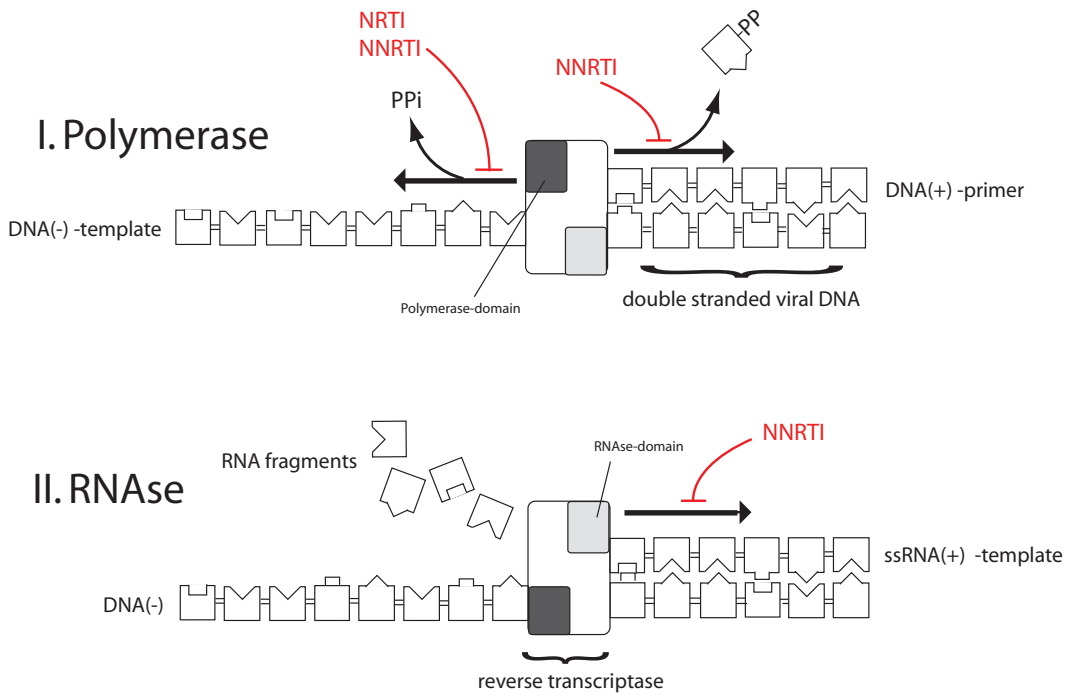

Figure 3.3: Illustration of the main functions performed by the reverse transcriptase and how reverse transcriptase inhibitors interfere with these functions.

Currently, NRTIs are the backbone of highly active anti-retroviral therapy (HAART), which typically consists of a combination of two NRTIs.

NRTIs are analogs of naturally occurring deoxynucleotides (dN). They can be divided into four subclasses: (i) Thymidine analogues: zidovudine (AZT) and stavudine (d4T), (ii) Cytidine analogues: dideoxycytidine (ddC), lamivudine (3TC) and emtricitabine (FTC), (iii) Adenosine analogues: didanosine (ddI) and tenofovir (TDF, PMPA) and (iv) Guanosine analogues: abacavir (ABC) (see also fig. 3.4). A full list of all currently approved NRTIs is given in table 3.1. NRTIs exert their effect intracellularly, at the site of reverse transcription. Due to their hydrophilic character, they are most likely taken up by active transport mechanisms [300], e.g. utilizing the host transporters that are responsible for the import of the endogeneous deoxynucleotides. All NRTIs are prodrugs, that have to pass at least three intracellular activation steps in order to exert their effect (see also fig. 3.4). The triphosphorylated form competes with deoxynucleotides triphosphates (dNTPs, the endogenous substrate) for the incorporation into the nascent viral DNA which is produced by RT [301]. All currently licensed NRTIs are chain terminators: they lack the hydroxyl-group which is necessary for further extension/polymerization of the DNA. This mechanism of action is selective for RT, because RT does not provide a proof reading mechanism, which can replace falsely incorporated NRTIs, unlike most cellular polymerases [302].

The efficacy and safety of nucleoside analogs depends on intracellular- and extracellular pharmacokinetics as well as the affinity of the NRTI for incorporation by RT, versus host polymerases [303]. NRTIs are active against both HIV-1 and HIV-2. Most NRTIs are excreted either unchanged, or after glucoronidation. Thus, there is little interaction with compound classes which are primarily metabolized through CYP P450-enzymes (like PIs and NNRTIs).

Prodrug activation. Nucleoside- and nucleotide (partially phosphorylated nucleosides) analogs are prodrugs that require intracellular phosphorylation to exert their activity (see fig. 3.4). For most NRTIs, uptake- and efflux is mediated by concentrative nucleoside transporters (CNT) and equilibrative nucleoside transporters (ENT), among others [304, 305]. A series of intracellular phosphorylation reactions are required to form an active triphosphate (TP) moiety, eventually creating a

pool of dideoxynucleoside analog triphosphates (NRTI-TP) that competes with the cell's endogenous deoxynucleotide triphosphates (dNTPs) for substrate binding to RT [306].

Although it has been established that the antiretroviral effect of NRTI is related to the active tri-phosphate form, patients are often treated with regimens based on extracellular (plasma) pharmacokinetics and not on intracellular triphosphate pharmacokinetics [307]. Intracellular phosphorylation data from NRTI-treated patients are limited. The effects of systemic or patient-related factors (e.g. infection status, concomitant drugs, genetic variability), cellular factors (cell cycle, cell type, activation status), and measurement factors are difficult to control adequately in clinical studies. Additionally, small samples, poor design, and comparison of study results also impose major limitations on clinical studies, when it comes to analysis of the complex interactions involved in NRTI phosphorylation [308, 309]. The relationship between intracellular phosphorylation and extracellular pharmacokinetics is not always concordant, and complex models are required to define this relationship [145].

The generic route for the activation of NRTIs involves the (active) uptake of the prodrug from the cell surrounding medium and sequential tri-phosphorylation.

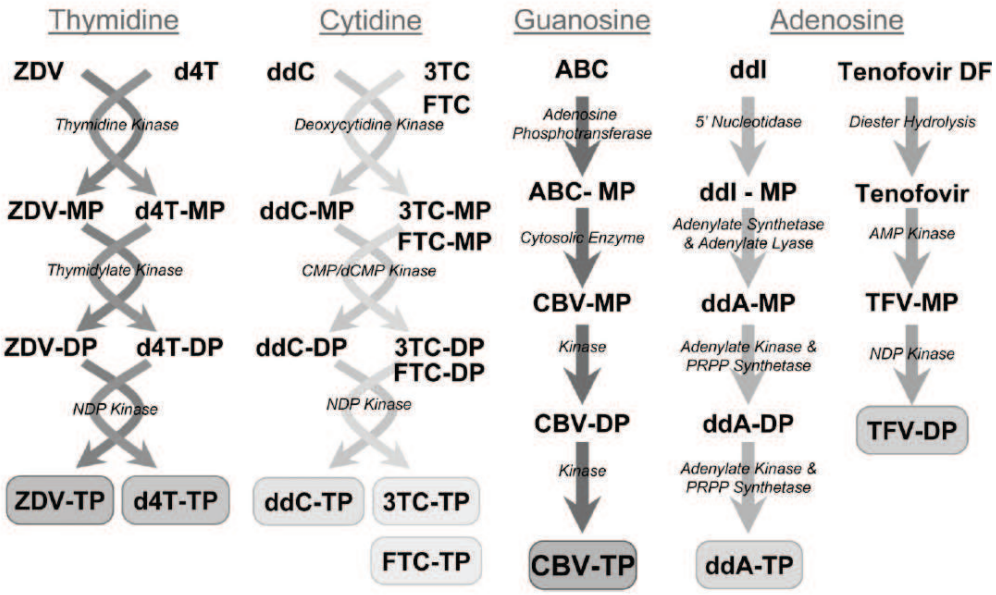

Figure 3.4: Intracellular steps required for the activation of NRTIs. Illustration from [303]

One or more steps in the sequential phosphorylation of NRTIs from initial -MP to -DP to -TP formation can be rate limiting. The efficiency and regulation of these pathways varies and has not been fully characterized for all agents. Studies have shown that the parent drug is often only partially converted to the active TP form (see e.g. [145, 310–315]).

In-vitro and ex-vivo studies with NRTIs indicate that the amount of phosphorylated products in different cell types and the differential phosphorylation kinetics are related to expression of cellular kinases, efficiency of cellular kinases, intracellular dNTP concentration (that might compete for activation) and expression of transporters [300, 314–316]. The extent of intracellular phosphorylation can be influenced by the type of cell (e.g. the difference in phosphorylating capacity) or the activation state of the cell (resting vs. actively replicating). The extent of phosphorylating activity in different cells varies for a given nucleoside analog [314, 315], depending on the predominant activation pathway

(see fig. 3.4).

NRTIs are usually co-administered as the backbone of HAART. Synergy between NRTIs is strongly influenced by how the two NRTIs are activated (see fig. 3.4). Analogs of the same dNTP are likely to use the same phosphorylating pathway, thus competing at the activation cascade level. The most beneficial combinations of NRTIs are those which combine drugs from different subclasses [317].

All NRTIs except for abacavir and tenofovir are activated through triphosphorylation, which involves different enzymes for the different analogues. Abacavir (ABC) has a unique intracellular phosphorylation pathway that first involves addition of a phosphate to form ABC-MP, then cytosolic deamination of ABC-MP forms CBV-MP, which is subsequently phosphorylated twice to form CBV-TP, the active moiety [318] (see fig. 3.4).

Nucleotide reverse transcriptase inhibitors (NtRTI) are partially phosphorylated nucleoside analogs. Enzymatic rate limitation during tri-phosphorylation of nucleoside agents was the driving principle behind their development. However, one limitation is that the highly polar phosphate moiety of NtRTIs restricts cellular penetration. Therefore, the polar phosphate moiety is masked by attaching labile lipophilic groups that would permit uptake through cellular membranes. Within the cell, enzymatic excision of the masking groups regenerates the monophosphate, and intracellular kinases produce the active nucleotide analog triphosphate. Enzymatic excision has the potential to become a further rate-limiting step in the activation of a nucleotide analog. The choice of masking groups, and hence the excision pathway, can significantly influence both the rate and the cell types in which the generation of active drug occurs for a given analog. The only licensed NtRTI so far is the deoxyadenosine-monophosphate (dAMP) analog tenofovir disoproxil fumarate (see fig. 3.4). After intracellular removal of the fumarate residues by intracellular esterase enzymes, tenofovir activation requires two consecutive phosphorylation steps (see fig. 3.4).

Equally important as the phosphorylation cascade are the dephosphorylation steps. The velocity of dephosphorylation determines the intracellular half-life (/clearance) of the active moiety. NRTI plasma elimination is usually fast [307], so that dosing schedules become feasible only in the context of rate-limiting dephosphorylation steps, leading to slow intracellular pharmacokinetics. However, intracellular dephosphorylation can depend on the concentration of intracellular phosphatases, which in turn are cell (and cell activation) dependent. This implies that if the dosing schedule has been adjusted to the intracellular halflife in a particular surrogate marker (e.g. peripheral blood mononuclear cells, PBMC), and the intracellular halflife in some target cell (e.g. macrophages) is smaller, then, insufficient concentrations of active intracellular drug might be achieved at the time before the next dosing. The currently licensed NRTIs with a the longest plasma halflife are lamivudine ($\approx$ 6h) and tenofovir ($\approx$ 17h) [307], while all other NRTIs have a plasma half-life of $\leq$ 3h (see section 5.5). Given the worst-case scenario; –the dephosphorylation of NRTIs in some target cell is fast, implies that only lamivudine and tenofovir are efficient as twice daily regimens. However, currently all NRTIs are given twice daily or less.

Effect. NRTIs compete with their analogous endogenous substrates for incorporation into the nascent viral DNA by RT (see fig. 3.5, a), where they, once incorporated, prohibit further strand prolongation [306, 319]. Three major determinants of NRTI-efficacy can be extracted from mechanistic effect-models [145, 320]: (i) the affinity and rate of incorporation of NRTIs versus the endogenous substrate, (ii) the ratio of NRTI-TP:dNTP and (iii) the total number of NRTI incorporation sites per reverse transcriptase event. From resistance mechanisms, especially to AZT, it is also clear that the rate and selectivity of excision of the NRTI versus the endogenous substrates is an important determinant of efficacy.

The affinity and rate of incorporation of NRTIs depends on the enzyme properties and is thus a major route of mutational escape (see e.g. [301]).

The importance of the NRTI-TP:dNTP ratio is clear from the effects of anti-metabolite agents

(agents that modulate nucleotide pool sizes) on the antiviral activity of NRTIs [321–323]. The relative increase in RT inhibition, and a greater antiviral effect, is achieved at a high ratio and is consistent with competition between NRTI-TP and dNTP for incorporation into DNA being shifted in favor of NRTI-TP [314, 320]. Similar to NRTI-TP levels, dNTP pools vary, depending on the cell type and activation state [315, 324]. This implies, that it is not only necessary to look at the ability of the cell to phosphorylate NRTIs, but also on the endogenous dNTP levels. This is especially important, since the cell's ability to phosphorylate NRTIs and dN are not always interrelated: dNTPs can be formed utilizing two different pathways, termed *de novo* and *salvage*. The *salvage* pathway is a complementary route for providing cells with DNA precursors, primarily utilizing uptake of nucleotides from the extracellular space, derived *in vivo* from nutrients or degraded DNA [325]. Most NRTIs are activated utilizing the *salvage* pathway, thus competing with endogenous nucleotides for this route of activation. However, the *salvage* pathway is not a requirement for the target cell, since the *de novo* synthesis can provide all the DNA precursors needed. In brief, the pool of intracellular NRTI-TP is dependent on the *salvage* pathway, while the pool of dNTP is not. Therefore, the NRTI-TP:dNTP ratio in a cell depends on the route that is primarily used by the target cells to provide supply with dNTPs. If the primary pathway is distinct from the pathway utilized by the NRTI for activation, then the NRTI-TP:dNTP ratio can be expected to be unfortunate and the NRTI is probably not very effective in this cell type.

The salvage pathway, however, has important implications for mitochondrial DNA (mtDNA) replication and metabolism. Interference of NRTIs with the salvage pathway might trigger toxic side effects [326–328].

The importance of the number of incorporation sites for the efficacy of NRTIs has to be viewed in the context of the chain reaction itself. The number of available sites to terminate the chain increases the propensity that the NRTI is incorporated and thus the probability that the NRTI terminates the nascent DNA-strand.

The effect of NRTIs will be exemplified in further detail in section 6.2.

Resistance. Resistance towards NRTIs is achieved by two distinct and generally exclusive mechanisms [301]: Resistance mutations can act either by (i) decreasing the incorporation efficiency of the NRTI-TP or (ii) increasing the removal of the incorporated NRTI. The former mechanism is observed with most NRTIs and most likely involves steric hindrance, decreased binding- [330] or rate of incorporation [331–333]. The later mechanism has been discovered in the context of AZT resistance. Since retroviral RTs lack 3'-exonuclease proofreading activity [334] is was believed that NRTIs, once incorporated, terminate and destroy the nascent DNA. However, reverse transcriptase is capable of pyrophosphorolysis (the reversal of the polymerization reaction, see fig. 3.3) [335] and transfer of the chain terminator to a nucleoside triphosphate, most likely ATP [336] (see also fig. 3.5, right). Transfer of the chain terminator to a nucleoside triphosphate is considered the main pathway of AZT resistance [301]. The two resistance pathways are orthogonal: The 3TC-resistant enzyme, for example, has very poor pyrophosphorolysis and ATP lysis properties on the 3TC-MP or AZT-MP terminated primer [337].

It can be speculated, that enhanced nucleoside excision due to resistance will have an impact on the fitness of the resistant virus, since it decelerates the overall progression of reverse transcription. Decreasing the binding- or incorporation efficacy of NRTIs will also have some collateral effects on the incorporation efficacy of dNs (which might explain the difficulty to detect e.g. 3TC resistant viral strains).

Toxicity. Class-wide long-term toxicity with NRTIs is linked to mitochondrial destruction [110]. The mitochondrial dysfunction has been explained with (i) the DNA polymerase-γ hypothesis, (ii) oxidative stress, and (iii) acquired mtDNA mutations, related to energy depletion [110]. Clinical, pharmacological, cell, and molecular biological evidence links mitochondrial dysfunction to the toxicity of NRTIs [338].

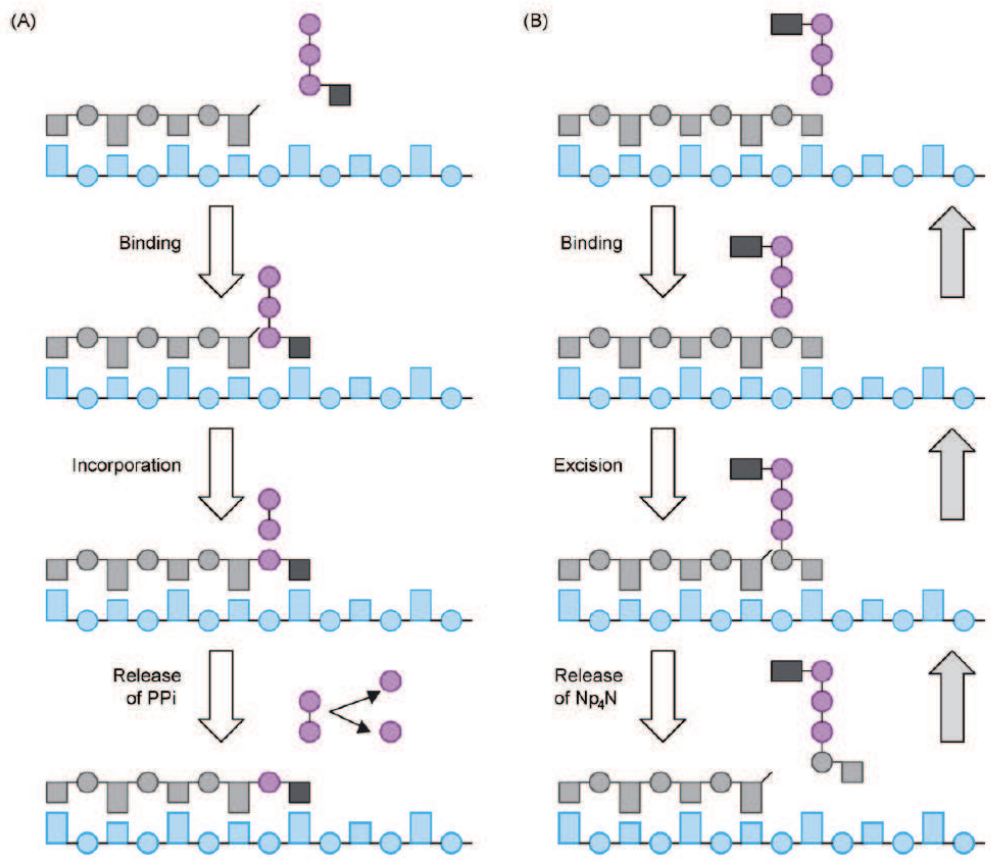

Figure 3.5: a) Polymerase action of RT. An incoming dNTP binds to the complementary dNTP on the complementary RNA/DNA strand. The dNTP is incorporated by ligating the monophosphate group to the hydroxyl-end of the nascent DNA. The remaining di-phosphate of the incoming dNTP is released. This process produces energy. b) Excision of NRTIs. With an NRTI-MP incorporated into the end of the nascent DNA there is no hydroxyl-end exposed for further prolongation of the DNA. An incoming dNTP (mainly ATP) binds to the phospho-diester bridge which connects the incorporated NRTI with its succeeding dNTP, releasing the NRTI from the nascent DNA. The NRTI is thereby excised from the nascent DNA, releasing a dNTP-NRTI complex. This process consumes energy. Picture taken from [329]

The dominant theory for NRTI toxicity is that NRTIs are incorporated into the mitochondrial genome by the mitochondrial polymerase-γ [110], leading to their functional impairment. Most NRTIs, serve as 5'-triphosphate substrates for mtDNA synthesis by DNA polymerase-γ. They compete with the natural nucleotides and also terminate nascent mtDNA chains because they lack 3'-OH for continued mtDNA polymerization. The exonuclease of DNA polymerase-γ may excise the inserted NRTI-MP at the time of its insertion into nascent mtDNA, if the NRTI is recognized as an erroneous substitute. If the NRTI is not recognizable, it remains in the chain, and mtDNA synthesis ceases because the 3'-OH necessary for DNA replication is absent in NRTIs.

When adjusting dosing regimes, the total amount of NRTIs incorporated into the mitochondria is therefore weighted against the potential to terminate reverse transcription, leading to a narrow therapeutic window for most NRTIs.

In a computational study, Wendelsdorf et al [339] have evaluated the DNA polymerase- γ hypothesis for different NRTIs. While the theory is able to explain the observed toxicity of most NRTIs, they found little correlation between observed AZT toxicity and expected toxicity based on the DNA polymerase- γ hypothesis. It is suggested that the association of AZT with mitochondrial toxicity is

a result of the depletion of mitochondrial TTP pools due to the inhibition of mitochondrial thymidine kinase (TK2) and TMP kinase by AZT and AZT-MP, respectively [340]. Similarly, whole cell TTP levels have previously been reported to be decreased by AZT [299,341]. While requiring further study, these results may help to explain the clinical observation of symptoms often associated with mitochondrial damage during AZT therapy [342], despite AZT-TP being a weak inhibitor of mtDNA polymerase-γ [343,344]. This also implies, that potentially not the AZT-TP levels, but rather AZT, or AZT-MP might more closely correlate with toxicity, necessitating a reconsideration of the therapeutic window for this drug [145].

Non-Nucleoside reverse transcriptase inhibitors (NNRTI)

After the discovery of NRTIs, non-nucleoside RT inhibitors (NNRTIs) were subsequently identified as a chemically diverse class of compounds. NNRTIs are chemically distinct from nucleosides and, unlike the NRTIs, do not require intracellular metabolism for activity. In general, NNRTIs are a group of small (<600 Da) hydrophobic compounds with diverse structures that specifically inhibit HIV-1 RT [345]. The four approved NNRTIs include nevirapine, delavirdine, efavirenz, and etravirine (see table 3.1). NNRTIs interact with the NNRTI binding pocket of HIV-1 RT (see e.g. [99] for a comprehensive review). Through induced fit binding they cause both short-range and long-range distortions of the HIV-1 RT structure [346], which affect the polymerase as well as the RNase activity of RT [347]. NNRTIs looked initially promising as potential anti-HIV drugs; *in vitro* data showed low toxicity combined with high potency [348, 349]. However, from clinical trials of the prototype NNRTI, nevirapine, as monotherapy [350], extremely rapid selection of resistant virus meant that the utility of this drug class appeared rather limited [351]. However, with the introduction of multi-drug combination therapy, an important role for NNRTIs has been established [352]. NNRTIs are primarily metabolized through the CYP-P450 pathway. In addition, they act as either inhibitors or inducers of various CYP enzymes (see fig 3.7). Thus, drug interactions are expected when NNRTIs are co-administered with other medications (e.g. PIs), necessitating an evaluation of potential drug-drug interactions [353]. Today, the greatest potential of NNRTIs lies in their use as part of combination therapy. Trials consisting of an NRTI backbone and an NNRTI have the highest success rates [354]. This might be partly due to better adherence to NNRTIs, which in general have very long half-lifes and are thus suitable for once daily dosing. Also, NNRTIs have favorable toxicity profiles, compared with PIs and NRTIs. However, major issues with the use of NNRTIs are rapid emergence of class-wide resistance, which has partly been overcome by recent developments, possibly allowing to sequence NNRTIs [355].

NNRTIs are non-competitive inhibitors of RT with respect to the dNTP substrate. Although NNRTIs represent, in terms of chemical structures, a heterogeneous class of inhibitors, they all interact with HIV-1 RT by binding to a single site termed the NNRTI-binding pocket that is in close proximity to the RT DNA polymerase active site [356]. Comparison of unliganded and NNRTI bound RT structures showed that the NNRTI pocket is only created by the binding of the inhibitor itself. Through binding to RT, NNRTIs inhibit HIV-1 reverse transcription. A number of different mechanisms for NNRTI inhibition of RT have been proposed. The proposed mechanisms can be divided into two categories: (i) Mechanisms that result in a selective inhibition of particular functions during the overall process of reverse transcription (see fig. 2.3) and (ii) local, kinetic modifications of RT activity (see fig. 3.3). The first mechanism is related to global conformational distortions in the RT enzyme, while the later refers to local distortions in the polymerase active site.

Global effects. RT requires functional- and conformational flexibility to perform its different enzymatic functions during the process of reverse transcription. The first strand transfer reaction, for example, is an essential step in reverse transcription and requires the co–ordination of both the DNA–polymerase and RNase–activities of HIV-1 RT. In [357] it was shown that nevirapine alters the mobility of RT that is required to complete reverse transcription (including several strand transfer operations) [358]. Nevirapine was shown to lower the pace of overall enzymatic activity through inhibiting the conformational, –and thus functional–, flexibility of RT. Locally, NNRTIs may cause these effects by shifting functional equilibria of RT [359]. During strand transfer, it was suggested

that NNRTIs affect the enzyme's ability to bind the RNA PPT primer/DNA template (see fig. 2.3) in a polymerase-dependent mode [360], preventing the functional switch to RNAse-dependent binding and thus halting the overall process of reverse transcription.

Local effects. Nevirapine increases the (metal-dependent) binding affinity of dNTPs (up to 130–times), but also decreases the velocity of dNTP incorporation into the growing DNA chain [361]. The slow rate of dNTP incorporation observed for NNRTI–RT–template/primer is probably due to an indirect effect through alteration/perturbation of the constellation of amino acids involved in positioning the active site for efficient phosphodiester bond formation (catalysis) [362]. These results have also been independently confirmed by molecular dynamics simulations [363].

Other effects. Some NNRTIs such as efavirenz and etravirine (TMC 125) have been shown to inhibit the late stages of HIV-1 replication by interfering with HIV-1 Gag-Pol polyprotein processing. Efavirenz enhances the processing kinetics of Pol compared to untreated and nevirapine treated cells [364]. Efavirenz mediates a concentration dependent increase in Pol/Pol dimerization [365], promoting the interaction between individual Gag–Pol polyproteins. This leads to premature activation of the HIV-1 PR embedded within Gag-Pol (see section 2.4), and the subsequent cleavage of the precursor polypeptides. As a consequence, the amount of full-length viral polyproteins available for assembly and budding from the host cell membrane decreases. Therefore, this enhancement of polyprotein processing is associated with a decrease in viral particle production. However, this collateral efficacy might also increase the amount in intracellular HIV building blocks, manifestation of infection and multi-integration of viral DNA, especially in long-lived cells.

Resistance. Most NNRTI resistance mutations are located in the hydrophobic core of the NNRTI pocket, impairing the stability of NNRTIs in the pocket [3, 366]. Another way of inducing resistance to NNRTIs is by limiting NNRTI entry into the pocket by altering "surface" residues. Resistance to bulkier NNRTIs, such as delavirdine can occur through modification of peripheral aminoacids that form contacts with the NNRTI. Second generation NNRTIs, such as efavirenz and etravirine, have been specifically designed to be less prone to first generation NNRTI resistance mutations. This has been achieved by allowing the novel NNRTIs to rearrange within the binding pocket. Efavirenz and etravirine can bind the NNRTI binding pocket in different conformations, thus conferring residual inhibition of RT that is resistant to first generation NNRTIs [366].

Although HIV-2 RT shows significant amino acid sequence homology to HIV-1 RT, most NNRTIs are completely inactive against HIV-2 [345]. This lack of activity is primarily due to amino acid residues in HIV-2 RT which prevent the drugs from binding [367].

3.5.3 Integration Inhibitors: InI

Although HIV-1 integrase is known to influence several stages of the HIV-1 replication cycle, including reverse transcription, integration, and viral assembly [368], the enzyme's primary role is in integration, the process wherein the viral DNA is irreversibly inserted into the cellular DNA of the host. Integrase is required for each of the three events critical for integration: assembly with the viral DNA, 3' processing, and strand transfer (see fig. 2.4). In the context of HIV-1 replication, these events proceed in a stepwise manner, with the rate-limiting event being strand transfer.

Integration is absolutely required to stably maintain the viral DNA in the infected cell. In biological systems, blocking integration allows the viral DNA to be metabolized by cellular enzymes. Therefore, within the viral life cycle, InI provide the last chance of a cell to fend-off irreversible infection through genome integration. The targeted process (integration) occurs intracellular, or even in the nucleus of the cell.

Integrase inhibitors were initially identified by random chemical library screening at Merck [369, 370]. Integrase inhibitors bind to the catalytic site of the integrase enzyme [371]. They consist of two

domains: (i) the enzyme-binding domain and (ii) the catalytic triad-binding domain. The enzyme binding domain facilitates and potentially stabilizes inhibitor binding to the integrase enzyme, thereby allowing the catalytic triad domain to be presented to the catalytic triad [372]. Unlike competitive inhibitors that compete for substrate binding, integrase inhibitors are catalytic inhibitors. Accumulating evidence suggests that integrase inhibitors sequester metal ions from the active site and thereby inhibit enzymatic catalysis [370, 373–378]. Metal ions are crucial for integrase catalysis, because they provide the positive charge necessary to bind the negatively charged DNA.

Integrase inhibitors only bind with high affinity to integrase when the enzyme is in a specific complex with viral DNA [379]. The inhibitor-bound complex is not competent to bind the cellular or target DNA substrate (because the metal ion for DNA binding are missing), and the net result is selective inhibition of strand transfer.

Although most of the unintegrated viral DNA may be degraded, alternate metabolic pathways involving recombination- and repair produce circular DNA by-products (see fig. 3.6). The net result of either process is an irreversible block of HIV-1 replication. Circular DNA has become a defining feature of integrase strand transfer inhibitors, but was first noted with integration-defective viruses containing mutations in the integrase coding region [380, 381].

As integrase inhibitors bind only to the enzyme in complex with viral DNA [377,379], they are not involved until several hours after infection, when the process of reverse transcription is complete.

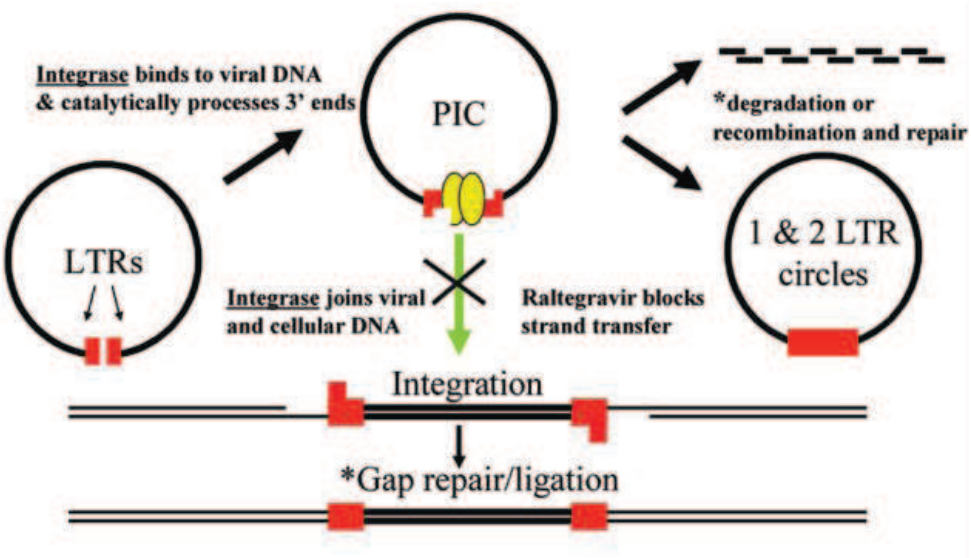

Figure 3.6: Mode of action of integrase (strand-transfer) inhibitors and mechanism of by-product synthesis

Raltegravir has been approved by the FDA in late 2007 as the first integrase inhibitor [382] (see table 3.1). It is mainly metabolized by glucoronidation and has thus little potential for drug-drug interaction with most of the approved anti-HIV drugs. Raltegravir has a moderate halflife of $\approx$ 9h and is recommended for twice daily dosing [383]. Little is known about the mechanism of resistance to raltegravir at this stage.

3.5.4 Protease Inhibitors: PI

HIV protease is an aspartyl-protease, that consists of two non-covalently bound identical subunits. The enzyme cleaves the Gag and Gag-Pol polyproteins of HIV at ten distinct sites (see fig. 2.6) and

is necessary for the maturation of the viral particles.

The importance of viral encoded protease was established around 1990 in *in vitro* studies that showed that the substitution or removal of amino acids in the HIV protease, by mutations- or deletions in the protease gene, eliminated the function of the HIV protease and resulted in the formation of non-infectious HIV particles [384, 385]. Further *in vitro* studies demonstrated that synthetic compounds could inhibit the HIV protease with similar results [386, 387]. Subsequently, HIV protease was targeted for pharmaceutical intervention.

Initial lead compounds for HIV-1 protease inhibitors were found within the pharmaceutical companies' libraries, which had been developed for another pharmaceutically interesting aspartyl protease, renin [388]. HIV protease cleaves amino acid sequences in Gag and Gag-Pol precursors (phenylalanine-proline and tyrosine-proline bonds), which are unusual sites of attack for mammalian aspartic proteases as well as other proteases [389]. The initial lead compounds, knowledge of the cleavage site sequences, a known catalytic mechanism and the ability to readily crystallize the protease with a bound inhibitor provided all the tools necessary for this successful and ongoing drug development effort [390].

In the life cycle of HIV, PIs prevent the production of infectious HIV, through suppression of Gag and Gag-Pol cleavage which inhibits the maturation of nascent HIV virions [391]. To be active against the HIV protease, PIs have to be located intracellularly, although the pharmacological effect is probably partly exerted in virions which have already been released from the cell [386].

Currently, there are nine protease inhibitors approved for treatment of HIV-1 infection (see table 3.1). Seven of these inhibitors (except Tipranavir and Darunavir) are peptido-mimetics [392], containing a variety of non-cleavable dipeptide analogues as core components. Peptido-mimetics are structurally similar to the intermediate that forms during cleavage of the targeted peptide bond of the natural substrate [392].

Effect. All available PIs act by binding to the catalytic site of the HIV protease and inhibit proteolytic processing of the natural substrate [393, 394]. The compounds mimic the transition state of substrate cleavage: PIs arrest the enzyme in a specific conformation, that is normally only transiently occupied to enable cleavage and is abandoned once cleavage has been accomplished. Although chemically different, many of the PIs have very closely overlapping structures and interactions, since they all target the same mechanism [388].

PIs are active against HIV-1 and -2 protease, but are inactive or weakly active against human aspartic proteases.

Development & **Evolution of PIs.** Saquinavir (SQV), ritonavir (RTV), indinavir (IDV), nelfinavir (NFV) and amprenavir (APV) are first generation PIs. Despite the success with these first generation PIs [393], early protease inhibitors have low bioavailabilities (4 % for SQV), short halflifes (range: 1.8 –5 h [393]) and very high plasma protein binding (see fig. 5.9). These pharmacokinetic characteristics lead to extremely high doses ($\geq$ 2000[mg] for e.g. SQV and IDV) and inconvenient dosing schedules (every 8 hours), resulting in collateral toxicity and poor adherence. Furthermore, there are dietary restrictions with some of the initial protease inhibitors and they have generally a low barrier to resistance (e.g [395–398]).

In the race to develop HIV-1 protease inhibitors, competing laboratories would co-crystallize compounds that their competitors patented in order to figure out alternative chemical scaffolds that would preserve the same contacts, but with better pharmacokinetics and bioavailability [388]. These efforts resulted in some of the second generation PIs (lopinavir (LPV), atazanavir (ATV), fosamprenavir (FPV)) that were mainly developed to overcome some of the pharmacokinetic issues of the first generation of PIs. Lopinavir has been co-formulated (LPV/RTV, discussed later) to improve the bioavailability, halflife and cellular penetration of LPV. FPV is a water-soluble prodrug of APV that has improved pharmacokinetics and no dietary restrictions. ATV has a very long halflife, allowing for

once daily dosing. It has been shown [399], that ATV has a distinct resistance profile relative to other PIs, with susceptibility maintained against 86% of isolates resistant to 1–2 PIs.

Third Generation PIs (tipranavir (TPV), and darunavir (DRV)) have been designed to further increase the genetic barrier to resistance and to maintain activity against other PI resistant strains.

In contrast to the previously approved PIs that are classified as peptido–mimetics, TPV was the first non-peptidic PI. *In vitro* studies demonstrated potent inhibition by TPV against clinical isolates resistant to multiple PIs. The molecular flexibility of TPV allows it to fit into the active site of protease, that has become resistant to other PIs [400, 401]. Phase II clinical trials have shown that as many as 16–20 mutations, including at least three PI resistance-associated mutations are needed to confer decreased susceptibility [400].

DRV is the second non-peptidic PI that has structural similarity to amprenavir [402]. DRV preserves its activity against protease by extremely tight binding to the enzymatic pocket [403]. The dissociative half-life of DRV is significantly greater and binding affinity of DRV is > 2 orders of magnitude higher vs. other PIs [404].

Pharmacokinetics and Potential Drug-Drug Interactions. Differences in the pharmacokinetic characteristics of PIs between patients are large [405] and are attributed to variability in binding proteins and polymorphisms in metabolizing enzymes and drug transporters.

The penetration of protease inhibitors into the central nervous system and testis is considered to be low [406], with only indinavir penetrating the blood–brain and blood-testis barrier in therapeutic concentrations [407–411].

Most protease inhibitors are metabolized, transported and bound by the same enzymes: (i) All PIs are metabolized with very high affinity by cytochrome (CYP) P–450 enzymes, mainly the 3A4 isoform [412–414]. CYP3A4 is present in the small intestine and contributes to the poor bioavailability of PIs, especially saquinavir [412]. Hepatic CYP3A4 contributes to the rapid elimination of PIs, but also displays significant inter-individual variability, which has been shown to be accentuated in HIV-infected patients.

(ii) Most PIs are also substrates of the P-glycoprotein (P-gp) efflux transporter system [415–419]. P-gp is an ATP-dependent drug-transporter located in the plasma membrane on the luminal (apical) side of various types of cells e.g. enterocytes, hepatocytes, renal tubular cells and the endothelial cells of the blood-testis and blood-brain barrier, but also $CD4^+$ cells [420, 421]. P-gp serves as a protective mechanism (efflux pump) against various compounds which the human body is exposed to, promoting intestinal, hepatobiliary and renal excretion of foreign compounds and preventing exposure of the testis and brain [422, 423].

Efflux by P-gp transporters is likely to be the main cause of poor blood-brain barrier penetration of most PIs [406]. The co-ordinated effect of CYP3A4 and P-gp has been shown to further enhance the removal of drugs that are substrates of both enzymes [424, 425].

(iii) All PIs except indinavir (61%) are highly protein-bound (see fig. 5.9) [405]. Plasma protein binding is primarily to α_1–acid glycoprotein, which occurs in low concentrations (concentration range: 15-170 mg/dl, median 79 mg/dl [426]).

As a consequence of the overlapping metabolism, transport and binding of PIs, the pharmacokinetic drug-drug interaction potential with PIs is considerable. Apart from being substrates for CYP isozymes, all PIs have effects on cytochrome P-450 enzymes, by acting as P–450 inhibitors or –inducers (see fig. 3.7). PIs, that are inhibitors of CYP3A4, exert mechanism-based inhibition, which involves inactivation of the enzyme by tight and irreversible binding of reactive metabolites that are formed as a result of the metabolism [427–431] (during longer eposure, RTV, NFV, APV and LPV can also

induce CYP3A4 [432, 433]). In *in vitro* studies, it has been shown that PIs are also P-glycoprotein inhibitors [416, 434, 435] (after prolonged exposure RTV, NFV, APV, LPV and ATV can also induce P-glycoprotein [420, 436, 437]). Ritonavir was shown to be the most potent inhibitor of CYP3A4 [413] and P-gp transport [417, 438–441].

Pharmacokinetic boosting. Most PIs have unfavorable pharmacokinetics, in terms of rapid elimination from the body. The rapid elimination of most PIs is contributed to CYP3A4 mediated metabolism and P-gp mediated efflux. Therefore, both the low bioavailability and the short halflife of PIs can be overcome by inactivating one- or both enzymes [442].

Because RTV is the most potent inhibitor of CYP3A4 and P-gp, the paradigm of PI-based therapies changed from using RTV as a single PI to "boosting" of other PIs with RTV to increase their halflifes and bioavailabilities [443]. By using RTV in low non-therapeutic doses (low-dose, 50-200 mg once or twice-a-day), it is possible to improve the pharmacokinetics of co-administered PIs, primarily by inhibition of intestinal- and hepatic CYP3A4 and P-gp [444,445]. "Ritonavir-boosting" has become the standard and maintains prolonged blood levels of the boosted PI, increases potency, decreases the required dosage, and minimizes PI side effects. In a similar fashion, RTV-boosting impacts the dosing requirements of other classes of antiviral agents, including the CCR5 co-receptor antagonist, Maraviroc.

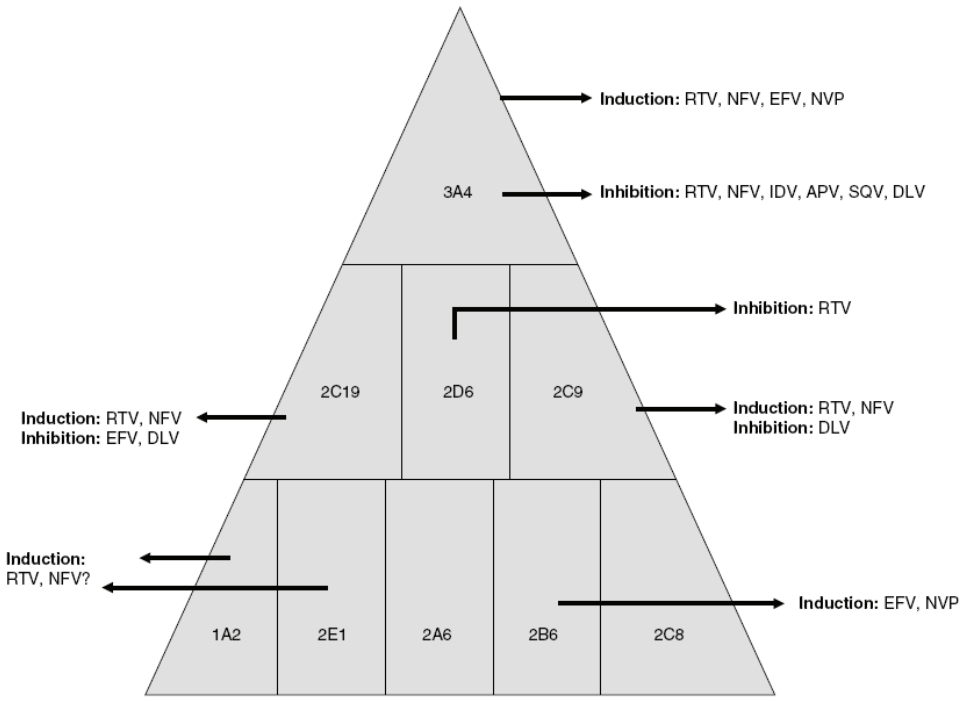

Figure 3.7: Impact of antivirals on CYP-P450 enzymes. Abbreviations: RTV = ritonavir, NFV = nelfinavir, IDV = indinavir, APV = amprenavir, SQV = saquinavir; EFV = efavirenz, NVP = nevirapine, DLV = delavirdine. Figure from [446].

Resistance. Nearly 70% of the 99 residues in HIV-1 protease are known to mutate [447–450]. The residues that are conserved appear to be primarily for enzymatic activity, or structural reasons (at the dimer interface, or for preserving flexibility) [388]. The extensiveness of the mutational patterns in both the enzyme and the substrates indicates that this is a very adaptable target.

Since all protease inhibitors are competitive active site inhibitors with the substrates, it is somewhat un-intuitive that resistance occurs without impacting substrate recognition. By comparing the

crystal structures of the substrate complexes with the crystal structures of the inhibitor complexes, it was found [451] that the inhibitors protrude from the "substrate envelope" at specific locations. The positions at which each inhibitor protrude away from the substrates and contact HIV-1 protease correspond very closely with the site of drug resistant mutations [452]. In fact, inhibitors that fit more tightly within the substrate envelope have a higher threshold for drug resistance [451].

Although some specific protease mutation sites are considered primary drug-resistant mutations, they usually occur in complex interdependent combinations with many other sites throughout the enzyme. In general, initial single amino acid mutations yield only a slight change (by less than a factor of 5) in drug sensitivity [453–456]. However, secondary mutations can lead to high-level drug resistance. Unlike the initial mutations, the secondary mutations overlap between different protease inhibitors [397, 457]. Prolonged treatment with one protease inhibitor can result in the emergence of virus with both primary- and secondary resistance mutations and might thus eliminate further PI treatment options.

Side-Effects. Protease inhibitors cause severe side-effects of which the mechanistic reasons are poorly understood. Lipodystrophy is one of the most common long-term class-wide toxicity of PIs [393]. Lipodystrophy is a fat redistribution with accumulation of neck and abdominal fat and is usually associated with loss of facial, buttocks, and extremity fat. It is resistant to treatment, often not reducing even with discontinuation of the offending agent. Some patients become unrecognizable from their pretreatment body habitus and facial features [458].

3.5.5 Investigational Drugs

Genome editing approaches. The finding that failure to express CCR5 is well-tolerated in individuals with this mutation, might allow the exploitation of modes of action on this target, that are not allosteric. This has led to the engagement in e.g. genome editing approaches. The compound SB-728-T of Sangamo BioSciences is a novel zinc-finger DNA-binding nuclease that permanently disrupts the CCR5 gene in $CD4^+$ T cells [459]. It has recently been approved for clinical phase I trials by the FDA [460]. While the virus eventually develops resistance to small molecules, this strategy aims to disrupt CCR5 viral entry permanently by modifying $CD4^+$ T cells. A recent publication [461], reporting that an HIV-infected patient treated with bone marrow from a CCR5-deficient donor had undetectable viral loads 20 months after transplantation, lends support to the notion that CCR5 depleted T cells may offer long-term protection against infection.

CXCR4 antagonists. Unlike CCR5, individuals with a natural loss of CXCR4 have not been identified yet. In mice, loss of natural CXCR4 function has been shown to be developmentally lethal, producing haematopoiesis and developmental defects in the cerebellum, heart and gastrointestinal tract [462–464]. Therefore, the freedom in the design of a CXCR4 modulator is far more restricted than for CCR5. In particular, CXCR4 modulators must be allosteric and permissive, blocking the function of this receptor as a mediator of X4 HIV virus entry (pathological effect) while preserving natural chemokine function [265].

CXCR4 antagonists have demonstrated anti-HIV activity in small clinical studies, although changes in the plasma concentration of CXCR4-tropic viruses have been inconsistent, with some subjects having no measurable response [465, 466].

Mutagenic nucleoside analogues. The high error rate of RT also has a detrimental effect on the virus. Most of the HIV virus particles found in infected blood are nonviable, most likely due to an accumulation of debilitating mutations. It has been proposed that the mutation rate could be artificially increased by the introduction of a mutagenic nucleoside [467, 468]. Mutagenic nucleotides are nucleotide analogs that incorporate randomly into HIV and pair with multiple bases. The increase in the mutation rate would lead the viral population to cross the threshold for error catastrophe and ablate the viral population as a whole [469].

The novel compound KP-1461 is the oral prodrug of the cytidine analogue KP-1212 [470]. KP-1212 is metabolized to a triphosphate and incorporated into the HIV-1 genome by RT. The drug is similarly incorporated into human mitochondrial DNA polymerase. The active substance KP-1212 has been shown to inhibit antiviral activity in tissues after just one pass; accumulation has been shown to eradicate the virus entirely. HIV strains treated with KP-1212 also showed increased sensitivity to NRTIs [470]. So far no toxicities have been reported, however, the nature of the mutagenicity raises concerns whether the drug might have long term genotoxic/cancerogenic effects in humans [243]

Maturation inhibitors Maturation Inhibitors (MI) inhibit maturation of nascent HIV virions, but unlike PIs they target the substrate of PR [214]. The processing of Gag is a highly ordered cascade of cleavages (see fig. 2.6), governed by differences in the inherent processing rates at each cleavage site [222,471]. The ordered processing suggests that a regulated cleavage cascade is needed for proper virion maturation and infectivity; mutations that either abrogate or alter the rate of cleavage of HIV Gag lead to the formation of aberrant, non-infectious particles [224, 472]. The slowest and last of the cleavages occurs within p25 between CA and the spacer peptide, p2 (see fig. 2.6). Maturation inhibitors shield the CA and the spacer peptide (p2) cleavage site [214], thus preventing the formation of a mature capsid and rendering the virus uninfective.

This unique specificity results in activity against PI-resistant HIV-1, while MI-resistant HIV-1 shows no cross-resistance with PIs.

The compound bevirimat of Panacos Pharmaceuticals showed very promising results and is currently in phase II clinical trials.

Virus Induction Therapy It is known that HIV infects cells (resting/quiescent T-cells) with a halflife of month or years [255, 473]. These cells, which originate from post-integration latency might get activated upon an external stimulus and start to produce virus. The decay of this reservoir is very slow and estimates for its eradication range from 8 [473] to 60 years [257].

Novel therapeutical strategies are under investigation to eliminate the reservoir of latently infected cells by viral induction therapy (see e.g. [474–477], summarized in [189]). Immune activation therapy aims at driving resting $CD4^+$ T cells out of latency.

Valproic acid (VPA) has been developed by Abbott Laboratories for viral induction therapy and is undergoing phase II clinical studies. VPA is a known chemical compound that has found clinical use as a spasm releasing- and mood-stabilizing drug, primarily in the treatment of epilepsy, bipolar disorder, migraine, schizophrenia and less commonly major depression. Valproic acid is a histone de-acetylase inhibitor and might therefore activate latently infected cells, if the main cause for latency is a restricting chromatin structure.

Results from clinical phase I studies have shown a reduction in latently infected $CD4^+$ T-cells in a subgroup of the patients [478]. The mechanistic reasons are unclear why VPA is successful in some patients and not in others. However, elimination of the latent reservoir can only be successful in combination with a potent antiviral regimen that prevents replenishment of the latent reservoir [479, 480], which has been strongly violated in some unsuccessful trials [481].

Biological Response Modifier. The compound Ampligen (Poly(I)-poly(C12U)) from Hemispherx Biopharma is an immunomodulatory double stranded RNA drug, that has completed clinical phase II trials. It induces human immune defenses against viruses and tumors by stimulating interferon production. Cells normally encounter double-stranded RNA molecules like Ampligen during infection with RNA viruses. The Toll-like receptor 3 (TLR3) on the cell surface detects pathogens, long before adaptive immunity can intervene against foreign invaders. This response therefore serves as a first line of immunological defense against a broad range of pathogens [482]. When TLR3 senses a double stranded RNA, it releases a message to the cell to produce interferon. Interferon alerts other

cells that an infection is present and produces a series of responses in nearby cells and the interferon-producing cell. One response is the stimulation of the RNase L (Ribonuclease, latent). This protein degrades viral RNA and can thus fend–off viral infection, or production of viral mRNA. RNase L can also degrade the cell's own RNA, leading to the apoptosis of virally compromised cells.

In clinical trials Ampligen was shown to be synergistic with most antivirals [483].

3.6 Summary and Perspective

Currently, the main goal in HIV treatment is to reduce AIDS-related morbidity. The goal of HIV eradication is currently not envisaged, because HIV seems to persist in long-lived reservoirs that prevent eradication. Treatment success is defined in terms of plasma viral load suppression and virological failure is defined in terms of not achieving one the endpoints. However, durable suppression of the virus is commonly not achieved, as a result of resistance development. The mutagenicity of HIV can lead to drug-class wide resistance. Drug resistance to established drugs is the driving principle behind the ongoing development of anti-HIV compounds. To overcome cross-resistance, new viral targets are being explored and established ones are targeted with novel mechanisms. Overall, HIV drug development is continuing and dynamic.

In this section, we have provided a comprehensive overview of all approved anti-HIV drugs. Each drug-class has its inherent advantages and disadvantages. FIs and CCR5-antagonists, for example, have the advantage that they exert their effect in the blood plasma. However, the target of FIs is only transiently exposed. CCR5-antagonists are only active against CCR5-tropic virus and have a unfavorable drug-target stoichiometry. NRTIs require intracellular activation, however, each molecule has many opportunities to interfere with the process of reverse transcription. NRTIs cause severe side-effects, leading to a narrow therapeutic window. NNRTI have very favorable characteristics in terms of pharmacokinetics and low toxicities. However, pharmacokinetic interactions with PIs limit their combined use. Furthermore, they have a small barrier to class-wide resistance. InIs target the last remaining enzyme of HIV. Little is known at this stage about toxicities or general barriers to resistance. However, in clinical trials, InIs produced a unique (rapid) viral decay (e.g. [484]), which has been subject to controversial discussion. PIs are very promising and potent inhibitors of HIV. They have an enormous drug-drug interactions potential, and generally poor pharmacokinetics, that can partly be overcome by co-formulation with ritonavir (RTV). A severe side-effect that is connected with the prolonged use of PIs is the development of lipodystrophy.

Drug-class wide resistance in a growing population of treatment-experienced patients has urged the regulatory agencies to make drug resistance data become an integral part of the approval process of a novel compound [485]. In this context, an antiviral with a novel resistance profile can become a life-saving entity that will be granted a priority review and an accelerated approval [485]. As a consequence, HIV drug development moves into a direction where the uniqueness of the drug's resistance pathway becomes a key criteria. Therefore, as already observed in recent years, novel drug targets will be explored and established targets will be targeted in a way that results in minimal overlap with existing drugs, in terms of resistance development. These efforts result in a growing repertoire of antivirals with orthogonal resistance profiles. While these efforts are primarily followed with the aim of treating (treatment-) experienced patients, we will in the next section make use of these recent developments in order to increase the likelihood of achieving treatment success.

3.7 Glossary: Basic Pharmacokinetic Terms

bioavailability: denotes the fraction of the dose that reaches the systemic (blood) circulation after oral administration.
halflife: the time when the drug concentration is halved in the blood plasma (assumes linear elimination).
plasma binding: Some fraction of the circulating drug might be bound to blood (plasma) proteins. Only the unbound fraction of the drug is available for penetration into cells, or for exerting effect. The most important blood (plasma) proteins are α_1-acidic glycoprotein and albumin. Albumin concentrations are very high (≈ 600 [μM]), while α_1-acidic glycoprotein concentrations are much lower (≈ 70 [μM]).
metabolism: Drugs are usually chemically modified by cellular enzymes to enable their excretion. Chemical modification usually also inactivates the drugs. The cytochrome P450 (CYP) -superfamily of enzymes catabolizes a broad spectrum of drugs (for HIV: PIs, NNRTIs, CCR5-A). CYPs are mainly located in the liver, but also in the intestine. The family of UDP-glucuronosyltransferases catabolize many drugs by glucuronidation (for HIV: NRTIs, the InI raltegravir). These enzymes are located mainly in the liver, but also the heart, kidneys, adrenal gland, spleen, and thymus.
transport: Cells express many transporters on their cellular membrane. Some of these transporters, like the P-glycoprotein (P-gp) are efflux transporters with a broad substrate spectrum, that aim at shielding body compartments from potential toxigens. These transporters are specifically expressed in the blood-brain-barrier and the blood-testis-barrier and at the apical membrane of the gut wall. P-gp are important for shuttling lipophilic substances (like, e.g. PIs) out of the cell. Nucleosides cannot pass into cells by passive diffusion, because they are too hydrophilic. The cell provides a number of transporters that can shuttle nucleosides. The family of concentrative nucleoside transporters (CNT) in- or effluxes nucleosides from the cell. Equilibrative nucleoside transporters (ENT) aim at eliminating the concentration gradient between the extra- and the intracellular space of the cell. CNTs and ENTs are required for NRTIs to enter cells.
BBB, BTS: The vascular epithelium is usually fenestrated, allowing small molecules and nutrients to pass from the blood to the extracellular space of tissues. However, this is not the case in the brain and the testis. These two tissues are especially protected by a solid vascular epithelium (the blood-brain-barrier BBB and the blood-testis-barrier BTB), that contains many transporters that strictly regulate which substances can pass into the tissue. Because of the selectivity of traffic into the brain and testis, they are likely to be sanctuary sites for pharmaceutics.

Part II

Mathematical Models of HIV

Chapter 4

HIV dynamics, Mutation and Impact of Drug treatment

If a patient with chronic HIV infection (asymptomatic stage) is repeatedly sampled and the viral load in the blood is measured, the viral load generally remains unchanged (see e.g. fig. 1.1). This could suggest that the rate of HIV replication is very slow. However, during studies with first protease inhibitors, the plasma level of HIV-1 RNA was observed to drop by one to two orders of magnitude during the first 2 weeks of therapy [11, 13, 486]. Since the levels of virus remain constant [487] in patients with chronic viral infection, the body must be producing and clearing virus at the same rate. This, as well as earlier observations, indicated that the virus might be replicating rapidly. However, in order to gain information on rates of viral production and clearance, the system has to be perturbed. For example, if virus production is fully blocked, then the viral load will fall and the rate at which it falls is the viral clearance rate. If production is not fully blocked, then the rate of viral-load decline will depend not only on the virion-clearance rate, but also on the rate of death of virus-producing cells and the efficacy of the drug being used to block viral production [488]. By fitting the kinetics of viral decay to mathematical models, the kinetic parameters governing viral infection and cell death can be revealed (see e.g. [11]). In this context, models were developed, that quantitatively describe

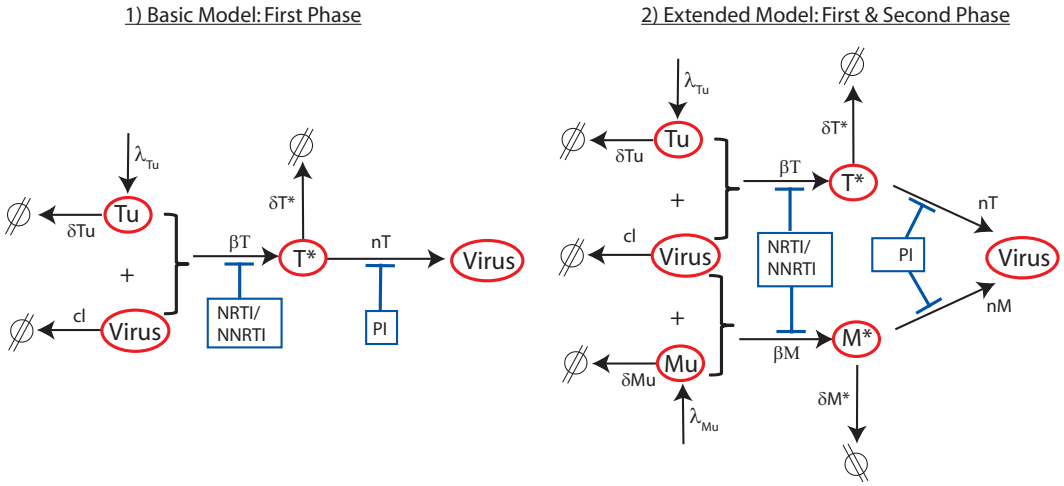

Figure 4.1: Existing Models that can describe the two phases of viral decay.

virus dynamics and improve our understanding of the timescales of virus dynamics.

4.1 Basic Viral Dynamics Models

The basic HIV-model considers a set of cells susceptible to infection, TU , which, through interactions with virus, V, become infected (rate β_{T}). Infected cells, T^*, are each assumed to produce new virus particles at a constant average rate $\mathrm{N}_{\mathrm{T}^*}$ and to die at rate δ_{T^*} per cell. In HIV infection, death might involve viral cytopathic effects or immune-mediated cellular destruction. Newly produced virus particles, V, can either infect new cells or be cleared from the body at rate CL per virion. This most simple model is shown in fig. 4.1 (left). The corresponding differential equations are shown below.

$$\begin{aligned} \frac{\mathrm{d}}{\mathrm{d}t}\mathrm{TU} &= \lambda_{\mathrm{TU}} - \beta_{\mathrm{T}} \cdot \mathrm{V} \cdot \mathrm{TU} - \mathrm{TU} \cdot \delta_{\mathrm{TU}} \\ \frac{\mathrm{d}}{\mathrm{d}t}\mathrm{T}^* &= \beta_{\mathrm{T}} \cdot \mathrm{V} \cdot \mathrm{TU} - \mathrm{T}^* \cdot \delta_{\mathrm{T}^*} \\ \frac{\mathrm{d}}{\mathrm{d}t}\mathrm{V} &= \mathrm{N}_{\mathrm{T}^*} \cdot \mathrm{T}^* - \mathrm{V} \cdot \mathrm{CL}, \end{aligned} \tag{4.1}$$

where λ_{TU} and δ_{TU} are the production and death rate of healthy susceptible cells [489].

In the presence of a 100% effective protease inhibitor, infectious virus production is inhibited ($\mathrm{N}_{\mathrm{T}^*} = 0$), and infectious virus should decay exponentially with slope CL. Measuring the rate of loss of viral infectivity was used by Perelson et al. [488] (see fig. 4.1, B) to determine CL. In some patients, infectivity decayed too rapidly to quantify. Therefore, another approach, called 'apheresis' (fig. 4.1, A) was used to estimate CL in the blood plasma [490]. This approach confirmed that HIV was cleared rapidly, with an average value of 23 per day [490].

The parameter estimates made in [488, 490] suggest that a minimum of 10^{10} virions is produced daily [488].

In [491] it was shown that not all six parameters in the model can be identified if only the viral load is measured. Instead only four parameters and the product of two parameters ($\mathrm{N}_{\mathrm{T}^*}$ and λ_{TU}) are identifiable. However, utilizing known initial values of the unobservable state variables can help to identify more parameters [491].

When three or more drugs are given to HIV-infected patients, plasma virus decays with an initial rapid exponential decline (first phase), followed by a slower exponential decline (second phase) that leads to the virus falling below levels of detection (see eg. fig. 1.4). To interpret the two-phase decline, a new model was introduced [12], which postulated that the second phase was due to sources of HIV-1 not included in the basic model (see fig. 4.1, right).

$$\begin{aligned} \frac{\mathrm{d}}{\mathrm{d}t}\mathrm{TU} &= \lambda_{\mathrm{TU}} - \beta_{\mathrm{T}} \cdot \mathrm{V} \cdot \mathrm{TU} - \mathrm{TU} \cdot \delta_{\mathrm{TU}} \\ \frac{\mathrm{d}}{\mathrm{d}t}\mathrm{T}^* &= \beta_{\mathrm{T}} \cdot \mathrm{V} \cdot \mathrm{TU} - \mathrm{T}^* \cdot \delta_{\mathrm{T}^*} \\ \frac{\mathrm{d}}{\mathrm{d}t}\mathrm{MU} &= \lambda_{\mathrm{MU}} - \beta_{\mathrm{M}} \cdot \mathrm{V} \cdot \mathrm{MU} - \mathrm{MU} \cdot \delta_{\mathrm{MU}} \\ \frac{\mathrm{d}}{\mathrm{d}t}\mathrm{M}^* &= \beta_{\mathrm{M}} \cdot \mathrm{V} \cdot \mathrm{MU} - \mathrm{M}^* \cdot \delta_{\mathrm{M}^*} \\ \frac{\mathrm{d}}{\mathrm{d}t}\mathrm{V} &= \mathrm{N}_{\mathrm{T}^*} \cdot \mathrm{T}^* + \mathrm{N}_{\mathrm{M}^*} \cdot \mathrm{M}^* - \mathrm{V} \cdot \mathrm{CL} \end{aligned} \tag{4.2}$$

where λ_{MU}, δ_{MU} and β_{M} are the production-, death- and infection rates of healthy M-cells and $\mathrm{N}_{\mathrm{M}^*}$ is the rate of virus production from M^* cells. Candidates were a longer-lived population of productively infected cells (e.g. infected macrophages), while the initial rapid decay was attributed to infected, activated T-cells.
A weakness of all the presented models so far (eqs. (4.1)-(4.3)) is the assumption that drugs block a viral process by 100 %. For example, when the virus clearance CL was estimated [11], it was assumed

that the protease inhibitors completely blocks the production of new virus. Drug concentrations, however, fluctuate and drugs distribute heterogeneously into different body compartments. Therefore, more elaborated models of drug efficacy are needed to elucidate the trade-off between residual replication under treatment and actual viral clearance by the immune system. We will present some approaches in section 4.2.1 and in part III.
Another point to consider is, that even if an inhibitor is 100 % effective against the wildtype virus, a resistant mutant will, after some time, be selected from the virus population, rendering the efficacy of the drug and altering the viral decay. This emphasizes, that viral mutation also has to be considered, in order to temporally resolve the decay characteristics of the virus.
On a) short time scales, however, if the b) majority of the virus is susceptible to the drug and the c) efficacy of the drug is close to 100 %, parameter estimations from simplified models such as eqs. (4.1)-(4.2) might be close to the the actual removal rates of virus and -infected compartments. On longer time scales, it can be expected that resistance development and residual influx from pharmacological sanctuaries alters the observed viral decay, even if the drugs were 100 % effective against the wildtype in the majority of HIV compartments. Therefore, estimates on second- and third phase decay of the virus may contain a lot of factors that are not considered by the models, resulting ultimately in the underestimation of the decay rates for these phases [11].
Resting $CD4^+$ memory T cells were identified as a long-lived latent reservoir [492], and their mean

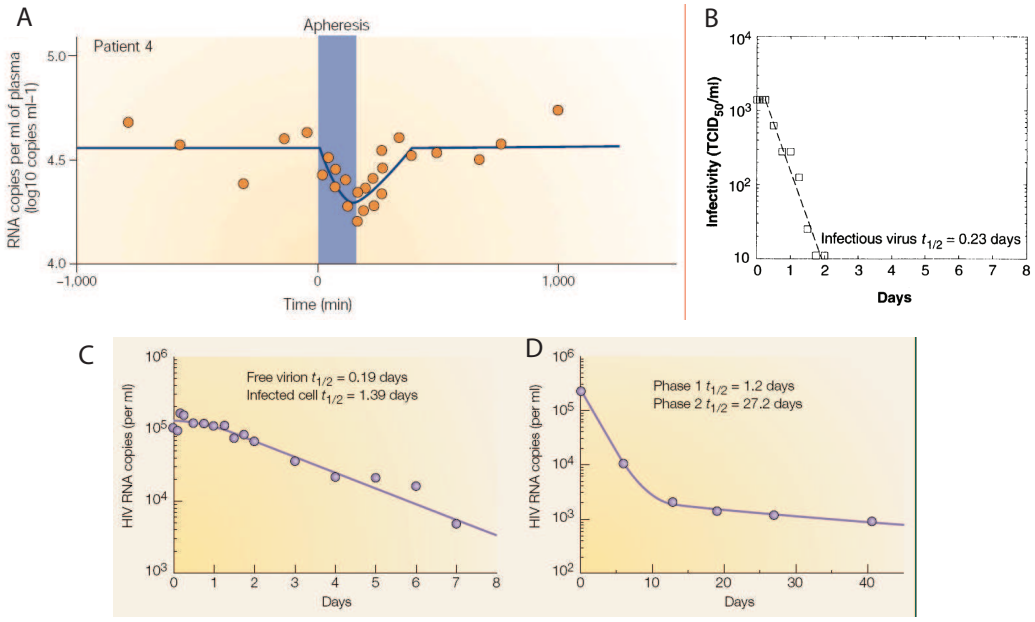

Figure 4.2: The three phases of HIV dynamics after treatment. Picture A taken from [27], picture B taken from [11] and pictures C and D taken from [488]

half-life was estimated in different studies as being as short as 6 months [492] or as long as 43.9 months [257]. Even though these estimates largely diverge, indicating un-identifiability of the decay, it has been shown, that resting CD^+-cells constitute an inducible reservoir in HIV-infected patients [115, 255, 256]. In either event, latently infected cells are decaying extremely slowly, possibly comprising a third phase of viral decay. However, despite the already mentioned reasons, it is difficult to accurately determine the decay of this reservoir, because, (i) using standard methods, this decay is not visible, (ii) data points using ultra-sensitive assays are very prone to errors e.g. [257] and (iii) current therapy does not seem to be 100% effective [61, 492–494]; in which case replenishment of this reservoir could occur as a result of low-level ongoing replication [495].
Many models, however, consider a pool of latently infected cells and National Institute of Health (NIH) bases its current treatment guidelines on the existence of this reservoir. In the basic model [11, 496] (see. eq. 4.3), $CD4^+$ -cells enter an activated- (T^*) or latent stage (L) upon infection with probabilities q_1 and q_2 respectively. $CD4^+$ cells might also obtain a defective provirus D with probability q_3.

Latently infected cells can become reactivated and turn into virus producing cells T^* with some rate α.

$$\begin{aligned}
\frac{d}{dt}TU &= \lambda_{TU} - \beta_T \cdot V \cdot TU - TU \cdot \delta_{TU} \\
\frac{d}{dt}T^* &= q_1 \cdot \beta_T \cdot V \cdot TU - T^* \cdot \delta_{T^*} + \alpha \cdot L \\
\frac{d}{dt}L &= q_2 \cdot \beta_T \cdot V \cdot TU - L \cdot \delta_L - \alpha \cdot L \\
\frac{d}{dt}D &= q_3 \cdot \beta_T \cdot V \cdot TU - D \cdot \delta_D \\
\frac{d}{dt}MU &= \lambda_{MU} - \beta_M \cdot V \cdot MU - MU \cdot \delta_{MU} \\
\frac{d}{dt}M^* &= \beta_M \cdot V \cdot MU - M^* \cdot \delta_{M^*} \\
\frac{d}{dt}V &= N_{T^*} \cdot T^* + N_{M^*} \cdot M^* - V \cdot CL
\end{aligned} \tag{4.3}$$

Antivirals have an impact on the viral parameters (that is β and N in eq. (4.1)). We will present models of drug efficacy in section 4.2.1 and part III. However, let us consider the following first: Since antiviral drugs have an impact on the viral parameters, the ability to model the drug's effect (mechanistically) depends on whether the inhibited process is reflected in the virus model. Eqs. (4.1)-(4.3) for example are very practical in terms of parameter estimation, however none of these models can reproduce the effect of e.g. an integrase inhibitor accurately, because the process of integration is not considered. Furthermore, no distinction can be made between entry inhibitors (FI and CCR5-antagionists) and reverse transcriptase inhibitors (NRTI and NNRTI), because infection is represented by a single parameter β. However, entry inhibitors block infection extracellular, before irreversible fusion, while reverse transcriptase inhibitors alter infection after irreversible fusion (thus contributing to the clearance of free virus).

As an example, the recent introduction of integrase inhibitors [383] lead to a novel characteristic viral decay [484]. An analysis based on the established models, e.g eqs. (4.1)-(4.3) lead to wild speculations of how such a decay can be achieved [497] and what decay can be expected in the third phase. The most simple explanation for the characteristic viral decay with integrase inhibitors, however, can be achieved by extending the established model (e.g. eq. (4.2)), explicitly incorporating the step of integration [498, 499]. The observable decay is then explained on the basis of the inhibited stage of the viral life cycle. In other words: based on the decay of the different types of infected cells (prior to genomic integration: T_1, M_1 and after integration: T_2, M_2).

To study the consequences of drug-class specific interference with the viral life cycle, we will initially propose a detailed model of host cell and viral dynamics (depicted in fig. 4.3). The detailed model explicitly accounts for the transitions between the different viral stages that are targeted by currently approved antiretrovirals and by antiretrovirals that are in late clinical development. In the following we will mechanistically simplify the detailed model, which allows the parametrization of the model and preserves the mechanistic detail, by which we model antiviral treatment.

4.2 Detailed Viral Life Cycle Model.

We propose the detailed virus-target cell interaction model depicted in Fig. 4.3 to allow for a mechanistic integration of the action of all anti-retroviral drugs that are approved for HIV treatment or in late clinical trials.

In summary, an infectious virus V_I reversibly binds (with effective rate constants k_{on} and k_{off}) to a target cell TU, forming a complex $V_I : TU$. After binding, the virus irreversibly fuses (with rate

constant k_{fus}) with the target cell and the viral capsid containing the viral genomic RNA is released; this state is denoted by $\mathrm{T_{RNA}}$. During reverse transcription (with effective rate constant k_{rev}), genomic viral RNA is irreversibly transformed into a more stable DNA. Viral DNA and viral proteins form the pre-integration complex (PIC), denoted by $\mathrm{T_1}$. In the next step, viral DNA of the PIC is irreversibly integrated into the DNA of the target cell, forming the provirus $\mathrm{T_2}$. After integration, the infected cell cannot return to an uninfected stage. From the proviral DNA, viral proteins are amplified and new viruses are released (with effective rate constant $\widehat{\mathrm{N}}_{\mathrm{T}}$). Only a given percentage $p > 0$ of the released viruses are correctly assembled premature viruses $\mathrm{V_{IM}}$, while the remaining percentage $(1 - p)$ are defective virions $\mathrm{V_D}$. During the final step, the viral protease, which is packed into the virions, is responsible for the maturation of the virus. A proportion $(1 - q)$ of the released virus maturates abnormally, contributing to the pool of defective virions $\mathrm{V_D}$. Successful maturation eventually leads to new infectious virus particles $\mathrm{V_I}$ (with rate constant k_{mat} and probability q).

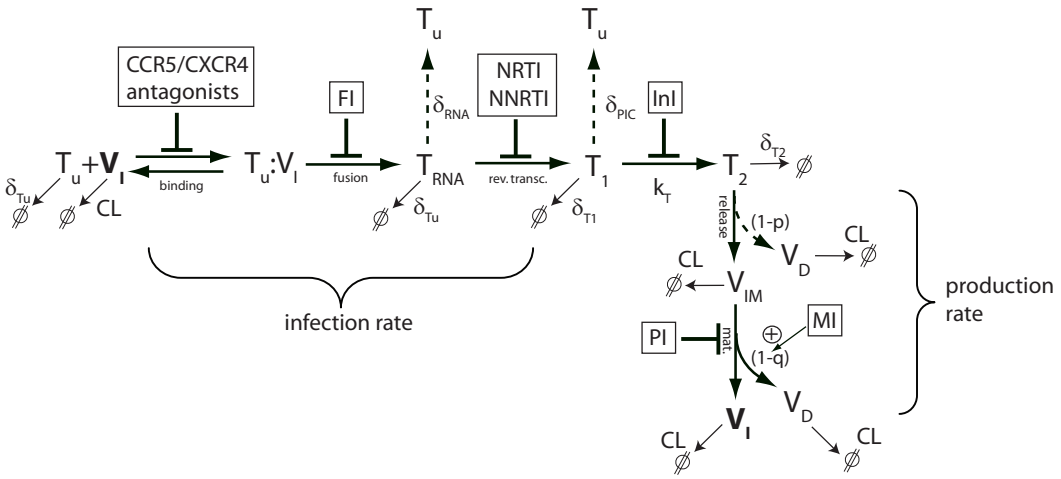

Figure 4.3: Highlighting the the distinct steps in the life cycle of HIV and the mechanistic basis of inhibition by antivirals.

Depending on the stage of the life cycle, the host organism has different abilities to clear the virus. It was assumed that infectious, premature and non-infectious virions $\mathrm{V_I}$, $\mathrm{V_{IM}}$, and $\mathrm{V_{NI}}$, respectively, are cleared with rate constant CL by the host. The uninfected target cell TU, the $\mathrm{T_{RNA}}$ stage and the early infected stage $\mathrm{T_1}$ are assumed to be cleared with rate constant δ_{TU}, since none of these stages express viral proteins, while the provirus $\mathrm{T_2}$ is assumed to be cleared with rate constant $\delta_{\mathrm{T2}} \gg \delta_{\mathrm{TU}}$. In addition to cell death, the target cell may fend-off the viral infection by degrading the viral RNA or the PIC, rendering the cell uninfected. RNA is very unstable with a half life ranging from seconds to a maximum of two hours [500, 501]. Therefore, through degradation or by hypermutation through APOBEC3G, the viral RNA can be cleared with rate constant δ_{RNA}. The cell might also destroy essential components of the PIC (with rate constant δ_{PIC}) to clear the virus.

The system of ODEs describing the rate of change of the different viral species and target cells in the detailed model (depicted in Fig. 4.3), is given below. As typically done in kinetic studies, complex aspects of the viral dynamics are subsumed by lumped parameters in the model. For instance, the rate constant of the reverse transcription k_{rev} contains all the steps necessary to transform the viral RNA into a double stranded DNA.

The model in fig. 4.3 involves all steps, which are currently targeted by anti-HIV drugs. Therefore, it allows us to incorporate the action of antiretroviral drugs explicitly. The rate of change in the detailed model of the viral life cycle is specified by the following system of ordinary differential

equations (ODEs):

$$\begin{aligned}
\frac{\mathrm{d}}{\mathrm{d}t}\mathrm{TU} &= \lambda - k_{\mathrm{on}}\mathrm{TU}\cdot\mathrm{V_I} + k_{\mathrm{off}}[\mathrm{V_I}:\mathrm{TU}] \\
&\quad +\delta_{\mathrm{RNA}}\cdot\mathrm{T_{RNA}} + \delta_{\mathrm{PIC}}\cdot\mathrm{T_1} - \delta_{\mathrm{TU}}\cdot\mathrm{TU} && (4.4)\\
\frac{\mathrm{d}}{\mathrm{d}t}[\mathrm{V_I}:\mathrm{TU}] &= k_{\mathrm{on}}\mathrm{TU}\cdot\mathrm{V_I} - k_{\mathrm{off}}[\mathrm{V_I}:\mathrm{TU}] - k_{\mathrm{fus}}[\mathrm{V_I}:\mathrm{TU}] && (4.5)\\
\frac{\mathrm{d}}{\mathrm{d}t}\mathrm{T_{RNA}} &= k_{\mathrm{fus}}\cdot[\mathrm{V_I}:\mathrm{TU}] - (\delta_{\mathrm{TU}}+\delta_{\mathrm{RNA}}+k_{\mathrm{rev}})\mathrm{T_{RNA}} && (4.6)\\
\frac{\mathrm{d}}{\mathrm{d}t}\mathrm{T_1} &= k_{\mathrm{rev}}\cdot\mathrm{T_{RNA}} - (\delta_{\mathrm{TU}}+\delta_{\mathrm{PIC}}+k_{\mathrm{T}})\mathrm{T_1} && (4.7)\\
\frac{\mathrm{d}}{\mathrm{d}t}\mathrm{T_2} &= k_{\mathrm{T}}\cdot\mathrm{T_1} - \delta_{\mathrm{T_2}}\cdot\mathrm{T_2} && (4.8)\\
\frac{\mathrm{d}}{\mathrm{d}t}\mathrm{V_{IM}} &= p\cdot\widehat{\mathrm{N_T}}\cdot\mathrm{T_2} - (\mathrm{CL}+k_{\mathrm{mat}})\mathrm{V_{IM}} && (4.9)\\
\frac{\mathrm{d}}{\mathrm{d}t}\mathrm{V_D} &= (1-p)\cdot\widehat{\mathrm{N_T}}\cdot\mathrm{T_2} + (1-q)\cdot k_{\mathrm{mat}}\cdot\mathrm{V_{IM}} - \mathrm{CL}\cdot\mathrm{V_D} && (4.10)\\
\frac{\mathrm{d}}{\mathrm{d}t}\mathrm{V_I} &= q\cdot k_{\mathrm{mat}}\cdot\mathrm{V_{IM}} - \mathrm{CL}\cdot\mathrm{V_I} - k_{\mathrm{on}}\mathrm{TU}\cdot\mathrm{V_I} + k_{\mathrm{off}}[\mathrm{V_I}:\mathrm{TU}]. && (4.11)
\end{aligned}$$

where k_{fus}, r_{rev}, k_{T} and k_{mat} are the fusion-, reverse transcription-, integration- and maturation rates. The probability p denotes which proportion of the released particle has all building blocks for being infective. The death rates of uninfected cells, intracellular genomic viral RNA, the pre-integration complex, infected cells with integrated proviral DNA and free virus are denoted by δ_{TU}, δ_{RNA}, δ_{PIC}, $\delta_{\mathrm{T_2}}$ and CL respectively. It was assumed that cells, that do not express viral proteins ($\mathrm{T_{RNA}}$, $\mathrm{T_1}$) are cleared at the same rate as uninfected cells. Furthermore, it was assumed that free virus of any kind is cleared with the same rate CL.

We have simulated infection with HIV, based on the model above (eq. (4.4)-(4.11)). The simulation results are shown in fig. 4.4 (left, starting with $\lambda/\delta_{\mathrm{T}}$ target cells and 100 viral particles). The infective compartments arrange according to the parameter choices. Under the parameters chosen, the infected state is asymptotically stable. The virus load ($V_{\mathrm{tot}} = [\mathrm{V_I}:\mathrm{TU}] + \mathrm{V_{IM}} + \mathrm{V_I} + \mathrm{V_D}$) initially overshoots and then sets to a stable level. The viral load is limited by the availability of target cells in the model. In fig. 4.4 (right) we show the ratio of total infective virus ($\mathrm{V_I} + [\mathrm{V_I}:\mathrm{TU}]$)-to-total virus ($\mathrm{V_{tot}}$). As the number of target cells decreases, less infectious virus is cleared through the cells (either by successful, or unsuccessful infection).

The presented model is able to describe infection and the asymptomatic phase of HIV infection. However, like all other presented models (eqs. (4.1)-(4.3)) is not able to model the evolution of disease, which involves the final rise in virus load and the decline in $\mathrm{CD4^+}$-cells (see fig. 1.1). For the purposes analyzed here, however, it is sufficient, because we are interested in the effects of drugs on the viral dynamics and to a lesser extend on the immune system dynamics.

4.2.1 Mechanism of Inhibition of Antivirals

The mechanism of action of the seven drug classes is based on interfering with the viral life cycle at the different stages. We assume that the effect of a drug on the targeted process is specified by some parameter $\varepsilon(t) \in [0,1]$.

$$(1-\varepsilon) = \left(1+\frac{C}{\mathrm{IC_{50}}}\right)^{-1} \qquad \text{(conc. dependent efficacy)} \qquad (4.12)$$

assuming some underlying averaged drug concentration $C = \widehat{C}$, see e.g. [20]. It is possible to also use time-varying drug concentration $C = C(t)$ resulting from some pharmacokinetic model, or to use more mechanistic effects models [21, 145].

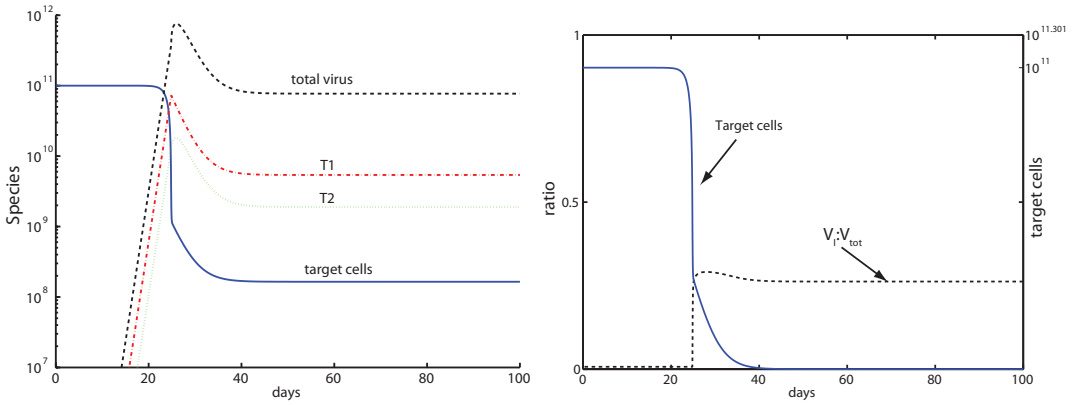

Figure 4.4: Left: Illustrative Example of the distribution of sub-species after infection. Right: ratio of infective virus-to-total virus (dashed black line) and abundance of uninfected T-cells (solid blue line). Arbitrary parameters used for simulation: $\mathrm{CL} = 23, \delta_\mathrm{T} = 0.02, \mathrm{N} = 1000, k_\mathrm{T} = 0.35, \delta_\mathrm{PIC} = 0.35, \lambda = 2 \cdot 10^9, \mathrm{K_D} = 1000, k_\mathrm{off} = 10^6, \delta_\mathrm{RNA} = 1440, r_\mathrm{fusion} = 1440, r_\mathrm{RT} = 48, r_\mathrm{InI} = 0.35, r_\mathrm{mat} = 12,\ q = 0.9$

The action of the different drug classes within the viral life cycle is shown in Fig. 4.3. CCR5 antagonist inhibit the association of HIV with the CCR5 receptor in CCR5-tropic virus. They thus affect the association constant k_on. Fusion inhibitors inhibit the process of HIV fusion k_fus. Activated NRTIs compete with endogenous deoxynucleoside triphosphates for prolongation of the growing DNA chain, while NNRTIs allosterically inhibit the function of the reverse transcriptase. The effect of both drugs results in a reduced rate at which the RNA is reversely transcribed into DNA. Integration inhibitors affect the integration of viral DNA into the host genome catalytically [370,376–378]. In the proposed model, this alters the transition rate k_T from early infected cells $\mathrm{T_1}$ to the lately infected cells $\mathrm{T_2}$. Protease inhibitors interfere with the functionality of the protease enzyme that mediates the transition of immature virus $\mathrm{V_{IM}}$ to infective virus $\mathrm{V_I}$. Finally, the novel class of maturation inhibitors perturb the ordered sequence of cleavages, decreasing the probability q that immature virus maturates normally, creating abnormally maturated, defective virus $\mathrm{V_D}$.

4.2.2 Effect of Antivirals on Different HIV-Subpopulations

We used the detailed virus-target cell interaction model to predict the effect of the different drug classes on the distinct stages of the viral infection cycle. In order to enable the direct comparison between the different drug classes, we artificially kept the uninfected target cell $\mathrm{TU_0}$ and the infective virions $\mathrm{V_{I,0}}$ constant, resulting in 'downstream' quasi-steady state numbers $\mathrm{T_{1,}}_{ss}$, $\mathrm{T_{2,}}_{ss}$, $\mathrm{V_{IM,ss}}$, $\mathrm{V_{I,ss}}$, and $\mathrm{V_{D,ss}}$. For a given drug (class) and local efficacy ε, the effect of the drug on the infection cycle was quantified by the four ratios

$$\frac{\mathrm{T_{1,}}_{ss}}{\mathrm{TU_0}}, \quad \frac{\mathrm{T_{2,}}_{ss}}{\mathrm{T_1}_{ss}}, \quad \frac{\mathrm{V_{I,ss}}}{\mathrm{V_{IM,ss}}}, \quad \frac{\mathrm{V_{I,ss}}}{\mathrm{V_{D,ss}}} \tag{4.13}$$

in Fig. 4.5. As expected, the drugs perturb the ratios of viral states that encompass their site of action within the viral life cycle. In the present example (Fig. 4.5), all states that lie downstream of the drugs' target site are affected, while the states that lie upstream are usually not affected. The exception are InIs, which increase the abundance of the preceding stage $\mathrm{T_1}$ (Fig. 4.5, upper left), despite decreasing the number of the subsequent infectious stage $\mathrm{T_2}$ (Fig. 4.5, lower left). This atypical behavior is due to the fact, that under the chosen parameters, k_T is responsible for $\approx 50\%$ of the observed decay of $\mathrm{T_1}$. Inhibiting k_T by InIs will therefore bottleneck the decay of $\mathrm{T_1}$.

Interestingly, the effect on the ratios is not always a linear function of drug efficacy. PIs and MIs show a different behavior (Fig. 4.5, lower right): PIs affect the ratio of infectious-to-defective virions through decreasing the number of infective virions, while MIs are increasing the number of defective

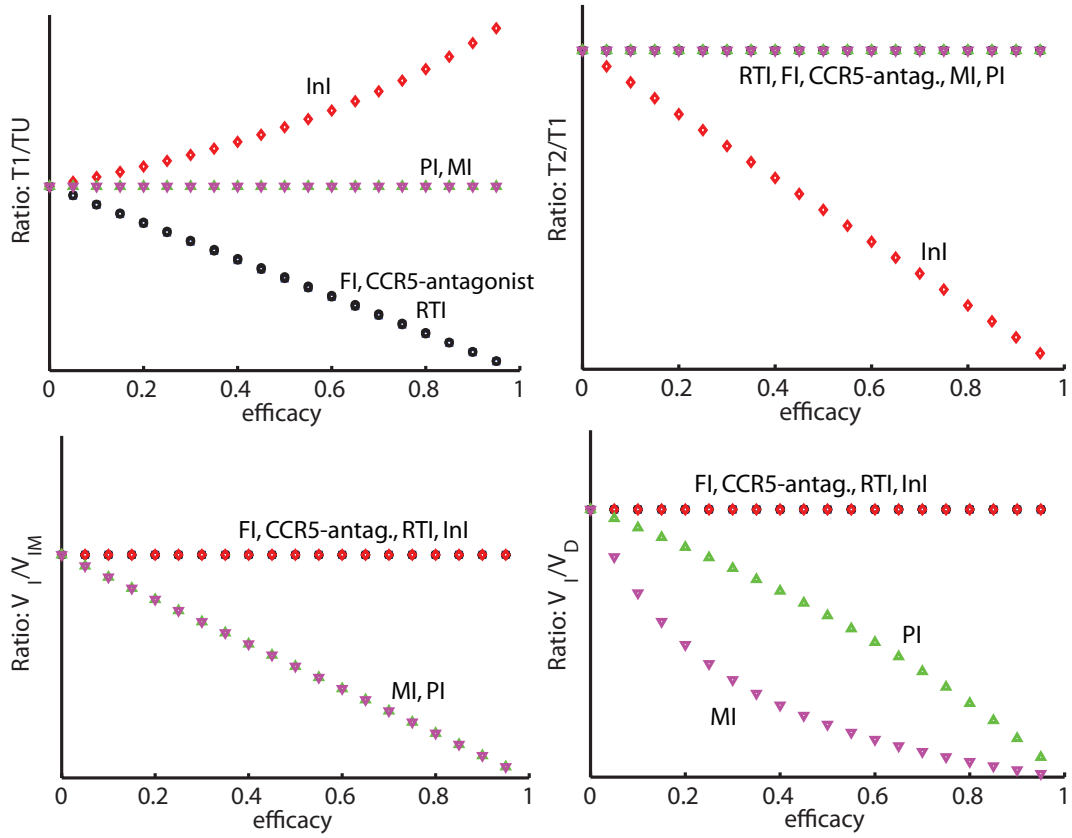

Figure 4.5: The illustrations shows how the ratios (linear scale) for HIV subspecies are shifted through treatment with different drug classes using the detailed model eqs. (4.4)-(4.11) and varying efficacies ε for each drug. Utilized parameters: $\mathrm{CL} = 23, \delta_{\mathrm{T}} = 0.02, \mathrm{N} = 1000, k_{\mathrm{T}} = 0.35, \delta_{\mathrm{PIC}} = 0.35, \lambda = 2 \cdot 10^9, \mathrm{K_D} = 1000, k_{\mathrm{off}} = 10^6, \delta_{\mathrm{RNA}} = 144, r_{\mathrm{fusion}} = 144, r_{\mathrm{RT}} = 48, r_{\mathrm{InI}} = 0.35, r_{\mathrm{mat}} = 12,\ q = 0.9$.

virions at the same time.

The detailed structural model contains parameters that are difficult to measure and currently not available. We therefore lump parts of the model based on quasi steady state assumptions to obtain a parameterizable model of viral and host cell dynamics. Using this technique, it is still possible to incorporate the effect of HIV antivirals mechanistically.

4.2.3 Mechanistic Parameter Lumping

Utilizing the detailed model eqs. (4.4)-(4.11) and under the reasonable assumption that $k_{\mathrm{off}} >> k_{\mathrm{fus}}$, we get

$$\frac{[\mathrm{V_I} : \mathrm{TU}]}{\mathrm{TU} \cdot \mathrm{V_I}} = \frac{1}{\mathrm{K_D}} \tag{4.14}$$

from eq. 4.5, where $\mathrm{K_D} = \frac{k_{\mathrm{off}}}{k_{\mathrm{on}}}$. Applying the quasi-steady state assumption to $\mathrm{T_{RNA}}$ yields

$$\frac{\mathrm{T_{RNA}}}{[\mathrm{V_I} : \mathrm{TU}]} = \frac{k_{\mathrm{fus}}}{k_{\mathrm{rev}} + \delta_{\mathrm{RNA}}}, \tag{4.15}$$

where we exploited that $\delta_{\mathrm{RNA}} \gg \delta_{\mathrm{TU}}$. We can now determine the effective infection rate by parameterizing the rate of new infections $k_{\mathrm{rev}} \cdot T_{\mathrm{RNA}}$ in terms of $\mathrm{TU} \cdot \mathrm{V_I}$. Using the above relationsships we

obtain

$$k_{\text{rev}} T_{\text{RNA}} = k_{\text{rev}} \frac{\text{T}_{\text{RNA}}}{[\text{V}_\text{I} : \text{TU}]} \cdot \frac{[\text{V}_\text{I} : \text{TU}]}{\text{TU} \cdot \text{V}_\text{I}} \cdot \text{TU} \cdot \text{V}_\text{I} \tag{4.16}$$

$$= \underbrace{\frac{k_{\text{fus}}}{\text{K}_\text{D}} \cdot \frac{k_{\text{rev}}}{k_{\text{rev}} + \delta_{\text{RNA}}}}_{\beta} \cdot \text{TU} \cdot \text{V}_\text{I}. \tag{4.17}$$

The parameter β describes the overall (lumped) basic infection rate up to the early infectious stage T_1. Since we want to eliminate the two intermediate stages $[\text{V}_\text{I} : \text{TU}]$ and T_{RNA}, we also have to take into account the clearance of viral particles associated with these stages. Aiming at a lumped clearance in terms of $\text{V}_\text{I} \cdot \text{TU}$ we exploit eqs. (4.14) and (4.15) to obtain

$$\begin{aligned} \text{CL}_\text{T} \cdot \text{V}_\text{I} \cdot \text{TU} &= (\delta_{\text{TU}} + \delta_{\text{RNA}}) \text{T}_{\text{RNA}} \\ &= \left(\frac{k_{\text{fus}}}{\text{K}_\text{D}} \cdot \frac{\delta_{\text{RNA}}}{k_{\text{rev}} + \delta_{\text{RNA}}} \right) \cdot \text{V}_\text{I} \cdot \text{TU} \\ &= \left(\beta \cdot \frac{k_{\text{rev}} + \delta_{\text{RNA}}}{k_{\text{rev}}} - \beta \right) \cdot \text{V}_\text{I} \cdot \text{TU} \end{aligned} \tag{4.18}$$

where we have assumed that $\delta_{\text{TU}} \ll \delta_{\text{RNA}}$. In most models, this term is not explicitly considered, but rather modelled as part of the overall constant viral clearance CL , thus ignoring the possible impact of unsuccessful infection on viral clearance.

Let us define the probability $\rho_{\text{rev},\phi}$ that reverse transcription is successfully finished in the absence of drugs:

$$\rho_{\text{rev},\phi} = \frac{k_{\text{rev}}}{k_{\text{rev}} + \delta_{\text{RNA}}}, \tag{4.19}$$

where we again used $\delta_{\text{TU}} \ll \delta_{\text{RNA}}$. Then eq, (4.18) becomes

$$\text{CL}_\text{T} = \left(\frac{\beta}{\rho_{\text{rev},\phi}} - \beta \right). \tag{4.20}$$

Along the same lines, we eliminate V_{IM} by assuming quasi-steady state conditions for the viral stage in eq. (4.9)

$$\text{V}_{\text{IM}} = p \cdot \frac{\widehat{\text{N}_\text{T}}}{\text{CL} + k_{\text{Mat}}} \text{T}_2. \tag{4.21}$$

Then the amount of maturated, released virions $q \cdot k_{\text{mat}} \cdot \text{V}_{\text{IM}}$ in terms of T_2 is given by

$$q \cdot k_{\text{mat}} \text{V}_{\text{IM}} = \underbrace{q \cdot p \cdot \frac{k_{\text{mat}}}{\text{CL} + k_{\text{mat}}} \cdot \widehat{\text{N}_\text{T}}}_{\text{N}_\text{T}} \cdot \text{T}_2. \tag{4.22}$$

This term can now be used to replace V_{IM} in eqs. (4.9)-(**??**). Finally we subsume the non-infectious virus $\text{V}_{\text{NI}} = \text{V}_{\text{IM}} + \text{V}_\text{D}$.

4.2.4 Lumped Model

Applying the lumping process, the simplified model is defined by the following system of ODEs:

$$\begin{aligned}
\frac{\mathrm{d}}{\mathrm{d}t}\mathrm{TU} &= \lambda_\mathrm{T} + \mathrm{T}_1 \cdot \delta_\mathrm{PIC} - \mathrm{TU} \cdot \delta_\mathrm{TU} - \beta \cdot \mathrm{V_I} \cdot \mathrm{TU} \\
\frac{\mathrm{d}}{\mathrm{d}t}\mathrm{T}_1 &= \beta \cdot \mathrm{V_I} \cdot \mathrm{TU} - \mathrm{T}_1 \left(\delta_{\mathrm{T}_1} + \delta_\mathrm{PIC} + k_\mathrm{T}\right) \\
\frac{\mathrm{d}}{\mathrm{d}t}\mathrm{T}_2 &= \mathrm{T}_1 \cdot k_\mathrm{T} - \mathrm{T}_2 \cdot \delta_{\mathrm{T}_2} \qquad (4.23) \\
\frac{\mathrm{d}}{\mathrm{d}t}\mathrm{V_I} &= \mathrm{N_T} \cdot \mathrm{T}_2 - \mathrm{V_I} \cdot \big(\mathrm{CL} + (\mathrm{CL_T} + \beta) \cdot \mathrm{TU}\big) \\
\frac{\mathrm{d}}{\mathrm{d}t}\mathrm{V_{NI}} &= \mathrm{T}_2 \cdot \big(\widehat{\mathrm{N_T}} - \mathrm{N_T}\big) - \mathrm{V_{NI}} \cdot \mathrm{CL} \qquad (4.24)
\end{aligned}$$

This model can now be extended for, e.g., macrophages or mutational dynamics to derive the model in Fig. 4.7.

4.2.5 Parameters

The novel parameter k_T can be derived by combining information from the literature [96, 156] with our model. Zhou et al. [96] have measured the decay of the pre-integration complex and estimated a halflife of 2 days ($\delta_\mathrm{PIC} = 0.35$[1/day]). This value was later confirmed by [156]. Furthermore, Zhou et al. [96] stated that approximately 50% of viral PICs undergo degradation in infected cells after infection. Therefore, the fraction of successful integration $\rho_{\text{integr.}}$ is also approximately 50%. From our model, we derive

$$\frac{k_\mathrm{T}}{k_\mathrm{T} + \delta_\mathrm{PIC} + \delta_\mathrm{TU}} \;=\; \rho_{\text{integr.}} \;\approx\; 0.5. \qquad (4.25)$$

Assuming $\delta_\mathrm{PIC} \gg \delta_\mathrm{TU}$, we finally obtain $k_\mathrm{T} = 0.35$ [1/day].
Values for $\rho_{\mathrm{rev},\phi}$ range from 15% [502] to 50% [96]. The parameter k_mat has been reported to be in the range of 12 [1/day] [222]. If we initially set $q = p = 1$, and assume that infected cells, which do not express viral proteins, are cleared at the same rate as uninfected cells ($\delta_{\mathrm{T}_1} = \delta_\mathrm{TU}$), then the remaining number of unknown parameters ($\beta, \widehat{\mathrm{N}}, \lambda, \delta_\mathrm{TU}, \delta_{\mathrm{T}_2}, \mathrm{CL}$) is the same as in the standard models [12].

4.2.6 Effect of Compounds on Lumped Parameters

In the following we will denote the local effects of compounds on the targeted processes in the detailed model by ε, while effects of drugs on lumped parameters in the simplified model (fig. 4.7) will be denoted by η.

Entry inhibitors and RTIs. We have determined the basic infection rate constant β in eq. (4.17). Locally, CCR5 inhibitors, FI and RTIs inhibit binding k_on, fusion k_fus and reverse transcription k_rev. The rate of successful infection $\beta_{\mathrm{CCR5,FI,RTI}}$ in the presence of inhibitors by is given by:

$$\beta_{\mathrm{CCR5,FI,RTI}} \;=\; (1-\varepsilon_\mathrm{FI}) \cdot (1-\varepsilon_\mathrm{CCR5}) \cdot \frac{k_\mathrm{fus}}{\mathrm{K_D}} \cdot \frac{(1-\varepsilon_\mathrm{RTI}) \cdot k_\mathrm{rev}}{(1-\varepsilon_\mathrm{RTI}) \cdot k_\mathrm{rev} + \delta_\mathrm{RNA}},$$

where $(1-\varepsilon) \in [0,1]$ denotes the residual activity of the targeted processes in the presence of the inhibitor. From the above equation it becomes clear that the local effect on the detailed parameters and the global effect on the lumped parameters are identical for FIs and CCR5-antagonists, i.e., $\varepsilon_\mathrm{FI} = \eta_\mathrm{FI}$, $\varepsilon_\mathrm{CCR5} = \eta_\mathrm{CCR5}$. For RTIs, however, the overall effect on the rate of successful infection β depends on the decay rate constant δ_RNA of viral RNA.

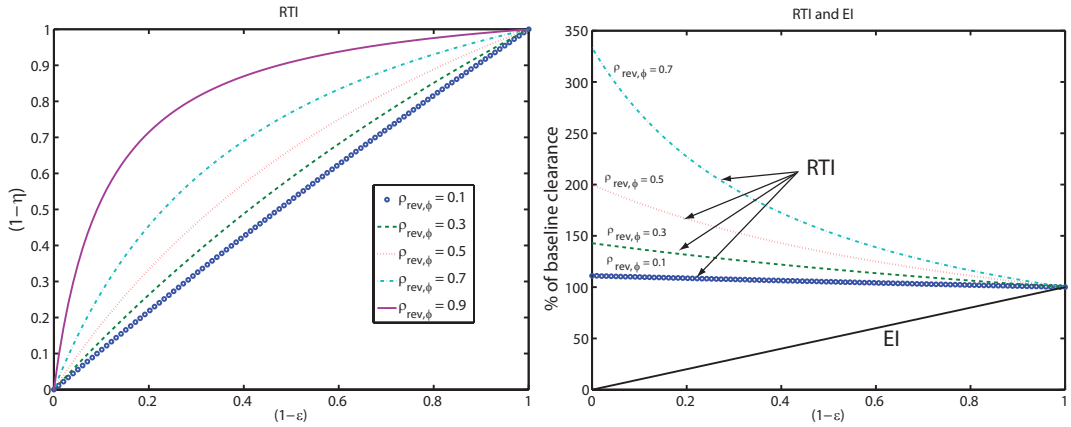

Figure 4.6: Left: Correlation between effect of RTIs on the reverse transcription $(1-\varepsilon_{\mathrm{RTI}})$ and effect on the infection rate $(1-\eta_{\mathrm{RTI}})$ for a parameter range that defines the probability to finalize reverse transcription in the absence of RTIs $\rho_{\mathrm{rev},\phi}$. Right: Effect of RTIs and EIs on the clearance through unsuccessful infection $\mathrm{CL_T}$.

Let $\rho_{\mathrm{rev,RTI}}$ denote the probability that reverse transcription is successfully completed in the presence of RTIs.

$$\rho_{\mathrm{rev,RTI}} \quad = \quad \frac{(1-\varepsilon_{\mathrm{RTI}})\cdot k_{\mathrm{rev}}}{(1-\varepsilon_{\mathrm{RTI}})\cdot k_{\mathrm{rev}}+\delta_{\mathrm{RNA}}}. \tag{4.26}$$

The effect of RTIs on the lumped infection rate β can now be interpreted as the reduction in the probability to successfully complete reverse transcription

$$1-\eta_{\mathrm{RTI}}(\rho_{\mathrm{rev},\phi}) \quad = \quad \frac{\rho_{\mathrm{rev,RTI}}}{\rho_{\mathrm{rev},\phi}}, \tag{4.27}$$

resulting from the reduced rate of reverse transcription, which increases the likelihood that parts of the viral RNA are degraded before being transformed into DNA.

$$\begin{aligned}(1-\eta_{\mathrm{RTI}}(\rho_{\mathrm{rev},\phi})) \quad &= \quad \frac{(1-\varepsilon_{\mathrm{RTI}})\cdot k_{\mathrm{rev}}}{(1-\varepsilon_{\mathrm{RTI}})\cdot k_{\mathrm{rev}}+\delta_{\mathrm{RNA}}}\cdot\frac{k_{\mathrm{rev}}+\delta_{\mathrm{RNA}}}{k_{\mathrm{rev}}}\\ &= \quad \frac{1}{\rho_{\mathrm{rev},\phi}+\frac{1-\rho_{\mathrm{rev},\phi}}{(1-\varepsilon_{\mathrm{RTI}})}}.\end{aligned} \tag{4.28}$$

Therefore, for RTIs, we derive a non-linear relationship between inhibition of reverse transcription and inhibition of infection, in contrast to CCR5-antagonists and FIs. The relation between the local effect of RTIs on reverse transcription $\varepsilon_{\mathrm{RTI}}$ and the effect of RTIs on the infection rate $\eta_{\mathrm{RTI}}(\rho_{\mathrm{rev},\phi})$ is illustrated in Fig. 4.6 (left). It can be seen that the non-linearity between $(1-\eta_{\mathrm{RTI}})$ and $(1-\varepsilon_{\mathrm{RTI}})$ is most pronounced if reverse transcription has a high likelihood of being finalized in the absence of drug, i.e, $\rho_{\mathrm{rev},\phi}\approx 1$. In this case $(1-\eta_{\mathrm{RTI}})>(1-\varepsilon_{\mathrm{RTI}})$ or $\varepsilon_{\mathrm{RTI}}>\eta_{\mathrm{RTI}}$, implying that the effect of RTIs on the infection rate is smaller than the effect on reverse transcription. If reverse transcription is rarely finalized in the absence of drug, i.e., $\rho_{\mathrm{rev},\phi}\approx 0$, then the effects on reverse transcription and on the infection rate become identical $(1-\eta_{\mathrm{RTI}})=(1-\varepsilon_{\mathrm{RTI}})$ or $\varepsilon_{\mathrm{RTI}}\approx\eta_{\mathrm{RTI}}$.

Using eq. (4.28), we obtain the rate of (successful) infection $\beta_{\mathrm{CCR5,FI,RTI}}$ in the presence of CCR5-antagonists, FIs and RTIs:

$$\beta_{\mathrm{CCR5,FI,RTI}} \quad = \quad (1-\eta_{\mathrm{CCR5}})\cdot(1-\eta_{\mathrm{FI}})\cdot(1-\eta_{\mathrm{RTI}}(\rho_{\mathrm{rev},\phi}))\cdot\beta, \tag{4.29}$$

where β denotes the basic infection rate in the absence of inhibitors. The equation above implies that the effect of CCR5-antagonists, FIs and RTIs can be modeled at the level of infection. We also illustrated that in the case of RTIs, there might be a discrepancy between the local effects on the enzyme (reverse transcriptase) and the effects on the lumped infection rate β. To elucidate whether

this discrepancy has any consequence *in vivo*, it is necessary to determine which fraction $\rho_{\mathrm{rev},\phi}$ of the viral RNA that enters the cell is successfully transcribed into full length DNA in the absence of drug.

Using the same considerations as above, we can derive the effect of CCR5 inhibitors, FI and RTIs on the clearance through unsuccessful infection (cf. eq. (4.18)):

$$\begin{aligned} \mathrm{CL}_{\mathrm{T,CCR5,FI,RTI}} &= (1-\varepsilon_{\mathrm{CCR5}})\cdot(1-\varepsilon_{\mathrm{FI}})\cdot\left(\frac{k_{\mathrm{fus}}\cdot\rho_{\mathrm{rev,RTI}}}{\mathrm{K_D}\cdot\rho_{\mathrm{rev,RTI}}}-\frac{k_{\mathrm{fus}}}{\mathrm{K_D}}\cdot\rho_{\mathrm{rev,RTI}}\right) \\ \mathrm{CL}_{\mathrm{T,CCR5,FI,RTI}} &= (1-\eta_{\mathrm{CCR5}})\cdot(1-\eta_{\mathrm{FI}})\cdot\left(\frac{\beta}{\rho_{\mathrm{rev},\phi}}-(1-\eta_{\mathrm{RTI}})\cdot\beta\right) \end{aligned} \tag{4.30}$$

From this equation it is clear that effective RTIs ($\eta_{\mathrm{RTI}}\approx 1$) significantly contribute to the clearance of virus through unsuccessful infection, whereas FIs and CCR5-antagonists lower the clearance of virus through unsuccessful infection, because they inhibit viral infection at steps that precede the step of viral RNA destruction δ_{RNA} (see Fig. 4.6, right).

Most models (see e.g. [503]) do not consider the clearance of virus through (unsuccessful) infection $\mathrm{CL_T}$ explicitly and treat it as part of the constant virus clearance CL. However, as we demonstrated, inhibitors can have an effect on the clearance. If one is only interested in the additional clearance, and not the baseline clearance of virus through unsuccessful infection, it can be derived by subtracting $\mathrm{CL}_{\mathrm{T,CCR5,FI,RTI}}-\mathrm{CL}_{\mathrm{T},\phi}$, using eq. (4.20) and eq. (4.30).

Integrase inhibitors. InIs inhibit the integration of viral DNA into the host DNA. We did not perform parameter lumping at this stage and therefore $\eta_{\mathrm{InI}}=\varepsilon_{\mathrm{InI}}$. The rate of integration is altered in the presence of InIs, according to:

$$k_{\mathrm{T,InI}} = (1-\eta_{\mathrm{InI}})\cdot k_{\mathrm{T}}. \tag{4.31}$$

Protease and maturation inhibitors. PIs inhibit the protease of HIV, resulting in a decreased maturation rate constant k_{mat}, and MIs decrease the probability that virions maturate normally q. Recalling eq. (4.22), the total input into the compartment of infective virus $\mathrm{V_I}$ is described by:

$$q\cdot k_{\mathrm{mat}}\mathrm{V_{IM}} = (1-\varepsilon_{\mathrm{MI}})\cdot q\cdot p\cdot\frac{(1-\varepsilon_{\mathrm{PI}})\cdot k_{\mathrm{mat}}}{\mathrm{CL}+(1-\varepsilon_{\mathrm{PI}})\cdot k_{\mathrm{mat}}}\cdot\widehat{\mathrm{N}}_{\mathrm{T}}\cdot\mathrm{T}_2. \tag{4.32}$$

In the case of MIs we have $\varepsilon_{\mathrm{MI}}=\eta_{\mathrm{MI}}$. However, in the case of PIs, their effect depends on the clearance of free virus CL. Similarly to the case with RTIs, we can define the probability that maturation is successfully finished in the absence of inhibitors $\rho_{\mathrm{PR},\phi}$ and in the presence of inhibitors $\rho_{\mathrm{PR,PI}}$

$$\rho_{\mathrm{PR},\phi} = \frac{k_{\mathrm{mat}}}{k_{\mathrm{mat}}+\mathrm{CL}} \tag{4.33}$$

$$\rho_{\mathrm{PR,PI}} = \frac{(1-\varepsilon_{\mathrm{PI}})\cdot k_{\mathrm{mat}}}{\mathrm{CL}+(1-\varepsilon_{\mathrm{PI}})\cdot k_{\mathrm{mat}}} \tag{4.34}$$

The effect of PIs can then be defined as the decrease in the likelihood that virions will successfully maturate, before they are cleared by the immune system $(1-\eta_{\mathrm{PI}})=\rho_{\mathrm{PR,PI}}/\rho_{\mathrm{PR},\phi}$. We derive:

$$(1-\eta_{\mathrm{PI}}(\rho_{\mathrm{PR},\phi})) = \frac{1}{\rho_{\mathrm{PR},\phi}+\frac{1-\rho_{\mathrm{PR},\phi}}{(1-\varepsilon_{\mathrm{PI}})}}, \tag{4.35}$$

analogously to eq. (4.28). Therefore in the case of PIs, we observe the same non-linearity between $(1-\eta_{\mathrm{PI}})$ and $(1-\varepsilon_{\mathrm{PI}})$ as in the case of RTIs (see fig. 4.6). The effect of MIs and PIs on the production of infectious particles N can be modelled accoring to:

$$\mathrm{N_{PI,MI}} = (1-\eta_{\mathrm{MI}})\cdot\big(1-\eta_{\mathrm{PI}}(\rho_{\mathrm{PR},\phi})\big)\cdot\mathrm{N_T} \tag{4.36}$$

Similarly, the above equation can be used to model the influence of PIs and MIs on the production of non-infectious Virus $\mathrm{V_{NI}}$.

4.3 Novel two-stage Viral Growth-Competition Model

The lumped model can be parameterized in terms of six unknown parameters ($\beta, \widehat{\mathrm{N}}, \lambda, \delta_{\mathrm{TU}}, \delta_{\mathrm{T}_2}, \mathrm{CL}$), which equals the number of estimated parameters using standard models [12]. For the remaining parameters, we have provided values from the literature (see section 4.2.5).

We specify two types of target cells (T-cells and macrophages) and finally incorporate the viral mutation process (resulting from erroneous reverse transcription) into the overall model. The proposed simplified two-stage virus dynamics model is shown in Fig. 4.7. It comprises T-cells, macrophages, free infectious- and uninfectious virus ($\mathrm{TU}, \mathrm{MU}, \mathrm{V_I}, \mathrm{V_{NI}}$, respectively) and four types of infected cells: infected T-cells and macrophages *prior* to proviral genomic integration ($\mathrm{T_1}$ and $\mathrm{M_1}$, respectively) and infected T-cells and macrophages *after* proviral genomic integration ($\mathrm{T_2}$ and $\mathrm{M_2}$, respectively).

The system of ordinary equations for the derived two-stage virus dynamics model is given below:

$$
\begin{aligned}
\frac{\mathrm{d}}{\mathrm{d}t}\mathrm{TU} &= \lambda_{\mathrm{T}} + \mathrm{T_1}(i)\cdot\delta_{\mathrm{PIC}} - \mathrm{TU}\cdot\delta_{\mathrm{TU}} - \sum_i \beta_{\mathrm{T}}(i)\cdot\mathrm{V}(i)\cdot\mathrm{TU} \\
\frac{\mathrm{d}}{\mathrm{d}t}\mathrm{MU} &= \lambda_{\mathrm{M}} + \mathrm{M_1}(i)\cdot\delta_{\mathrm{PIC}} - \mathrm{MU}\cdot\delta_{\mathrm{MU}} - \sum_i \beta_{\mathrm{M}}(i)\cdot\mathrm{V}(i)\cdot\mathrm{MU} \\
\frac{\mathrm{d}}{\mathrm{d}t}\mathrm{T_1}(i) &= \beta_{\mathrm{T}}(i)\cdot\mathrm{V}(i)\cdot\mathrm{TU} - \mathrm{T_1}(i)\big(\delta_{\mathrm{T_1}} + \delta_{\mathrm{PIC}} + k_{\mathrm{T}}(i)\big) \\
\frac{\mathrm{d}}{\mathrm{d}t}\mathrm{T_2}(i) &= \sum_k \big(\mathrm{T_1}(k)\cdot k_{\mathrm{T}}(k)\cdot p_{k\to i}\big) - \mathrm{T_2}(i)\cdot\delta_{\mathrm{T_2}} \\
\frac{\mathrm{d}}{\mathrm{d}t}\mathrm{M_1}(i) &= \beta_{\mathrm{M}}(i)\cdot\mathrm{V}(i)\cdot\mathrm{MU} - \mathrm{M_1}(i)\big(\delta_{\mathrm{M_1}} + \delta_{\mathrm{PIC}} + k_{\mathrm{M}}(i)\big) \\
\frac{\mathrm{d}}{\mathrm{d}t}\mathrm{M_2}(i) &= \sum_k \big(\mathrm{M_1}(k)\cdot k_{\mathrm{M}}(k)\cdot p_{k\to i}\big) - \mathrm{M_2}(i)\cdot\delta_{\mathrm{M_2}} \\
\frac{\mathrm{d}}{\mathrm{d}t}\mathrm{V_I}(i) &= \mathrm{N_M}(i)\cdot\mathrm{M_2}(i) + \mathrm{N_T}(i)\cdot\mathrm{T_2}(i) \\
&\quad -\mathrm{V}(i)\cdot\Big(\mathrm{CL} + \big(\mathrm{CL_T}(i) + \beta_{\mathrm{T}}(i)\big)\cdot\mathrm{TU} + \big(\mathrm{CL_M}(i) + \beta_{\mathrm{M}}(i)\big)\cdot\mathrm{MU}\Big) \\
\frac{\mathrm{d}}{\mathrm{d}t}\mathrm{V_{NI}} &= \sum_i \Big(\big(\widehat{\mathrm{N}}_{\mathrm{M}}(i) - \mathrm{N_M}(i)\big)\cdot\mathrm{M_2}(i) + \big(\widehat{\mathrm{N}}_{\mathrm{T}}(i) - \mathrm{N_T}(i)\big)\cdot\mathrm{T_2}(i)\Big) - \mathrm{CL}\cdot\mathrm{V_{NI}}
\end{aligned}
\tag{4.37}
$$

where λ_{T} and λ_{M} are the birth rates of uninfected T-cells and macrophages and δ_{TU} and δ_{MU} are their death rates. The parameters $k_{\mathrm{T}}(k)$ and $k_{\mathrm{M}}(k)$ are the integration rates of mutant strain k. The parameters $\delta_{\mathrm{T1}}, \delta_{\mathrm{T2}}, \delta_{\mathrm{M1}}$ and δ_{M2} are the death rates of T1, T2, M1 and M2 cells. The parameter δ_{PIC} refers to the intracellular clearance of essential components of the pre-integration complex (PIC), e.g. by the host cell proteasome. The parameter $p_{k\to i}$ defines the probability to mutate from strain k to strain i and will be defined in section 4.3.3.

4.3.1 Effect of Antivirals on Model Parameters

The effect of drugs on lumped parameters in the model is implemented as previously described (sec. 4.2.6). For the ease of completeness, we will summarize them in the context of the novel model.

$$
\begin{aligned}
\beta_{\mathrm{T/M(CCR5,FI,RTI)}} &= (1-\eta_{\mathrm{CCR5}})\cdot(1-\eta_{\mathrm{FI}})\cdot(1-\eta_{\mathrm{RTI}}(\rho_{\mathrm{rev},\phi}))\cdot\beta_{\mathrm{T/M}} \\
\mathrm{CL}_{\mathrm{T/M(CCR5,FI,RTI)}} &= (1-\eta_{\mathrm{CCR5}})\cdot(1-\eta_{\mathrm{FI}})\cdot\left(\frac{\beta_{\mathrm{T/M}}}{\rho_{\mathrm{rev},\phi}} - (1-\eta_{\mathrm{RTI}})\cdot\beta_{\mathrm{T/M}}\right) \\
k_{\mathrm{T/M(InI)}} &= (1-\eta_{\mathrm{InI}})\cdot k_{\mathrm{T/M}} \\
\mathrm{N}_{\mathrm{T/M(PI,MI)}} &= (1-\eta_{\mathrm{MI}})\cdot\big(1-\eta_{\mathrm{PI}}(\rho_{\mathrm{PR},\phi})\big)\cdot\mathrm{N_{T/M}}
\end{aligned}
$$

where β is the basic infection rate and $(1-\eta)$ denotes the effect of the compund on the model parameter (see sec. 4.2.6).

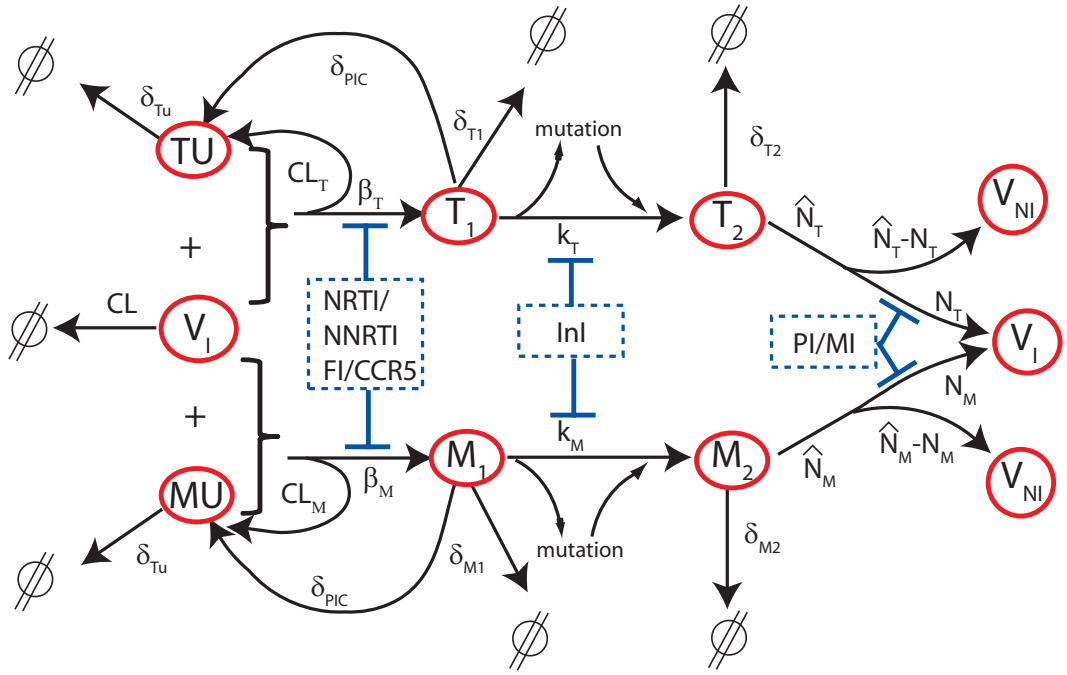

Figure 4.7: Simplified Two Stage Virus Dynamics Model. Species are circled in red. Reactions are indicated by black arrows. Drugs and their interference in the life cycle of HIV are indicated in blue.

4.3.2 Strain-associated Reproduction and Resistance

There are two basic determinants, which allow us to create any possible fitness landscape in the quasi-species space: The endogenous ability of the mutant strain to proliferate and the impact of inhibitors on this activity. Since the endogenous activity of every mutant strain is most likely not known, we denote it by some selective disadvantage s, which describes the ability of the mutant strain to proliferate, relative to the wildtype. The effectivity of some inhibitor η is usually measured with reference to the wildtype and some mutant strain i confers a resistance r to the drug, where the resistance of the wildtype is assumed to be 0%.

Therefore, we have modeled the ability of a mutant strain i to proliferate based on three parameters s, r and η, which allow us to create any possible fitness landscape (e.g. fig. 4.11, 4.12) in the quasi-species space.

- the endogenous ability to proliferate relative to the wildtype $(1 - s(i))$, where $s(i) \in [0, 1]$ is the selective disadvantage of the mutant strain i for a particular proliferative process (e.g. fusion, reverse transcription, etc.).
- the efficacy of drug treatment $(1 - \eta(j))$, where $\eta(j) \in [0, 1]$ is the efficacy of drug j in inhibiting a targeted proliferative process in the wildtype.
- the resistance against a certain treatment $\big(1 - r(i, j)\big)$ of mutant strain i against drug j.

As an example, consider two drugs $d1$ and $d2$, which are 90% and 80% effective in inhibiting the infection β_{wt} in the wildtype. Then,

$$\beta(d1, d2)_{\text{wt}} \quad = \quad (1 - 0.9) \cdot (1 - 0.8) \cdot \beta, \tag{4.38}$$

and infection will be 2% as effective as in the absence of drugs. A mutant strain $m1$ can infect cells only 80 % as effectively as the wildtype ($s_{\text{m1}} = 0.2$). Thus,

$$\beta(d1, d2)_{\text{m1}} \quad = \quad (1 - 0.9) \cdot (1 - 0.8) \cdot (1 - 0.2) \cdot \beta, \tag{4.39}$$

and infection is only 1.6% as effective as for the wildtype in the absence of drug. Some other mutant $m2$ is 99% resistant against $d1$. Thus,

$$\beta(d1, d2)_{\mathrm{m2}} \quad = \quad \big(1 - 0.9 \cdot (1 - 0.99)\big) \cdot (1 - 0.8) \cdot (1 - 0.2) \cdot \beta, \tag{4.40}$$

and infection with type $m2$ in the presence of drugs $d1$ and $d2$ is 16% effective compared to the wildtype in the absence of drugs.

4.3.3 Mutation

The observed efficacy of a drug, -or a combination of drugs will decrease over time due to the emergence of resistance mutations, because the HIV population within the body is very adaptable and because adaptation can occur on a very short time scale (see e.g. [395]). Therefore, it is essential to incorporate some kind of resistance development, if longer term viral dynamics are modelled, or if the virological failure is a phenomenon studied by the model.

Huang et al. [15] have have proposed the most simple approach. In their model, emergence of resistance was modeled by a linear decrease of drug efficacy (increase in IC_{50}, see fig. 4.8). This way, it is not necessary to explicitly model the evolution of mutants. However, the limitations of such an approach are obvious: Under such an approach, it is completely unclear what the underlying dynamics of resistance development are and there is no possibility to study them within the model. It is not possible to incorporate potential fitness loss and regain [504,505] of mutant virus. Therefore, it is also not possible to study the effects of different fitness landscapes [7, 10] on the timing and emergence of resistance. In other words: it is not possible to study if, or if not resistance emerges and ways to possibly overcome it.

For these reasons, we have decided to explicitly model viral quasi-species dynamics in a growth-competition model.

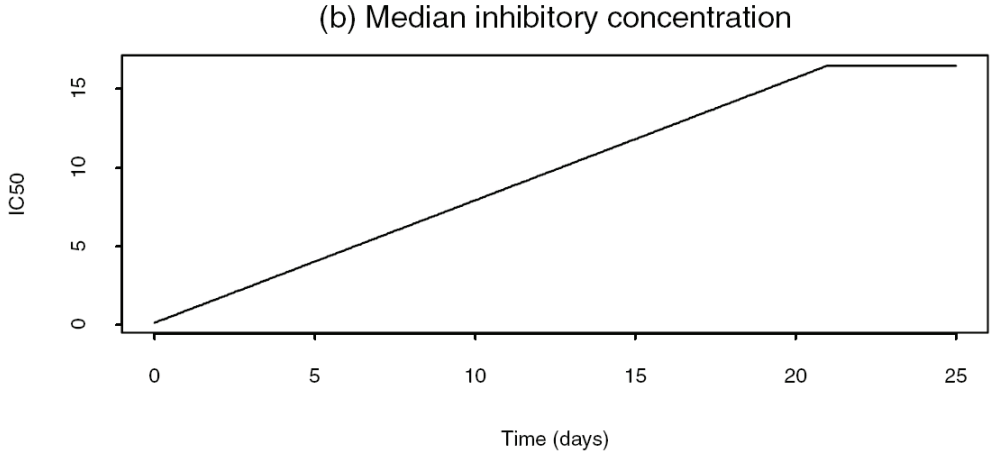

Figure 4.8: Most simple approach to model emergence of drug resistance implemented by Huang [15]

Our overall viral dynamics model (eq. (4.37)) comprises a complete mutagenic graph. In HIV infection, genomic mutation occurs during the reverse transcription process [4]. The reverse transcriptase of HIV lacks a proof reading mechanism in contrast to host polymerase enzymatic reactions. However, viral proteins from newly mutated viral genomes are only produced after integration of the viral genome into the host cell DNA. The proteins required for the stable integration of the newly mutated viral genome originate from the founder virus. Therefore, phenotypically, drug resistance

of new mutants will only be observed after integration, i.e., in the infectious stages T_2 and M_2. In total, the model includes 2^N different viral strains that contain point mutations in any pattern of the modelled N possible mutations. For two distinct mutations, the mutagenic graph is shown in Fig. 4.9. Each mutant i can mutate to every other mutant k in one step. The probability $p_{k\to i}$ to mutate from any strain k to any strain i can be directly derived from the mutagenic tree in Fig. 4.9 (left):

$$p_{k\to i} = \mu^{h(i,k)} \cdot (1-\mu)^{N-h(i,k)}, \tag{4.41}$$

where μ denotes the mutation probability per base and reverse transcription process ($\approx 3 \cdot 10^{-5}$ [4]), $h(i,k)$ is the hamming distance between strain k and strain i, and N is the total number of different positions that may mutate. Since some viral strains are present only in very low copy numbers, we use a hybrid stochastic-deterministic setting [506] to model the overall virus dynamics model (see section 4.6.2 for details).

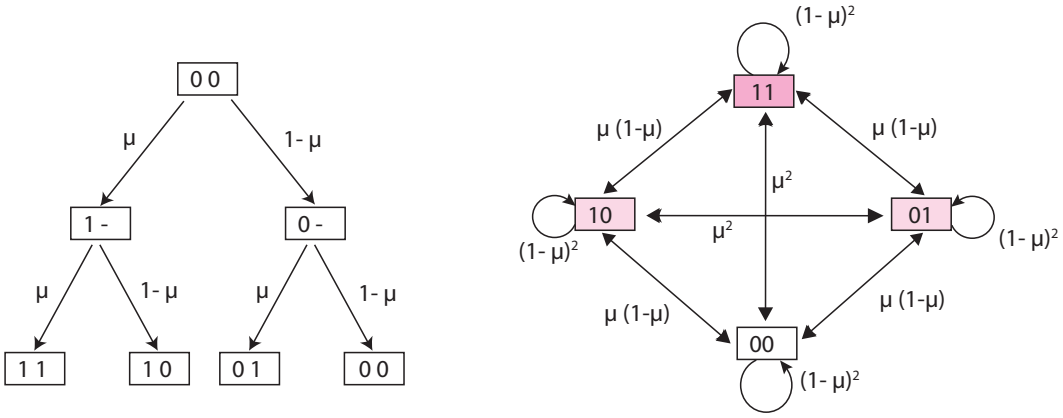

Figure 4.9: Left: Decision tree for the transition pathway on the right. Right: Transition pathways, if two mutations are considered

Using this model, we ignore mutations that do not occur at drug-resistance sites. Some of these mutations might be deleterious for the virus. Therefore, it is possible that we overestimate the amount of replication-capable offspring. In view of mutagenic nucleoside analogs, it might require a more accurate model to study the effects of these inhibitors on the dynamics of the virus.

4.3.4 Abundance of Resistant Mutants Prior to Treatment Initiation

One reason for treatment failure can be the selection of pre-exiting resistant strains.
Our quasi-species model (eq. (4.37)) allows to compute the expected number of resistant mutants, prior to treatment initiation. In fig. 4.10, we show the abundance of resistant mutants in the drug-free steady state, based on our model. In this example, we have assumed a graded fitness landscape: Each mutation away from the wild type is associated with a fitness loss s. In figure 4.10 it can be seen that the probability for the presence of multiply mutated strains is decreasing with a lower fitness (greater selective disadvantage). If a drug resistance is associated with a fitness loss of 30%, it is unlikely that mutants pre-exist, that confer resistance to three- or more drugs. A similar analysis has been performed by Ribero et al. [507] based on the frequency of resistant strains.
One could infer from fig. 4.10, that mutants will not pre-exist, if they are sufficiently unfit. However, there is a minimal abundance of mutant strains: Assume, that drug-resistant strains are not replicating efficiently alongside the wildtype. The total amount of infected cells with integrated viral DNA has been estimated to be $\approx 10^7$ [115] and the mutation rate per base per round of reverse transcription has been estimated to be $3 \cdot 10^{-5}$ [4]. Therefore, even under the assumption that drug-resistant strains are not replicating, the expected number of mutant strains with a specific point mutation is ≈ 300. This means, that any one point mutation, irrespectively of how fit it is, is likely to be present at the start of therapy.

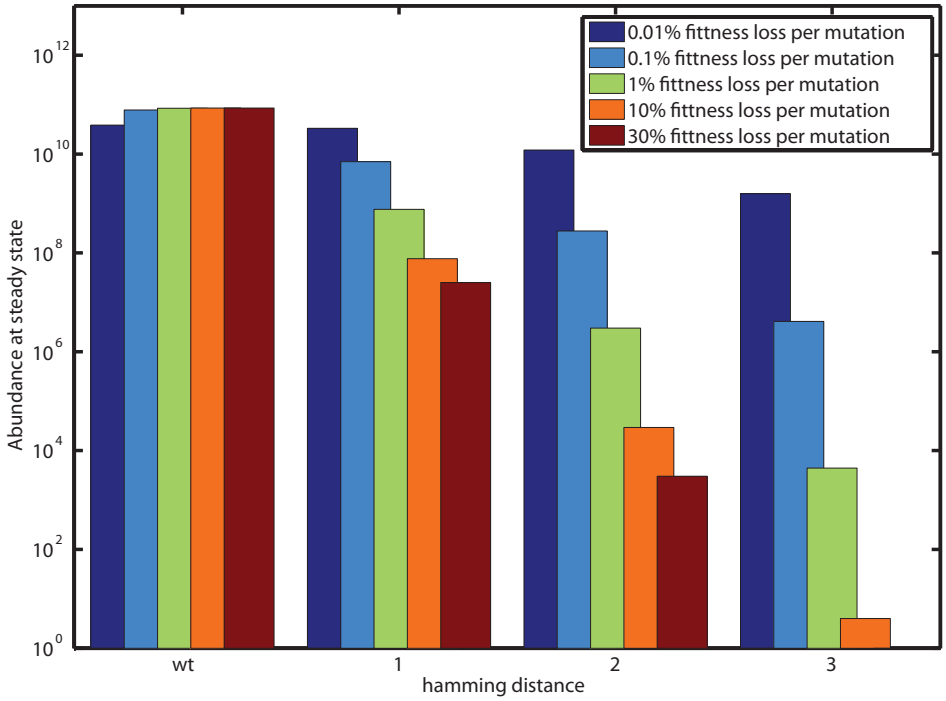

Figure 4.10: The presence of drug resistant (one point) mutants prior to treatment depends on the fitness of the mutants in the drug-free environment (only if the path from wt to mutant is steady/graded fitness landscape).

4.4 Fitness & Drug Resistance

Fitness describes the capability of an individual (of certain genotype) to reproduce in a certain environment. If differences in individual genotypes affect fitness, then, through adaptation, the frequencies of the genotypes will change over generations and the genotypes with higher fitness become more common.
In the case of HIV, the natural environment is provided by the host individual. Pharmacological intervention (through the application of drugs) can modify this environment drastically, disabling most viral strains from reproduction and selecting resistant strains that are able to reproduce in the pharmacologically modified environment. Whether the viral population can survive as a whole is ultimately determined by the ability of some resistant strain to sustain the viral population.
The threshold parameter, which determines if a strain- or a population as a whole can sustain, expand, or will be eradicated, is denoted by the reproductive number R_0 [508].

4.4.1 The Reproductive Number R_0

The reproductive number R_0 denotes the average number of offspring that is produced within the lifetime of one individual pathogen. The basic reproductive number can be interpreted as a threshold parameter: for $R_0 > 0$, the pathogen is able to replicate, however, if $R_0 < 1$, the pathogen will die out after some time. For $R_0 = 1$ the infection is stabilized and for $R_0 > 1$ the infection will expand.
There are two ways to calculate R_0: Using the (i) *survival function* and (ii) the *next generation method* [509]:
Survival function. The survival function is defined as follows:

$$R_0 = \int_0^\infty L(s) \cdot P(s) \mathrm{d}s \tag{4.42}$$

where the expected lifetime of the pathogen, L, is the reciprocal of its decline. The productivity P is the number of newly infected individuals that will be produced per unit time (the product of all

proliferative terms).
If R_0 is calculated using the survival function, it will capture the expected offspring in the same compartment (e.g. virus-to-virus).
Next generation operator. We define the matrix $F_i(x)$ as the rate of new infections in the compartment i and $V_i(x) = V_i^-(x) - V_i^+(x)$, where $V_i^-(x)$ denotes the rate of transfer of individuals out of compartment i and $V_i^+(x)$ the rate of transfer of individuals into of compartment i. R_0 is then given by the dominant eigenvalue of the *next generation* operator FV^{-1}.
The *next generation* method is particularly useful, if many infectious compartments (= infectious stages) are considered and if the main interest is in the transfer from the founder compartment into some other infectious compartment (not a complete replicative circle). For the complete life cycle (e.g. virus-to-virus), both methods yield the same result for R_0.
We are particularly interested in the whole life cycle of HIV, which captures the effects of all drug classes. Therefore, in our example, it is not necessary to choose one of the methods over the other.
Example. Considering one infectious cycle (virus-to-virus), for the model in eq. (4.1), we derive

$$F = \begin{pmatrix} 0 & \beta \cdot \mathrm{TU} \\ 0 & 0 \end{pmatrix} \tag{4.43}$$

and

$$V = \begin{pmatrix} \delta_\mathrm{T} & 0 \\ -N & \mathrm{CL} \end{pmatrix} \tag{4.44}$$

Utilizing the next generation operator, we get

$$R_0 = \frac{\beta \cdot \mathrm{TU} \cdot N}{\delta_\mathrm{T} \cdot \mathrm{CL}}. \tag{4.45}$$

Which we also derive using the *survival function*. If initial infection is modeled, we can use the approximation $\mathrm{TU} \approx \lambda/\delta_\mathrm{TU}$, which will describe the initial expansion of infection.
Impact of drug treatment. Inhibitors have an impact on the proliferative terms in the virus dynamics model, as discussed previously in section 4.2.1. As an example, we consider the treatment with entry inhibitors EI and protease inhibitors PI, which decrease the rate of infection β and the amount of infectious virus that is released N, respectively. The basic reproductive number under treatment in the present example (eq. (4.45)) is described by:

$$R_0(\mathrm{EI}) = \frac{(1-\eta_\mathrm{EI})\beta \cdot \mathrm{TU} \cdot N}{\delta_\mathrm{T} \cdot \mathrm{CL}}. \tag{4.46}$$

$$R_0(\mathrm{PI}) = \frac{\beta \cdot \mathrm{TU} \cdot (1-\eta_\mathrm{PI})N}{\delta_\mathrm{T} \cdot \mathrm{CL}}. \tag{4.47}$$

$$R_0(\mathrm{EI},\mathrm{PI}) = \frac{(1-\eta_\mathrm{EI})\beta \cdot \mathrm{TU} \cdot (1-\eta_\mathrm{PI})N}{\delta_\mathrm{T} \cdot \mathrm{CL}}. \tag{4.48}$$

In the basic model, which does not include mutation and drug resistance, the population will go to extinction, if the drug decreases R_0 below 1.

R_0 of the Novel Two-Stage Model (eq. (4.37))

For our novel model eq. (4.37), we can derive the reproductive numbers for each mutant i under treatment j. In the model, we consider 5 infectious stages ($\mathrm{T}_1, \mathrm{T}_2, \mathrm{M}_1, \mathrm{M}_2$ and V). For the virus, we derive:

$$R_\mathrm{V}(i,j) = \frac{\beta_\mathrm{T}(i,j)\mathrm{TU} \cdot k_\mathrm{T}(i,j) \cdot \mathrm{N_T}(i,j)}{r_u \cdot r_T \cdot \delta_\mathrm{T2}} + \frac{\beta_\mathrm{M}(i,j)\mathrm{MU} \cdot k_\mathrm{M}(i,j) \cdot \mathrm{N_M}(i,j)}{r_u \cdot r_M \cdot \delta_\mathrm{M2}}$$

with constants

$$\begin{aligned} r_u &= \mathrm{CL} + \{\mathrm{CL_T}(i,j) + \beta_\mathrm{T}(i,j)\}\,\mathrm{TU} + \{\mathrm{CL_M}(i,j) + \beta_\mathrm{M}(i,j)\}\,\mathrm{MU} \\ r_T &= \delta_\mathrm{T1} + \delta_\mathrm{PIC} + k_\mathrm{T}(i,j) \\ r_M &= \delta_\mathrm{M1} + \delta_\mathrm{PIC} + k_\mathrm{M}(i,j) \end{aligned}$$

Since infected cells are also pathogens, which can lead to a rebound of the disease, even in the absence of any virus, we also determined their reproductive numbers under a given treatment j. The reproductive numbers $R_{\mathrm{T1}}(i,j)$ and $R_{\mathrm{M1}}(i,j)$ of the infectious stages T1 and M1, belonging to the viral strain i, are given by

$$\begin{aligned} R_{\mathrm{T1}}(i,j) &= \frac{k_{\mathrm{T}}(i,j)\cdot \mathrm{N_T}(i,j)}{r_T\cdot\delta_{\mathrm{T2}}}\cdot\frac{\beta_{\mathrm{T}}(i,j)\mathrm{TU}+\beta_{\mathrm{M}}(i,j)\mathrm{MU}}{r_u} \\ R_{\mathrm{M1}}(i,j) &= \frac{k_{\mathrm{M}}(i,j)\cdot \mathrm{N_M}(i,j)}{r_M\cdot\delta_{\mathrm{M2}}}\cdot\frac{\beta_{\mathrm{T}}(i,j)\mathrm{TU}+\beta_{\mathrm{M}}(i,j)\mathrm{MU}}{r_u}. \end{aligned}$$

The reproductive numbers $R_{\mathrm{T2}}(i,j)$ and $R_{\mathrm{M2}}(i,j)$ of the infectious stages T2 and M2 corresponding to the viral strain i are given by

$$\begin{aligned} R_{\mathrm{T2}}(i,j) &= \frac{\mathrm{N_T}(i,j)}{\delta_{\mathrm{T2}}}\cdot\left\{\frac{k_{\mathrm{T}}(i,j)\mathrm{TU}\cdot\beta_{\mathrm{T}}(i,j)}{r_u\cdot r_T}+\frac{k_{\mathrm{M}}(i,j)\mathrm{MU}\cdot\beta_{\mathrm{M}}(i,j)}{r_u\cdot r_M}\right\} \\ R_{\mathrm{M2}}(i,j) &= \frac{\mathrm{N_M}(i,j)}{\delta_{\mathrm{M2}}}\cdot\left\{\frac{k_{\mathrm{T}}(i,j)\mathrm{TU}\cdot\beta_{\mathrm{T}}(i,j)}{r_u\cdot r_T}+\frac{k_{\mathrm{M}}(i,j)\mathrm{MU}\cdot\beta_{\mathrm{M}}(i,j)}{r_u\cdot r_M}\right\} \end{aligned}$$

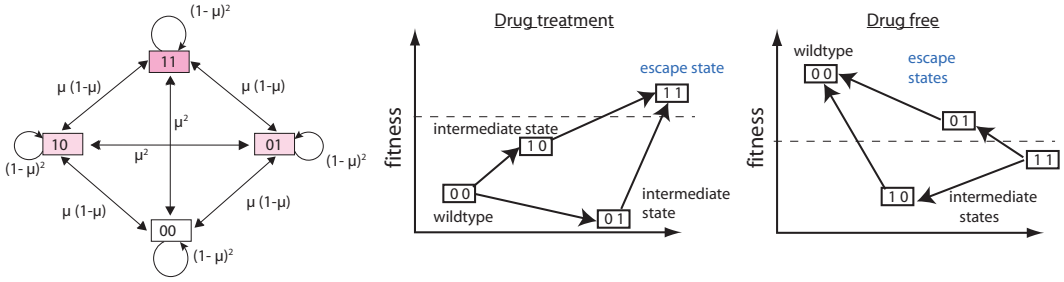

Figure 4.11: Fitness and possible mutational pathways depend on the environment. Left: General transition pathways. Central: Fitness in the presence of drug. Right: Fitness in the absence of drug. Dashed line: critical fitness that allows the strain to survive ($R0(i) > 1$)

In our novel model which includes mutation, drug resistance and endogenous fitness, we can look at every mutant i in any possible (pharmacological) environment j and evaluate whether this mutant is able to sustain the viral population ($R_0(i,j) \geq 1$), or not ($R_0(i,j) < 1$). This is highlighted in fig. 4.11 for two possible mutations. The leftmost figure shows the general transition paths, the central figure shows the fitness landscape in the presence of some drug j and the rightmost figure shows the fitness landscapes in the absence of any drug. The critical fitness $R_0 = 1$ is indicated by a dashed line. Viral strains, that can reproduce sufficiently in some (pharmacological) environment j ($R_0(i,j) \geq 1$) are termed "escape state".

The example in the central and right panels of figure 4.11, can be interpreted as follows: mutant type "10" confers high-level resistance to the drug, at the price of a reduced endogenous ability to proliferate. Mutant type "01" confers moderate resistance to treatment and has a slight selective disadvantage. The escape state "11" combines the high-level resistance of type "10" with the fitness of type "01". In the presence of strong drug treatment (central figure), it is more convenient to mutate from $00 \rightarrow 10 \rightarrow 11$, because even though "10" has impaired enzymatic abilities, it can still produce more offspring than "01". However "10" alone cannot sustain the population $R_0(10) < 1$, but it can delay the decline, because $R_0(10)$ is close to 1. In the absence of drug treatment the preferred mutational pathway is from $11 \rightarrow 01 \rightarrow 00$, because "01" has the smaller selective disadvantage compared to "10" and is thus able to produce most offspring in the drug-free environment. Also, type "01" is able to sustain the population in the drug-free environment on its own $R_0(01) > 1$.

4.4.2 Resistance Pathways

In fig. 4.12, we show examples of resistance pathways. In panel A, we have illustrated a resistance pathway that involves a single point mutation. This kind of resistance pathway has been observed e.g. with the NRTI lamivudine (3TC). A single-point mutation can be assumed to be readily present at the start of therapy.

In panel B, we show a resistance pathway, which involves an initial mutation that confers resistance to the drug, but also reduces the fitness of the affected enzyme considerably. Subsequent mutations restore the functionality of the enzyme. A similar resistance pathway has been suggested for zidovudine (AZT) resistance and some protease inhibitors [454, 510]. A resistance pathway, like the one shown in panel B, might develop after some initial delay.

In the case of some PIs, high-level resistance can emerge through accumulation of resistance-associated mutations [400]. This is highlighted in panel C.

In the last example (panel D), we show a case, where resistance can only develop after multiple steps of fitness loss, which then enable the emergence of mutants that are fit enough to sustain the population. This kind of resistance pathway has been suggested e.g. for influenza in the case of adaptation to a new host-species [511], and might also be likely for HIV. The emergence of resistance under such a pathway requires a chain of multiple chance events to occur and might therefore emerge only after a very long time, if at all.

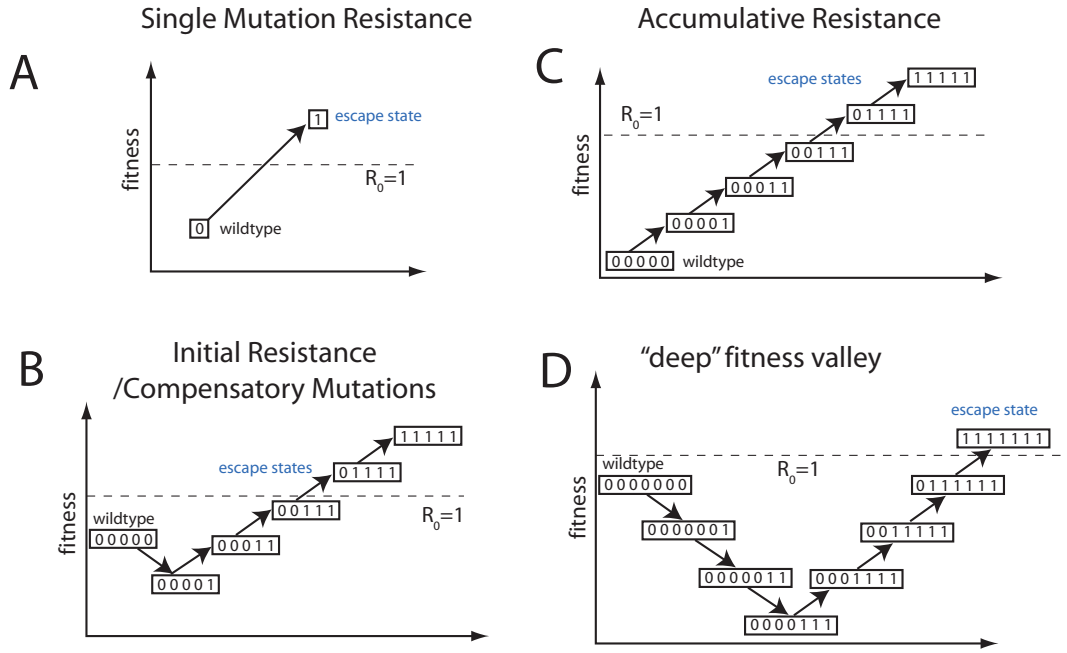

Figure 4.12: Examples of utilized resistance pathways. In panel A, B, C, D, we show the respective genotypes and their fitness in the presence of a drug j ($R_0(i,j)$) under drug pressure

With our model it is generally possible to implement each of these resistance pathways. However, our model eq. (4.37) becomes very high-dimensional: The number of species is $\#\text{Species} = (3+5\cdot\#\text{Mutants})$. If we consider all possible combinations of mutations/attributes, then the number of mutants is $\#\text{Mutants} = 2^{\text{pos}}$, where 'pos' refers to the number of positions/attributes, which are considered. In order to compute all transition rates, it is necessary to perform $\mathcal{O}(\#\text{Species})^2$ calculations, due to the nested loop in the mutation/transition paths. Therefore, there are computational limits on the number of mutations to be considered.

4.5 The Reproductive Capacity R_{cap}

The previously introduced reproductive number $R_0(i,j)$ evaluates the ability of each strain i to reproduce in a (pharmacologically modified) environment j, however it does not provide any information about the actual viral population within the host. If $R_0(i)$ is defined for each mutant strain i in a quasi-species model (as above), then the general threshold that has previously been defined might not hold. Imagine an example with two viral strains $m1$ and $m2$. One mutant strain is fit $R_0(m1) > 1$ and one is very unfit $R_0(m2) < 1$. There is a transition between the two variants due to mutation. The unfit strain $m2$ might not produce enough offspring to sustain its own population size, however, because there is a influx (due to mutation) from the fitter strain $m1$ it might nevertheless not die out. This problem is particularly due to the fact that R_0 does not consider the population (and possible transition paths therein), but rather each mutant i for itself. To overcome this limitation, we introduce the reproductive capacity R_{cap}.

The reproductive capacity R_{cap} combines the state of infection, with the reproductive numbers $R0(i,j)$, which evaluate the reproduction of each mutant i from the perspectives of a treatment j. The reproductive capacity R_{cap} of the entire HIV population is the summation over the reproductive capacity of all pathogens (in our model: free virus, infected T-cells and infected macrophages) belonging to all mutant strains i. Therefore, $R_{cap}(j)$ denotes the expected total number of offspring that the infection will produce in one round of replication under a certain treatment j, starting from the current state of the infection.

$$\begin{aligned} R_{cap}(j) &= \sum_i \Big\{ V(i)R_V(i,j) + T_1(i)R_{T1}(i,j) + M_1(i)R_{M1}(i,j) \\ &\qquad + T_2(i)R_{T2}(i,j) + M_2(i)R_{M2}(i,j) \Big\} \end{aligned} \tag{4.49}$$

Eq. (4.49) also implies that $R_{cap}(j)$ (of treatment j) only considers mutants, which are able to produce offspring ($R_0(i,j) > 0$) under treatment j.

Replication and resistance emergence. Besides the possible pre-existence of resistance strains, as discussed earlier, a second major challenge to effective drug treatment is the emergence of resistant viral strains through ongoing replication. The probability for new mutants to emerge is correlated with the extend of replication, since new mutations can only emerge, if new viral RNA is reversely transcribed (genotypically) and integrated into the host genome (phenotypically). In the asymptomatic stages of an HIV infection, the level of infectives (virus, infected cells) is kept roughly constant and the entire population of infected cells is replaced every 1.2 days [512] – 1.4 days [11]. Utilizing the previously introduced numbers ($\approx 10^7$ infected cells [115] and a mutation rate of $3 \cdot 10^{-5}$ per round of reverse transcription per base [4]), we therefore expect to have ≈ 230 new mutant strains with any specific point mutation per day. If a treatment decreases the amount of infection to 1 % (e.g. 99 % effective treatment), then the probability, that a new mutant strain is produced within a day is still 230 %. The previously introduced reproductive capacity provides a good estimate for the probability that new mutations emerge, because $R_{cap}(j)$ estimates the total amount of replication, which is directly correlated to the probability that new mutations emerge. Secondly, because $R_{cap}(j)$ considers the population of infectives, it is also a good indicator of the state of infection.

4.5.1 R_0 of the Whole Population

There are two possible ways to implement R_0 in a quasi-species model: (i) R_0 can be considered for each viral strain, and will therefore be a constant. (ii) The reproductive ratio is defined for the whole population (including all mutants), and is therefore not constant, as the composition of viral strains might change and impair the overall productivity P and the lifetime L of the viral population. If at initiation of a selective pressure (e.g. antiviral treatment), the overall population is unfit ($R_0 < 1$), adaption might change the population composition, increase the overall R_0 and lead to the survival of the population of infectives (see fig. 4.13, dashed red line).

If we normalize eq. (4.49) with the total population size , we receive the mean reproductive number of the total virus population $\overline{R_0}(j)$, which is time-varying (not constant), because the population composition changes, in contrast to the previously defined $R_0(i,j)$ of every mutant i. The mean reproductive number of the total population $\overline{R_0}(j)$ is defined by:

$$\overline{R_0}(j) \quad = \quad \frac{1}{\sum_i \mathrm{V}(i) + \mathrm{T}_1(i) + \mathrm{M}_1(i) + \mathrm{T}_2(i) + \mathrm{M}_2(i)} \cdot \mathrm{R}_{\mathrm{cap}}(j) \tag{4.50}$$

for our model in eq. (4.37).

4.5.2 Evaluation of Markers of Virological Failure

In figure 4.13 we illustrate the virus load (left), the mean total reproductive number $\overline{R_0}(j)$ (dashed red line, right) and the reproductive capacity $\mathrm{R}_{\mathrm{cap}}(j)$ (solid blue line, right) in the event of a drug failure, due to resistance emergence. On the left figure, it can be seen that total virus load (solid

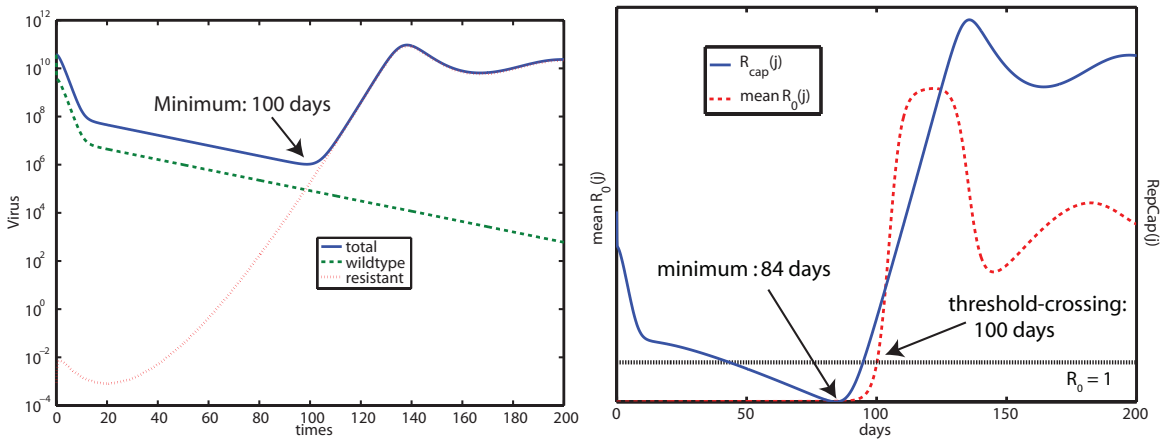

Figure 4.13: Markers of virological failure. Left: total viral load (solid blue line), wildtype strain (dashed green line) and resistant strain (dotted blue line). Right: Corresponding mean total reproductive number $\overline{R_0}(j)$ (dashed red line, left y-axis) reproductive capacity (solid blue line, right y-axis). Utilized parameters: Applied drug combination: 1 PI + 2 NRTI, all 90% efficient against the wildtype. s = 0.7 per mutation. One point-mutation caused 90% resistance against the respective drug. The fraction of un-infectious virus particles was assumed to be 50% in the absence of drug. The simulation was started from a steady-state distribution (in the absence of drug). Other parameters: $\lambda_{\mathrm{T}} = 2 \cdot 10^9, \lambda_{\mathrm{M}} = 4.95 \cdot 10^8, \delta_{\mathrm{T}} = \delta_{\mathrm{T}_1} = 0.02, \delta_{\mathrm{T}_2} = 1, \delta_{\mathrm{M}} = \delta_{\mathrm{M}_1} = \delta_{\mathrm{M}_2} = 0.0495, \delta_{\mathrm{PIC}} = 0.35, \beta_{\mathrm{T}} = 9 \cdot 10^{-12}, \beta_{\mathrm{M}} = 1.5 \cdot 10^{-14}, k_{\mathrm{T/M}} = 0.35, N_{\mathrm{T}} = 1000, N_{\mathrm{M}} = 100, \mathrm{CL} = 23$

blue line) declines upon treatment initiation, reaches a minimum at $\approx$ 100 days and then rebounds and stabilizes. The rebound is solely contributed to the emergence of a resistant strain (dotted red line), while the wildtype virus (dashed green line) declines. In the right figure, we have illustrated the corresponding $\overline{R_0}(j)$ (dashed red line) and $\mathrm{R}_{\mathrm{cap}}(j)$ (solid blue line). The reproductive capacity $\mathrm{R}_{\mathrm{cap}}(j)$ reaches a minimum at $\approx$ 84 days, which is much earlier than the corresponding minimum for the viral load. This is because $\mathrm{R}_{\mathrm{cap}}(j)$ indicates a tradeoff between the population size of susceptible- and resistant resistant strains in terms of their ability to produce offspring. In other words, in $\mathrm{R}_{\mathrm{cap}}(j)$, we use the reproductive numbers $R_0(i,j)$ as weighting functions for the respective mutant populations. Therefore, the "risk potential" of a mutant strain under a certain treatment j is evaluated. For treatment j, failure starts when the minimum in $\mathrm{R}_{\mathrm{cap}}(j)$ has passed, because from this moment onwards, treatment j cannot reduce the overall number of expected offspring.

In fig. 4.13 (right), we have illustrated the mean reproductive number $\overline{R_0}(j)$ (dashed red line). $\overline{R_0}(j)$ indicates whether the total population is expected to decrease- or increase, respectively if $\overline{R_0}(j) < 1$ or $\overline{R_0}(j) > 1$. Since the virus is usually the most abundant species with the fastest dynamics, a threshold-crossing ($\overline{R_0}(j) = 1$) and a minimum in the viral load appear at the same time

($\approx$ 100 days).

While the viral load and the mean reproductive number $\overline{R_0}(j)$ evaluate the trajectory of the total population of infectives, $R_{cap}(j)$ has the ability to evaluate the "risk potential" of a population under a certain treatment and is able to detect viral failure prior to any of the other markers. Therefore, $R_{cap}(j)$ has the ability to forecast events, such as virological failure, in contrast to virus load and $\overline{R_0}(j)$, which are descriptors of the actual state of infection and -change.

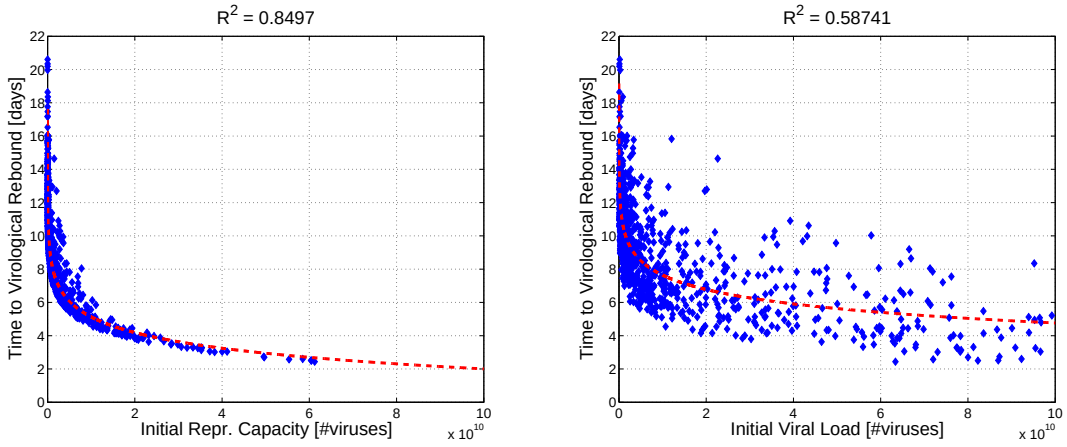

Figure 4.14: **Reproductive Capacity vs. Viral Load as a Predictor of Virological Failure.** The time to virological rebound is much better correlated to the initial reproductive capacity (left panel) than to the initial viral load (right panel). The data (marked by '♦') shows the time to virological rebound with respect to initial viral load and reproductive capacity, respectively, observed in a set of 1000 simulations for a treatment containing PI/MI + (2 x NRTI). The initial viral population for each simulation was chosen randomly, the selective disadvantage s was 1%, the drug efficacy was assumed to be 90%, and the fraction of uninfectious viruses was set to 0.67. The dashed red lines show the exponential fit of the data.

We demonstrate in Fig. 4.14 that the reproductive capacity is a much more precise indicator of treatment failure than the decay of total viral load for a drug combination consisting of a PI and 2 NRTIs. We also tested other drug combinations (EI + 2 NRTI, InI + 2 NRTI and NNRTI + 2 NRTI) and parameter sets in [513] and derive the same conclusion.

4.5.3 Evaluation of Markers for Drug Efficacy

We evaluated the impact of antiviral drugs on viral load (fig. 4.15, left) and reproductive capacity (fig. 4.15, right).

All drugs, except for the novel class of integrase inhibitors (InIs) produce identical viral load declines. Based on our detailed model and the subsequently derived simplified model, this can be explained as follows: EI and RTIs decrease the infection rate and thus the number of new infections. This has an impact on the release of virus (and therefore on the virus decline) indirectly through the viral life cycle. MIs and PIs do not interfere with the total amount of virus that is being released (rate $\widehat{N}$), but rather shift the ratio of infective virus-to-total virus $V_I : V_{tot}$ (see fig. 4.3 and fig. 4.15, inset) by affecting rate N (eq. (4.36)). Therefore, the immediate effect of PIs and MIs is not on total virus release, but rather on infective virus, which has an impact on the number of new infections. Subsequently, their impact on virus release is indirect through the viral life cycle.

$$\text{new infections} \quad = \quad \overbrace{\beta}^{\text{EI, RTI}} \cdot \text{TU} \cdot \underbrace{V_I}_{\text{PI,MI}} \stackrel{\text{life-cycle}}{\longrightarrow} \text{virus release} \tag{4.51}$$

Therefore, EIs, RTIs, PIs and MIs produce identical viral decays (see Fig. 4.15), if they are equally potent inhibitors. InIs on the other hand, decrease the amount of late infected cells (see fig. 4.5),

which has an immediate impact on virus release.

$$\text{virus release} \quad = \quad \widehat{\mathrm{N}} \cdot \underbrace{\mathrm{T}_2}_{\mathrm{InI}} \tag{4.52}$$

Thus, the onset of observed viral decay is faster for InIs, than with other compounds, irrespective of their potency (which was set equal for all compounds in fig. 4.15, left), because the impact is immediate and not delayed by the viral replication cycle as in the case of all other compounds.

This also implies, that the efficacy η of all compounds, except InIs can be related on the basis of viral load decay, as it is currently done. Inferring that novel integrase inhibitors are more potent than existing drugs, based on viral load decline alone, might produce false conclusions. Murray et al. [484, 497] have implied that novel InIs might be more potent than existing drugs, based on viral load decline. However, Sedaghat et al. [498,499] have argued that the efficacy of InIs, relative to other drug-classes, cannot be assessed, based on viral load. Finally, Shen et al. [131] have shown *ex vivo*, that integrase inhibitors are among the least potent antiviral drug-classes.

We show the reproductive capacity $\mathrm{R}_{\mathrm{cap}}(\phi)$ (evaluated at the drug-free setting) for the same simulation in fig. 4.15 (right). In contrast to total viral load, the reproductive capacity discriminates between RTIs, FIs, CCR5-antagonists, PIs and MIs.

Protease and maturation inhibitors are most efficiently reducing the reproductive capacity. The reproductive capacity $\mathrm{R}_{\mathrm{cap}}(\phi)$ after PI/MI application in fig. 4.15 sets to an overall lower level. Because of the high turnover of free virus [490], the compartment of infective virus $\mathrm{V_I}$ is eliminated completely by a 100 % effective PI/MI, in contrast to the other inhibitors, in which case $\mathrm{V_I}$ is proportional to either T_2 or M_2.

InIs are reducing $\mathrm{R}_{\mathrm{cap}}$ more efficiently than RTIs and EIs. A side-effect of the inhibition by InIs is the reduction of the clearance of the proceeding compartment (see fig. 4.5). This clearance term appears in the denominator of the reproductive capacities $\mathrm{R}_{\mathrm{cap}}$ and thus explains the higher starting value for the reproductive capacity in fig. 4.15 (right). Clearance of the post-integration compartment results in a proportional clearance of virus, as the netto production of virus shrinks (fig. 4.15, left).

The instantaneous effect of NRTIs, NNRTIs, CCR5 inhibitors and FIs on $\mathrm{R}_{\mathrm{cap}}(\phi)$ is comparable (fig. 4.15). The difference between entry inhibitors and reverse transcriptase inhibitors is marginal, because, under the chosen parameter set, the clearance of virus by infection is negligible compared to the clearance by the immune system. A 'side effect' of entry inhibitors (FI/CCR5) and RTIs (NRTIs/NNRTIs) is an increased number of uninfected cells, thus leading to an initial increase in the reproductive capacity, as more potential targets become available.

4.5.4 Determinants of Drug Efficacy *in vivo*

The reproductive capacity does not only take the potency of a drug into account, but also the impact of the host defence mechanism on the viral dynamics.

In figure 4.15 (right) we have assumed equal potencies for all tested drug classes. The different decay patterns for the reproductive capacity $\mathrm{R}_{\mathrm{cap}}$ are therefore solely contributed to the decay patterns of the infective compartments ($\mathrm{V_I}$, T_1, M_1, T_2, M_2) after drug application. In our model, we generally have the following relation [490]: $\mathrm{CL} \cdot \mathrm{V_I} > \delta_{\mathrm{T}_2} \cdot \mathrm{T}_2 > \delta_{\mathrm{T}_1} \cdot \mathrm{T}_1$. Thus, PIs and MIs, which constrain the production of $\mathrm{V_I}$, reduce $\mathrm{R}_{\mathrm{cap}}$ most efficient in the initial phase followed by InIs, which constrain the production of T_2, and finally RTIs and EIs, which impair the production of T_1. Infectious virus $\mathrm{V_I}$ is the most abundant compartment after treatment with EIs, RTIs and InIs, dominating $\mathrm{R}_{\mathrm{cap}}$. However, under effective PI/MI treatment $\mathrm{N_{T,M}}$ is close to zero and thus $\mathrm{V_I}$ might be become smaller than the other infective compartments. This pushes $\mathrm{R}_{\mathrm{cap}}$ in the case of PI/MI application below the levels achieved by other inhibitor classes.

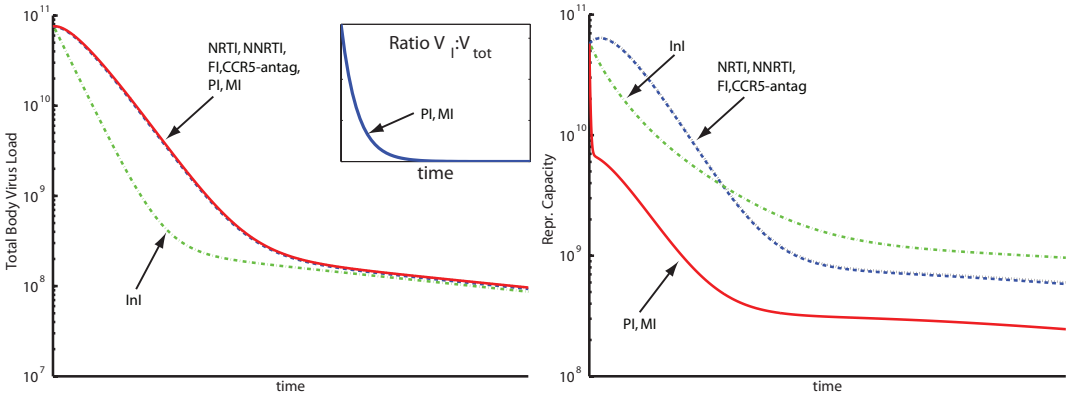

Figure 4.15: Left Panel: Total virus load decay after treatment initiation. Integrase inhibitors (InI) produce a faster decay of virus load than all other compound classes. Inset: Protease- and maturation inhibitors (PI and MI) change the ratio of infectious-to-total virus. Right panel: The reproductive capacity takes the total amount of expected viral offspring into account. Protease inhibitors (PI) and maturation inhibitors (MI) most effectively reduce the reproductive capacity. The reproductive capacity decreases more rapidly with integrase inhibitors (InI) compared to NRTIs, NNRTIs, FIs and CCR5-antagonists, but reaches the same level after some time. Initial infection was assumed to be all wild type. Drug efficacy was assumed to be 100%.

Average Time to Virological Rebound (days)							
Combination	30%	25%	20%	15%	10%	5%	1%
InI	73.4	66.1	60.2	55.3	51.3	47.8	45.6
FI/CCR5-antag.	133.4	105.5	81.6	68.2	58.7	51.0	46.5
NNRTI	140.5	107.6	85.7	69.5	59.1	51.3	46.7
PI/MI	142.9	107.6	86.0	70.0	59.6	51.3	46.9
InI	0.514	0.462	0.421	0.387	0.359	0.334	0.319
FI/CCR5-antag.	0.934	0.738	0.571	0.477	0.411	0.357	0.326
NNRTI	0.983	0.753	0.600	0.487	0.414	0.359	0.327
PI/MI	1.000	0.753	0.602	0.490	0.417	0.359	0.328

Table 4.1: The time to virological rebound depends on both the cost of resistance s and the choice of drugs. Each table entry shows the average time to virological rebound in an ensemble of 1000 hybrid stochastic-deterministic simulations, where we assumed that the efficacy of the drugs against the wildtype was 90%. The drug was 45% effective against a one-mutation strain and completely inefficient against the double-mutant. The fraction of uninfectious viruses was set to two-thirds.

Thus, we conclude that the target half life is another important factor for the *in vivo* efficacy of an HIV compound, besides the affinity of a drug to its molecular target, its pharmaceutical penetration into target cells and its genetic barrier to resistance.

The different decay patterns also manifest in the time to virological rebound that is shown for the different drug classes in Table 4.1. However, for InIs, another factor gains importance: Since InIs reduce the decay of T_1 (see fig. 4.5), T_1 accumulates, which increases the probability to develop resistance (see eq. (4.37)):

$$\text{new mutations:} \qquad \mu \cdot \underbrace{T_1(k)}_{\text{increased by InI}} \cdot k_{T/M}(k) \cdot p_{k \to i}. \tag{4.53}$$

4.5.5 Experimental Equivalents of Model-derived Reproductive Capacity

Phenotypic assays [514] are the experimental counterpart to the calculated reproductive capacity $R_{cap}(j)$. These assays can take patient derived viral sequences, which are inserted into a modified viral vector, which possesses a reporter gene and lacks the Env (envelope) gene that is required for

infection. These modified viruses are then co-transfected with murine leukemia virus Env-genes into cells to produce infective viral particles, which are subsequently harvested (fig. 4.16). The harvested virus is incubated together with target cells. Through transcription and translation, this modified virus will produce the reporter gene product intracellularly, which can be measured as output. Therefore, phenotypic assays monitor the entire viral life-cycle (single-round infectivity), starting from the production of particles after co-transfection, to infection and amplification of gene products.

Phenotypic assays/single-round infectivity assays can assess the reproductive capacity R_{cap} of patient virus samples under different drugs combinations and dosages [130]. Because PIs alter the maturation of virus, they are applied during the step of transfection, while all other drugs are applied during the step of infection (see fig. 4.16).

Originally, these assays were restricted to patient-derived Pol gene fragments [514], which harbor resistance mutations against PIs, and RTIs. However, Shen et al. [131] have extended these assays and used them for PIs, InIs, RTIs and FIs, to compare class-specific efficacy of anti-HIV drugs.

To date, these assays have two major disadvantages, which limit their utility in clinical practice: (i) Minor viral strains are being lost during the initial amplifications procedures. (ii) The turnover time is a few weeks (personal communication with R. F. Siliciano).

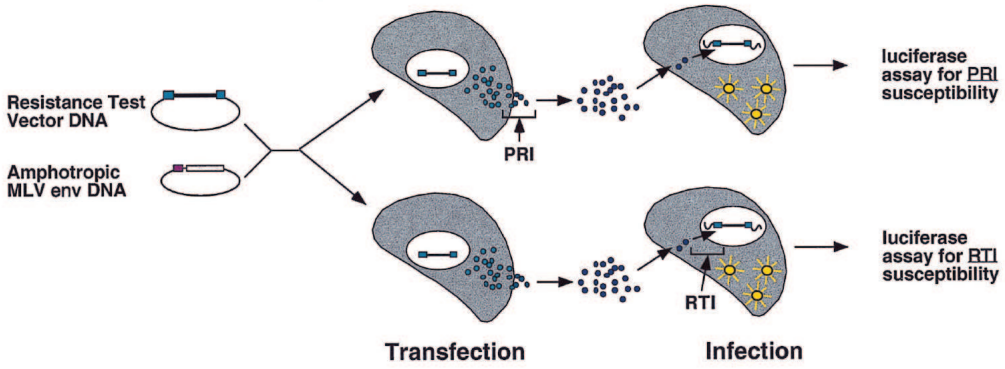

Figure 4.16: Principles of a phenotypic single-round infectivity assay. Illustration taken from [514].

4.6 Treatment Sequencing to Minimize Drug Resistance Development

The existence of a reservoir of latently infected cells has motivated the National Institute of Health (NIH) to re-define the treatment goals for HAART, with the primary goal being the management of the disease, rather than the attempt to eradicate the virus [2]. However, the goal of virological suppression is achieved in only ≈50% of patients who receive HAART in a non-clinical trial setting [245–248]. One of the main reasons for therapy failure is the rapid emergence of drug resistance [515, 516], due to the enormous viral mutation rate [4].

Up to now, new means to address the problem of drug resistance have arisen, as the breadth of available treatment options continuously expands. Today, there are 25 antivirals from 6 distinct drug classes on the market (see e.g. [108]) and many more in late clinical trials (see e.g. [243]). In order to overcome resistance development, we propose to use the novel antiviral tools, which for the first time, allow strategic sequencing of therapy across multiple treatment lines. In HAART, treatment change is largely restricted to treatment failure/viral relapse [517] and there is little consensus when a treatment change would be optimal [2, 518]. Considering the rapid viral turnover [13], treatment

change in the context of viral relapse presumably lies beyond an optimal point of treatment switching.

In the following, we will present a mathematical method to determine the optimal switching time and to choose the optimal drug combination for the *next* treatment period. The method uses only information that is available at the time of decision. The rationale of the strategy is thus transferable to clinical decision making. We will analyze our strategy in a model of virus dynamics (eq. (4.37)), that allows the mechanistic incorporation of all novel (and most prospective) HIV drugs. The virus dynamics model considers viral resistance development to any pharmacological challenge by mutation.

4.6.1 Idea.

HAART therapy is switched in the case of virological rebound [2]. In figure 4.17 we have illustrated the expected time course (based on the model in fig. 4.7) of the viral population in the context of a failing drug regimen: In the first phase the total virus load declines (solid black line, shaded area). This is because susceptible strains, that make up the majority of the viral population, are decreased in numbers (dashed blue line, wt). Beneath the total viral kinetics, viral strains, that are resistant to the current drug regimen are selected from the population of viruses (dash-dotted green line, m1). In the second phase, resistant strains have become more abundant than susceptible strains and therefore dominate the kinetics of total viral load. This subsequently leads to the rebound of total virus and the restoration of infection (solid black line, shaded area).

We argue that drug switching in the case of virological rebound confers little benefit for the *next* drug combination: As the viral population size increases, it becomes more likely that viral strains arise, that are resistant to the *next* drug combination (that is 'm2' in the upper panels of figure 4.17 and the dotted line in the lower panel) and subsequently it becomes more likely that the *prospective* combination will fail. Therefore, it is unfavorable to wait until virological failure, in view of any *prospective* treatment: In the case of virological failure, the likelihood that viral strains exist, that readily confer resistance against the *prospective* treatment is similar compared to the time of treatment initiation (see figure 4.17, upper panels).

In view of a treatment switching strategy, the main idea is to evaluate the actual state of infection in terms of a *prospective* treatment: E.g. "when does the *actual* treatment not confer benefit for a *prospective* treatment". We will introduce the mathematical criteria in section 4.6.3. However, we will first discuss the requirements from the simulation perspective in order to model a drug switching strategy mathematically.

4.6.2 Modelling Requirements & Simulation Technique

The overall virus dynamics in our model (eq. (4.37)) comprises different viral strains with copy numbers that can vary over several orders of magnitude. If the amount of at least some of the reactant species are not too many orders of magnitude larger than one, discreteness and stochasticity may play important roles for the evolution of the system [519]. Whenever that happens, then continuous rate equation models do not accurately describe the system's true behavior. In our application this has particular relevance, since deterministically, it is not possible to simulate eradication of certain viral strains. We have illustrated the difference between the continuous- (deterministic) and a stochastic solution (using the direct method [520, 521]) of a viral dynamics system in fig. 4.18 (left). In fig. 4.18 (left), a treatment (treatment 1) is applied, that reduces the abundance of a viral mutant that confers resistance against the *next* treatment (treatment 2). In the stochastic setting, the viral mutant is eradicated at $t \approx 20$, whereas in the deterministic setting, the abundance of the viral mutant falls below the threshold of one (which might be interpreted as the expectation of eradication). After treatment change (fig. 4.18, left), virus immediately relapses in the deterministic solution of the system, whereas this is not the case in the stochastic implementation, because the virus had already been cleared at $t \approx 20$.

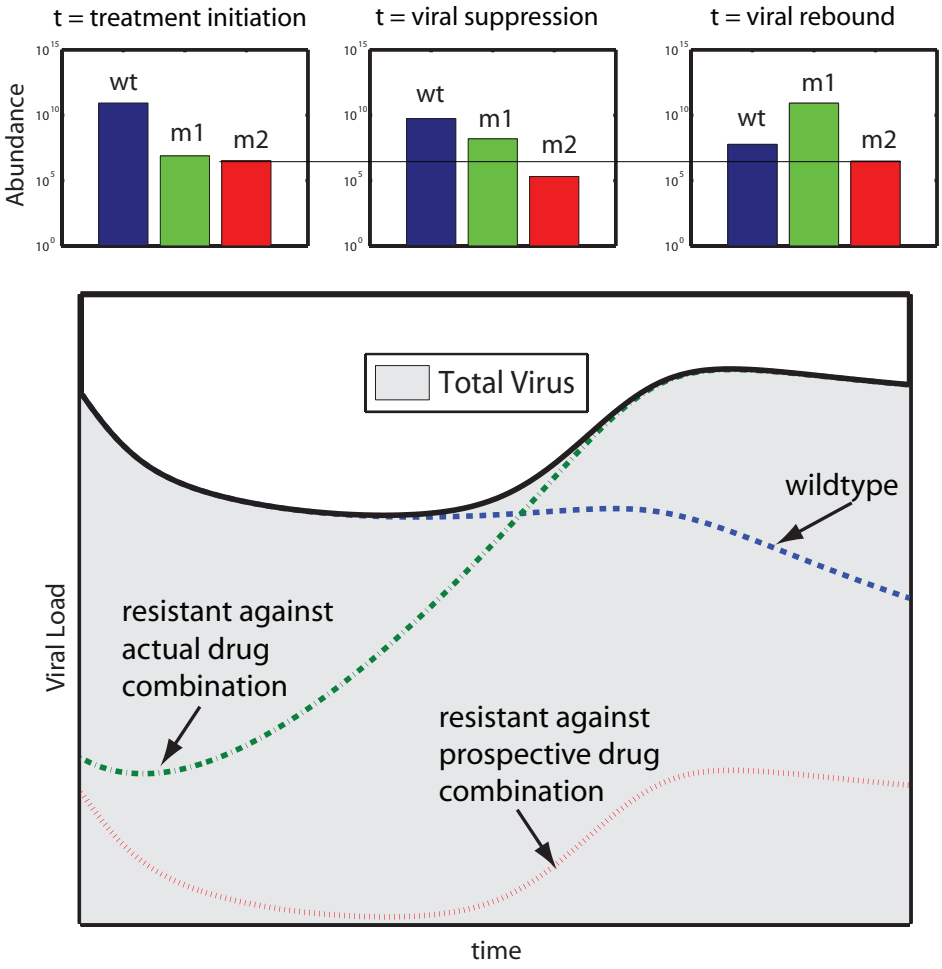

Figure 4.17: Time course of infectious compartments between treatment initiation and failure. Inset I, II & III: Frequency of mutants at the start of therapy, at the minimal total viral load and after treatment failure.

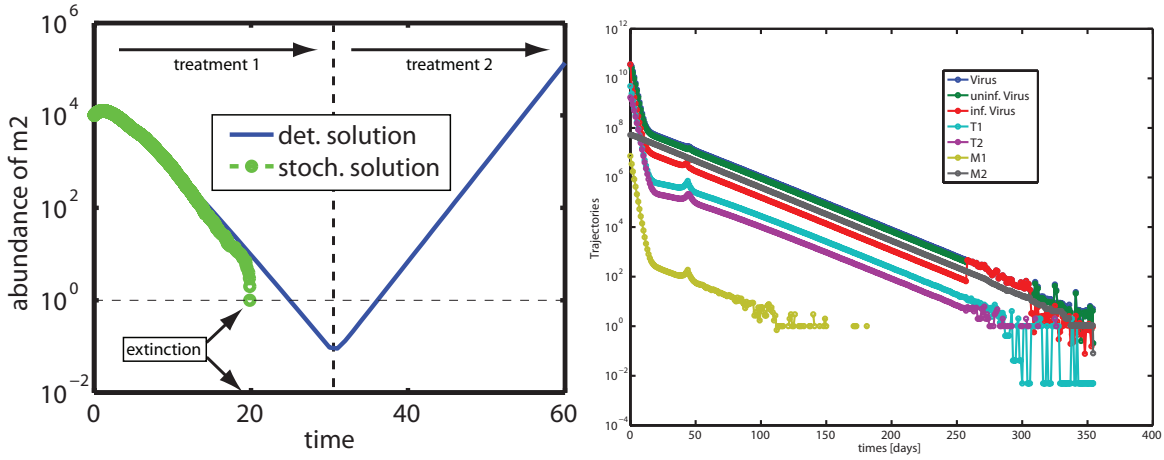

Figure 4.18: Left: The time course of a virus, that is resistant against treatment 2, modelled deterministically (blue line) and stochastically (green circles). In the stochastic simulation the virus dies out, whereas it cannot die out in the deterministic simulation, subsequently causing the virus to rebound after treatment change. Right: Sample trajectory of viral infectives utilizing hybrid stochastic-deterministic modelling techniques in the case of complete eradication. For simulations, the model in eq. 4.37 was utilized with optimal treatment switching criteria (eq. (4.54), (4.55)).

Stochastic kinetics describe the time evolution of a well-stirred reacting system in a way that takes honest account of the systems discreteness and stochasticity. In the presented example, this provides a much more accurate description of the system's kinetic behavior, when low numbers of reactants are involved. However, for a large number of reactants, the deterministic solution works quite well (fig. 4.18, left part). For this reason we have chosen a hybrid (stochastic-deterministic) setting for numerical simulation; We thus (i) take stochastic fluctuations in the slow reaction processes into account and (ii) reduce the computational costs for the simulation of the fast (deterministic) system dynamics. We use the direct hybrid method proposed in [506]. Elementary reactions were treated stochastically, whenever their propensity function or the quantity of at least one of their reactants has fallen below a certain threshold (for all numerical simulations this threshold was set to five).

In fig. 4.18 (right) we show a sample trajectory of HIV decay, simulated using the hybrid simulation approach and the model in fig. 4.7. As can be seen in the figure, the kinetics of different infectious compartments behave deterministically, until their abundance decreases below a certain threshold, after which they behave stochastically, eventually being eradicated.

4.6.3 Switching Strategy

Knowing that virological failure does not constitute an optimal switching time, what are the parameters, that determine the optimal switching time and which strategy might possibly improve the performance of HIV-therapy?

We have previously introduced the reproductive capacity in section 4.5 (eq. (4.49)). The reproductive capacity $\mathrm{R}_{\mathrm{cap}}(j)$ denotes the expected amount of offspring under treatment j. It provides a balance between the abundance of a mutant strain i and its ability to produce offspring. It can therefore forecast the effects that any potential treatment $j \in J$ would have, at each state of the infection. We have shown in fig. 4.13 that $\mathrm{R}_{\mathrm{cap}}(j)$ can detect virological failure prior to other markers, like e.g. viral load or $\overline{R_0}$. $\mathrm{R}_{\mathrm{cap}}$ constitutes, therefore, a good function for optimization.

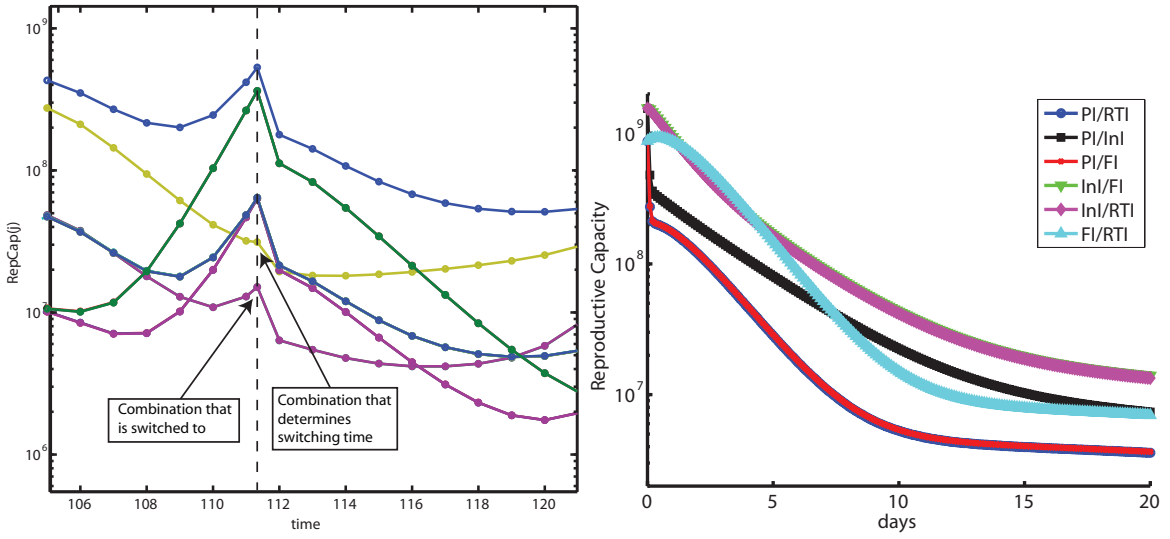

Figure 4.19: Left: **When to switch:** Time course of the reproductive capacity $\mathrm{R}_{\mathrm{cap}}(j)$ for all available treatments. At any timepoint t it is not known whether the overall minimum in $\mathrm{R}_{\mathrm{cap}}(j)$ has been reached, as long as the $\mathrm{R}_{\mathrm{cap}}(j)$ is decreasing for some alternative treatment. Therefore, we choose the point in time, when the last $\mathrm{R}_{\mathrm{cap}}(j)$ has reached its minimum (the yellow line) as switching time. **What to switch to:** It is best to choose the treatment that has the smallest $\mathrm{R}_{\mathrm{cap}}(j)$ (thus the best starting condition) after the time for switching has been determined (magenta line). Right: Impact of various drug combinations on the initial reduction in the reproductive capacity. $\mathrm{R}_{\mathrm{cap}}(\phi)$ evaluated at the drug free state.

When to Switch.

Given an *actual* treatment $k \neq j$ we want to assess: when does k stop to be beneficial in terms of the viral population for the *next* treatment j? Upon the initiation of a treatment regimen, the reproductive capacity $\mathrm{R_{cap}}(j)$ decreases (see figure 4.19), because susceptible strains are cleared. When viral rebound begins, the population of replication-competent infectives, that might confer resistance to any prospective treatment j, increases. A saddle point in $\mathrm{R_{cap}}(j)$ denotes the point in time where the trade-off between increase of susceptible- and decrease of resistant viral strains is reached.

The saddle point can be determined by taking the derivative of $\mathrm{R_{cap}}(j)$ as the objective function. Under the previously described assumptions, the derivative should turn from negative to positive.

$$\begin{aligned} &\text{switch if:} \\ \min_{j \in J} \left(\frac{\mathrm{d}}{\mathrm{d}t} \mathrm{R_{cap}}(j) \right) &= 0. \end{aligned} \tag{4.54}$$

The time, when the last saddle point in $\mathrm{R_{cap}}(j)$ for all $j \in J$ is reached, is our criteria to switch treatment, because at the actual time it is not certain whether some $\mathrm{R_{cap}}(j)$ might reach the overall smallest value of all possible drug combinations J, as long as it is still decreasing (see fig. 4.19).

What to switch to.

When a treatment switching point is being detected, it is best to choose the treatment as the *next* regimen, that allows the smallest amount of replication (= resistance development). The reproductive capacity $\mathrm{R_{cap}}(j)$ determines exactly this quantity. Therefore, treatment regimen j is chosen, if $\mathrm{R_{cap}}(j)$ is minimal over all alternative treatment options J.

$$\begin{aligned} &\text{switch to j if:} \\ \mathrm{R_{cap}}(j) &= \min_{j \in J} \left(\mathrm{R_{cap}} \right). \end{aligned} \tag{4.55}$$

4.6.4 First Combination

In table. 4.1 we have shown that the time to virological rebound depends on the compound, or more precisely on the half life of the drug's target. In terms of the reproductive capacity, we have shown that different drug classes induce different decay dynamics for the reproductive capacity. For combinations of drugs this decay behavior is shown in fig. 4.19 (right). From fig. 4.19 (right) we infer that a combination of protease inhibitors (PI) and reverse transcriptase inhibitors (RTI) is most efficiently reducing the reproductive capacity initially.

We speculate, that it is important to reduce the infection's ability to produce offspring rapidly, because it would decrease the cumulative probability to develop resistance against any treatment. This speculation is visualized in fig. 4.15. In fig. 4.15 one drug (drug A) has a very rapid effect on the infection, that levels off quickly, while another drug (drug B) has a slower, but more sustained effect. In this example it might be of advantage to apply the drug with the rapid effect first, in order to minimize the initial propensity of resistance development and then to continue with a drug that exhibits a more sustained effect. Thus, the second drug makes use of the beneficial starting position and reduces the propensity of resistance development subsequently, minimizing the overall probability to develop resistance. The probability to develop resistance within a certain time-frame is related to the area-under-the-curve (AUC) of the propensity to develop resistance (fig. 4.15, left). The solid and the dashed line in fig. 4.15 represent a different sequence of the drugs (solid: first drug A, then B, dashed: first B, then A). It can be seen from this illustration that using a drug which has a rapid, but not sustained effect, prior to using a drug with a sustained effect, results in a decreased AUC.

For the considerations above, we choose an initial combination consisting of PI + RTI.

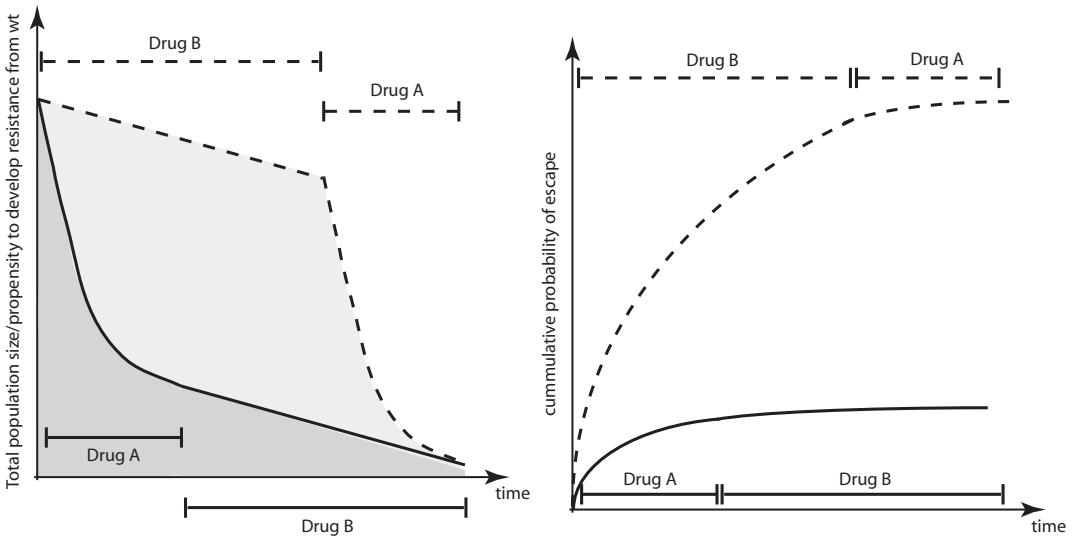

Figure 4.20: The probability to develop resistance might depend on the sequence of drugs. Left: The total population of infectives decreases faster, when a 'fast acting' drug (solid line) is applied first. The propensity to develop resistance can be assumed to be proportional to the population size. Right: The corresponding cumulative probability of escape for the two sequences of drugs. Drugs, which decrease the population of infectives very fast (act on infectives with short life-spans) are ideal in initial combinations.

4.6.5 Simulations

In figure 4.21 we show the trajectory of the reproductive capacity $\mathrm{R}_{\mathrm{cap}}(j)$ in the case of successful drug sequencing (eradication of all productively infected cells). The blue trajectory that lies above the other trajectories is the reproductive capacity evaluated in the absence of treatment $\mathrm{R}_{\mathrm{cap}}(\phi)$. Drug switching (indicated by dashed vertical lines) occurs at irregular patterns with longer periods of drug application as the infection approaches eradication ($t > 300$ days). The 'stairs' in the reproductive capacity (that coincide with drug switches) are related to the application of PI/MIs, which primarily affect the free infectious virus, which is cleared rapidly (thus causing 'stairs').

Since hybrid simulations represent one possible realization (subject to randomness), it is necessary to run multiple simulations to achieve statistically significant insights. In figure 4.22 (left) we show a Kaplan-Meier plot of the rate of success (defined as eradication of productively infected cells) as a function of time for 100 hybrids stochastic-deterministic simulations. In the example shown in figure 4.22 (left), treatment leads to viral rebound in 100% of all cases.

In fig. 4.22 (right) we show the average runtime of a single hybrid realization of the model (eq. (4.37)) with the indicated number of possible mutants. With the current implementation of the model, it is possible to consider 8 resistance mutations (average runtime = 35h on a single cpu with 2.833 Ghz).

4.6.6 Success-rate Depends on Number of Sequencable Drugs

We have evaluated the optimal treatment sequencing strategy with the virus dynamics model in table 4.2 (and fig. 4.7). For the evaluation in table 4.2, we have taken various worst-case scenario assumptions. (i) A single point mutation confers high level resistance to each drug. (ii) All free virus is infectious ($q \cdot p \cdot \rho_{\mathrm{PR}} = 1$). (iii) The initial composition of the viral population consists of both mutants and wildtype according to their fitness. Therefore, each resistance to a single drug is readily present at the initiation of the first therapy and multiply resistant mutants are likely to be present. In the simulation example, we chose to administer two compounds in parallel, which sets a lower barrier to resistance to each combination, but allows more combinations to be sequenced (and thus the algorithm to be tested). We evaluated combinations of selective disadvantage s and number of compounds that can be sequenced. For each field in table 4.2, we evaluated 100 simulations.

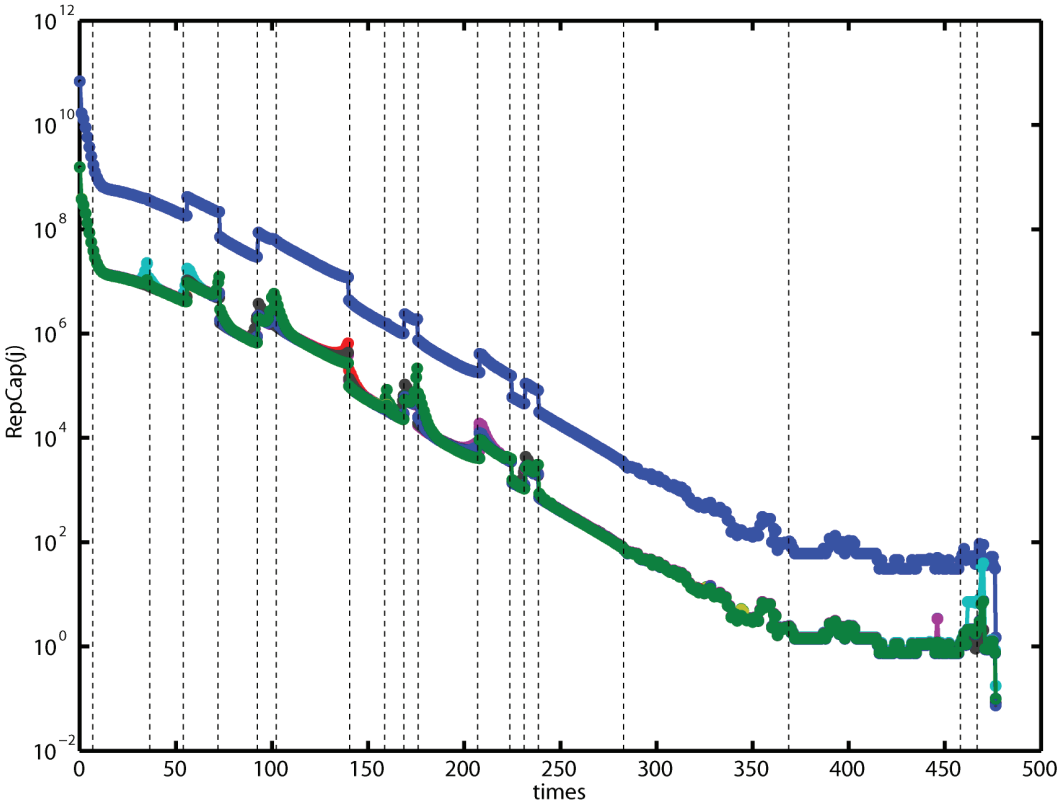

Figure 4.21: The reproductive capacity in the context of a succeeding drug sequencing strategy. blue line: $R_{cap}(\phi)$. Vertical dashed lines: switching times. Two drugs were given in parallel. Available drugs were 2 PIs, 1 NRTI, 1 NNRTI, 1 FI, 1 InI. The selective disadvantage of a resistance mutation $s = 0.7$. The drug efficacy was assumed to be 85 %. Single resistance mutations conferred 90 % resistance against the drug. 80 % of the virus was assumed to be infectious in the absence of any drugs. Other parameters: $\lambda_T = 2 \cdot 10^9$, $\lambda_M = 4.95 \cdot 10^8$, $\delta_T = \delta_{T1} = 0.02$, $\delta_{T2} = 1$, $\delta_M = \delta_{M1} = \delta_{M2} = 0.0495$, $\beta_T = 8 \cdot 10^{-12}$, $\beta_M = 8 \cdot 10^{-15}$, $k_T = 0.35$, $k_M = 0.35$, $N_T = 1000$, $N_M = 100$, cl = 23, $\delta_{PIC} = 0.35$. The lower threshold for the frequency of drug switching: 7days.

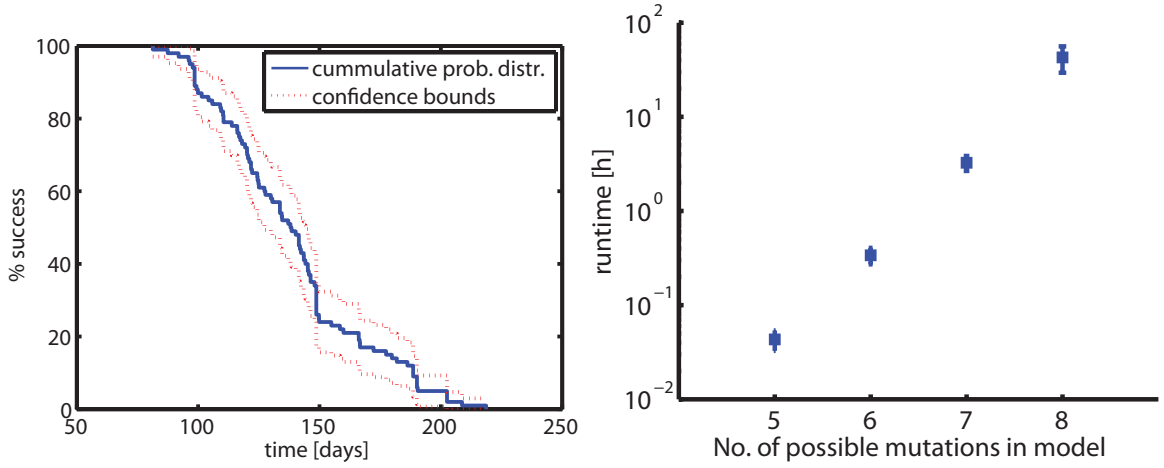

Figure 4.22: Left: Cumulative probability distribution of success in an ensemble of 100 hybrid stochastic-deterministic simulations. In the present example treatment is unsuccessful in 100 % of all cases (Simulation details: seven sequenceable drugs and a selective disadvantage of 20 % per resistance mutation). Right: The average runtime for hybrid simulations containing the indicated number of possible mutants. Error bars indicate standard deviation.

The simulation results show that the rate of success with our novel strategy increases with the number of drugs that can be sequenced. Therefore, with the exploitation of novel targets against

# ortho. drugs	4	5	6	7	8
$s = 0.6$	100%	100%	100%	100%	100%
$s = 0.55$	65 %	100%	100%	100%	100%
$s = 0.5$	15 %	100%	100%	100%	100%
$s = 0.45$	0 %	100%	100%	100%	100%
$s = 0.4$	0 %	91,92[1]%	99,100[1]%	100%	100%
$s = 0.35$	0 %	44,40[1]%	92,96[1]%	95,100[1]%	97,94[1]%
$s = 0.3$	0 %	0,1[1] %	59,78[1] %	67,71[1]%	79,88[1]%
$s = 0.25$	0 %	0 %	5,7[1]%	8,16[1]%	22,34[1]%
$s = 0.2$	0 %	0 %	0 %	0 %	1,1[1]%
$s = 0.15$	0 %	0 %	0 %	0 %	0 %

Table 4.2: % treatment success (no virological rebound during 1000 days) based on 100 simulations for each field. Simulations started in a steady-state distribution over all mutants (each single drug mutation present). Two drugs were given in parallel. 4 drugs were 2 PIs, 1 NRTI, 1 NNRTI 5: + FI, 6: +InI, 7: + CCR5-antagonist, 8: + MI. The selective disadvantage of a resistance mutation s as indicated. The drug efficacy was assumed to be 85 %. Single resistance mutations conferred 90 % resistance against the drug. Other parameters: $\lambda_T = 2 \cdot 10^9$, $\lambda_M = 4.95 \cdot 10^8$, $\delta_T = \delta_{T1} = 0.02$, $\delta_{T2} = 1$, $\delta_M = \delta_{M1} = \delta_{M2} = 0.0495$, $\beta_T = 8 \cdot 10^{-12}$, $\beta_M = 8 \cdot 10^{-15}$, $k_T = 0.35$, $k_M = 0.35$, $N_T = 1000$, $N_M = 100$, cl $= 23$, $\delta_{PIC} = 0.35$. The lower threshold for the frequency of drug switching 7days, or 3days (indicated with [1]).

HIV (discussed in chapter 3), more drugs, which can be sequenced become available and it becomes more likely, that a drug sequencing strategy, as the one presented, might be successful in eradicating productively infected cells.

4.6.7 Clinical Implementation of Optimal Strategy Requires High-resolution Resistance Assays

In fig. 4.23, we show the abundance of drug resistant strains in the case where the proposed strategy (eq.(4.54), (4.55)) was successful (left) and where it failed (right).

In the case of success (fig. 4.23, left), resistant strains become abundant in less than 20% of the population, which is the critical detection limit in standard phenotypical and genotypical assays [125, 126]. Ignoring all other limitations (laboratory delay, sampling frequency), it can therefore be inferred that standard assays cannot detect the optimal treatment switching time. However, novel developments, such as the pyrosequencing technology [129, 522–524] might possibly overcome these limitations in the future.

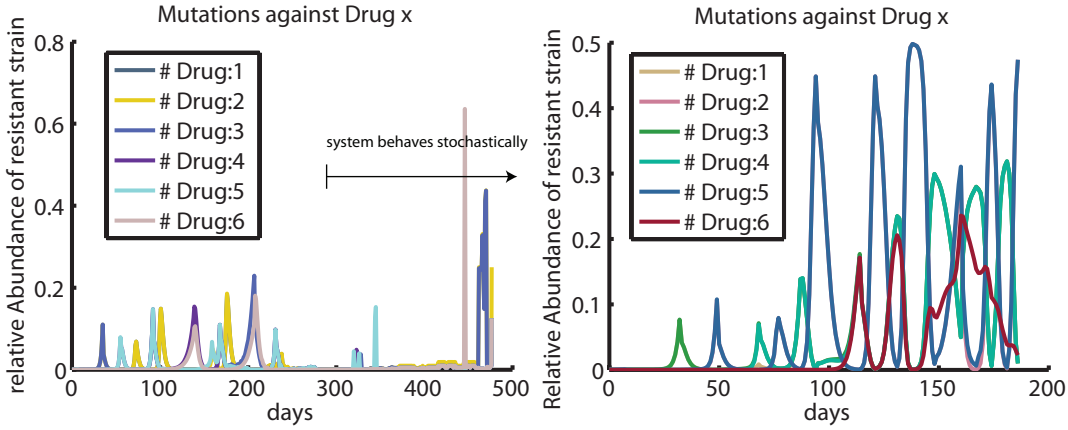

Figure 4.23: Left: Abundance of mutant strains in the case of succeeding drug sequencing strategy. Right: Abundance of mutant strains in the case of failing drug sequencing strategy.

4.7 Summary

In HIV therapy, mathematical models are a valuable tool to interpret the time course of virological markers (e.g. HIV RNA) during HIV treatment [11–14, 525] and contribute much to our current understanding of the *in vivo* dynamics of HIV. However, established models cannot accurately incorporate the mechanism of action of novel antivirals.

With the growing repertoire of novel antiviral drug classes, there is a demand for mathematical models that can help to interpret clinical markers of drug efficacy. We explain in section 4.2.6 how the action of established-, novel- and prospective drugs can be incorporated in a structural model of the viral replication cycle.

Viral decay rates are often used to assess the efficacy of HAART regimens (e.g. [526–528]). In clinical studies, the first approved integrase inhibitor, raltegravir, induced an extremely rapid decline in viral load both when applied as monotherapy [529] and in combination with an optimized NRTI background therapy [484, 530–532]. While it was initially speculated that the observed decline might be a result of superior potency of raltegravir, it is now emerging that the viral decline in InI-based therapy might be a class-specific phenomenon [533, 534]. To the contrary, superior potency of InIs was not confirmed by single-round infectivity assays [131]. The mechanisms underlying the decay dynamics are still not clear [535] and controversially discussed [484, 498].

From the discussion above, three major questions arise: (i) How do InIs cause the rapid viral decay? (ii) Is The viral load decay a good marker to assess the *in vivo* drug potency? (iii) Are there better markers to assess the *in vivo* potency of antivirals?

In section 4.5.3 we have explained that the rapid viral decay, that is observed with InIs is not necessarily an indicator of greater potency, but rather a result of their target location within the viral life cycle. The impact on viral load is delayed by the viral life cycle, for all drugs (EI, RTI, PI, MI) except InIs. InIs, to the contrary, have a direct impact on the amount of viral release (thus viral decay) by reducing the number of virus producing, late-stage infected cells (T_2, M_2). Thus, the onset of observed viral decay is faster for InIs, than with other compounds, irrespective of their potency (which was set equal for all compounds in fig. 4.15, left). Our insight was derived from our detailed, mechanistic model and confirms the result in [498], who claim that the decay dynamics depend on the inhibited stage of the viral life cycle.

For antivirals that affect the viral load in an identical way (see eq. (4.51)), it is possible to relate their potencies by comparing viral load decline. However, if the effect on viral load decline is not identical (e.g. between NRTIs and InIs), it is not possible to compare the compounds' potency, based on viral load decay. Therefore, before the introduction of InIs, viral load decline served as a good marker of drug potency at the enzymatic level. However, when comparing e.g. InIs with other drug classes, it might lead to false conclusions about the potencies of these drugs at the enzymatic level.

Antivirals affect the virus' ability to replicate. Phenotypic/single round infectivity assays assess the *in vitro* efficacy of antivirals by measuring the virus' ability to produce offspring. However, *in vitro*, the host response to infection that occurs *in vivo* (e.g. by clearance of virus and infected cells) cannot be accurately represented. We therefore transfer the concepts of validated *in vitro* experiments (the compounds' effect on offspring production) into a mathematical framework, which we use in our novel virus-dynamics model to estimate the *in vivo* efficacy of different drug classes. We call this novel term the 'reproductive capacity'. The reproductive capacity allows to extract and analyze key characteristics and differences between drug classes that have an impact on the overall efficacy of HIV drugs. The reproductive capacity can be used to distinguish class-specific *in vivo* efficacy of antivirals based on the hosts' ability to clear the targeted infective in the viral life cycle. The main conclusion is that the *in vivo* efficacy (in terms of the reproductive capacity) is larger for compounds that target viral life-stages that are cleared at a fast rate. It is generally assumed, that the free virus is cleared at the fastest rate [11, 490]. Since MIs and PIs reduce the production of infective Virus V_I

(see fig. 4.5), they therefore reduce the virus' ability to produce offspring faster than all other drug classes. Furthermore, since resistance development is correlated with the extend of replication, it can be inferred that PIs and MIs, based on their viral target, are the most efficient drug classes in terms of reducing the probability of resistance development. This assumption correlates well with the observed rebound times in table 4.1 and is also supported by the fact that the introduction of PIs marked the success of HAART.

In the present example, to analyze differences in class-wide *in vivo* drug efficacies, we have not focussed on compound-specific attributes, such as the inhibitory concentration (typically assessed by the IC_{50} value), pharmacokinetics and the genetic barriers to resistance. The results can therefore be used to generally rate pharmaceutical targets within the viral life cycle. Our findings suggest for drug discovery that the target half life is another important factor for the overall success of an HIV compound, besides the affinity of a drug to its molecular target, its pharmaceutical penetration into target cells and its genetic barrier to resistance.

The reproductive capacity has been shown to be a predictive tool for drug failure (see table 4.1) and might be a valuable tool to determine drug regime change- and selection, prior to virological failure [536].

We have evaluated this in sec. 4.6 where we propose an optimal drug switching strategy. In contrast to all currently applied drug switching strategies (that are based on viral load), the novel strategy evaluates the ability to produce offspring. Instead of focussing on the failure of the *actual* treatment, it evaluates if the *actual* treatment is of any advantage to the *prospective* treatment. One of the main results from the extensive analysis is that the rate of success of our proposed strategy increases with the number of sequencable drugs (see table 4.2). The overall trend in HIV drug discovery goes towards the exploitation of novel targets (see section 3), thus supporting a strategy that is based on the availability of many alternative treatment options.

The central component of our novel drug switching strategy is the reproductive capacity. Utilization of the reproductive capacity in clinical practice requires a detailed knowledge about the viral quasi-species composition. In the past, it has only been possible to detect viral mutants that occur at least in 20% of the viral population, using phenotypic assays [125], and in $20 - 50\%$ of the viral population using genotypic assays [126]. The recent introduction of pyrosequencing technologies, however, allows to detect minor viral mutant forms [129, 522–524] and might therefore enable the use of markers for virological failure, like the reproductive capacity, in order to determine the optimal time for regimen change and the optimal follow-up combination, prior to the event of virological rebound.

4.8 Glossary: Viral Dynamics

viral quasi-species: Group of viruses related by a similar mutation or mutations, competing within a highly mutagenic environment.
fitness landscape: fitness landscapes are adaptive landscapes that visualize the relationship between genotypes (or phenotypes) and reproductive success. In the fitness landscapes, fitness is denoted by the height of the landscape. Genotypes which are very similar are said to be close to each other, while those that are very different are far from each other. The two concepts of height and distance are sufficient to form the concept of a landscape. The set of all possible genotypes, their degree of similarity, and their related fitness values is then called a fitness landscape.

Part III

Pharmacokinetic- & Pharmacodynamic Modelling

Pharmacokinetics (PK) is defined as the study of the motion of drugs within biological systems (concentration-time, see fig 4.24, upper left). In other words "what the body does to the drug". Pharmacodynamics (PD) on the other hand is defined as the study of how chemical substances interfere with biological systems (response-concentration, fig. 4.24, upper right); -"what the drug does to the system".

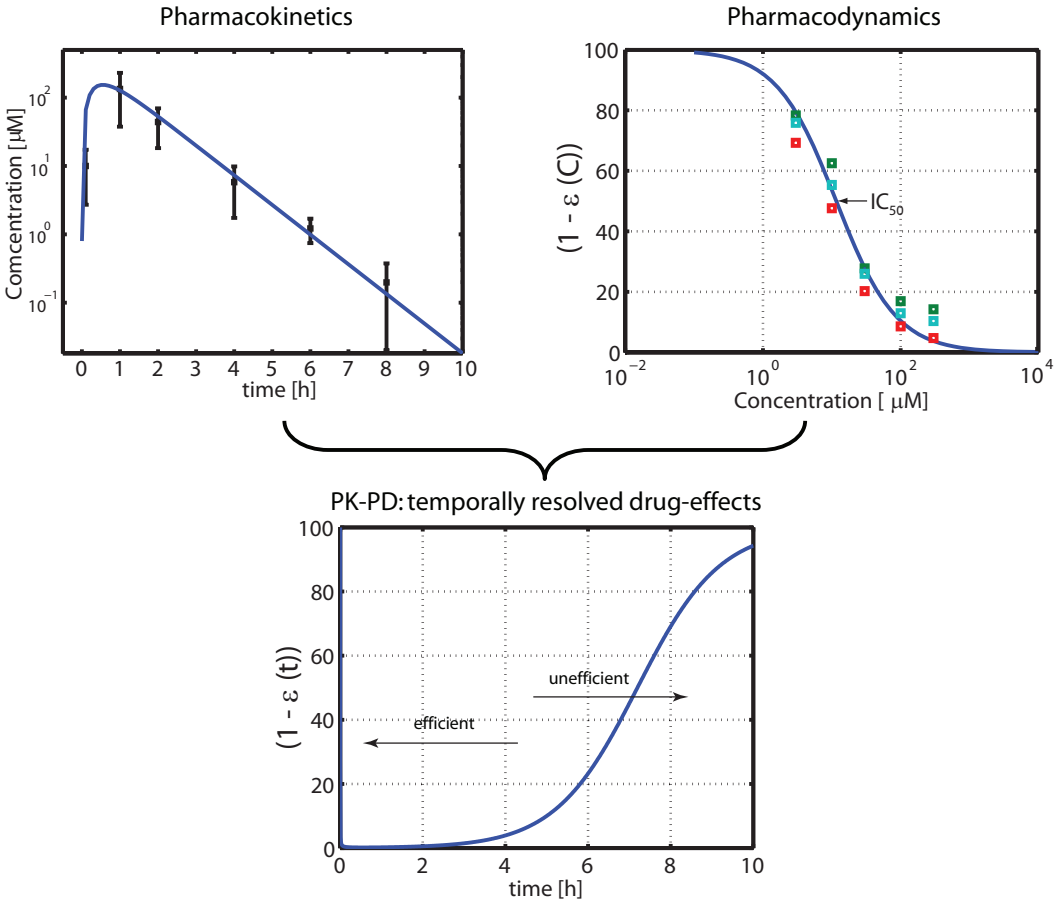

Figure 4.24: Pharmacokinetics, pharmacodynamics and the PK-PD-relationship

From pharmacodynamic studies, the relationship is established between the concentration of the drug (e.g. at a target site) and the expected effect. This is typically done *in vitro* on the basis of constant drug concentrations. However, *in vivo* drug concentrations are not static. The temporal resolution of drug exposure is revealed in pharmacokinetic studies. By combining pharmacokinetics and pharmacodynamics (pk-pd) it is possible to predict the temporal drug effects (fig. 4.24, lower figure) as they would appear *in vivo*. It is very important to establish this relation, because generally, once a drug is approved, the only adjustments in a clinical setting are: (i) What amount of drug to give and (ii) how often to give it.

In HIV treatment, the clinical endpoints (e.g. viral load) under therapy are always a result of the temporal drug effects (pk-pd).

In the previous chapter, we have introduced a novel model that can incorporate drug effects mechanistically. We have analyzed the effects of anti-HIV drugs on clinical markers, utilizing constant efficacy terms.

$$(1-\varepsilon) = \quad \text{const.} \quad \text{(constant efficacy)} \tag{4.56}$$

This model, however, neglects two important aspects: (i) The drug concentration at the target site is responsible for the intensity of a drug response. The link between (a fixed) drug concentration and response is established by the pharmacodynamic model. (ii) In order to resolve the temporal aspects of pharmacological response it is necessary to resolve the temporal aspects of drug concentration by pharmacokinetic modelling. In this chapter, we will explore realistic pharmacokinetic and pharmacodynamic models, that allow to resolve drug efficacies temporally $(1 - \varepsilon(t))$.

In the first section, we will present pharmacokinetic models, followed by a section on pharmacodynamic models. Finally, we will give several distinct modelling examples.

Chapter 5

Pharmacokinetic Modelling

In pharmacokinetics, the time-course of drugs (in relevant compartments) is studied [537]. The concentration-time profile of a drug is usually assessed within the blood-plasma, because the drug is usually transported to the effect-site via the blood stream and because blood-samples can easily be derived from patients. For model validation, it is therefore necessary to accurately capture the blood-plasma pharmacokinetics. Drug concentrations at the site of effect are rarely available. However, often they can be related to the blood-plasma concentrations from patients, either by some linear- or non-linear functions.

The simplest model is the one-compartment model, which assumes instantaneous distribution of the drug into all body compartments. It is described by the following differential equation:

$$\underbrace{V_{\mathrm{ss}}}_{\text{distribution}} \frac{\mathrm{d}}{\mathrm{d}t}C = \overbrace{v_{\mathrm{in}}(t)}^{\text{absorption}} - \underbrace{C \cdot \mathrm{CL}(t)}_{\text{elimination}} \tag{5.1}$$

where V_{ss} [volume] denotes the 'volume of distribution', which is a hypothetical volume with the same distribution characteristics as the blood plasma [538]. As an example: if the drug distributes instantaneously into the blood (volume of 5L) and three times more intensely into the adipose tissue (10L) and nowhere else, then the 'volume of distribution' is 5L + 3x10L = 35L. We will present modelling approaches for drug distribition in section 5.3. The parameter $v_{\mathrm{in}}(t)$ in eq. (5.1) describes the influx of drug into the system (the amount of drug that reaches the circulation/blood-plasma) through e.g. oral application of a pill or an intravenous injection. Models for drug absorption will be discussed in section 5.2. Finally, $\mathrm{CL}(t)$ [volume/time] describes the elimination of the drug from the body, e.g. through metabolic degradation, or urinary/bilary/fecal excretion. In the most simple case $\mathrm{CL}(t)$ is a constant.

The example shows, that the pharmacokinetics of a drug can be described by modelling the following three processes:

- absorption
- distribution
- elimination

We will present models for absorption, distribution and elimination respectively in sections 5.2-5.4.

5.1 Modelling Approaches

There are different approaches in pharmacokinetics, such as 'non-compartmental' analysis, 'compartmental' modelling and 'physiologically-based' modelling [539]. Generally, the availability of data and the study objectives determine the modelling approach.

The non-compartmental approach attempts to model the response rather than the structure of a process and is mainly used to derive pharmacokinetic parameters from *in vitro/in vivo* data. The underlying principles are often based on a one-compartment model with linear kinetics (e.g. [540]).

The 'compartmental' approach utilizes 'kinetic compartments' (see glossary), which by themselves have little physiological and anatomical meaning. The 'compartmental' approach follows the principle, that 'simpler is better' [541]. A minimum number of compartments is used. Additional compartments are included, only if the data suggests that they are necessary. Thus, a one-compartment model will be used unless the data indicates to "require" a more complex model, such as a two-compartment model. Thus, the study objectives, as-well as the available data provide the structure of the model.

Physiologically based pharmacokinetic (PBPK) models are specific compartmental models that utilize 'anatomical compartments' (see glossary). The PBPK compartments represent physiological compartments, such as organs [542, 543]. Therefore, the compartments are more meaningful than in the previously discussed model approaches. PBPK models include blood flow, distribution- and elimination from individual organs and tissue groups. They thus provide a more mechanistic basis of the observed pharmacokinetics. However, PBPK models require an improved theoretical basis for predicting pharmacokinetic effects. Because of the complexity of this approach, many parameters and assumptions may not be verified.

However, one strength of this approach is that it can take *in vitro* or *in vivo* data as input, combine it with known physiological data and predict *in vivo* profiles [544]. The model assumptions remain disclosed and testable *in vitro*, in contrast to lumped parameters in e.g. compartmental approaches.

The basic structure of a PBPK model is provided by the exchange of drug through the blood flow between different anatomical compartments (see fig. 5.1). The lung 'lun' gets input from the vene 'ven' and drug leaving the lung enters the artery 'art'. The gut 'gut', spleen 'spl' and pancreas 'pan' get input from the artery and emit drug into the portal vein 'hep, art', that feeds into the liver 'liv'. Drug leaving the liver enters the vene. All other tissues 'tis' receive input from the artery and drug

leaving these compartments enters the vene. The differential equations are as follows

$$
\begin{aligned}
V_{\text{lun}} \frac{\mathrm{d}}{\mathrm{d}t} C_{\text{lun}} &= Q_{\text{lun}} \left(C_{\text{ven}} - C_{v,\text{lun}} \right); && (5.2)\\
C_{v,\text{lun}} &= \frac{C_{\text{lun}}}{K^{\text{lun}:b}} \\
V_{\text{art}} \frac{\mathrm{d}}{\mathrm{d}t} C_{\text{art}} &= Q_{\text{lun}} \left(C_{v,\text{lun}} - C_{\text{art}} \right) && (5.3)\\
V_{\text{tis}} \frac{\mathrm{d}}{\mathrm{d}t} C_{\text{tis}} &= Q_{\text{tis}} \left(C_{\text{art}} - C_{v,\text{tis}} \right); && (5.4)\\
C_{v,\text{tis}} &= \frac{C_{\text{tis}}}{K^{\text{tis}:b}} \\
&\quad \text{tis} = \text{all tissues except liv and lun} \\
V_{\text{liv}} \frac{\mathrm{d}}{\mathrm{d}t} C_{\text{liv}} &= Q_{\text{liv}} \left(C_{\text{in}} - C_{v,\text{liv}} \right) - \text{CL}_{\text{int}} \cdot C_{v,\text{liv}}; && (5.5)\\
C_{v,\text{liv}} &= \frac{C_{\text{liv}}}{K^{\text{liv}:b}} \\
C_{\text{in}} &= \frac{Q_{\text{pan}} C_{v,\text{pan}} + Q_{\text{gut}} C_{v,\text{gut}} + Q_{\text{spl}} C_{v,\text{spl}} + Q_{\text{hep,art}} C_{v,\text{art}}}{Q_{\text{liv}}} \\
V_{\text{ven}} \frac{\mathrm{d}}{\mathrm{d}t} C_{\text{ven}} &= Q_{\text{lun}} \left(C_{v,\text{in}} - C_{\text{ven}} \right) + v_{\text{i.v.}}(t), && (5.6)\\
C_{v,\text{in}} &= \sum_{\text{tis}} \frac{Q_{\text{tis}} C_{v,\text{tis}}}{Q_{\text{lun}}}, \\
&\quad \text{tis} = \text{all tissues except lun, gut, spl and pan}
\end{aligned}
$$

$C_{v,\text{tis}}$ is the venous-blood-leaving-tissue drug concentration. The parameter Q denotes the respective blood flow in- or out of the organ and the parameters $v_{\text{i.v.}}(t)$ and CL_{int} denote the influx of drug by intravenous administration and the metabolic clearance of drug, discussed further in section 5.2 and 5.4, respectively. The tissue-to-blood partition coefficients $K^{\text{tis}:b}$ are one of the most important input parameters in PBPK modelling. Their derivation will be discussed in section 5.3. One attribute of the PBPK model is that is does not assume instantaneous drug distribution into all tissue *per se*.

In summary, PBPK models offer the advantage that data from various sources (e.g. *in vivo, in vitro* and *in silico*) can be integrated in a mechanistic way to predict *in vivo* profiles. Therefore, PBPK models can readily be used in the early stages of drug discovery [545–547] and throughout drug development [548], enabling the integration of novel insights, as they emerge. However, one problem is their increased complexity and the non-identifiability of many model parameters and -assumptions and the verifiability of predictions in compartments for which no data exists. Furthermore, the complexity of the PBPK model does not reveal the underlying kinetic structure.

However, PBPK models can be reduced to derive compartmental models that more intuitively reveal the kinetic structure and allow for elaborated model analysis [549–551]. Since compartmental models usually compromise a limited number of (lumped) parameters, they are also suitable for parameter estimation and analysis of population effects (e.g. using NLME techniques). Therefore, through combining PBPK modelling and compartmental modelling, it is possible to make use of the strengths of both approaches and eliminate the weaknesses of each individual approach (as suggested by [548]). We have illustrated the general pharmacokinetic modelling strategy in fig. 5.1. Generic physiologically based pharmacokinetic (PBPK) models require a small number of *in vitro* parameters to produce *in vivo* predictions [544–547]. This model can subsequently be simplified to reveal the underlying kinetic structure and validated- or falsified with experimental data. In any case, the PBPK model can be refined based on any data that becomes available, possibly changing the structure of the compartmental (kinetic) model.

In the next sections, we will present models on absorption, distribution and elimination in the light of the discussed overall modelling strategy (fig. 5.1).

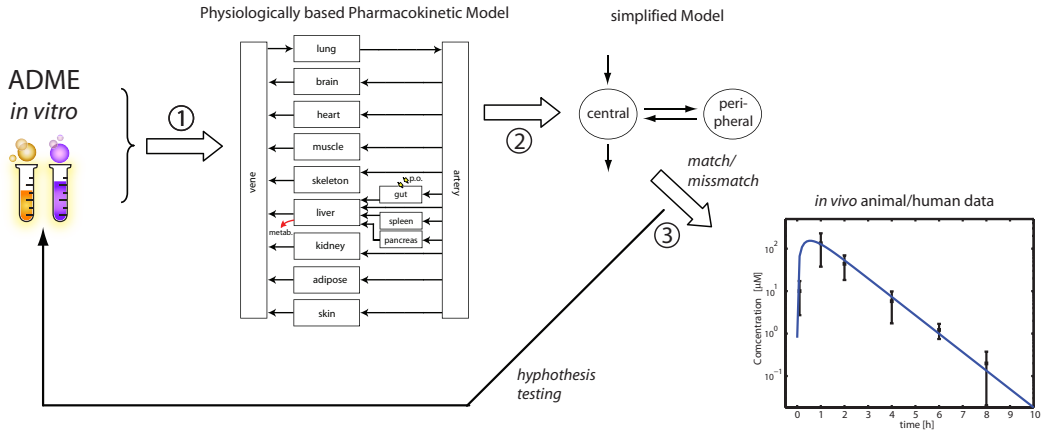

Figure 5.1: Proposed pharmacokinetic modelling pipeline. 1. *In vitro* data can be integrated into a physiologically based pharmacokinetic (PBPK) model. 2. the complexity of the PBPK model is reduced ("lumping"), which allows more elaborated model analysis and use. 3. If *in vivo* data suggests that an important process is not considered by the model, new experiments are carried out. The results of these experiments can be integrated into the PBPK model, etc...

5.2 Absorption

Drugs can be applied through several routes: intra-venous, orally, intro-muscular, subcutaneous, by inhalation, intranasal and transdermal. Amongst these routes, intravenous (i.v.) and oral (p.o.) administration are the most common. All anti HIV drugs are applied orally or intravenous, with the exception of the fusion inhibitor enfuvirtide, which is applied by subcutaneous injection or intravenously. A model for the subcutaneous injection of enfuvirtide is readily provided in [552]. For these reasons we will only focus on models of oral absorption and intravenous injection.

5.2.1 Intravenous Administration

The easiest absorption model is a constant bolus infusion. Denote by T_0 the starting time of the injection, by ΔT the duration of the injection, by dose the amount of drug to be injected. Then, the mass inflow is given by

$$v_{\text{in}} = \begin{cases} \text{dose}/\Delta T; & t \in [T_0, T_0 + \Delta T] \\ 0; & \text{otherwise.} \end{cases} \tag{5.7}$$

This model can readily be integrated into a compartmental model (central blood compartment) or into a PBPK model (venous blood compartment).

5.2.2 Oral Administration

Modelling an oral application is much more demanding compared to an intravenous application. Whereas 100% of the i.v. administered dose enters the blood stream, this is not necessarily the case for orally administered drugs. This might have various reasons (fig. 5.2) [538]:

- only a fraction of the drug that has been swallowed might be absorbed into the gastrointestinal cells. This parameter is denoted the 'fraction absorbed' ($\int_0^\infty F_{\text{abs}}(s)\mathrm{d}s$). The residual fraction will be excreted without ever having entered the body.
- Some proportion of the absorbed drug might readily be degraded within the gut cells (enterocytes). We call this parameter the gastrointestinal extraction E_{gut}.

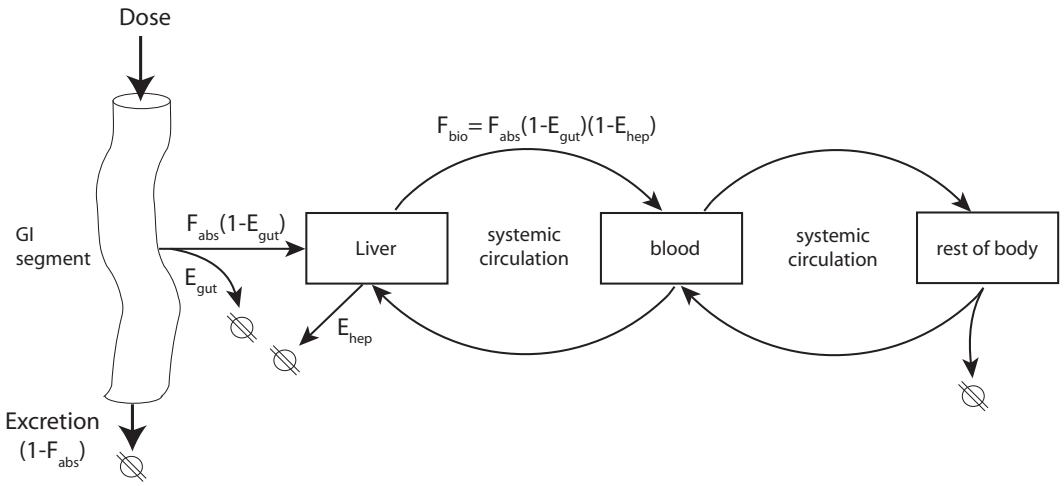

Figure 5.2: Schematic illustration of the distinct obstacles that an orally administered drug has to master in order to enter the blood stream.

- After having passed the gastrointestinal wall, the drug enters the portal vene, which transports the drug into the liver. Many drugs are converted into metabolites, that do not confer any efficacy. The proportion of drug that is extracted here is denoted by E_{hep}. After having passed the liver, the drug enters the systemic circulation.

Thus, only a fraction of the administered dose ever enters the systemic circulation, where it could potentially exert its effect. This fraction is called the bioavailability F_{bio} of the drug [538].

$$F_{\text{bio}} \quad = \quad (1 - E_{\text{gut}}) \cdot (1 - E_{\text{hep}}) \cdot \int_0^\infty F_{\text{abs}}(s)\mathrm{d}s. \tag{5.8}$$

Models for drug elimination will be discussed later in section 5.4.

The bioavailability can be experimentally determined if *in vivo* pharmacokinetic data for i.v. administration and p.o. administration is available [538], by

$$F_{\text{bio}} = \frac{\text{dose}_{\text{p.o.}} \cdot \text{AUC}_{\text{p.o.}}}{\text{dose}_{\text{i.v.}} \cdot \text{AUC}_{\text{i.v.}}} \tag{5.9}$$

where AUC refers to the area under the plasma concentration curve. Alternatively, if insufficient data is available, F_{bio} can be estimated from *in vitro/in vivo* using physiologically based modelling.

In fig. 5.3 we show F_{bio} of some anti-HIV drugs. Some protease inhibitors (especially saquinavir and darunavir) and the novel CCR5-antagonist maraviroc have very low intrinsic bioavailabilities. This is mainly due to poor absorption (affecting F_{abs}) (extensive efflux from gut cells into the GI-lumen) and extensive metabolic degradation, both in the enterocytes (affecting E_{gut}) and the liver (affecting E_{hep}). The PI ritonavir can block the efflux transporters, that are responsible for the poor absorption of these compounds and the enzymes that are responsible for the degradation. Therefore, co-administration with low-dose ritonavir, can sufficiently increase F_{bio} for these compounds (see fig. 5.3) [443]. In the case of zidovudine, didanosine and tenofovir, different transporters and enzymes are responsible for their poor bioavailability. Therefore, ritonavir-boosting cannot improve their bioavailability.

Compared to an i.v administration, there might be a substantial delay between the oral administration of a drug and the time when the drug reaches the blood stream. Therefore, there might ultimately be a delay between the administration of the pill and the commence of a drug-effect. The length of the human small intestine (where most drugs are absorbed) is about 300 cm [559] and the transit time is $\approx$ 3.5h [560]. Depending where the compound is primarily absorbed, will ultimately

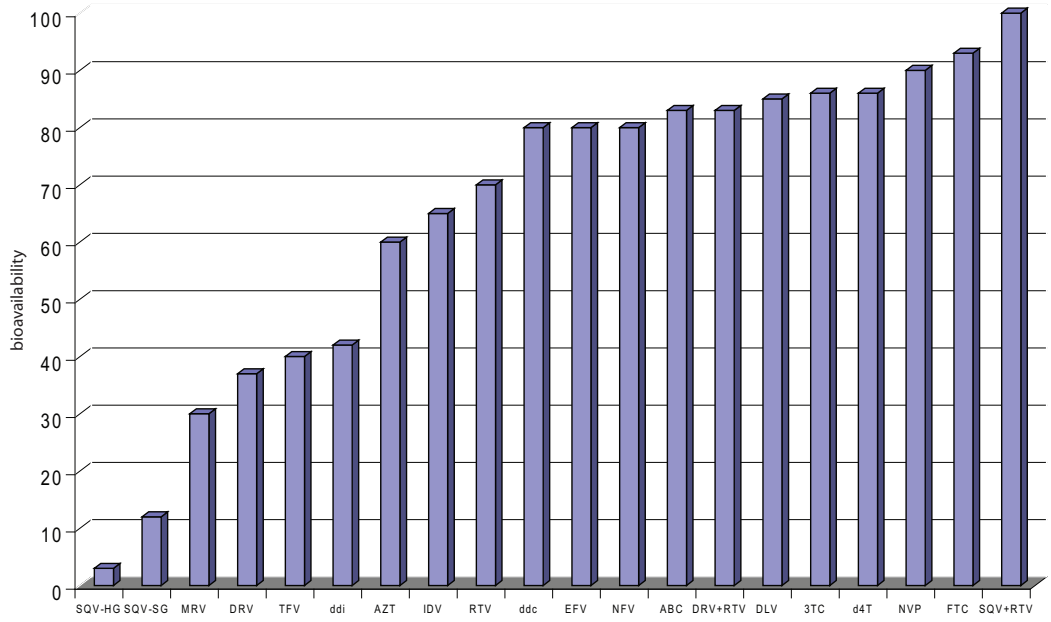

Figure 5.3: Bioavailabilities of various anti-HIV compounds. Data from [393, 405, 553–558] . SQV = Saquinavir, MRV = maraviroc, DRV = darunavir, TFV = tenofovir, DDI = didanosine, AZT = zidovudine, IDV = indinavir, RTV = ritonavir, DDC = zalcitabine, EFV = efavirenz, NFV = nefinavir, ABC = abacavir, DLV = delavirdine, 3TC = lamivudine, d4T = stavudine, NVP = nevirapine, FTC = emtricitabine. SG: soft-gel formulation. HG: hard-gel formulation

determine when it appears in the blood circulation after an oral administration. Therefore, the drug absorbtion over time (determined by $F_{\text{abs}}(t)$) determines the delay in oral input.

In fig. 5.4, we show some pharmacokinetic profiles after an oral absorption. While intravenously administered drug appears instantaneously in the blood stream, orally applied drugs might appear with delays (e.g. fig. 5.4).

Depending on the availability of pharmacokinetic data it might require various approaches to model drug absorption:

- **Empirical Models**, if *in vivo* pharmacokinetic profiles are available and the bioavailability is known.
- **Mechanistic Models**, if F_{bio} is unknown, if *in vivo* data is not available, or both.

Empirical Models

The most simple absorption model is the first-order absorption model (see fig. 5.5, left panel). This model assumes that drug is absorbed from the intestine with some constant rate [537].

$$\frac{\mathrm{d}}{\mathrm{d}t}C_{\text{depot}} = -k_a \cdot C_{\text{depot}} \tag{5.10}$$

$$\frac{\mathrm{d}}{\mathrm{d}t}C_{\text{central}} = k_a \cdot C_{\text{depot}} - ... \tag{5.11}$$

where k_a is the absorption rate constant (the release of drug into the blood compartment). If we set $C_{\text{depot}}(0) = F_{\text{bio}} \cdot \text{dose}$, we can replace the depot-compartment with $C_{\text{depot}}(t) = F_{\text{bio}} \cdot \text{dose} \cdot e^{-k_a t}$ and derive

$$v_{\text{in}}(t) = k_a \cdot F_{\text{bio}} \cdot \text{dose} \cdot e^{-k_a t}. \tag{5.12}$$

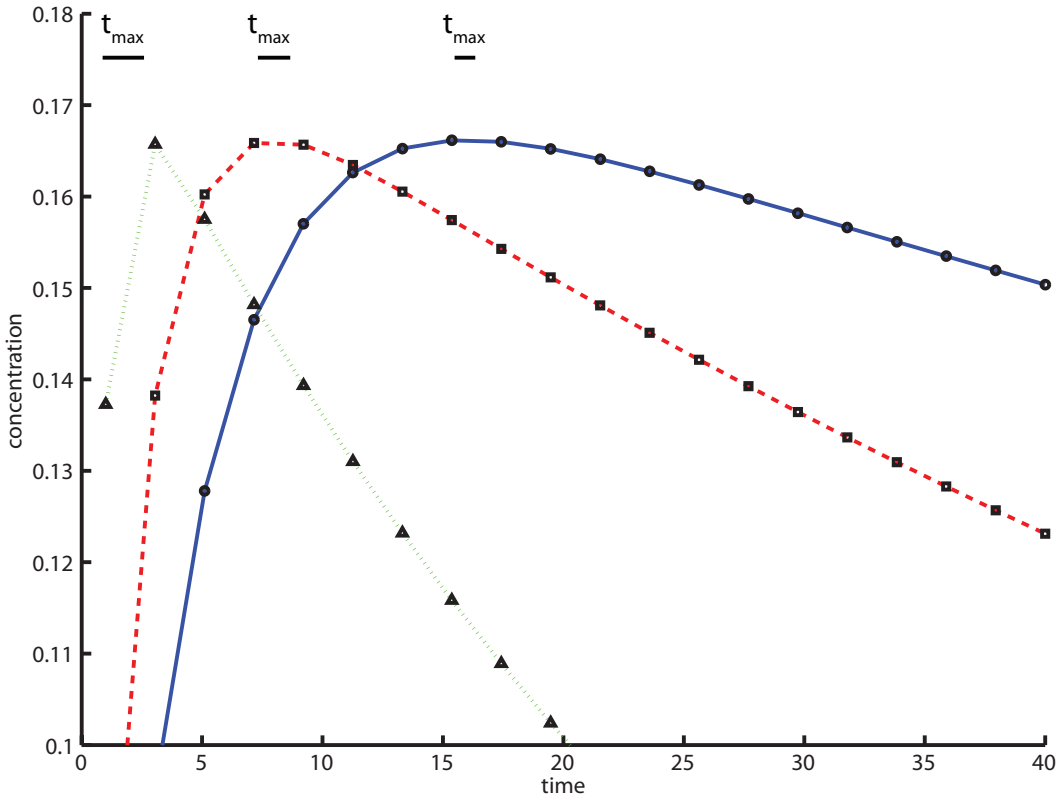

Figure 5.4: Examples of delayed oral absorption. We used a one-compartment model with linear kinetics $C(t) = \frac{F_{\text{bio}} \cdot \text{dose}}{V_{\text{ss}}} \frac{k_a}{k_a - k_e} \cdot (e^{-t \cdot k_e} - e^{-t \cdot k_a})$ and set $k_e = 50 \cdot k_a$. k_e = elimination rate constant. k_a = absorption rate constant.

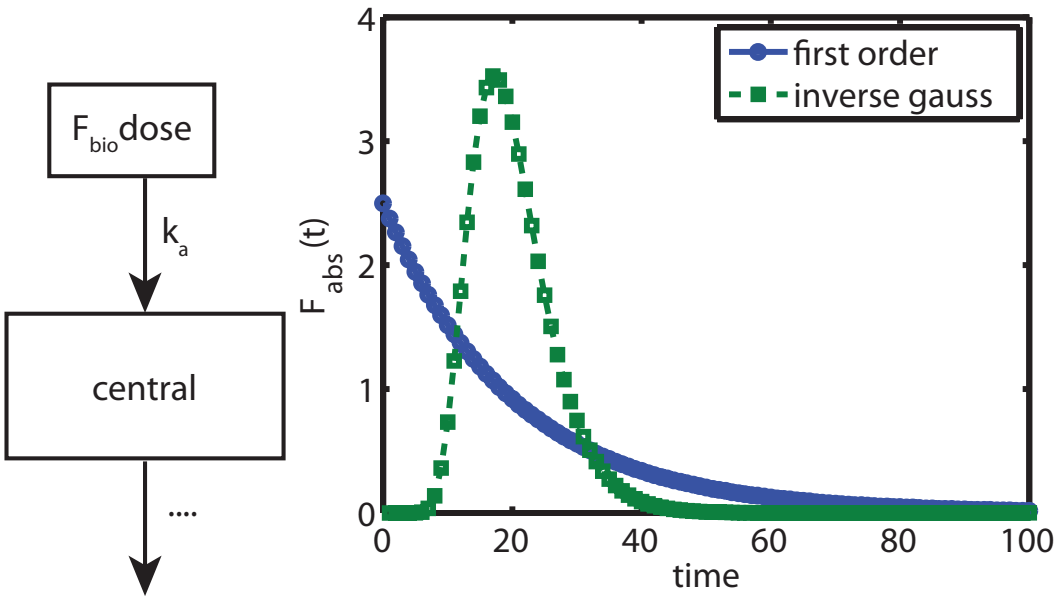

Figure 5.5: Right:First-order absorption model

This model is very useful due to its simplicity and it takes only one parameter, that could eventually be estimated from the *in vivo* profile. However, absorption rate constants k_a are very difficult to estimate by parameter-fitting. If the elimination of the drug is also given by some constant term, e.g.

$v_{\text{out}}(t)/V_{\text{ss}} = k_e$, then a good estimate of the absorption rate constant can be derived, by evaluating $t_{\max}$ from the *in vivo* profile (see fig. 5.4) utilizing the following relation:

$$t_{\max} = \frac{1}{k_a - k_e} \ln\left(\frac{k_a}{k_e}\right). \tag{5.13}$$

However, eq. (5.12) assumes that drugs are constantly absorbed (see fig. 5.5, right panel). The absorption of many drugs, however, might not occur within the first compartments of the gastrointestinal tract and might therefore be orderly delayed. This is a feature that cannot be captured by the first-order model. For this reason, the inverse gaussian absorption model was proposed [561].

$$v_{\text{in}}(t) \quad = \quad F_{\text{bio}} \cdot \text{dose} \cdot \sqrt{\frac{\text{MAT}}{2\pi \text{CV} t^3}} \exp\left(-\frac{(t-\text{MAT})^2}{2\text{CV}t\text{MAT}}\right), \tag{5.14}$$

where MAT denotes the mean absorption time and CV is the normalized variance of the distribution. The inverse gaussian absorption model produces one peak absorption (see fig. 5.5, right), that can be shifted on the time-axis. Although this model can produce potentially more realistic absorption profiles, its main disadvantage is that it requires two parameters as input, that are very difficult to estimate from *in vivo* pharmacokinetic profiles.

The empirical models (eqs. (5.12), (5.14)) can either be embedded into the central compartment of a compartmental model, or they can be integrated into the blood-compartment of a physiologically-based model.

Mechanistic Models

Mechanistic absorption models can be parameterized in terms of *in vitro* data and physiological data. Several different models have been proposed: The Compartmental Absorption and Transit model (CAT) [560, 562–564], the Advanced Compartmental Absorption and Transit model (ACAT) [565] and the GastroIntestinal Transit and Absorption model (GITA) [566–568]. A common feature of all of these approaches is that they represent the intestine by a chain of transit compartments from which drug is absorbed into the portal vein. Willmann et al. [559, 569, 570] proposed a continuous transit model that will not be discussed here.

In [560], Yu and Amidon proposed the compartmental absorption and transit (CAT) model. The model considers the stomach, the small intestine (divided into seven compartments) and the colon, which serves as a sink. For the model it is assumed that absorption takes place only in the intestine compartments, and that the drug is present in the dissolved form. Furthermore, the intestinal compartments are not defined based on anatomical segmentation, but rather based on identical transit times. The CAT model is defined by the following set of equations

$$\begin{aligned}
\frac{\mathrm{d}}{\mathrm{d}t}A_s &= -k_s A_s \qquad \text{(stomach)} \\
\frac{\mathrm{d}}{\mathrm{d}t}A_2 &= k_s A_s - k_t A_2 - k_a A_2 \qquad \text{(intestine, } n = 2\text{)} \\
\frac{\mathrm{d}}{\mathrm{d}t}A_n &= k_t A_{n-1} - k_t A_n - k_a A_n \qquad \text{(intestine, } n = 3, \ldots, 8\text{)} \\
\frac{\mathrm{d}}{\mathrm{d}t}A_c &= k_t A_8 \qquad \text{(colon),}
\end{aligned}$$

where k_s denotes the rate of gastric emptying, k_t denotes the small intestine transit rate, and k_a denotes the absorption rate constant. The initial condition for the above set of equations is $A_s(0) = \text{dose}$, $A_n(0) = A_c(0) = 0$ for $n = 2, \ldots, 8$. In [560], the rate constants are further specified as

$$k_t = \frac{7}{\text{T}_{\text{si}}} \quad \text{and} \quad k_a = \frac{2P_{\text{eff}}}{r_{\text{SI}}} \tag{5.15}$$

The absorption rate constant has been derived, by assuming $k_a = \mathrm{SA} \cdot P_{\mathrm{eff}}/V$ and substituting the surface area SA and the volume V with the corresponding parameters under the assumption of a cylindric shape. Therefore, the model can be parameterized in terms of the mean small intestine transit time $\mathrm{T_{si}}$ (reference value: 3.32 [h] for humans [560]), the radius of the small intestine r_{SI} (reference value: 1.75 [cm] for humans [560]), the rate constant k_s (reference value: 2 [1/h] [559]). The effective permeability P_{eff} is usually determined from *in vitro* experiments in Caco-2 mono-cell-layers. Given the input parameters (dose and P_{eff}), the mass inflow is given by

$$F_{\mathrm{abs}}(t) \quad = \quad \sum_{n=2}^{8} k_a A_n(t).$$

Correct representation of the gastrointestinal tract as a series of compartments requires an analysis of small intestine (SI) transit time frequency distribution to determine the correct number of compartments. Analysis of more than 400 human SI transit times revealed a log normal distribution with mean transit time of 3.32 [h]. The authors [560] determined that seven equal transit time small intestine compartments gave the best fit to the observed cumulative frequency distribution. The seven-compartment transit model may be visualized as having the first half of the first compartment representing the duodenum, the second half of the first compartment, along with the second and third representing the jejunum, and the rest representing the ileum [565]. The corresponding transit times in the duodenum, jejunum, and ileum are 14, 71, and 114 [min].

The GITA-model [566–568] takes anatomical transit compartments (stomach, duodenum, jejunum, ileum, cecum and large intestine) with corresponding transit rates k_t in rats [568] and humans [567] (for stomach, jejunum, ileum, cecum and below), but otherwise follows the same structure as the CAT model. The absorption rate constants in [568] were determined experimentally. However, it is also possible to use the absorption model in eq. (5.15) and calculate the absorption rate constants k_a based on anatomical GI-segment radii [559]. In fig. 5.6 we show the absorption profile of the NRTI zidovudine in human, based on a transit compartment parameterized with physiological data from [559,567] and drug-specific data from [571].

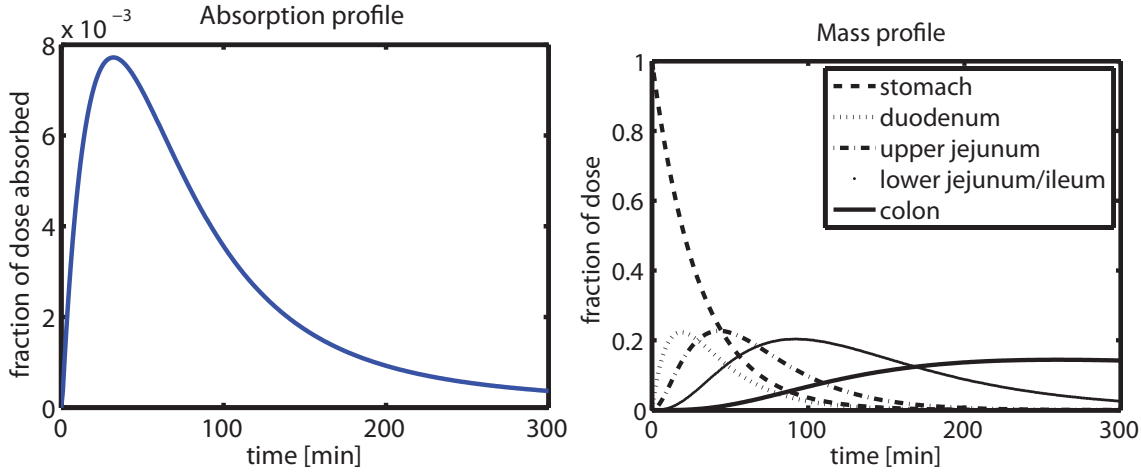

Figure 5.6: Left: $F_{\mathrm{abs}}(t)$ for zidovudine in human based on a transit compartment approach. Right: Drug mass in different anatomical GI-compartments. Parameters from [559, 567, 571]

In order to account for drug dissolution effects, Yu et al. [572] proposed the **extended CAT** model. Based on the same assumption as for the CAT model, the drug is now considered in crystalized, undissolved form A_C, and in dissolved form A_D (see fig. 5.7). The resulting set of equation is

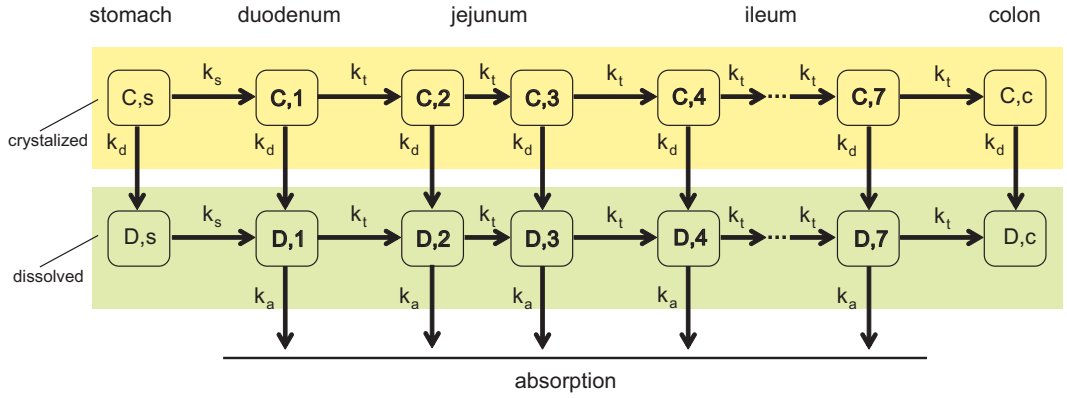

Figure 5.7: The extended Compartmental Absorption and Transit model.

$$
\begin{aligned}
\frac{\mathrm{d}}{\mathrm{d}t}A_{C,s} &= -k_s A_{C,s} - k_d(A_{C,s}) \cdot A_{C,s} \qquad \text{(stomach)},\\
\frac{\mathrm{d}}{\mathrm{d}t}A_{D,s} &= -k_s A_{D,s} + k_d(A_{C,s}) \cdot A_{C,s}\\
\frac{\mathrm{d}}{\mathrm{d}t}A_{C,2} &= k_s A_{C,s} - k_t A_{C,2} - k_d(A_{C,2}) \cdot A_{C,2} \qquad \text{(intestine, n = 2)},\\
\frac{\mathrm{d}}{\mathrm{d}t}A_{D,2} &= k_s A_{D,s} - k_t A_{D,2} + k_d(A_{C,2}) \cdot A_{C,2} - k_a A_{D,n}\\
\frac{\mathrm{d}}{\mathrm{d}t}A_{C,n} &= k_t \left(A_{C,n-1} - A_{C,n}\right) - k_d(A_{C,n}) \cdot A_{C,n} \qquad \text{(intestine, n = 3,...,8)},\\
\frac{\mathrm{d}}{\mathrm{d}t}A_{D,n} &= k_t \left(A_{D,n-1} - A_{D,n}\right) + k_d(A_{C,n}) \cdot A_{C,n} - k_a A_{D,n}\\
\frac{\mathrm{d}}{\mathrm{d}t}A_{C,c} &= k_t A_{C,8} \qquad \text{(colon)},\\
\frac{\mathrm{d}}{\mathrm{d}t}A_{D,c} &= k_t A_{D,8},
\end{aligned}
$$

In addition to the parameters of the CAT model, the (concentration dependent) dissolution rate k_d has been introduced

$$
k_d(A_{C,n}) = \frac{3D \cdot \mathrm{MW}}{\rho\, r h}\left(S_w - \frac{A_{C,n}}{V_n}\right)
$$

in terms of the diffusion coefficient D in [area/time] (reference value: 5×10^{-6} [cm^2/sec] in [572]), the density of the drug ρ in [mass/volume] (reference value: 1200 [mg/cm^3] [572]), the initial radius of the drug particles r in [length], the diffusion layer thickness h (reference value: 30 μm in [572]), and the aqueous solubility S_w in [mol/volume]. V_n is the volume of the nth compartment which has not been specified in the original publication.

Given the input parameters dose, k_s, r, S_w and P_{eff}, the mass inflow is given by

$$
F_{\mathrm{abs}}(t) = \frac{1}{\mathrm{MW}} \sum_{n=2}^{8} k_a A_{D,n}(t).
$$

A further advanced version is implemented in the commercially available GastroPlus© software. The underlying absorption model is called the ACAT (advanced CAT) model, which explicitly takes the unreleased, undissolved and the dissolved species into account. The number of GI-compartments is identical to the number of compartments in the extended CAT model.

5.3 Drug Distribution

Drug binding and retention. It is often assumed, that only the unbound drug C_{u} can pass the cellular membrane by passive diffusion, or interact with macromolecules that facilitate- or direct membrane permeation [541]. Within the blood-plasma compartment, drugs can be aggregated with the plasma proteins albumin and α_1-acid glycoprotein (highlighted in fig. 5.9 for some HIV-compounds), that prevent their movement across anatomical barriers like the plasma membrane of cells, or the vascular membrane of blood vessels. The extent of plasma protein binding can usually be measured *ex vivo* using human- or animal blood plasma and will therefore not be discussed in detail here.

Cells consists of chemically different subspaces. Within cells, the unbound drug is usually considered as the amount of drug that is dissolved in the aqueous space of the cell. Drugs can have a considerable affinity to some of the constituents and concentrate within confining subspaces of the cell. The timescales for the dissolution of drugs in tissue constituents (e.g. lipids) is assumed to be much faster than the timescales of interest. Within cells and tissues, we will therefore estimate a lumped parameter, the fraction of unbound drug $\mathrm{f_u}$, that indicates the extent of drug binging in cells/tissues (see fig. 5.8, leftmost panel) at quasi steady-state.

Drug exchange through membranes. Unbound drug C_{u} can be exchanged between two adjacent compartments that are separated by a membrane, (e.g. cell and interstitial space, plasma and interstitial space, see fig. 5.8, center left panel). The transfer over the membrane can eliminate a possible concentration gradient (equilibrating), or build up a gradient (concentrative). Furthermore, transfer across the cellular membrane can be rate-limiting (see Glossary) on the timescales of interest. Subcellular binding and exchange of drugs through e.g. the cellular membrane can be subsumed into the tissue-to-plasma partition coefficient $K^{\mathrm{t:p}}$, which characterizes drug distribution in the whole tissue, typically under steady-state assumptions. However, possible membrane-limitation (see Glossary) cannot be accurately modelled this way. For most tissues, however, membrane limitation is not expected, nor does it effect the primary study objective.

Drug distribution with blood flow. A physiologically based pharmacokinetic (PBPK) model (see fig. 5.8, center right panel) utilizes tissue-to-plasma partition coefficients $K^{\mathrm{t:p}}$ to model drug distribution into various tissues on the basis of the blood flow into tissues. The blood flow can limit the distribution of drugs on the timescales of interest (see Glossary). However, if the tissue concentration is not a study endpoint, then tissue compartments can be lumped into kinetic compartments (see Glossary).

Extraction of kinetic features. It is possible to lump parts of the PBPK model to derive a simplistic compartment model (see fig. 5.8, rightmost panel) that uses a minimal number of parameters and compartments to accurately capture the drugs' pharmacokinetics. This is especially useful, if verifying assumptions for the PBPK model are missing, if the main purpose lies is the mathematical analysis of the model, in parameter estimation or if only a subset of compartments are of importance (like e.g. the central (blood) compartment).

In order to resolve drug distribution we will first introduce the concept of drug binding to tissue constituents, then derive equations for the exchange of free drug C_{u} of adjacent compartments and present models that predict the extent of tissue binding. Finally, we will introduce equations which allow us to lump tissues compartments into kinetic compartments, that can be used in a compartmental approach. While in this section we will use the concepts to lump compartments, we will in section 5.5 conserve as much detail as possible at the effect site.

5.3.1 Drug Binding and Retention

In case of a linear, i.e., non-saturable relationship between the unbound aqueous and the total drug concentration, we can define

$$C_{\mathrm{u}}^{\mathrm{x}} = {\mathrm{f_u}}^{\mathrm{x}} \cdot C^{\mathrm{x}}, \tag{5.16}$$

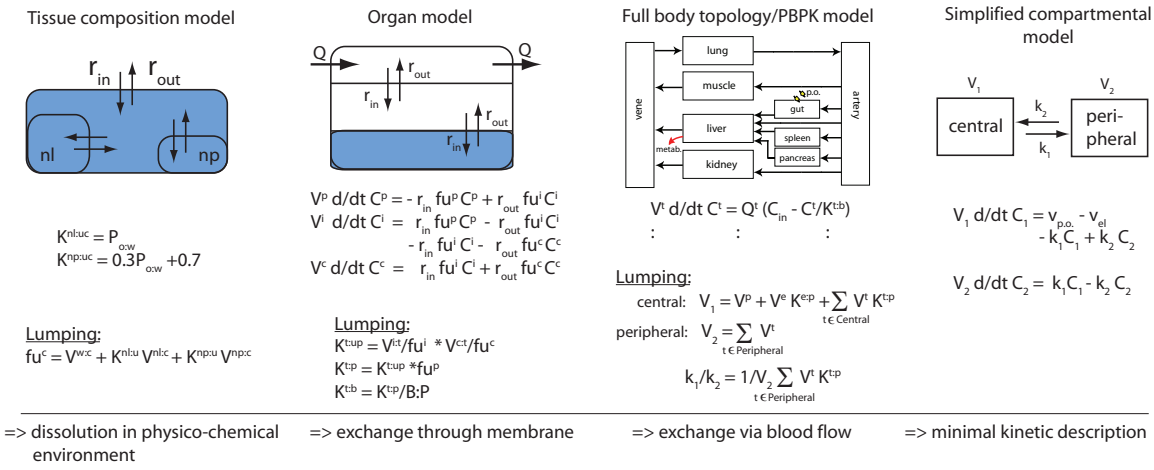

Figure 5.8: Drug distribution: Left: Distribution in sub-cellular spaces. Center-left: Distribution in organ sub-compartments (e.g. cell and interstitial space). Center-right: PBPK model (exchange of drug between organs via blood flow). Right: Extraction of kinetic features underlying drug distribution in a simplified model

where $f_u{}^x$ denotes the unbound fraction of drug in the sub-compartment x, which is defined as the steady state distribution between the unbound aqueous concentration and the total concentration $f_u{}^x = C_u^x/C^x$. If the relation between the total concentration C and the unbound aqueous concentration C_u is assumed to be non-linear, e.g., due to saturable binding processes, equation (5.16) has to be replaced. We will comment on this and illustrate possible extensions below.

First, we consider a linear relation between the unbound aqueous and the total drug concentration. We restrict our consideration to a single sub-compartment x to derive a predictive equation for $f_u{}^x$. Let us assume that within the compartment x, the compound distributes into neutral lipids or phospholipids, and is present in water in dissolved form or bound to proteins; other effects are considered neglectable. Then, the total amount of drug A^x in the sub-compartment x is given by [573–575]

$$A^x = A_u + A^{pr} + A^{nl} + A^{np}, \tag{5.17}$$

where A_u denotes the amount of unbound drug in water, A^{pr} the amount of bound drug in the water, A^{nl} and A^{np} the amount of drug partitioned into neutral lipids (nl) and phospholipids (np). Let us denote by $V^{z:x}$ the fractional volume of the constituent z (e.g., water, neutral or phospholipids) with respect to the total volume of the sub-compartment x, i.e.,

$$V^{z:x} = \frac{V^z}{V^x}. \tag{5.18}$$

Dividing eq. (5.17) by the total sub-compartment volume V^x yields

$$C^x = (C_u + C^{pr}) \cdot V^{w:x} + C^{nl} \cdot V^{nl:x} + C^{np} \cdot V^{np:x} \tag{5.19}$$

with $C_u = A_u/V^w$, $C^{pr} = A^{pr}/V^w$, $C^{nl} = A^{nl}/V^{nl}$, and $C^{np} = A^{np}/V^{np}$. Dividing by the unbound aqueous concentration C_u and exploiting linear binding and distribution processes such that $C_u = f_u{}^x C^x$, we finally obtain

$$\frac{1}{f_u{}^x} = \left(1 + \frac{C^{pr}}{C_u}\right) V^{w:x} + \left(\frac{C^{nl}}{C_u}\right) V^{nl:x} + \left(\frac{C^{np}}{C_u}\right) V^{np:x}. \tag{5.20}$$

The concentration ratios on the right hand side of eq. (5.20) can be interpreted as partition coefficients associated with the different sub-compartment constituents: the protein-unbound, neutral lipids-unbound and neutral phospholipids-unbound partition coefficients

$$K^{pr:u} = \frac{C^{pr}}{C_u}, \qquad K^{nl:u} = \frac{C^{nl}}{C_u}, \qquad K^{np:u} = \frac{C^{np}}{C_u}. \tag{5.21}$$

This finally yields

$$\frac{1}{{f_u}^x} = (1 + K^{pr:u}) \cdot V^{w:x} + K^{nl:u} \cdot V^{nl:x} + K^{np:u} \cdot V^{np:x}. \quad (5.22)$$

Hence, the inverse of the unbound fraction is a weighted sum of different constituent partition coefficients. The weighting factors are given by the volume fractions of the tissue constituents. The above relation is not restricted to the chosen example, but is much more general: Assume that the sub-compartment comprises water and constituents $z \in \{a, b, c, \ldots\}$ in which drug can be retained. Then, the unbound fraction ${f_u}^x$ satisfies

$$\frac{1}{{f_u}^x} = V^{w:x} + \sum_{z \in \{a,b,c,\ldots\}} K^{z:u} \cdot V^{z:x}. \quad (5.23)$$

In order to derive *a priori* predictive models, the tissue constituents partition coefficients are approximated by parameters that can be approximated by *in vitro* surrogate measurements. To recognize this and to find appropriate experimental realizations was the break-through in *a priori* determination of partition coefficients [576, 577]. The differences between existing tissue distribution models regard (i) the tissue constituents that are taken into account and (ii) the approximation of partition coefficients for the resulting constituents by *in vitro* data. Typically, ionization effects, potential binding to acidic phospholipids and partitioning into the neutral- and phospholipids are processes associated with the cellular space. Important processes in the interstitial space include binding to macro-molecules and ionization effects. Plasma and erythrocytes partitioning are typically measured directly by *in vitro* experiments.

Finally, let us consider a non-linear relation between the unbound and total concentration. E.g., assume that binding in the interstitial space is saturable, specified in terms of the dissociation constant K_D and the maximum number of possible binding sites B. Then, eq. (5.16) for $x = i$ has to be replaced by the equation

$$C_u^i = \frac{1}{2}\left(C^i - B - K_D + \sqrt{(C^i - B - K_D)^2 + 4K_D C^i}\right). \quad (5.24)$$

Further extensions can be realized in a similar way.

The unbound fraction in plasma ${f_u}^p$ can directly be determined by *in vitro* measurements. We will therefore not discuss it further here. In fig. 5.9 we show experimentally determined plasma binding $1 - {f_u}^p$ for some HIV compounds.

5.3.2 Drug Exchange Through Membranes and Partition Coefficients.

So far, we have derived the unbound concentration C_u of a drug with respect to the aqueous phase within an anatomical compartment. It is usually assumed, that only the unbound drug C_u can pass the cellular membrane by passive diffusion, or interact with macromolecules that facilitate- or direct membrane permeation [541].

An organ is considered to consist of capillaries (blood), the interstitial space (the space between cells) and the cells. We neglect the erythrocytes within the blood for a moment because they are not in direct exchange with the tissues. Drug can be exchanged between the blood-plasma p and the interstitium i and between the interstitium and the cells c. We can therefore derive the following set of equations, that describe the exchange of drugs between the adjacent tissue sub-compartments:

$$V^p \frac{d}{dt} C^p = +\text{advection} \quad (5.25)$$

$$-r^{p\to i} \cdot C_u^p + r^{i\to p} \cdot C_u^i \quad (5.26)$$

$$V^i \frac{d}{dt} C^i = r^{p\to i} \cdot C_u^p - r^{i\to p} \cdot C_u^i - r^{i\to c} \cdot C_u^i + r^{c\to i} \cdot C_u^c \quad (5.27)$$

$$V^c \frac{d}{dt} C^c = r^{i\to c} \cdot C_u^i + r^{c\to i} \cdot C_u^c \quad (5.28)$$

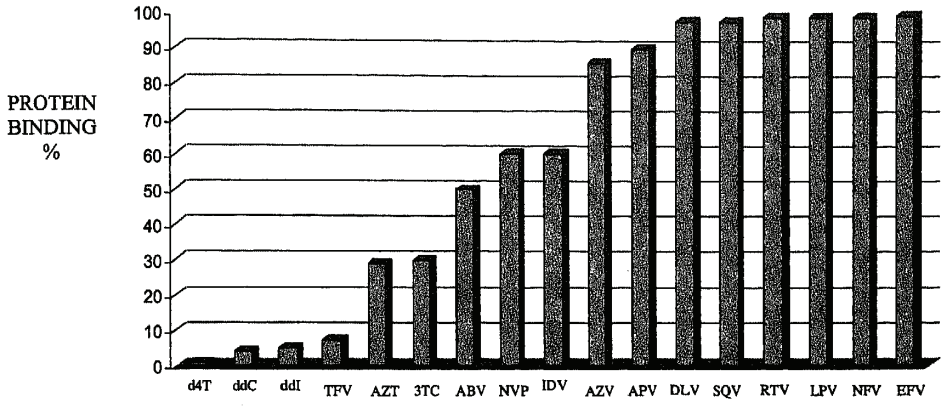

Abbreviations: d4T, stavudine; ddC, zalcitabine; ddI, didanosine; TFV, tenofovir; AZT, zidovudine; 3TC, lamivudine; ABV, abacavir; NVP, nevirapine; IDV, indinavir; AZV, atazanavir; APV, amprenavir; DLV, delavirdine; SQV, saquinavir; RTV, ritonavir; LPV, lopinavir; NFV, nelfinavir; EFV, efavirenz.

Figure 5.9: Protein Binding of antivirals. Figure from [578]

where $r^{\mathrm{p}\to\mathrm{i}}, r^{\mathrm{i}\to\mathrm{p}}, r^{\mathrm{i}\to\mathrm{c}}, r^{\mathrm{c}\to\mathrm{i}}$ are the fluxes [volume/time] of drug from the plasma to the interstitial space, the interstitial space to the plasma, the interstitial space to the cell and the cell to the interstitial space, respectively.

Example 1: Equilibrating Transport. If the drug exchange is primarily governed by passive diffusion or equilibrating transport, then, $r^{\mathrm{p}\to\mathrm{i}} = r^{\mathrm{i}\to\mathrm{p}}$ and $r^{\mathrm{i}\to\mathrm{c}} = r^{\mathrm{c}\to\mathrm{i}}$ and for the dynamical equilibrium (steady state), we derive

Assumption: Equilibrating Transport

$$C_{\mathrm{u}}^{\mathrm{p}} = C_{\mathrm{u}}^{\mathrm{i}} = C_{\mathrm{u}}^{\mathrm{c}}. \tag{5.29}$$

Recalling that the unbound aqueous concentration is defined with respect to water volume and exploiting eq. (5.29), we obtain for the unbound fraction in the tissue

$$\frac{1}{{\mathrm{f_u}}^{\mathrm{t}}} = \frac{C^{\mathrm{t}}}{C_{\mathrm{u}}^{\mathrm{t}}} = \frac{(V^{\mathrm{i}}C^{\mathrm{i}} + V^{\mathrm{c}}C^{\mathrm{c}})/V^{\mathrm{t}}}{(V^{\mathrm{wi}}C_u^{\mathrm{i}} + V^{\mathrm{wc}}C_{\mathrm{u}}^{\mathrm{c}})/V^{\mathrm{wt}}} \tag{5.30}$$

$$= \left(\frac{V^{\mathrm{i}}}{{\mathrm{f_u}}^{\mathrm{i}}} + \frac{V^{\mathrm{c}}}{{\mathrm{f_u}}^{\mathrm{c}}}\right)\left(V^{\mathrm{wi}} + V^{\mathrm{wc}}\right)^{-1} \cdot \frac{V^{\mathrm{wt}}}{V^{\mathrm{t}}}, \tag{5.31}$$

where the subscripts wt, wi and wc refer to the tissue-, interstitial- and cellular water, and $V^{\mathrm{t}} = V^{\mathrm{i}} + V^{\mathrm{c}}$ and $V^{\mathrm{wt}} = V^{\mathrm{wi}} + V^{\mathrm{wc}}$. We end up with the relation

$$\frac{V^{\mathrm{t}}}{{\mathrm{f_u}}^{\mathrm{t}}} = \frac{V^{\mathrm{i}}}{{\mathrm{f_u}}^{\mathrm{i}}} + \frac{V^{\mathrm{c}}}{{\mathrm{f_u}}^{\mathrm{c}}}. \tag{5.32}$$

By definition, the tissue-unbound plasma partition coefficient is given by $K^{\mathrm{t:up}} = C^{\mathrm{t}}/C_{\mathrm{u}}^{\mathrm{p}}$. This yields

$$K^{\mathrm{t:up}} = \frac{1}{{\mathrm{f_u}}^{\mathrm{t}}}, \tag{5.33}$$

where we have again exploited that at steady state the unbound aqueous concentration are identical, i.e., $C_{\mathrm{u}}^{\mathrm{p}} = C_{\mathrm{u}}^{\mathrm{t}}$. Combining eqs. (5.32) and (5.33), we get the central relation between the tissue-unbound plasma partition coefficient and the unbound fractions in the different sub-compartments:

Partitioning: Equilibrating Transport.

$$K^{\mathrm{t:up}} = \frac{V^{\mathrm{i:t}}}{{f_u}^{\mathrm{i}}} + \frac{V^{\mathrm{c:t}}}{{f_u}^{\mathrm{c}}} \tag{5.34}$$

Since we have $K^{\mathrm{t:p}} = {f_u}^{\mathrm{p}} \cdot K^{\mathrm{t:up}}$, we may alternatively predict the tissue-plasma partition coefficient $K^{\mathrm{t:p}}$. Eq. (5.34) easily generalizes to more than two tissue sub-compartments.

Example 2: Concentrative Transport. We assume that the drug exchange is primarily governed by passive diffusion between the plasma p and the interstitial space i and we assume that the drug is actively taken up into the cell c by some concentrative mechanism, in addition to passive diffusion. $r^{\mathrm{p}\to\mathrm{i}} = r^{\mathrm{i}\to\mathrm{p}}$ and $r^{\mathrm{i}\to\mathrm{c}} \neq r^{\mathrm{c}\to\mathrm{i}}$ and for the dynamical equilibrium (steady state), we derive

Assumption: Concentrative Transport

$$C_u^{\mathrm{p}} = C_u^{\mathrm{i}} = C_u^{\mathrm{c}}/\alpha \ , \tag{5.35}$$

where $\alpha = r^{\mathrm{i}\to\mathrm{c}}/r^{\mathrm{c}\to\mathrm{i}}$ is the "influx ratio". In this example, the influx is given by $r^{\mathrm{i}\to\mathrm{c}} = r_{\mathrm{eq}}^{\mathrm{i}\to\mathrm{c}} + r_{\mathrm{conc}}^{\mathrm{i}\to\mathrm{c}}$, where $r_{\mathrm{eq}}^{\mathrm{i}\to\mathrm{c}}$ denotes the equilibrating mechanism (e.g. passive diffusion) and $r_{\mathrm{conc}}^{\mathrm{i}\to\mathrm{c}}$ denotes the concentrative mechanism. For simplicity we assume that $r_{\mathrm{eq}}^{\mathrm{i}\to\mathrm{c}}$ and $r_{\mathrm{conc}}^{\mathrm{i}\to\mathrm{c}}$ are linear. From eq. 5.35 we derive two relations:

$$C_u^{\mathrm{c}} = \alpha \cdot C_u^{\mathrm{p}} \tag{5.36}$$

$$\alpha = C_u^{\mathrm{c}}/C_u^{\mathrm{i}}. \tag{5.37}$$

Under these conditions, we derive

$$\frac{1}{{f_u}^{\mathrm{t}}} = \left(\frac{V^{\mathrm{i}}}{{f_u}^{\mathrm{i}}} + \frac{\alpha \cdot V^{\mathrm{c}}}{{f_u}^{\mathrm{c}}}\right) \cdot \frac{V^{\mathrm{wt}}}{(V^{\mathrm{wi}} + \alpha \cdot V^{\mathrm{wc}})V^{\mathrm{t}}}. \tag{5.38}$$

utilizing eqs. (5.36) and (5.35). The tissue to unbound plasma partitioning coefficient ($K^{\mathrm{t:up}}$) is defined as

$$\begin{aligned} K^{\mathrm{t:up}} &= \frac{C^{\mathrm{t}}}{C_u^{\mathrm{p}}} = \frac{1}{{f_u}^{\mathrm{t}}} \cdot \frac{C_u^{\mathrm{t}}}{C_u^{\mathrm{p}}} = \frac{1}{{f_u}^{\mathrm{t}}} \cdot \frac{V^{\mathrm{wi}} C_u^{\mathrm{i}} + V^{\mathrm{wc}} C_u^{\mathrm{c}}}{V^{\mathrm{wt}} C_u^{\mathrm{p}}} \\ &= \frac{1}{{f_u}^{\mathrm{t}}} \cdot \frac{V^{\mathrm{wi}} + \alpha \cdot V^{\mathrm{wc}}}{V^{\mathrm{wt}}} \end{aligned} \tag{5.39}$$

where we used eq. (5.37). Combining eq. (5.38) and (5.39) yields the final equation for the tissue to unbound plasma partition coefficient:

Partitioning: Concentrative Transport

$$K^{\mathrm{t:up}} = \frac{V^{\mathrm{i:t}}}{{f_u}^{\mathrm{i}}} + \frac{\alpha \cdot V^{\mathrm{c:t}}}{{f_u}^{\mathrm{c}}}. \tag{5.40}$$

Example 3: Passive diffusion of uncharged compound. Most drugs are weak electrolytes (e.g. acids or bases). In solution, they can exist in an un-ionized (neutral) and ionized (charged) form. Because the ionized form of the drug has a decreased lipid-solubility, it is stated in the **pH partition hypothesis**, that the un-ionized (neutral) drug penetrates the membrane by many magnitudes faster

than the charged form and that ionization is instantaneously achieved. As a consequence, the concentrations of the un-ionized species will equilibrate on both sides of the membrane. The concentrations of the ionized species and therefore the total concentration may be different, depending on the solute pH on either side of the membrane.

Based on the compounds pK_a and the physiological pH in an anatomical compartment [573, 579], it is possible to calculate the neutral (uncharged) fraction fn for a compound in this compartment. The derivation of fn is given in appendix A.

We assume that the unionized, unbound aqueous concentration is identical in all sub-compartments, i.e.,

Assumption: Passive Diffusion of unionized drug

$$\mathrm{fn}^{\mathrm{p}} C_{\mathrm{u}}^{\mathrm{p}} = \mathrm{fn}^{\mathrm{i}} C_{\mathrm{u}}^{\mathrm{i}} = \mathrm{fn}^{\mathrm{c}} C_{\mathrm{u}}^{\mathrm{c}}. \tag{5.41}$$

Recalling that the unbound aqueous concentration is defined with respect to water volume and exploiting eq. (5.41), we obtain for the unbound fraction in the tissue

$$\frac{1}{{\mathrm{f_u}}^{\mathrm{t}}} = \frac{C^{\mathrm{t}}}{C_{\mathrm{u}}^{\mathrm{t}}} = \frac{(V^{\mathrm{i}} C^{\mathrm{i}} + V^{\mathrm{c}} C^{\mathrm{c}})/V^{\mathrm{t}}}{(V^{\mathrm{wi}} C_{\mathrm{u}}^{\mathrm{i}} + V^{\mathrm{wc}} C_{\mathrm{u}}^{\mathrm{c}})/V^{\mathrm{wt}}} \tag{5.42}$$

$$= \left(\frac{V^{\mathrm{i}}}{\mathrm{fn}^{\mathrm{i}}\, {\mathrm{f_u}}^{\mathrm{i}}} + \frac{V^{\mathrm{c}}}{\mathrm{fn}^{\mathrm{c}}\, {\mathrm{f_u}}^{\mathrm{c}}} \right) \left(\frac{V^{\mathrm{wi}}}{\mathrm{fn}^{\mathrm{i}}} + \frac{V^{\mathrm{wc}}}{\mathrm{fn}^{\mathrm{c}}} \right)^{-1} \cdot \frac{V^{\mathrm{wt}}}{V^{\mathrm{t}}}, \tag{5.43}$$

Defining the neutral fraction in tissue fn^{t} by

$$\frac{V^{\mathrm{wt}}}{\mathrm{fn}^{\mathrm{t}}} = \frac{V^{\mathrm{wi}}}{\mathrm{fn}^{\mathrm{i}}} + \frac{V^{\mathrm{wc}}}{\mathrm{fn}^{\mathrm{c}}}, \tag{5.44}$$

we end up with the relation

$$\frac{V^{\mathrm{t}}}{\mathrm{fn}^{\mathrm{t}}\, {\mathrm{f_u}}^{\mathrm{t}}} = \frac{V^{\mathrm{i}}}{\mathrm{fn}^{\mathrm{i}}\, {\mathrm{f_u}}^{\mathrm{i}}} + \frac{V^{\mathrm{c}}}{\mathrm{fn}^{\mathrm{c}}\, {\mathrm{f_u}}^{\mathrm{c}}}. \tag{5.45}$$

By definition, the tissue-unbound plasma partition coefficient is given by $K^{\mathrm{t:up}} = C^{\mathrm{t}}/C_{\mathrm{u}}^{\mathrm{p}}$. This yields

Partitioning: Passive Diffusion of unionized drug

$$K^{\mathrm{t:up}} = \frac{\mathrm{fn}^{\mathrm{p}}}{\mathrm{fn}^{\mathrm{t}} {\mathrm{f_u}}^{\mathrm{t}}}, \tag{5.46}$$

where we have again exploited that at steady state the unionized, unbound aqueous concentration are identical, i.e., $\mathrm{fn}^{\mathrm{p}} C_{\mathrm{u}}^{\mathrm{p}} = \mathrm{fn}^{\mathrm{t}} C_{\mathrm{u}}^{\mathrm{t}}$. Combining eqs. (5.45) and (5.46), we get the central relation between the tissue-unbound plasma partition coefficient and the unbound fractions in the different sub-compartments:

Partitioning: Passive Diffusion of unionized drug

$$K^{\mathrm{t:up}} = \frac{\mathrm{fn}^{\mathrm{p}}}{\mathrm{fn}^{\mathrm{i}}} \cdot \frac{V^{\mathrm{i:t}}}{{\mathrm{f_u}}^{\mathrm{i}}} + \frac{\mathrm{fn}^{\mathrm{p}}}{\mathrm{fn}^{\mathrm{c}}} \cdot \frac{V^{\mathrm{c:t}}}{{\mathrm{f_u}}^{\mathrm{c}}}. \tag{5.47}$$

Erythrocytes. Drug might also be distributed and retained in erythrocytes. The blood-plasma ratio B : P is commonly measured *in vitro*. Using the hematocrit hct (reference: 0.45 in human), it is possible to derive the erythrocyte-to-plasma partition coefficient $K^{\mathrm{e:p}}$:

$$K^{\mathrm{e:p}} = \frac{\mathrm{B:P} - (1 - \mathrm{hct})}{\mathrm{hct}}. \tag{5.48}$$

5.3.3 Parametrization

Partition coefficients $K^{\mathrm{x:y}}$ measure the ratio of drug concentration between two compartments x, y, typically at steady state [537]. Partition coefficients between tissue and plasma $K^{\mathrm{t:p}}$ or tissue and blood $K^{\mathrm{t:b}}$ can be measured experimentally in animals. However, obtaining these parameters is costly and time-consuming, as the animals are usually sacrificed and tissues are extracted for measurement. It is not possible to obtain these parameters for the human. A common approach is to assume that the processes that underlie the distribution of a drug in the animal tissue are identical in the human [580]. However, this assumption might, in many cases, not be justified and consequently animal tissue partition coefficients might be of little value to extrapolate to human.

To overcome the dilemma of potentially investing a large amount of money and time into an uncertain benefit, it was proposed [573, 574, 576, 577, 579, 581] to estimate tissue partition coefficients *a priori* from physiological- and *in vitro* data.

The published models predict the amount of bound (retained) drug in each tissue subspace (e.g. interstitial space $f_u{}^i$, cell $f_u{}^c$, whole tissue $f_u{}^t$) and then assume generic processes (like passive diffusion, eqs. (5.33),(5.47)) to estimate the distribution of drugs within the subspaces of the organ and to derive the tissue-to-plasma partition coefficients $K^{\mathrm{t:p}}$. The models can, in principle, be also tailored to specific compounds, by incorporating active (concentrative) transport (e.g. eq. (5.40)).

Published Models.

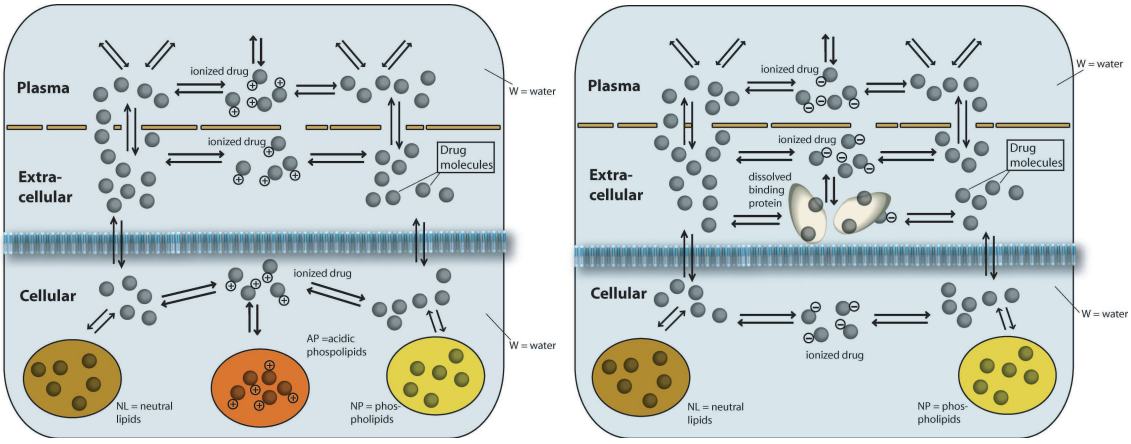

Figure 5.10: Tissue decomposition and processes underlying the *a priori* partition coefficient models for moderate to strong bases by Rodgers et al. (left), and for neutrals and acids by Rodgers and Rowland (right). For details, see the text.

Moderate to strong bases and type 1 zwitterions Rodgers et al. [573, 574] developed mechanistic equations to predict the tissue-unbound plasma partition coefficient for moderate to strong bases ($\mathrm{pK_a} \geq 7.0$) and type 1 zwitterions (at least one $\mathrm{pK_a} \geq 7.0$). The model assumes that the unbound (dissolved) drug is possibly ionized in the extra-cellular and intra-cellular space. In the intra-cellular space, the ionized drug may bind to acidic phospholipids (rem), while the neutral form may distribute into neutral lipids (nl) and phospholipids (np). Furthermore it is assumed that only

the neutral species can cross membranes by passive diffusion; see Fig. 5.10, left for illustration. In the following derivation, we identify the extra-cellular and intra-cellular space in [573, 574] with the interstitial and cellular space. Moreover, we denote the water in the interstitial and cellular space by (wi) and (wc).

The model is based on the following approximations of the constituent partition coefficients: (i) cellular residual tissue components-unbound drug partitioning:

$$K^{\text{rem:uc}} = \big(1 - \text{fn}^{\text{c}}\big) K_{\text{A,AP}} [\text{AP}^-]^{\text{rem}}, \tag{5.49}$$

where $[\text{AP}^-]^{\text{rem}}$ denotes the concentration of acidic phospholipids in the residual space, with corresponding association constant $K_{\text{A,AP}}$. (ii) Neutral lipids-unbound drug partitioning:

$$K^{\text{nl:uc}} = \text{fn}^{\text{c}} P_{*:\text{w}}, \tag{5.50}$$

where $P_{*:\text{w}}$ is chosen to be the octanol-water partition coefficient $P_{\text{o:w}}$ for non-adipose tissue and the vegetable oil-water partition coefficient $P_{\text{vo:w}}$ for adipose tissue. (iii) Neutral phospholipids-unbound drug partitioning:

$$K^{\text{np:uc}} = \text{fn}^{\text{c}} \big(0.3 \cdot P_{*:\text{w}} + 0.7\,\big) \tag{5.51}$$

assuming that neutral phospholipids behave like a mixture of 30% neutral lipids and 70% water (as initially suggested by Poulin and Theil in [576]).

Sub-compartmentalized tissue distribution model. Since no interstitial binding is considered, the unbound fraction in the interstitial space is

$$\frac{1}{\text{f}_{\text{u}}{}^{\text{i}}} \;=\; 1, \tag{5.52}$$

while we obtain

$$\begin{aligned} \frac{1}{\text{f}_{\text{u}}{}^{\text{c}}} \;=\;& V^{\text{wc:c}} + \text{fn}^{\text{c}} P_{*:\text{w}} V^{\text{nl:c}} + \text{fn}^{\text{c}} \big(0.3\; P_{*:\text{w}} + 0.7\big) V^{\text{np:c}} + \\ & (1 - \text{fn}^{\text{c}}) K_{\text{A,AP}} [\text{AP}^-]^{\text{c}} \end{aligned} \tag{5.53}$$

for the cellular unbound fraction, where we exploited the relation $[\text{AP}^-]^{\text{c}} = [\text{AP}^-]^{\text{rem}} V^{\text{rem:c}}$. Note that $V^{x:\text{c}} = V^{x:\text{t}} \cdot V^{\text{t}}/V^{\text{c}}$, so that volume fractions with reference to the cellular space can easily be converted into those with reference to the tissue space (and thus we can use the readily available data in [573, 574, 582]).

Lumped steady state model. Exploiting eq. (5.47) we obtain the tissue-unbound plasma partition coefficient for moderate to strong bases:

$$\begin{aligned} K^{\text{t:up}} \;=\;& V^{\text{wi:t}} + \frac{\text{fn}^{\text{p}}}{\text{fn}^{\text{c}}} V^{\text{wc:t}} + \text{fn}^{\text{p}} P_{*:\text{w}} V^{\text{nl:t}} + \text{fn}^{\text{p}} \big(0.3\; P_{*:\text{w}} + 0.7\big) V^{\text{np:t}} + \\ & \text{fn}^{\text{p}} \frac{1 - \text{fn}^{\text{c}}}{\text{fn}^{\text{c}}} K_{\text{A,AP}} [\text{AP}^-]^{\text{t}}, \end{aligned} \tag{5.54}$$

where $[\text{AP}^-]^{\text{t}}$ denotes the concentration of acidic phospholipids in tissue, which is related to the corresponding cellular concentration $[\text{AP}^-]^{\text{c}}$ by $[\text{AP}^-]^{\text{c}} V^{\text{c:t}} = [\text{AP}^-]^{\text{t}}$. We remark that

$$\frac{1 - \text{fn}^{\text{c}}}{\text{fn}^{\text{c}}} \;=\; 10^{-(\text{pH}_{\text{c}} - \text{pK}_{\text{a}})} \tag{5.55}$$

for mono-protonic bases. Typically, values for $K_{\text{A,AP}}$ are not readily available for the different tissues. In order to estimate the unknown association constants, Rodgers et al. suggested to determine $K_{\text{A,AP}}$ for the erythrocytes from the blood-plasma ratio B : P and use this value as an approximation for the association constants in the other tissues. For details see [573, 583]. Parameter values can be found in [573, 574] for the species rat.

Very weak bases, neutrals, acids and type 2 zwitterions In [574] Rodgers and Rowland developed mechanistic equations to predict tissue-unbound plasma partition coefficients for very weak bases ($pK_a < 7.0$), neutrals, acids and type 2 zwitterions (no $pK_a \geq 7.0$). The model assumes that the drug is dissolved and possibly ionized (for acids, very weak bases, and type 2 zwitterions) in the extra-cellular and intra-cellular space. It may bind in either form macromolecules (albumin for acids and weak bases, lipoproteins for neutrals) in the extra-cellular space, and distribute into neutral lipids and phospholipids in unionized form in the intra-cellular space. Furthermore it is assumed that only the neutral species can passively diffuse across membranes; see Fig. 5.10 (right) for illustration. In the following derivation, we again identify the extra-cellular and intra-cellular space in [574] with the interstitial and cellular space.

The model is based on the following approximations of the constituents partition coefficients: (i) Interstitial protein-unbound drug partitioning:

$$K^{\text{pr:ui}} = \text{K}_{\text{A,PR}}\text{PR}^{\text{wi}}, \tag{5.56}$$

where PR^{wi} denotes the concentration of interstitial binding protein (albumin in the case of *acidic*, *very weak basic* and type 2 *zwitterions*, or lipoproteins in the case of *neutral* compounds), and $\text{K}_{\text{A,PR}}$ refers to the corresponding association constant. (ii) Neutral lipids-unbound drug partitioning:

$$K^{\text{nl:uc}} = \text{fn}^{\text{c}} P_{*:\text{w}}, \tag{5.57}$$

where $P_{*:\text{w}}$ is chosen to be the octanol-water partition coefficient $P_{\text{o:w}}$ for non-adipose tissue and the vegetable oil-water partition coefficient $P_{\text{vo:w}}$ for adipose tissue. (iii) Neutral phospholipids-unbound drug partitioning:

$$K^{\text{np:uc}} = \text{fn}^{\text{c}}\big(0.3P_{*:\text{w}} + 0.7\big) \tag{5.58}$$

assuming that neutral phospholipids behave like a mixture of 30% neutral lipids and 70% water (as above).

Sub-compartmentalized tissue distribution model. For the unbound fraction in the interstitial space, eq. (5.23) yields

$$\frac{1}{\text{f}_{\text{u}}{}^{\text{i}}} \quad = \quad 1 + \text{K}_{\text{A,PR}}\text{PR}^{\text{i}}, \tag{5.59}$$

while we obtain

$$\frac{1}{\text{f}_{\text{u}}{}^{\text{c}}} \quad = V^{\text{wc:c}} + \text{fn}^{\text{c}} P_{*:\text{w}} V^{\text{nl:c}} + \text{fn}^{\text{c}}\big(0.3\ P_{*:\text{w}} + 0.7\big) V^{\text{np:c}} \tag{5.60}$$

for the cellular unbound fraction.

Lumped steady state model. Exploiting eq. (5.47) we obtain the tissue-unbound plasma partition coefficient for very weak bases, acids, neutrals and group 2 zwitterions

$$\begin{aligned} K^{\text{t:up}} \quad = \quad & V^{\text{i:t}} + \text{K}_{\text{A,PR}}\text{PR}^{\text{t}} + \frac{\text{fn}^{\text{p}}}{\text{fn}^{\text{c}}} V^{\text{wc:t}} + \text{fn}^{\text{p}} P_{*:\text{w}} V^{\text{nl:t}} \\ & + \text{fn}^{\text{p}}\big(0.3P_{*:\text{w}} + 0.7\big) V^{\text{np:t}}, \end{aligned} \tag{5.61}$$

where we have exploited that $\text{PR}^{\text{t}} = \text{PR}^{\text{i}}\ V^{\text{i:t}}$. Rodgers and Rowland suggest to determine $\text{K}_{\text{A,PR}}$ in plasma from $\text{f}_{\text{u}}{}^{\text{p}}$ and $P_{\text{o:w}}$. For details see [574, eq. (13)]. Parameter values can be found in [574, 583] for the species rat.

Poulin-Theil model In their seminal papers in 2000/01 [576, 577], Poulin and Theil proposed an *in silico* approach to *a priori* predict tissue-plasma partition coefficients solely based on few compound specific *in vitro* data. They assumed that the compound is present in dissolved form in tissue water, that it may bind to macromolecules in the interstitial space, and distribute into neutral lipids

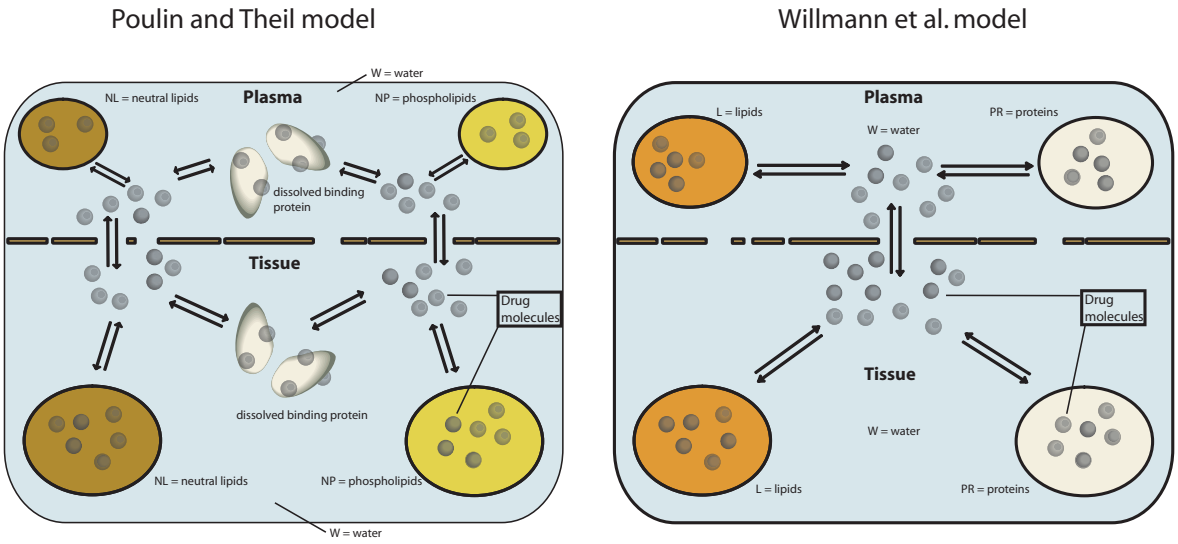

Figure 5.11: Tissue decomposition and processes underlying the *a priori* partition coefficient models by Poulin and Theil (left), and by Willmann et al. (right). For details, see the text.

or phospholipids in the cellular space, while other effects are considered negligible. These equations have subsequently been corrected by Berezhovskiy [575, eq. (64)] (see also [574]). For the present model we will only derive the unbound fraction in the tissue $f_u{}^t$, since only the total tissue water is considered by Poulin and Theil rather than a distinction between the interstitial and cellular water as in the previous models. The unbound fraction in tissue is linked to the tissue partition coefficient via $K^{t:p} = f_u{}^p / f_u{}^t$, if ionization is not considered.

The model (including the corrections) is based on the following approximations: (i) Protein-unbound drug partitioning:

$$K^{pr:ut} = \begin{cases} 1/(2f_u{}^p) - 1/2; & \text{non-adipose tissue,} \\ 0; & \text{adipose tissue,} \\ 1/f_u{}^p - 1; & \text{plasma} \end{cases} \tag{5.62}$$

where $f_u{}^p$ denotes the unbound fraction in plasma as measured by *in vitro* assays. (ii) Neutral lipids-unbound drug partitioning:

$$K^{nl:ut} = P_{*:w}, \tag{5.63}$$

where $P_{*:w}$ is chosen to be the octanol-water partition coefficient $P_{o:w}$ for non-adipose tissue and the vegetable oil-water partition coefficient $P_{vo:w}$ for adipose tissue. (iii) Neutral phospholipids-unbound drug partitioning:

$$K^{np:ut} = 0.3 \cdot K^{nl:ut} + 0.7, \tag{5.64}$$

where it is assumed that neutral phospholipids behave like a mixture of 30% neutral lipids and 70% water. For ionizable compounds, $P_{vo:w}$ has to be replaced by $fn \cdot P_{vo:w}$. In view of eq. (5.63) and (5.64) this implies that a correction for ionizable compounds is only made for adipose tissue (see discussion in [584]).

Sub-compartmentalized tissue distribution model. Based on the fundamental relation (5.22), the unbound fraction in *non-adipose* tissue $f_u{}^t$ is given by

$$\frac{1}{f_u{}^t} = \left(\frac{1}{2f_u{}^p} + \frac{1}{2}\right) V^{wt:t} + P_{o:w} V^{nl:t} + \big(0.3\, P_{o:w} + 0.7\big) V^{np:t}. \tag{5.65}$$

For *adipose* tissue it is

$$\frac{1}{{f_u}^t} = V^{wt:t} + P_{vo:w}V^{nl:t} + \big(0.3\ P_{vo:w} + 0.7\big)V^{np:t}. \tag{5.66}$$

Lumped steady state model. By neglecting ionization (fn = 1), as in [576], we exploit eq. (5.46) and $K^{t:p} = K^{t:up} \cdot {f_u}^p$ to obtain the tissue-plasma partition coefficient as published by Poulin and Theil, with subsequent corrections according to Berezhovskiy. For *non-adipose tissue* it is

$$K^{t:p} = \frac{\big(1/(2{f_u}^p) + 1/2\big)V^{w:t} + P_{o:w}V^{nl:t} + \big(0.3\ P_{o:w} + 0.7\big)V^{np:t}}{(1/{f_u}^p)V^{w:p} + P_{o:w}V^{nl:p} + \big(0.3\ P_{o:w} + 0.7\big)V^{np:p}}, \tag{5.67}$$

and for *adipose tissue* it is

$$K^{t:p} = \frac{V^{w:t} + P_{vo:w}V^{nl:t} + \big(0.3\ P_{vo:w} + 0.7\big)V^{np:t}}{(1/{f_u}^p)V^{w:p} + P_{vo:w}V^{nl:p} + \big(0.3\ P_{vo:w} + 0.7\big)V^{np:p}}, \tag{5.68}$$

where $V^{w:p}$, $V^{nl:p}$, $V^{np:p}$ are the respective fractions of water, neutral lipids and phospholipids in plasma. Parameter values can be found in [576, 585] for the species rabbit, rat, mouse and human.

Willmann et al. model In [581], Willmann et al. proposed an alternative mechanistic model for the calculation of the tissue-plasma partition coefficient $K^{t:p}$. In contrast to the previous models, Willmann et al. use the membrane affinity to quantify binding to lipids. It is assumed that the compound can dissolve in tissue water, bind to proteins (pr) and membrane lipids (l). In distinction to the previous models, Willmann et al. consider the proteins as a separate phase.

The model is based on the following approximations [581]: (i) Protein-unbound drug partitioning:

$$K^{pr:ut} = \begin{cases} \mathrm{PR}/\mathrm{K_D}; & \text{plasma} \\ 10^{-5}\ \mathrm{MA}; & \text{tissue} \end{cases} \tag{5.69}$$

where PR denotes the concentration of albumin in the blood plasma, and $\mathrm{K_D}$ denotes the dissociation constant for serum proteins. (ii) Lipids-unbound drug partitioning:

$$K^{l:ut} = \mathrm{MA} \tag{5.70}$$

where MA denotes the membrane affinity. For ionizable compounds, the tissue protein-unbound drug partitioning is corrected with the ionization constant $\mathrm{pK_a}$ yielding

$$K^{pr:ut} = 10^{-5}\left(9.9\frac{1}{1 + (8/\mathrm{pK_a})^{18}} + 0.1\right)\mathrm{MA}. \tag{5.71}$$

Sub-compartmentalized tissue distribution model. Based on the fundamental relation (5.22), the unbound fraction in tissue ${f_u}^t$ is given by

$$\frac{1}{{f_u}^t} = V^{wt:t} + K^{pr:wt}V^{pr:t} + \mathrm{MA} \cdot V^{l:t}. \tag{5.72}$$

Lumped steady state model. Exploiting eq. (5.46) and $K^{t:p} = K^{t:up} \cdot {f_u}^p$ we obtain the tissue-plasma partition coefficient

$$K^{t:p} = \frac{V^{w:t} + K^{pr:ut}V^{pr:t} + \mathrm{MA} \cdot V^{l:t}}{V^{w:p} + K^{pr:up}V^{pr:p} + \mathrm{MA} \cdot V^{l:p}}. \tag{5.73}$$

Parameter values can be found in [586].

5.3.4 Lumping Tissue Distribution

One problem with PBPK models is their complexity and the non-verifiability of their parameters and predictions. The complexity and the bulk of information that is provided by the PBPK model is partly a result of its generic structure. However, one might rather be interested in certain aspects of the pharmacokinetics and drug distribution of a compound. Compartmental models are much more suitable to analyze certain aspects of the drugs pharmacokinetics that are important for the study endpoint. Compartmental models are minimal models, tailored to the compound of interest and to the study objective. Their simplicity allows for elaborated model analysis. Compartmental models can be derived from PBPK models, but not vice versa.

In almost all cases, a main interest is in the blood pharmacokinetics, because they are verifiable with patient *in vivo* data. The plasma provides the drug input in pharmacodynamically relevant compartments and therefore, drug concentrations at the effect site can be related to the concentrations in the plasma.

We have previously mentioned that drug distribution may be limited by membrane permeation and blood flow (see Glossary). For blood flow limited distribution, the distribution rate constant is given by [537]:

$$k_t = \frac{Q^{\mathrm{t}}}{V^{\mathrm{t}} \cdot K^{\mathrm{t:b}}} \tag{5.74}$$

where Q^{t} denotes the blood flow of the tissue. The distribution half life is given by $\ln(2)/k_t$ and distribution is finished after approximately four half lives [537]. Eq. (5.74) indicates that rate limiting distribution is of importance for compounds with very high tissue-plasma partitioning coefficients. However, limiting distribution will only have a considerable impact on plasma pharmacokinetics compartment, if the amount of drug that is distributed by the limiting process is large in relation to the rest of the body (as can be seen from eq. 5.80).

In most cases, limiting distribution is a phenomenon, that is only observed during the first doses of the drug or when a large amount of drug enters the blood plasma compartment within a short time, as in the case of an i.v. infusion. However, most HIV drugs are given chronically so that the impact of (membrane/blood flow) limited distribution disappears. If the main modelling focuss lies in the pharmacokinetics of chronically applied pharmaceutics and not in the potential initial distribution phase, then a one compartment model might sufficiently capture the plasma pharmacokinetics.

Example: One compartment model. In the case of a one compartment model, the concentration within the central compartment C_1 reflects the concentration within the blood-plasma compartment C^{p} (which is typically measured). The volume of the compartment V_{ss} is a parameter, that adjusts the concentrations in the central compartment C_1 to the plasma concentrations C^{p}.

The total amount of drug in the body is the sum over the drug amount in each anatomical compartment:

$$A^{\mathrm{tot}} = A^{\mathrm{p}} + A^{\mathrm{e}} + \sum_{\mathrm{t}} A^{\mathrm{t}}, \tag{5.75}$$

where A^{tot} denotes the total amount of drug in the body and $A^{\mathrm{p}}, A^{\mathrm{e}}$ and A^{t} are the amounts of drug in the plasma, the erythrocytes and the tissues respectively. We can now replace A^{tot} with $A^{\mathrm{tot}} = V_{\mathrm{ss}} \cdot C_1$, where the 'volume of distribution' at steady state V_{ss}, denotes a theoretical volume of fluid into which the total administered drug would have to be diluted to produce the concentration in blood-plasma ($C_1 = C^{\mathrm{p}}_{ss}$). From eq. (5.75), assuming steady state distribution, we derive

$$V_{\mathrm{ss}} \cdot C_1 = V^{\mathrm{p}} \cdot C^{\mathrm{p}}_{ss} + V^{\mathrm{e}} \cdot C^{\mathrm{e}}_{ss} + \sum_{\mathrm{t}} \left(V^{\mathrm{t}} \cdot C^{\mathrm{t}}_{ss}\right) \tag{5.76}$$

$$V_{\mathrm{ss}} = V^{\mathrm{p}} + V^{\mathrm{e}} \cdot \frac{C^{\mathrm{e}}_{ss}}{C^{\mathrm{p}}_{ss}} + \sum_{\mathrm{t}} \left(V^{\mathrm{t}} \cdot \frac{C^{\mathrm{t}}_{ss}}{C^{\mathrm{p}}_{ss}}\right) \tag{5.77}$$

where $C^{\mathrm{p}}_{ss}, C^{\mathrm{e}}_{ss}$ and C^{t}_{ss} denote the concentration of drug in the blood plasma, the erythrocytes and the tissue at the distribution equilibrium and $V^{\mathrm{p}}, V^{\mathrm{e}}$ and V^{t} are the corresponding volumes. By replacing the concentration ratios with the corresponding partition coefficients, e.g. $K^{\mathrm{e:p}} = \frac{C^{\mathrm{e}}_{ss}}{C^{\mathrm{p}}_{ss}}$ and $K^{\mathrm{t:p}} = \frac{C^{\mathrm{t}}_{ss}}{C^{\mathrm{p}}_{ss}}$, we can determine V_{ss} [537].

$$V_{\mathrm{ss}} \quad = \quad V^{\mathrm{p}} + V^{\mathrm{e}} \cdot K^{\mathrm{e:p}} + \sum_{\mathrm{t}} \big(V^{\mathrm{t}} \cdot K^{\mathrm{t:p}}\big). \tag{5.78}$$

The central equation for the one-compartment model is given by:

$$V_{\mathrm{ss}} \frac{\mathrm{d}}{\mathrm{d}t} C_1 = v_{\mathrm{in}}(t) - C_1 \cdot v_{\mathrm{out}}(t), \tag{5.79}$$

where $v_{\mathrm{in}}(t)$ and $v_{\mathrm{out}}(t)$ denote the influx of drug into the body through drug absorption and the elimination of drug from the body respectively.

Eq. (5.78) also holds in the non-steady-state:

$$V_{\mathrm{d}}(t) \quad = \quad V^{\mathrm{p}} + V^{\mathrm{e}} \cdot K^{\mathrm{e:p}}(t) + \sum_{\mathrm{t}} \big(V^{\mathrm{t}} \cdot K^{\mathrm{t:p}}(t)\big). \tag{5.80}$$

with $V_{\mathrm{d}}(t)$ being the apparent volume of distribution at time t and $K^{\mathrm{x:p}}(t) = \frac{C^{\mathrm{x}}(t)}{C^{\mathrm{p}}(t)}$ being the apparent partition coefficient between compartments x and the blood plasma.

The volume of distribution V_{ss} or V_{d} can alternatively be estimated from the *in vivo* concentration-time profile in the blood-plasma, following an i.v. administration [538].

Example: Two compartment model. A model that includes more than one compartments might be utilized in the case, where e.g. the distribution phase of the drug is important for the modelling purpose. We will exemplify here, how to derive a two-compartment model from the PBPK model. The basic assumption is that one set of compartments has non-instantaneous distribution (peripheral compartment with concentration C_2 and volume V_2) and another set of compartments has instantaneous distribution (central compartment with concentration C_1 and volume V_1). Furthermore, the concentrations in the central compartment can be identified with the (measurable) concentrations in the blood-plasma. The volume of the central compartment V_1 is determined similarly to eq. (5.78):

$$V_1 \quad = \quad V^{\mathrm{p}} + V^{\mathrm{e}} \cdot K^{\mathrm{e:p}} + \sum_{\mathrm{t} \in \mathrm{central}} \big(V^{\mathrm{t}} \cdot K^{\mathrm{t:p}}\big). \tag{5.81}$$

where we have assumed that the distribution into erythrocytes e is instantaneous. The volume of the peripheral compartment V_2 is given by

$$V_2 \quad = \quad \sum_{\mathrm{t} \in \mathrm{peripheral}} V^{\mathrm{t}}, \tag{5.82}$$

which includes all tissues with rate-limiting distribution. The equations for this model are given by

$$V_1 \frac{\mathrm{d}}{\mathrm{d}t} C_1 \quad = \quad v_{\mathrm{in}}(t) - C_1 \cdot v_{\mathrm{out}}(t) - r_1 \cdot C_1 + r_2 \cdot C_2 \tag{5.83}$$

$$V_2 \frac{\mathrm{d}}{\mathrm{d}t} C_2 \quad = \quad r_1 \cdot C_1 - r_2 \cdot C_2 \tag{5.84}$$

with fluxes [volume/time] r_1 and r_2. From the tissue to plasma partition coefficients of the peripheral compartment we can also derive the additional constraint

$$\frac{r_1}{r_2} \quad = \quad \frac{1}{V_2} \sum_{\mathrm{t} \in \mathrm{peripheral}} \big(V^{\mathrm{t}} \cdot K^{\mathrm{t:p}}\big). \tag{5.85}$$

Similarly, lumping can be performed to derive e.g. three compartment models.

5.4 Drug Elimination

Drug can be eliminated from the body by two mechanisms [538]: (i) enzymatic degradation that produces inactive metabolites and (ii) urinary/fecal/pulmonal excretion of the parent compound. For HIV compounds, the most important processes are enzymatic degradation and urinary excretion. For these reasons we will focuss on these two aspects only.

5.4.1 Drug Metabolism

At an early stage of the drug discovery process, *in vitro* experiments using recombinant cytocrome P450 iso-enzymes, microsomes, hepatocytes or liver slices [587] are used to measure hepatic degradation. Consider the unbound substance $\mathbf{C}_\mathrm{u}$ being metabolized by an enzyme $\mathbf{E}$ according to

$$\mathbf{C}_\mathrm{u} + \mathbf{E} \underset{k_\mathrm{off}}{\overset{k_\mathrm{on}}{\longleftrightarrow}} \mathbf{C}:\mathbf{E} \xrightarrow{k_\mathrm{cat}} \mathbf{M} + \mathbf{E}$$

where $\mathbf{C}:\mathbf{E}$ denotes the substance-enzyme complex, $\mathbf{M}$ denotes the metabolite of the enzymatic reaction, and k_on, k_off, and k_cat denote the corresponding rate constants. Following the widely used *Michaelis–Menten–approximation* (see, e.g., [588]), the reaction rate in **saturable metabolism** is given by

$$r_\mathrm{out,invitro} = \frac{V_\mathrm{max}}{K_\mathrm{M} + C_\mathrm{u}} \cdot C_\mathrm{u} \tag{5.86}$$

where $K_\mathrm{M} = (k_\mathrm{off} + k_\mathrm{cat})/k_\mathrm{on}$ is the Michaelis–Menten constant. The parameter $V_\mathrm{max} = k_\mathrm{cat} \cdot \mathbf{E}$ is the flux at saturation. In the case of linear protein binding, it is $C_\mathrm{u} = \mathrm{f_u} \cdot C_\mathrm{tot}$ and thus

$$r_\mathrm{out,invitro} = \frac{V_\mathrm{max}}{(K_\mathrm{M}/\mathrm{f_u}) + C_\mathrm{tot}} \cdot C_\mathrm{tot}.$$

Depending on the experimental setting, either K_M or $K_\mathrm{M}/\mathrm{f_u}$ is determined as Michaelis constant. The regime of **linear metabolism** can be derived from the Michaelis–Menten model as a special case by assuming that $C_\mathrm{u} \ll K_\mathrm{M}$, yielding

$$\mathrm{CL}_\mathrm{int,invitro} \cdot C_\mathrm{u} = \frac{V_\mathrm{max}}{K_\mathrm{M}} \cdot C_\mathrm{u} \tag{5.87}$$

where $\mathrm{CL}_\mathrm{int,invitro}$ denotes the intrinsic *in vitro* clearance in units [μL/min/10^6 cells] or [μL/min/mg microsomes] [547]. Using a scaling factor SF (number of cells per g liver, or mg microsomal protein per g liver) we end up with the predicted *in vivo* intrinsic clearance $\mathrm{CL}_\mathrm{int,invivo}$ (see [547] and references therein).

$$\mathrm{CL}_\mathrm{int,invivo} = \mathrm{CL}_\mathrm{int,invitro} \cdot \mathrm{SF}, \tag{5.88}$$

Typical scaling factors for rat and human can be found in [547,589–591]. The above equation accounts for linear non-saturable metabolism. In the experimental setting, the intrinsic clearance might already incorporate protein binding effects, such that the unbound concentration C_u has to be replaced by the total concentration C.

Lumping

Several models, e.g. the well-stirred model and the parallel-tube model [592], have been proposed in order to lump the hepatic degradation of drugs in a way that it can be related to the blood, or blood-plasma concentration, instead of the drug concentration in the liver. Here, we will only focuss on the well-stirred model and relate the clearance to the blood-plasma concentration $\mathrm{CL}_\mathrm{plasma}$.

The well-stirred liver model assumes that the tissue concentration is homogeneous ('well-stirred'). Based on saturable enzyme kinetics, we get

$$V_{\text{liv}}\frac{\mathrm{d}}{\mathrm{d}t}C_{\text{liv}} = Q_{\text{liv}}\left(C^{\text{p}}_{\text{in}} - \frac{C_{\text{liv}}}{K^{\text{liv:p}}}\right) - \frac{V_{\max}\cdot C_{\text{liv}}}{K_{\text{M}}/\text{f}_{\text{uliv}} + C_{\text{liv}}}. \tag{5.89}$$

In the linear regime based on the intrinsic *in vivo* clearance CL_{int} (i.e., the rate of intra-cellular degradation), the ODE for the liver is given by

$$V_{\text{liv}}\frac{\mathrm{d}}{\mathrm{d}t}C_{\text{liv}} = Q_{\text{liv}}\left(C^{\text{p}}_{\text{in}} - \frac{C_{\text{liv}}}{K^{\text{liv:p}}}\right) - \text{CL}_{\text{int}}C_{\text{liv}}. \tag{5.90}$$

where $Q_{\text{liv}} = (1-\text{hct})Q^{\text{b}}_{\text{liv}}$ denotes the blood flow that is associated with the blood-plasma (hct = hematocrit value). Sometimes, the term $\text{CL}_{\text{int}}\text{f}_{\text{uliv}}C_{\text{liv}}$ is used instead of $\text{CL}_{\text{int}}C_{\text{liv}}$ in order to account for the fact that only the unbound concentration can form a complex with the enzyme. Whether or not this is a better model is likely to be dependent on the experimental setup that was used to determine CL_{int}.

The aim of the well-stirred liver (clearance) model is to express $\text{CL}_{\text{int}}C_{\text{liv}}$ in terms of $\text{CL}_{\text{plasma}}C^{\text{p}}_{\text{in}}$. To do so, we assume that the the exchange of drug via the blood flow and the degradation in the liver is in quasi-steady state. Formally, we set $dC_{\text{liv}}/dt = 0$ and obtain

$$Q_{\text{liv}}C^{\text{p}}_{\text{in}} = \left(\frac{Q_{\text{liv}}}{\text{CL}_{\text{int}}\cdot K^{\text{liv:p}}} + 1\right)\text{CL}_{\text{int}}C_{\text{liv}} \tag{5.91}$$

and thus

$$\text{CL}_{\text{int}}C_{\text{liv}} = \frac{Q_{\text{liv}}\text{CL}_{\text{int}}K^{\text{liv:p}}}{Q_{\text{liv}} + \text{CL}_{\text{int}}K^{\text{liv:p}}}\cdot C^{\text{p}}_{\text{in}}. \tag{5.92}$$

The term

$$\text{CL}_{\text{plasma}} = Q_{\text{liv}}\cdot E_{\text{hep}} \tag{5.93}$$

is called the hepatic plasma clearance with hepatic extraction ratio $0 \le E_{\text{hep}} \le 1$

$$E_{\text{hep}} = \frac{\text{CL}_{\text{int}}K^{\text{liv:p}}}{Q_{\text{liv}} + \text{CL}_{\text{int}}K^{\text{liv:p}}}. \tag{5.94}$$

Thus, the ratio of liver blood flow to the appropriately scaled intrinsic clearance determines the hepatic extraction ratio. Since E_{hep} can be at most 1, the hepatic plasma clearance is bound from above by the liver blood flow. Using $\text{CL}_{\text{plasma}}$ we may rewrite the above eq. (5.90) as

$$V_{\text{liv}}\frac{\mathrm{d}}{\mathrm{d}t}C_{\text{liv}} = Q_{\text{liv}}\left(C^{\text{p}}_{\text{in}} - \frac{C_{\text{liv}}}{K^{\text{liv:p}}}\right) - \text{CL}_{\text{plasma}}\cdot C^{\text{p}}_{\text{in}}. \tag{5.95}$$

Alternatively in a compartmental model, we can model hepatic metabolism with respect to the central compartment C_1

$$V_{\text{ss}}\frac{\mathrm{d}}{\mathrm{d}t}C_1 = v_{\text{in}} - C_1\cdot Q_{\text{liv}}\cdot E_{\text{hep}} \tag{5.96}$$

During the process of absorption (see section 5.2) drug might already be metabolized in the enterocytes (gut cells) and in the liver before entering the systemic circulation. In a lumped model, this can be modelled appropriately utilizing F_{bio} (eq. (5.8)) and inserting the respective extraction ratios (e.g. eq. (5.94)).

5.4.2 Renal Excretion

Renal excretion involves a component that is governed by passive processes and a component that is governed by active processes (see fig. 5.13 for an overview over all processes).

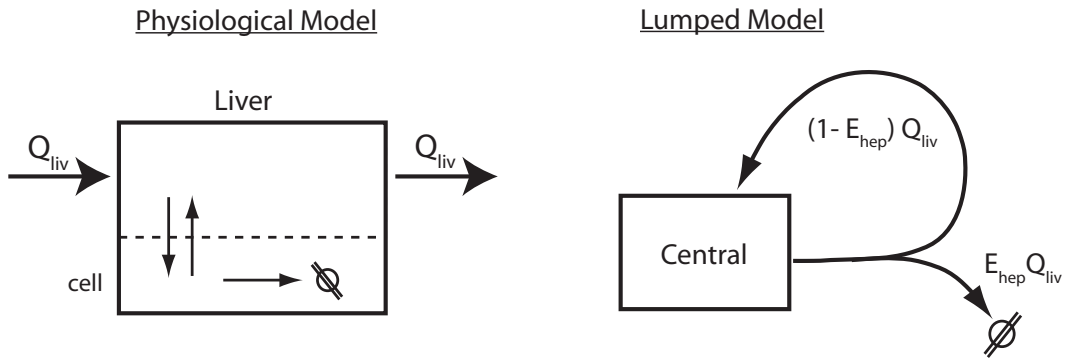

Figure 5.12: Liver metabolism models. Left: Possible implementation of liver metabolism in a physiologically based model. Right: Implementation of metabolic degradation in the liver in a compartmental model.

Passive Processes. Some HIV compounds with high water-solubility, like NRTIs are renally excreted by passive mechanisms. Molecules with a diameter less than 15Å (e.g. unbound drugs C_{u}) are filtered through the glomerular capillaries (by the arterial blood pressure) and excreted into the proximal tubuli (1. in fig. 5.13) with flux GFR (glomerular filtration rate, reference value: 117 [ml/(min·1.73m^2)] [593, 594]). This process is called glomerular filtration. A concentration gradient between primary urine and proximal tubulus is responsible for reabsorption by passive diffusion (2. in fig. 5.13). Depending on the $\mathrm{pK_a}$ of the drug, the urinary pH (average: 6.3 [538]) and the urine flow, complete reabsorption might occur. Lipophilic drugs will be re-absorbed to a greater extent than hydrophilic and charged compounds (see appendix A). We will denote the proportion of re-absorbed drug by the fraction f_{RE}.

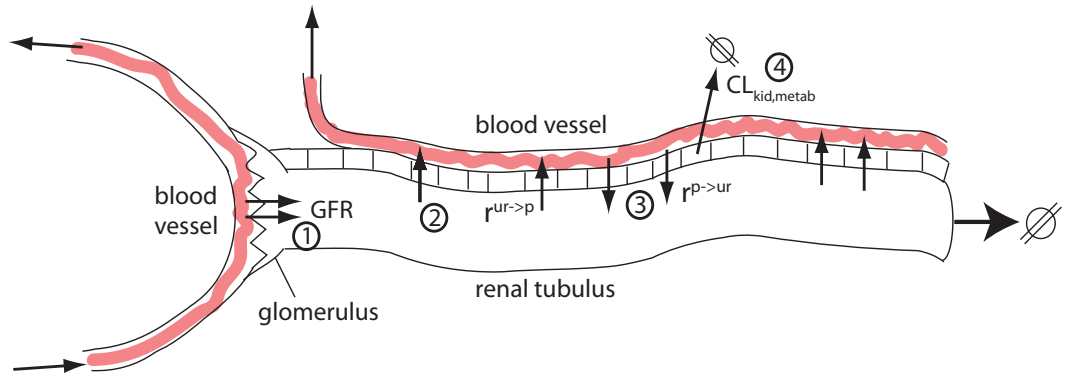

Figure 5.13: Renal excretion. 1: Unbound drug reaches the tubuli after glomerular filtration. 2: Most drugs are reabsorbed by passive diffusion. However, if the drug cannot pass the apical membrane of the tubular cells, it remains in the primary urine and will ultimately be excreted. 3 & 4: drugs can also be actively excreted from the tubular cells into the tubular lumen, or they can be metabolized by the tubular cells.

Let us the define the renal clearance through passive processes by

$$\mathrm{CL_{GFR}} = (1 - f_{\mathrm{RE}})\mathrm{GFR} \cdot \mathrm{f_u}^{\mathrm{p}}. \tag{5.97}$$

While GFR is usually assessed using exo- and endogenous markers [595], f_{RE} can be determined in this model by using e.g. urinary samples. The differential equation that describes the evolution of drug concentration in the kidney becomes

$$V_{\mathrm{kid}}^{\mathrm{p}} \frac{\mathrm{d}}{\mathrm{d}t} C_{\mathrm{kid}}^{\mathrm{p}} = Q_{\mathrm{kid}}\big(C_{\mathrm{in}} - C_{\mathrm{kid}}^{\mathrm{p}}\big) - \mathrm{CL_{GFR}} \cdot C_{\mathrm{kid}}^{\mathrm{p}} \tag{5.98}$$

where C_{in} is the concentration of drug in the arterial blood-plasma and Q_{kid} is the blood flow of the blood-plasma in the kidney. Utilizing this equation, $\mathrm{CL_{GFR}}$ is defined in terms of the concentration

of drug in the plasma of the kidney $C^{\mathrm{p}}_{\mathrm{kid}}$.

Lumping. We can derive the glomerular extraction ratio E_{GFR} and $\mathrm{CL}_{\mathrm{GFR,plasma}}$ in terms of the incoming plasma concentration:

$$E_{\mathrm{GFR}} = \frac{\mathrm{CL}_{\mathrm{GFR}}}{Q_{\mathrm{kid}} + \mathrm{CL}_{\mathrm{GFR}}}, \tag{5.99}$$

$$\mathrm{CL}_{\mathrm{GFR,plasma}} = Q_{\mathrm{kid}} \cdot E_{\mathrm{GFR}}. \tag{5.100}$$

The equations above imply, that the maximum amount of drug elimination through the kidney ($\mathrm{f_u} = 1$, $f_{\mathrm{RE}} = 0$) is determined by the product of glomerular extraction E_{GFR} and the blood flow of the kidney Q_{kid}.

Active Processes Drugs can be secreted from the blood-plasma of the kidneys through the tubular cells into the tubular lumen (active tubular secretion, 3. in fig. 5.13). We will denote this process with the parameter $r^{\mathrm{p}\rightarrow\mathrm{ur}}$. Active tubular secretion requires two steps: First, drug is taken up from the blood into tubular cells and then excreted by efflux transport from the cytosol of the cells into the lumen [596]. Some drugs might also be metabolized within the tubular cells. We denote this process by $\mathrm{CL}_{\mathrm{meta,kid}}$. For simplicity, lets subsume the processes of degradation and excretion $\mathrm{CL}_{\mathrm{act}} = r^{\mathrm{p}\rightarrow\mathrm{ur}} + \mathrm{CL}_{\mathrm{meta,kid}}$.

$$V_{\mathrm{kid}} \frac{\mathrm{d}}{\mathrm{d}t} C_{\mathrm{kid}} = Q_{\mathrm{kid}} \left(C_{\mathrm{in}} - \frac{C_{\mathrm{kid}}}{K^{\mathrm{liv:p}}} \right) - \mathrm{CL}_{\mathrm{act}} \cdot C_{\mathrm{kid}}. \tag{5.101}$$

As in the case with hepatic metabolism, drug is eliminated from the tissue. The blood flow Q_{kid} in the equation above refers to the blood flow that is assigned to the blood-plasma of the kidney ($Q_{\mathrm{kid}} = (1 - \mathrm{hct}) Q^{\mathrm{b}}_{\mathrm{kid}}$).

Lumping. Analogous to hepatic metabolism, we can apply the well-stirred model and derive the clearance terms with reference to the incoming concentration (central compartment, blood-plasma).

$$E_{\mathrm{act}} = \frac{\mathrm{CL}_{\mathrm{act}} \cdot K^{\mathrm{kid:p}}}{Q_{\mathrm{kid}} + \mathrm{CL}_{\mathrm{act}} \cdot K^{\mathrm{kid:p}}}, \tag{5.102}$$

$$\mathrm{CL}_{\mathrm{act,plasma}} = Q_{\mathrm{kid}} \cdot E_{\mathrm{act}}. \tag{5.103}$$

5.4.3 Summary

Drug can be metabolized in the hepatic tissue and actively excreted from the kidney tissue. In contrast, if drug is excreted by glomerular filtration, it is eliminated from the blood plasma of the kidney. The clearance by hepatic metabolism, renal excretion and renal filtration can be modelled within a PBPK model within the appropriate tissues. However, elimination via these routes can also be modelled in a compartmental model. We have shown how to derive the respective clearance parameter with reference to the blood-plasma (central compartment) concentration.

Finally, we want to give an example of a drug that is eliminated by glomerular filtration and hepatic degradation. In a one-compartmental model, the pharmacokinetics of drug elimination can be modelled according to

$$V_{\mathrm{ss}} \frac{\mathrm{d}}{\mathrm{d}t} C_1 = (1 - E_{\mathrm{hep,p.o.}}) \cdot F_{\mathrm{abs}}(t) - C_1 (\mathrm{CL}_{\mathrm{hep,plasma}} + \mathrm{CL}_{\mathrm{GFR,plasma}})$$

where $E_{\mathrm{hep,p.o.}} = \frac{\mathrm{CL}_{\mathrm{int}} K^{\mathrm{liv:p}}}{Q_{\mathrm{gut}} + \mathrm{CL}_{\mathrm{int}} K^{\mathrm{liv:p}}}$ denotes the extraction ratio that is associated with the first-pass effect and $\mathrm{CL}_{\mathrm{hep,plasma}}$ and $\mathrm{CL}_{\mathrm{GFR,plasma}}$ are defined in eq. (5.93) and eq. (5.100) respectively.

5.5 The Effect Compartment

In most cases, patient drug concentrations in the blood plasma will be available, while drug concentrations at the site of effect will only occasionally be analyzed. Most antivirals exert their effects in anatomical compartments other than the blood-plasma. The majority of cells that are susceptible to viral infection reside in the lymphoid tissues, thymus, cental nervous system and genitourinary tract (e.g. testis) [57]. We have discussed previously, that blood flow limitation might create an initial discrepancy between plasma concentration and tissue concentration (see section 5.3.4). The potential delay due to blood flow limitation can be assessed using eq. (5.74). If eq. (5.74) indicates, that a blood flow limitation is not expected, then the concentrations in the capillaries of target tissue can be identified with the plasma concentrations in the blood.

CCR5	FI	NRTI[a]/NNRTI	InI	PI/MI
extra-cell.	extra-cell endosome[b]	cytosol	cytosol nucleus[c]	cytosol virion[d]

Table 5.1: Site of effect of various classes of anti-HIV compounds.

[a] requires intracellular activation.
[b] A large proportion of HIV-particles fuses in the endosome [294].
[c] site of strand transfer action
[d] protease is active within the virion

Extracellular target location. Entry inhibitors (CCR5-antagonists and fusion inhibitors) exert their effect in the extracellular space (see table 5.1). Therefore, unbound plasma drug concentrations and unbound concentrations at the extracellular space might be identical (at steady state) for most tissues, because the endothelial membrane of the tissue capillaries, which forms the only potential barrier for drug penetration, is fenestrated in most tissues. For entry inhibitors, like CCR5-antagonists, we can therefore derive the general relationship between the available concentration at the effect site $C_{\mathrm{u}}^{\mathrm{e}}$ and the blood-plasma concentration:

$$C_{\mathrm{u}}^{\mathrm{e}}(t) = C_{\mathrm{u}}^{\mathrm{p}}(t) \text{ (example: CCR5-antagonists, e = extracellular)} \tag{5.104}$$

A recent study suggests [294], that fusion of HIV particles might occur after HIV-particles have been taken up by endocytosis. The endosomes are not in direct exchange with the extracellular medium, so that the concentration of FIs at the effect-site might be different to the concentration of FIs in the cell-surrounding liquid.

Specialized tissues, like the brain and the testis are protected by a solid vascular membrane (blood-brain-barrier and blood-testis-barrier), which might restrict the entry of drugs into these compartments. Crossing of the blood-brain-barrier or the blood-testis-barrier can be rate-limiting, concentrative and saturable. In animals, the plasma-to-cerebrospinal fluid (CSF) ratio can be determined in order to assess blood-brain-barrier crossing. The concentration in the semen can be used as a marker for blood-testis-barrier crossing in humans.

For target cells that reside within e.g. the brain, eq. (5.104) will generally not hold to establish the relation between blood plasma concentrations and the concentration of drug in the fluid surrounding the cells of the brain. The concepts used in section 5.3.2 can, however, be used to model this relation.

Intracellular target location. NRTIs, NNRTIs, InIs, PIs and MIs have to cross the plasma membrane of target cells in order to exert their effect (see table 5.1). We have discussed previously in section 5.3.2 that membrane transport can be rate-limiting, concentrative and possibly saturable (see e.g. fig. 5.14). Furthermore, membrane crossing might depend on the transporters present on the surface of a particular cell type [597, 598].

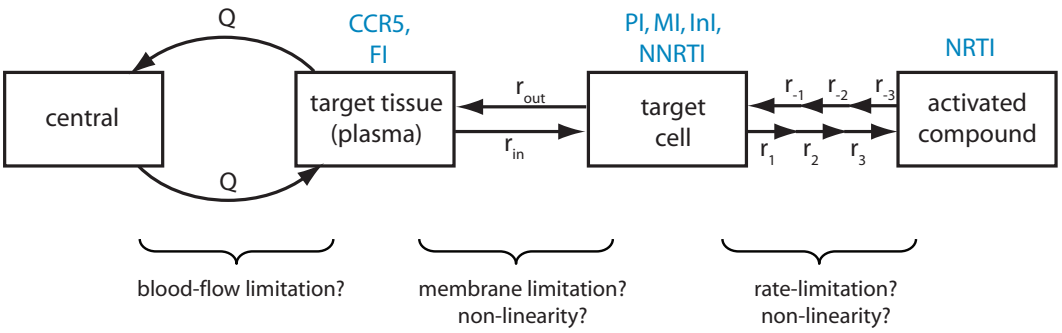

Figure 5.14: Left: Relation between the concentration at the effect site and the blood-plasma concentration (central compartment concentration)

Most HIV target cells reside in poorly accessible parts of the body and therefore do not qualify as markers for intracellular penetration of anti-HIV compounds [57]. There are some circulating cells of the immune system, that qualify as good surrogate markers for intracellular penetration of antivirals into target cells. The peripheral mononuclear blood cells (PMBC) can be derived from the blood, after erythrocytes and blood plasma are being removed. PMBCs contain an ensemble of different cells (see fig. 5.15) that might confer different intracellular kinetics. Drug kinetics within PMBCs, therefore, reflect "average kinetics", that might be a result of very diverse intracellular drug kinetics in each cell type that is contained in the PMBC compartment.

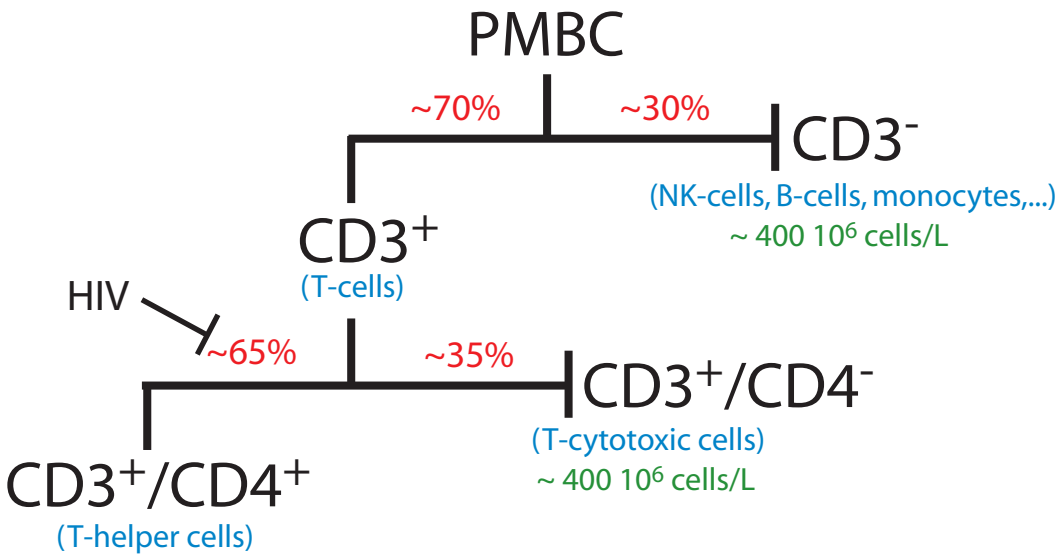

Figure 5.15: The composition of PBMCs in a healthy donor [599]. Cell types are distinguished based on the receptors present at the cellular surface. $CD4^+$ T-cells express the $CD3^+$ receptor (T-cells) and the $CD4^+$ receptor.

Example: Efavirenz. NNRTIs are small molecules, that, due to their lipid-solubility, have the ability to cross membranes by passive diffusion. We will test this assumption (passive diffusion) for the NNRTI efavirenz. In the case of PBMCs, exchange between plasma and cell is direct, since the interstitial space, that is associated with tissues, is missing. Assuming passive diffusion, we derive $fn^p \cdot C_u^p = fn^e \cdot C_u^e$, where 'e' refers to the concentration at the effect site, in this case the intracellular space of the PBMCs. Efavirenz in a very weak base ($pK_a = 10.2$ [600]) that is neither charged in the plasma (pH = 7.4), nor in the cell (pH = 7). Therefore, we can set fn = 1 and neglect ionization. Utilizing these assumtions and simplifications, we derive $K^{e:up} = 1/f_u{}^e$. The log octanol-

water partitioning coefficient ($\log P_{\text{o:w}}$) is 4.6 for efavirenz, therefore eq. (5.60) reduces to

$$K^{\text{e:up}} = \frac{1}{f_u{}^{e}} = P_{\text{o:w}} \cdot V^{\text{nl:e}} + 0.3\, P_{\text{o:w}} \cdot V^{\text{np:e}}$$

with $V^{\text{nl:e}} \approx 0.02$ and $V^{\text{np:e}} \approx 0.01$ [585]. The results of our estimation are shown in figure 5.16 (solid

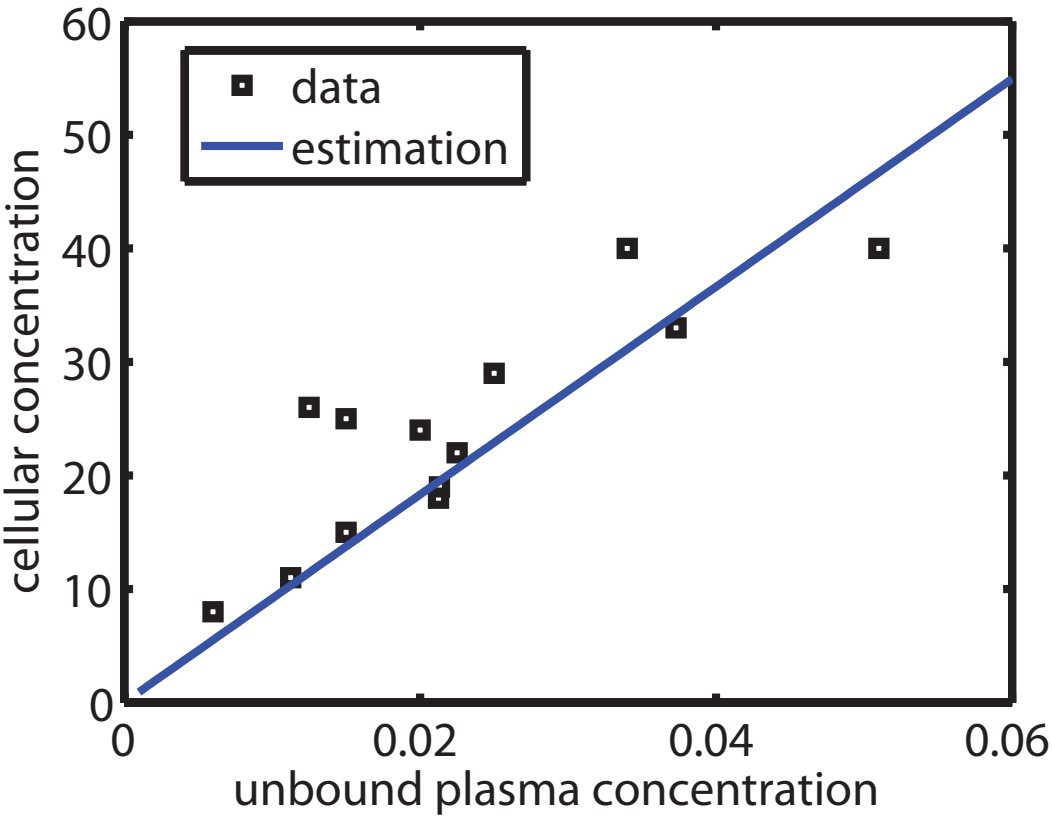

Figure 5.16: Correlation between unbound plasma concentration and intracellular efavirenz concentration in PBMCs. Data from [601] includes 13 patient samples.

blue line) together with patient data from [601]. As can be seen in the figure, there is a very good agreement between the model-estimated cellular concentration and the observed data, indicating that the assumption of passive diffusion as the dominant mechanism for membrane exchange might be true in the case of efavirenz and thus the unbound plasma concentration can be used in a pharmacodynamic model (after initial blood flow limitation has been overcome).

$$C_u^e(t) = C_u^p(t) \text{ (example: Efavirenz, e = cellular).}$$

For other drugs, especially PIs, which are substrates of efflux transporters (e.g. [602–605]), the assumption of an equilibrium between unbound cellular concentration and unbound plasma concentration might not hold. If data on cellular uptake- and efflux is available, models similar to eq. (5.35) can be used to describe the concentration of drug at the effect site. However, in the case of carrier-mediated transport, the expression of transporters on the surface of an HIV susceptible cell-type will determine the pharmacological penetration of the drug. In most cases it is not fully resolved which transporters are involved in the uptake- or efflux of a drug. Furthermore, it is not fully understood which transporter proteins are expressed on the surface of HIV susceptible cells (and to which extent they are expressed). This implies, that carrier-mediated penetration of drugs has to be resolved for each cell type and that different cell types not necessarily need to take up drugs in an identical way.

NRTIs. In addition to the previously discussed obstacles for HIV-drugs to reach their target site, NRTIs require intracellular phosphorylation (see fig. 3.4) to form an active triphosphate (NRTI-TP),

that exerts the effect [303].

NRTIs are small hydrophilic compounds ($\log P_{\text{o:w}} \ll 1$) [307]. They are poorly bound in the plasma (${f_u}^{\text{p}} > 0.5$ [578], see fig. 5.9) and, due to their hydrophilicity, they are not expected to be excessively bound to cell lipids. Their hydrophilicity permits passive diffusion into the cellular space. Many NRTIs are substrates of nucleoside transporters, due to their structural similarity to naturally occurring nucleosides (that is adenosine, guanine, cytosine and thymidine) [304]. The family of nucleoside transporters consists of concentrative transporters (CNT) [606] and equilibrative transporters (ENT) [607]. Cellular penetration of the prodrug (the un-phosphorylated NRTI) can therefore be modelled using the assumptions in eq. (5.35). Furthermore, since lipid binding is not expected, we can set ${f_u}^{\text{c}} \approx 1$.

$$C_{\text{u}}^{\text{p}}(t) = C_{\text{u}}^{\text{c}}(t)/\alpha \rightleftharpoons \text{phosphorylation} \rightarrow C_{\text{u}}^{\text{e}}(t) \text{ (example: NRTI, e = NRTI-TP).}$$

For NRTIs, each of the phosphorylation steps is likely to produce a disequilibrium between substrate and product, has the potential to be rate-limiting (induce transient behavior) and to create non-linearities between substrate and product [145]. Furthermore, expression of phosphorylating enzymes (kinases) is likely to be cell- and cell-cycle specific.

Intracellular phosphorylation data is limited in most cases, so that it is very difficult to resolve the phosphorylation kinetics of NRTIs. If phosphorylation data is available, it is usually measured within the PBMCs and it is subsequently assumed that the concentrations in $CD4^+$-cells are identical. The generic phosphorylation cascade is shown below:

$$\text{NRTI}^{\text{c}} \rightleftharpoons \text{NRTI-MP} \rightleftharpoons \text{NRTI-DP} \rightleftharpoons \text{NRTI-TP}.$$

For the phosphorylation direction NRTI → NRTI-TP, linear kinetics, that are not rate limiting, are of advantage. In this case, the intensity of the effect (caused by NRTI-TP) can be controlled by the dose given and the onset of effect can be estimated from the plasma concentration. For the de-phosphorylating direction NRTI-TP → NRTI, the opposite is of advantage. Since most NRTIs have short plasma halflifes [307], a rate-limiting de-phosphorylation can cause a prolonged intracellular halflife of the active triphosphate, resulting in less frequent dosing. We have illustrated the ratio of intracellular triphosphate halflife in PBMCs-to-plasma halflife in fig. 5.17. For all approved NRTIs (except TDF), current NRTI dosing schedules rely on the rate-limiting de-phosphorylation in PBMCs [307]. In other cell types, this ratio might, however, be quite different. In the worst case, if de-phosphorylation is not rate-limiting, the intracellular halflife might be identical to the plasma halflife (which is typically in the range of 1–2 h [307]). Therefore, a dosing schedule that relies on the rate-limitation in one cellular marker, might create a window of insufficient suppression in another HIV target cell, if the de-phosphorylation is fast in this cell type (e.g. by increased expression of the enzyme).
We will give a detailed example of the intracellular pharmacokinetics based on the NRTI zidovudine later in chapter 7, where we also combine the pharmacokinetics of zidovudine with its pharmacodynamics (section 6.2) and deduce the consequences of intracellular pharmacokinetics on viral quasi-species dynamics in chapter 7.

5.6 Summary

Pharmacokinetics can be divided into three sub-processes: absorption, distribution and elimination. We have presented different models to describe each of these processes. Each of the presented models for absorption, distribution and elimination requires different input parameters. Therefore, a set of models can be chosen, that can be parameterized based on the available *in vitro* and *in vivo* data in order to estimate concentration-time profiles.

The general approach presented herein is to:

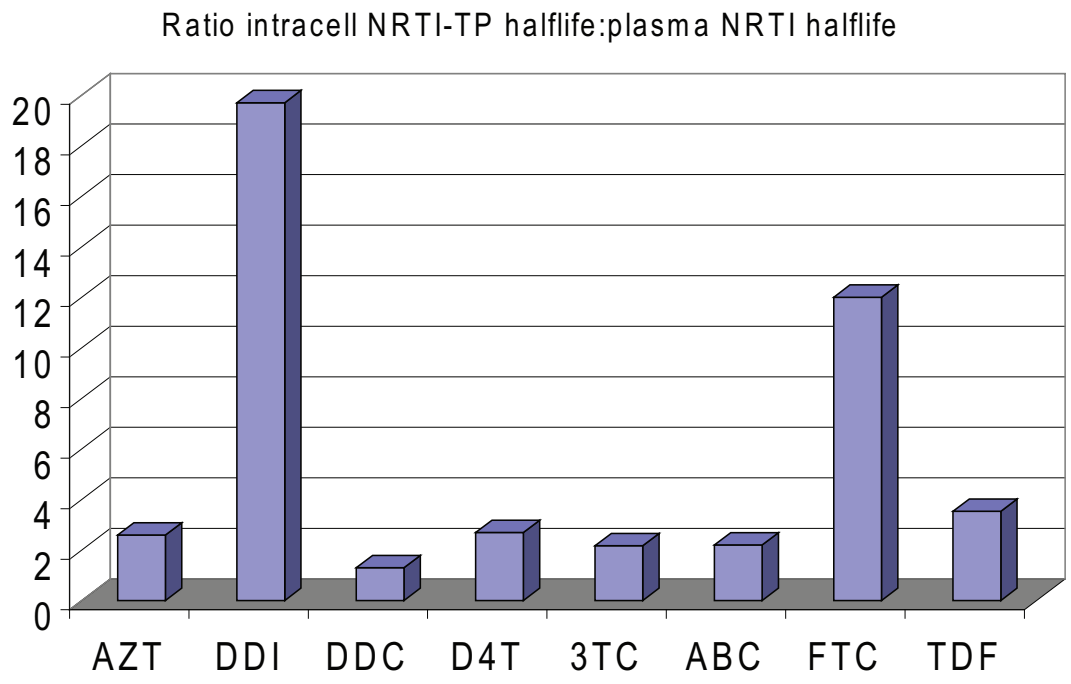

Figure 5.17: Intracellular halflifes of NRTIs in PBMCs in relation to the plasma halflifes. Data taken from [307]

1) build a model that accurately captures the pharmacokinetics of the compound in the blood-plasma and that can therefore be verified with *in vivo* data. The model building process starts with a detailed PBPK model, whose assumptions remain disclosed and whose parameters are testable in *in vitro* experiments. A detailed PBPK model can be transformed into a simplified compartment model, that allows for elaborated model- and kinetic analysis. However, back-transformation from a simple model to a PBPK model is not possible. Therefore, the PBPK model cannot be discarded, but can rather serve as a platform to incorporate new biological insights and to generate simplified models.

2) Once the plasma pharmacokinetics are accurately represented by the model, it is necessary to establish the link between (verifiable) plasma pharmacokinetics and the drug concentration at the effect site. In most cases there will be limited (if at all) data available to verify the kinetics that establish the link between the blood-plasma concentration and the concentration in the effect compartment. In the case of entry inhibitors (CCR5-antagonists, FIs), drug concentrations at the effect site might be identical with blood-plasma concentrations. For drugs that exert their effect intracellular (NNRTIs, InIs, PIs, MIs), it has to be evaluated whether concentrative transport creates discrepancies and non-linearities between unbound plasma concentrations and unbound intracellular concentrations. In the case of NRTIs, the relation between unbound plasma concentrations and activated cellular concentrations is not only influenced by transporters, but also by sequential intracellular phosphorylation (at least 3 steps), of which each one might be rate-limiting or saturated at physiological drug concentrations.

5.7 Glossary: Pharmacokinetic Terms

Anatomical Compartment. An anatomical compartment is a part of the body, often an organ or a collection of tissues, e.g., muscle or adipose tissue.

Kinetic Compartment. A kinetic compartment is a collection of anatomical spaces of the body that are considered kinetically identical, i.e., whose rate of change of drug amount or concentration is considered identical.

Membrane limited case. The membrane limited situation applies when the transfer across the cellular membrane is the rate-limiting step, while in comparison the exchange between the vascular and the interstitial space is rapid. As a consequence the vascular and the interstitial space are assumed to be in quasi-steady state.

Blood flow limited case. In the case of blood flow limitation, transfer across the capillary wall and the cellular membrane is rapid, leading to a distribution equilibrium within the organ. However, the amount of drug reaching the organ is limited by the blood flow, creating a disequilibrium between the concentration in the central blood compartment and the vascular space of the organ. The blood flow limited assumption can apply to organs that are not well perfused by the circulatory system.

Chapter 6

Pharmacodynamic Modelling

Pharmacodynamics aims at describing the concentration-response relationship of a drug. Depending on the definition of 'response' and 'concentration', a variety of models, such as indirect- or delayed response models have been proposed (see e.g. [608]). In this chapter we will define 'response' as the effect of the drug on the targeted molecular process, that is binding, fusion, reverse transcription, integration and maturation respectively for CCR5-antagonists, FIs, RTIs, InIs and PI/MIs. With 'concentration', we will refer to the concentration in the effect-compartment, which is defined in table 5.1 for the approved HIV drugs. Since we have also derived the quasi-species model in eqs. (4.37), we will define an effect against each viral mutant, rather than against the total viral population. Using these definitions, the effect of a drug ε is described by [608]:

$$\varepsilon(t) = G\big[t, C(t)\big] \tag{6.1}$$

where $C(t)$ is the concentration of drug at the effect site and G is a function that relates the drug concentration to the observed effect ε.

In the previous chapters we have considered constant drug concentrations for simplicity. In this chapter we will derive time-varying efficacies, that originate from time-varying drug concentrations.

In the following, we will first introduce empirical concentration-response relationships and in the second part we will give a mechanistic derivation of the concentration-response relationship with NRTIs.

6.1 Empirical Pharmacodynamic Models

Empirical models emphasize phenomenological relationships. In the extreme case they fit data without any regard of the mechanistic underpinnings. The simplest concentration-dependent pharmacodynamic model relates the concentration of the drug and the effect of the drug in a linear- or log-linear way [609, 610]. However, this model is only valid when the effect is less than 20% (linear), or within 20–80% (log-linear) [608]. Because of these limiting assumptions, we will not consider these types of models here. Another weakness with these models is that the maximum effect is not limited and will continue to increase with increasing concentration. This deficiency is removed in the $\mathrm{E}_{\max}$ model [611], which has its mechanistic basis in the law of mass action.

Let us assume that the reaction velocity v is proportional to the amount of enzyme-substrate complex $E:S$.

$$v \quad = \quad k_{\mathrm{cat}} \cdot E:S, \tag{6.2}$$

where k_{cat} is the catalytic rate and $E:S$ is the amount of substrate in complex with the enzyme. Let us assume that the substrate and the drug compete for binding to the same site on the inhibited enzyme. Therefore, if the drug I is present, than $E:S$ in eq. (6.2) is decreased (e.g. fig. 6.1, right).

Thus, the residual activity of the reaction, in the presence of the inhibitor, can be described in terms of an alteration in the amount of enzyme-substrate complex.

$$(1-\varepsilon) \quad = \quad \frac{E:S_I}{E:S_\phi} \tag{6.3}$$

where $E:S_\phi$ and $E:S_I$ denote the amount of enzyme-substrate without drug and the amount of enzyme-substrate in the presence of drug. Solving the reaction system (fig. 6.1, right) for the amount of complex yields:

$$\begin{aligned} E:S_\phi &= \frac{E_{\text{tot}} \cdot S}{K_{\text{M}} + S} \\ E:S_I &= \frac{E_{\text{tot}} \cdot S}{K_{\text{M}}(1+\frac{I}{K_I}) + S} \end{aligned} \tag{6.4}$$

where E_{tot} denotes the total amount of enzyme, $K_{\text{M}} = \frac{k_{\text{off,S}}+k_{\text{cat}}}{k_{\text{on,S}}}$ is the Michaelis-Menten constant and $K_I = \frac{k_{\text{off,I}}}{k_{\text{on,I}}}$ is the dissociation constant of the inhibitor. Combining eqs. (6.3)-(6.4) yields

$$(1-\varepsilon) \quad = \quad \frac{1}{1+\frac{K_{\text{M}} \cdot I}{K_I(S+K_{\text{M}})}} = \frac{1}{1+\frac{I}{\text{IC}_{50}(S)}} \tag{6.5}$$

Thus, the 50% inhibitory concentration $\text{IC}_{50}(S) = \frac{K_{\text{M}}}{K_I(S+K_{\text{M}})}$ depends on the amount of endogenous substrate, the binding affinity of the endogenous substrate and the inhibitor, and on the catalytic rate constant [612]. Typically, however, IC_{50} is just estimated as a lumped parameter, disregarding

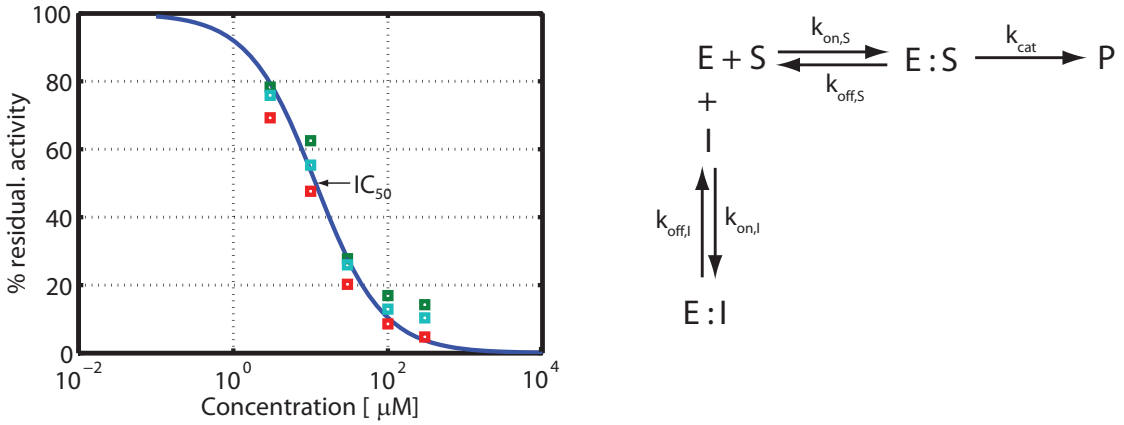

Figure 6.1: Left: Illustration of the basic concentration dependent effect model (eq. (6.5)). Right:reaction scheme

the endogenous substrate concentration in *cell-based* assays or *in vivo*. Therefore, large variations between published IC_{50} values from different experiments are often encountered.

In summary, the E_{max} model (eq. (6.5)) takes (i) an orthosteric mode of inhibition into account and (ii) often assumes a constant (unidentifyable) endogenous substrate concentration in terms of IC_{50}.

The sigmoidal shape of eq. (6.5) is illustrated in fig 6.1, left panel, and the proposed reaction scheme is shown in the right panel.

With the addition of an exponent γ to the E_{max} model, the slope of the log-linear region in fig 6.1 can be controlled [613]. The resulting model is known as the sigmoidal E_{max} model [614]:

$$(1-\eta) \quad = \quad \frac{1}{1+\frac{I^\gamma}{\text{IC}_{50}{}^\gamma}} \tag{6.6}$$

The E_{max} model has tremendous utility in pharmaceutical research: at low concentrations, it predicts a linear concentration-effect relationship, at higher concentrations it predicts a log-linear concentration-effect relationship and at very high concentrations it predicts a constant effect, independent of concentration.

Other empirical pharmacodynamic modelling techniques are polynomial fitting and spline fitting. However, these models lack any mechanistic substantiation [614].

6.1.1 Modelling the Impact of Resistance.

The output of phenotypic assays, when performed with drug resistant viral strains, is typically denoted as a fold-increase in the drug concentration needed to suppress the resistant virus in comparison to the wildtype (e.g. [514]). This translates into a proportional increase in IC_{50}. In the context of the standard model (eq. (6.5)), drug resistance can thus be implemented by utilizing the altered IC_{50} of the drug resistant mutant.

6.2 Enzymatic Pharmacodynamics of NRTIs

The target of phosphorylated (activated) NRTIs is the process of reverse transcription. The effect is based on decreasing the likelihood of successful viral reverse transcription, i.e, DNA chain completion. NRTI triphosphates (NRTI-TP) compete with the natural substrates (dNTP) for binding to the reverse transcriptase (RT) and subsequent insertion into the DNA (see e.g. fig. 6.2): zidovudine (AZT) and stavudine (d4T) compete with deoxythymidine triphosphate (dTTP); dideoxycytidine (ddC), lamivudine (3TC) and emtricitabine (FTC) compete with deoxycytosine triphosphate (dCTP); didanosine (ddI) and tenofovir (TDF) compete with deoxyadenosine triphosphate (dATP) and abacavir (ABC) competes with deoxyguanosine triphosphate (dGTP).

The starting point for modelling the effect of NRTI-TP is to consider the likelihood of a single dNTP insertion, depending on competition with NRTI-TP. If the discreteness of the reaction events and its sequence are important, the stochastic model of chemical reaction kinetics [615] is a much more appropriate description than the deterministic reaction rate model. In the stochastic setting, a biochemical reaction R is specified in terms of a so-called propensity functions a_R that is the probability that the reaction will take place in the next infinitesimal time interval. The propensity depends on the reaction constants and the abundance of the involved reactants. It is related to the next reaction time τ by $E(\tau) = 1/a_R$, where $E(\tau)$ denotes the expected (mean) time to the next reaction event. In the case of two competing reactions R_1 and R_2 the expected time to the next reaction (either R_1 or R_2) is $E(\tau) = 1/(a_{R1} + a_{R2})$. After this time, reaction R_1 will take place with probability $a_{R_1}/(a_{R1} + a_{R2})$ and reaction R_2 will take place with probability $a_{R2}/(a_{R1} + a_{R2})$ [521].

The two processes of chain prolongation and termination can be expressed by their respective propensities. For chain prolongation in the presence of an NRTI, it is:

$$a_+ = \frac{k_{\mathrm{cat,dNTP}} \cdot \mathrm{RT} \cdot \mathrm{dNTP}}{K_{\mathrm{M,dNTP}}(1 + \frac{\mathrm{NRTI}}{K_{\mathrm{M,NRTI}}}) + \mathrm{dNTP})} \tag{6.7}$$

and for chain termination it is:

$$a_0 = \frac{k_{\mathrm{cat,NRTI}} \cdot \mathrm{RT} \cdot \mathrm{NRTI}}{K_{\mathrm{M,NRTI}}(1 + \frac{\mathrm{dNTP}}{K_{\mathrm{M,dNTP}}}) + \mathrm{NRTI})} \tag{6.8}$$

where $k_{\mathrm{cat,NRTI}}$ and $k_{\mathrm{cat,dNTP}}$ denote the catalytic rate constants for termination and prolongation respectively and $K_{\mathrm{M,NRTI}}$ and $K_{\mathrm{M,dNTP}}$ denote the Michaelis-Menten parameters for NRTI and dNTP binding. Utilizing the propensities of the two possible reactions, the probability of chain prolongation at each nucleotide base, in the presence of chain terminators, is determined by

$$q = \frac{a_+}{a_0 + a_+}. \tag{6.9}$$

It follows, that in the absence of NRTI-TPs, we get q = 1. Rearranging yields

$$q = \frac{1}{1 + \frac{\mathrm{NRTI} \cdot k_{\mathrm{cat,NRTI}}}{\mathrm{dNTP} \cdot k_{\mathrm{cat,dNTP}}} \cdot \frac{K_{\mathrm{M,dNTP}}}{K_{\mathrm{M,NRTI}}}} \tag{6.10}$$

For many NRTIs [616] the catalytic rate constants k_{cat} are approximately equal to the catalytic rate constants of the natural substrates, so that eq. (7.11) only depends on the ratio of K_{M} values and the ratio of concentrations.

$$q = \frac{1}{1 + \frac{\mathrm{NRTI}}{\mathrm{dNTP}} \cdot \frac{K_{\mathrm{M,dNTP}}}{K_{\mathrm{M,NRTI}}}} \tag{6.11}$$

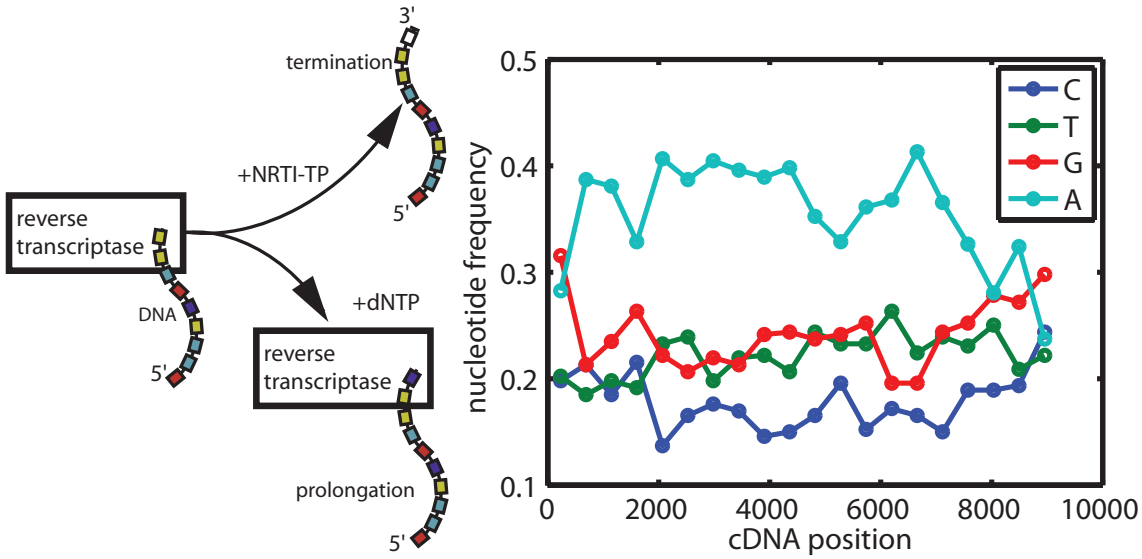

Figure 6.2: Left: Nucleoside reverse transcriptase inhibitors (NRTI-TPs) compete with the natural substrates (dNTP) for the incorporation into the nascent viral DNA. One incorporated, they terminate chain prolongation, because they lack the hydroxy-group that is required for the binding of the next incoming dNTP. Right: Nucleotide frequency in the HIV cDNA(GenBank accession no. **AF033819**). Each dot represents the nucleotide frequency per (≈ 460 base long) section of the viral genome.

The full length DNA of HIV is approximately 9200 bases long (GenBank accession no. **AF033819**). Successful completion of the viral double stranded DNA requires the incorporation of 2·9200 nucleotide bases in total (9200 for the DNA-DNA and RNA-DNA direction, respectively). NRTIs compete only with one type of nucleoside base for the incorporation into the nascent DNA (see above). We have illustrated the abundance of the different nucleotide bases in the HIV cDNA in figure. 6.2. In summary, reverse transcription requires the incorporation of ≈ 5300 thymidine- and adenosine bases (for thymidine: RNA → DNA: 2000 + DNA → DNA: 3300, for adenosine in reversed order) and ≈ 3900 guanine- and cytosine bases (for guanine: RNA → DNA: 2200 + DNA → DNA: 1700, for cytosine in reversed order). Therefore, there are ≈ 5300 or 3900 opportunities respectively for the incorporation of the NRTI-TPs during the process of reverse transcription.

It is generally believed that NRTI-TP insertion into the nascent DNA chain leads to chain termination, because NRTI-TPs lack the hydroxy-group that is required for the binding of the next incoming dNTP [617]. This can be realized in two different scenarios (see fig. 6.3 and 6.4):

- **Template limited case.** If a limited amount of RNA template is available for reverse transcription, then chain termination will cease reverse transcription. This scenario is likely when a previously uninfected cell gets into contact with an infective virus, because only a limited number of viral RNA genomes are packed into the virion.

- **Enzyme limited case.** If a limited amount of enzyme is abundant, then chain termination will decelerate the velocity of reverse transcription in the sense that reverse transcription has to start from the beginning, once a nascent DNA is terminated by NRTIs. This scenario reflects the situation in single nucleotide extension assays (e.g. [616, 618, 619]), that are typically used to determine kinetic constants for the action of NRTIs on the reverse transcriptase. *In vivo*, this scenario can occur in long lived cells when multiple integration is regarded [620, 621] and a supply of intracellular genomic RNA is provided by the infected cell. This scenario becomes even more likely, if the intracellular supply of RT is limited, e.g. by concomitant application of PIs.

Limited amount of template.

If the amount of template is the limiting factor for reverse transcription, inhibition by NRTIs will result in a depletion of viral genome. In this case, the important determinant of NRTI efficacy is the number of template terminations, -hence template destructions (see fig. 6.3). The probability that the reverse transcription is successful (will not be terminated) in the presence of an NRTI is denoted by

$$\big(1-\eta\big)= p = q^N, \tag{6.12}$$

where N denotes the number of targets (analog bases) for the respective NRTI. A similar model has been presented by Goody et al. [320]. This model is similar to the sigmoidal $\mathrm{E}_{\max}$ model (eq. (6.6)), with the exception that the contribution of the substrate concentration remains disclosed (see eq. (6.11)) and the exponent, that can cause identifiability problems in parameter estimation [622], is given by the genomic sequence of HIV.

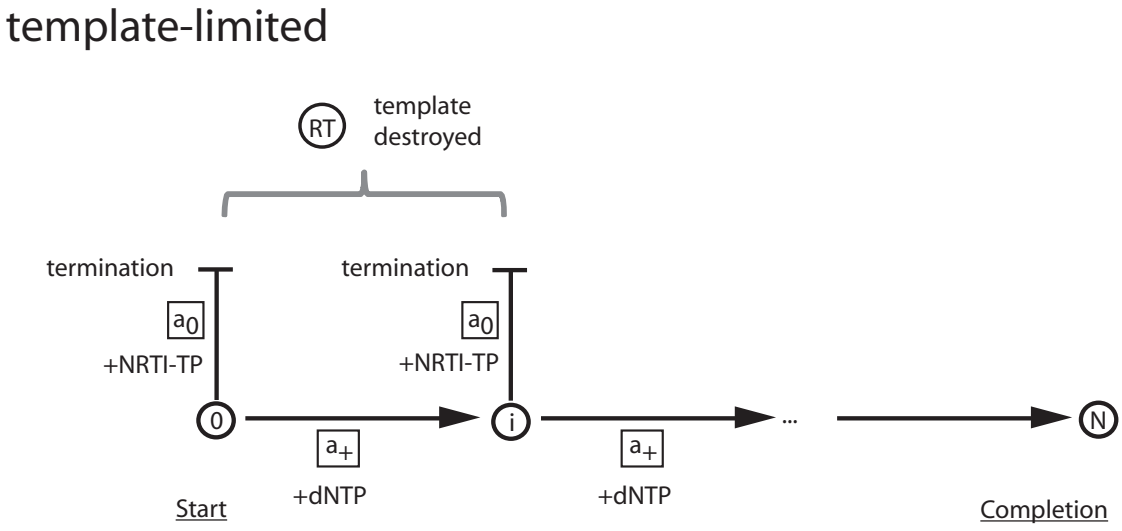

Figure 6.3: Model of the impact of NRTIs on reverse transcription in the RNA template-limited case

In this model, the effect describes the probability that reverse transcription will be successful. However, when it is successful, it will take the same amount of time, compared to the case when no inhibitor is present. Therefore, the effect of NRTIs on the infection rate in viral dynamics (e.g. eq. (4.37)) in the template-limited case can be modelled in the following way:

$$\beta_{\mathrm{NRTI}} = p \cdot \beta = \big(1-\eta\big)\cdot\beta. \tag{6.13}$$

Whereas the clearance through unsuccessful infection becomes

$$\mathrm{CL}_{\mathrm{NRTI}} \quad = \quad \left(\frac{\beta}{\rho_{\mathrm{rev},\phi}} - (1-\eta)\cdot\beta\right). \tag{6.14}$$

where β and $\rho_{\mathrm{rev},\phi}$ are the basic infection rate and the probability that reverse transcription will successfully be finalized in the absence of drug, respectively, as previously defined (section 4.2.3).

Limited amount of enzyme.

If the amount of RT is the limiting factor for reverse transcription, then the amount of free RT and the average time to completion of reverse transcription determines the overall velocity of reverse transcription. In contrast to the previous model, in which reverse transcription is aborted when the unfinished DNA chain is terminated, in this scenario, the RT can start over, using a new template that is available in excess (see fig. 6.4). Therefore, the reverse transcription might take many rounds before it is successfully finished. This increases the average time of reverse transcription $E_{\mathrm{NRTI}}[\tau_{\mathrm{DNA}}]$ in the presence of a chain terminator, in contrast to the average time to successful reverse transcription $E_{\phi}[\tau_{\mathrm{DNA}}]$ in the absence of drug. The effect of NRTIs in this scenario can thus be expressed as the increase in time to successful finalization of the reverse transcription process:

$$\big(1-\varepsilon\big)= p = E_0[\tau_{\mathrm{DNA}}]/E_{\mathrm{NRTI}}[\tau_{\mathrm{DNA}}]. \tag{6.15}$$

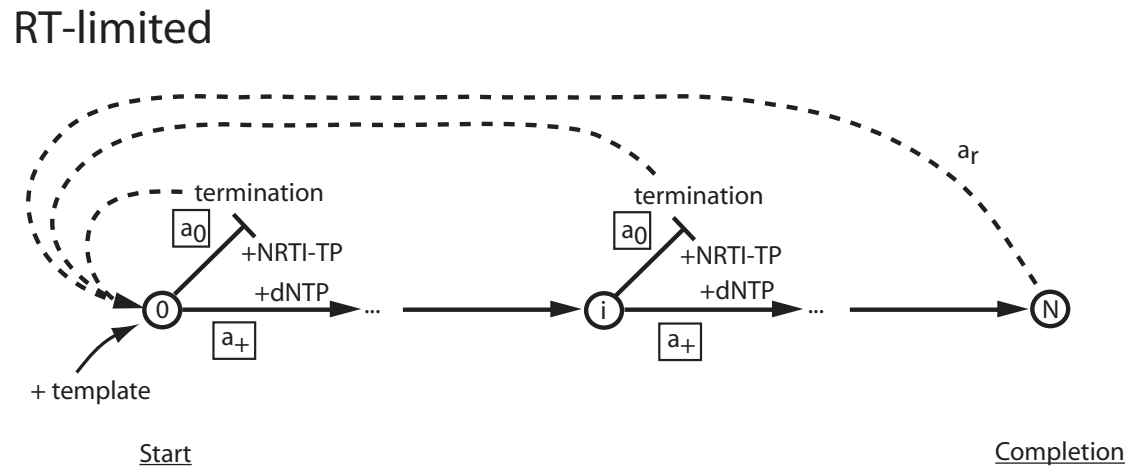

Figure 6.4: Model of the impact of NRTIs on reverse transcription in the RT-enzyme limited case

The process of DNA chain prolongation, termination and completion defines a Markov process with states $n = 0, 1, \ldots, N$, corresponding to the number of RTs with DNA chain containing n dNTP. The effect NRTIs is the deceleration of the reverse transcription process, i.e., the fraction p of successful DNA chain completion per unit time in comparison to the untreated situation. Equivalently, the effect can be interpreted as the increase $1/p$ in the mean time needed to successfully complete reverse transcription in comparison to the situation with no drug.

In terms of the above Markov process, the mean time τ_{DNA} to completion can be computed using the stationary distribution $\pi = (\pi_0, \ldots, \pi_N)$ of the Markov process and the rate a_r of leaving state N:

$$E[\tau_{\mathrm{DNA}}] = \frac{1}{a_r \cdot \pi_N} - \frac{1}{a_r}. \tag{6.16}$$

The term $1/a_r$ denotes the mean time of release of the completed DNA chain and return of the RT to its initial state. In the absence of an NRTI, resulting in $a_0 = 0$ and $q = 1$, the mean time of successful reverse transcription is given by

$$E_{\phi}[\tau_{\mathrm{DNA}}] \quad = \quad \frac{N}{a_+(\phi)}, \tag{6.17}$$

which follows from eq. (6.16) using the rule of l´Hopital. In the presence of one NRTI the stationary distribution has the following form:

$$\pi = (1, q, q^2, \ldots, q^{N-1}, \frac{a_+ + a_0}{a_r} q^N) \frac{1}{\frac{1-q^N}{1-q} + \frac{a_0+a_+}{a_r} q^N} \tag{6.18}$$

where N denotes the number of natural bases that compete with the NRTI of interest for the incorporation into the viral cDNA. After rearrangement we derive:

$$\pi = (1, q, q^2, \ldots, q^{N-1}, \frac{a_+}{a_r} q^{N-1}) \frac{1}{\frac{1-q^N}{1-q} + \frac{a_+}{a_r} q^{N-1}}. \tag{6.19}$$

Combining eq. (6.16), (6.17) and (6.19), we can compute the effect of one NRTI on decreasing the velocity of successful reverse transcription:

$$\big(1 - \varepsilon\big) = p = \frac{a_+}{a_+(\phi)} \cdot N q^{N-1} \; \frac{1-q}{1-q^N}. \tag{6.20}$$

The effect of NRTIs in the enzyme-limited case can be interpreted as a deceleration of the reverse transcription process. This is very similar to case discussed in eq. (4.26) (chapter 4). We therefore derive

$$\beta_{\mathrm{NRTI}} \quad = \quad (1 - \eta_{\mathrm{NRTI}}(\rho_{\mathrm{rev},\phi})) \cdot \beta, \tag{6.21}$$

with

$$(1 - \eta_{\mathrm{NRTI}}(\rho_{\mathrm{rev},\phi})) = \frac{1}{\rho_{\mathrm{rev},\phi} + \frac{1-\rho_{\mathrm{rev},\phi}}{(1-\varepsilon_{\mathrm{NRTI}})}}. \tag{6.22}$$

for the effect of NRTIs on the infection rate in viral dynamics (e.g. eq. (4.37)). The clearance through unsuccessful infection becomes

$$\mathrm{CL}_{\mathrm{NRTI}} \quad = \quad \left(\frac{\beta}{\rho_{\mathrm{rev},\phi}} - \big(1 - \eta_{\mathrm{RTI}}(\rho_{\mathrm{rev},\phi})\big) \cdot \beta \right). \tag{6.23}$$

6.2.1 Impact of Resistance.

Mutations in the RT-coding region, selected during treatment with nucleoside analogues confer resistance through different mechanisms: (i) altering discrimination between nucleoside RT inhibitors and natural substrates (dNTPs) by e.g. inferring with polymerization (e.g. L74V [623–625]), binding, or both (e.g. M184V [331, 625, 626]), or (ii) by increasing the RTs phosphorolytic activity 'excision' (e.g. M41L, T215Y and other thymidine analogue resistance mutations), which in the presence of a pyrophosphate donor (usually ATP) allow the removal of chain-terminating inhibitors from the 3' end of the primer [301].

Both mechanisms can be implemented by modifying $K_{\mathrm{M,NRTI}}$ and $k_{\mathrm{cat,NRTI}}$ in eq. (6.10). However, as the removal mechanism already suggests, to accurately analyze the impact of resistance, in particular excision, the directed reactions in model in fig.6.4 (a_+ and a_0) should be replaced by reversible reactions. Since NRTI incorporation is not marking the termination of the nascent DNA in these cases, it is important to consider the expected time to complete reverse transcription, $E_{\mathrm{NRTI}}[\tau_{\mathrm{DNA}}]$, along the same lines as the previously discussed enzyme-limited case.

6.3 Summary

We have presented two general approaches to pharmacodynamic modelling: empirical and mechanistic. The $\mathrm{E}_{\max}$ model can be derived mechanistically, as demonstrated in eqs. (6.2)-(6.5), by assuming

competitive binding. However, it is often used in an empirical context. The model is particularly appealing due to its simplicity and due to the fact that it only requires one input parameter: the fifty percent inhibitory concentration IC_{50}. Mechanistically, the IC_{50} incorporates the endogenous substrate concentration (that competes with the inhibitor for binding). In cell free *in vitro* assays (e.g. assays using purified enzyme), the endogenous substrate concentration can be controlled and inhibitory measures can be derived [612], which are independent of the endogenous substrate concentration (K_{M} and K_I). This is different in cellular assays (e.g. assays using cell populations), and consequently IC_{50} estimates from distinct cellular assays might lead to discrepancies in parameter estimates. More importantly, if the endogenous substrate concentration is very different in the assay and *in vivo*, the IC_{50}s might deviate; subsequently resulting in inaccurate or false dose recommendations.

The sigmoidal E_{max} model is an empirical extension of the standard E_{max} model. It includes an exponent, which can help to control the log-linear slope in the model.

We introduced a mechanistic model of the mechanism of action of NRTIs. The model is based on the competitive mode of incorporation of NRTIs into the nascent DNA. Based on the conditions within the assay/infected cell, two scenarios can be extracted: The situation in which NRTI incorporation ceases reverse transcription (template-limited case), or the situation in which incorporation of NRTIs decelerates the velocity of chain prolongation (enzyme-limited case).

The final mechanistic model of NRTIs pharmacodynamics (eq. (6.12) and eq. (6.20)) has some structural similarities with the sigmoidal E_{max} model. However, three important determinants of NRTI efficacy become visible:

1. The concentration of the NRTI versus the natural substrate. This parameter is most likely cell-dependent and therefore indicates that the efficacy of NRTIs might diverge between different HIV-infected cell-types.

2. The affinity of the NRTI to RT versus the natural substrate. This parameter is most likely subject to evolutionary optimization and might thus be the major route of resistance development.

3. The number of incorporation sites n. The number of incorporation sites determines the exponent in the model. The apparently large exponent explains why NRTIs, besides being poor substrates for RT, efficiently inhibit reverse transcription.

In summary, it might be sufficient to use empirical pharmacodynamic models if the main interest is in the reproduction of pharmacodynamic profiles. However, if novel insights are to be made by investigating the mechanism of action, then mechanistic models are required.

Chapter 7

Example: PK-PD of Zidovudine

In this chapter we will give an example of the pharmacokinetics and the pharmacodynamics of the NRTI zidovudine (AZT), see [145]. In the case of AZT, the active triphosphate (AZT-TP) competes with the natural substrate deoxythymidine triphosphate (dTTP) for the reverse transcriptase of HIV. AZT-TP, once incorporated into the viral DNA chain, leads to chain termination and thereby inhibits virus proliferation [617].

Many studies focus on the pharmacokinetics of the prodrug, assuming a linear relationship between AZT and its active anabolite (e.g. [627, 628]). However, the relation between AZT and AZT-TP was shown to be non-linear [629–633].

Since NRTIs exert their pharmacological activity through competition with naturally occurring deoxynucleotide triphosphates, it has been shown for the class of NRTIs [634], and specifically for AZT [635], that the nucleoside analogue triphosphate-to-deoxynucleotide triphosphate ratio is a major determinant for successful chain termination by NRTIs. In the case of AZT it has been shown that the main anabolite, zidovudine monophosphate (AZT-MP), causes depletion of dTTP levels [299,635], which might be synergistic to the effect of AZT-TP on the reverse transcriptase of HIV.

So far there is no pharmacokinetic model which explicitly includes the complete phosphorylation cascade of AZT to AZT-TP, although an earlier model includes AZT and AZT-MP [636]. The objective of the present study is to build a detailed PBPK model for zidovudine and all of its anabolites, based on *in vitro* and *in vivo* data. This allows us to study the origins of drug heterogeneity and the extent, to which temporal fluctuations can create windows of insufficient viral suppression—with the aim to help interpret outcomes of clinical trials [637, 638].

7.1 Plasma Pharmacokinetics

We focuss on AZT and its monophosphate (AZT-MP) only, when modelling blood-plasma pharmacokinetics. This has the following rationale: Only AZT and AZT-MP are able to permeate cellular membranes, while the di- and triphosphate moiety are confined to the cellular spaces [639, 640]. Furthermore, It has been observed that the cellular amounts of zidovudine diphosphate (AZT-DP) and AZT-TP are significantly smaller than the corresponding AZT and AZT-MP levels (approximately 1:100) [299, 629, 632, 633, 636, 640–642]. Therefore, phosphorylation of AZT- or AZT-MP to the di- and triphosphates in the tissue-cells insignificantly influences the kinetics of AZT and AZT-MP [639].

We will, however, model the di- and tri-phosphate species in the effect compartment, i.e., the peripheral blood mononuclear cells (PBMC).

7.1.1 Distribution

AZT can enter cells by both passive diffusion [643–645] and active transport mechanisms [304,643,645]. Based on [639], the average tissue-to-plasma partitioning coefficient is 0.86. Zidovudine has a mean blood-to-plasma partitioning coefficient B : P of 0.86 [646]. Based on B : P = 0.86, we obtained a

tissue-to-blood partitioning coefficient of 1.

AZT-MP is produced intracellularly from AZT. The ratio of AZT-MP to AZT in the rest of the body ($K^{\mathrm{r}}_{\mathrm{MP:AZT}}$) has been measured experimentally in various tissues in mice [639], resulting in an average value of $K^{\mathrm{r}}_{\mathrm{MP:AZT}} = 0.071$. The rate of AZT-MP production was assumed to be fast on the time scales of interest, so that AZT-MP is proportional to AZT (by the factor $K^{\mathrm{r}}_{\mathrm{MP:AZT}} = 0.071$) in the rest of the body.

In summary, neither AZT- nor AZT-MP are extensively tissue bound. Taking the tissue-plasma partition coefficients [639] into account and utilizing eq. (5.74), we deduce that distribution into the tissues of the body is not limiting (distribution into tissues is completed at t $\ll$ 10 [min]). Therefore, it is sufficient to use a one-compartment model to accurately describe the plasma pharmacokinetics of AZT and AZT-MP in contrast to [145]. Utilizing this approach requires to estimate the volume of distribution V_{ss}. Since $K^{\mathrm{r}}_{\mathrm{MP:AZT}} \ll 1$, we can assume that the total volume of distribution of the drug is determined by the volume of distribution of AZT $V_{\mathrm{ss}} \approx V_{\mathrm{ss,AZT}}$. Utilizing the experimental partition coefficients [639], eq. (5.78) and (5.48) with hematocrit (hct = 0.45) and physiological data (e.g. [585, 647]), we derive $V_{\mathrm{ss}} \approx 47$ [L] in a 70 [kg] human.

7.1.2 Elimination

AZT is cleared linearly from the body [648] at physiological concentrations (following oral dosage in the range of 2 - 15 [mg/kg]) with a total plasma clearance of CL = 1.56 [L/min] [648]. The clearance term reflects all breakdown processes involved in zidovudine elimination, regardless of the actual pathways.

Utilizing the volume of distribution $V_{\mathrm{ss}} \approx 47$ [L], we derive an elimination constant $k_e = 0.033$ [1/min].

7.1.3 Absorption

The prodrug (AZT) is administered orally. However, we do not know the kinetics that underlie the absorption of AZT. For simplicity and parameter identifiability, we assume a first-order absorption model (see eq. (5.12)) with absorption rate k_a. Since the elimination of AZT is linear and the distribution instantaneous, we can estimate k_a using equation (5.13) with median *in vivo* $t_{\max} = 45$ [min] [234, 627, 648–650] and the previously mentioned elimination constant, resulting in $k_a = 0.013$ [1/min].

The bioavailability of AZT is $F_{\mathrm{bio}} = 0.64$ [649]. AZT is usually administered in doses of 100mg, 300mg and 600mg.

7.1.4 Validation with Clinical Data

The final model for the plasma pharmacokinetics is the explicit solution of a one-compartment model with linear absorption- and elimination kinetics and takes the following form:

$$\mathrm{AZT}(t)^{\mathrm{p}} = \frac{F_{\mathrm{bio}} \cdot \mathrm{dose}}{V_{\mathrm{ss}}} \frac{k_a}{k_a - k_e} \cdot \left(e^{-t \cdot k_e} - e^{-t \cdot k_a}\right) \tag{7.1}$$

$$\mathrm{MP}(t)^{\mathrm{p}} = K^{\mathrm{r}}_{\mathrm{MP:AZT}} \cdot \mathrm{AZT}(t), \tag{7.2}$$

where MP^{p} denotes the concentration of AZT-MP in the blood plasma. An explicit solution for multiple dosings can be found e.g. in [18].

The concentration-time profile of AZT in the blood-plasma, following a single dose of 100mg AZT is shown in figure 7.1 together with clinical data. In contrast to the two-compartment model in the original publication [145], we have used a one-compartment model here, which yields identical kinetic profiles and indicates that additional compartments are not needed.

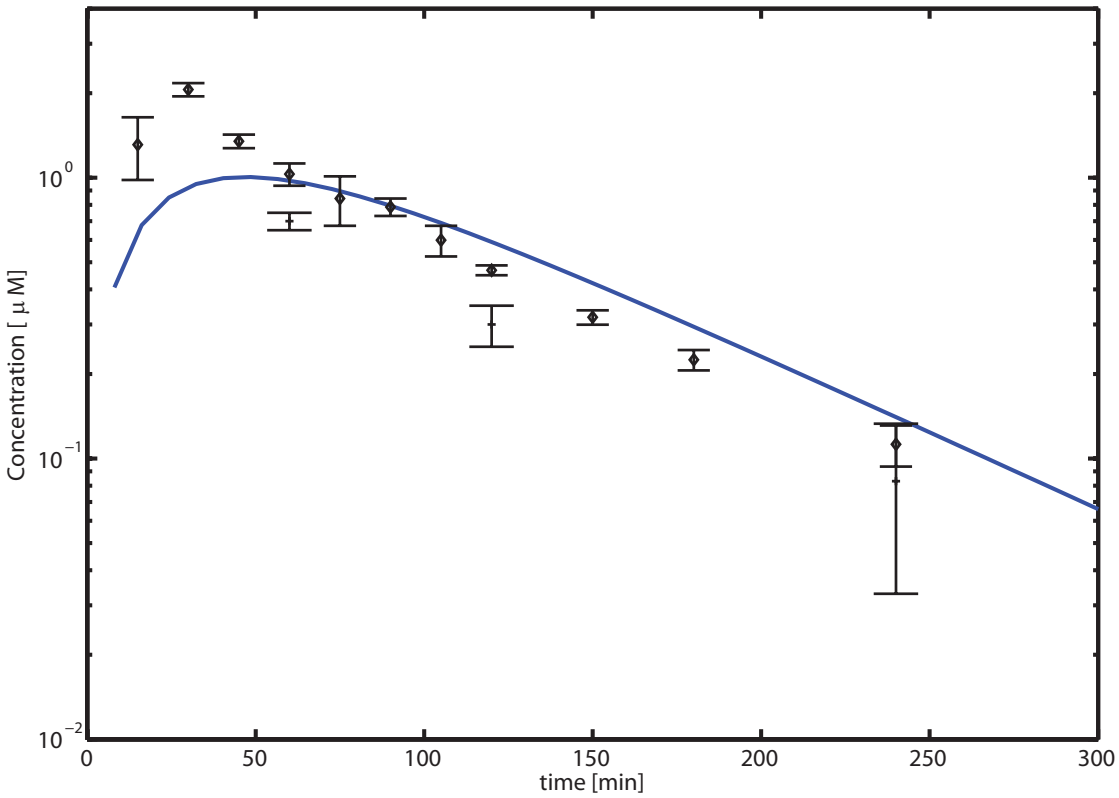

Figure 7.1: AZT Plasma Concentration after a 100mg dose together with clinical data from Barry et al. [632] (+) and Serra et al [650] (◇)

param.	value	ref.	param.	value	ref.
F_{bio}	0.64	[649]	k_e	0.033 [1/min]	see text
V_{ss}	47 [L]	see text	$K^{\text{r}}_{\text{MP:AZT}}$	0.071	[639]
k_a	0.025 [1/min]	see text	-	-	-

Table 7.1: Parameters for modelling the plasma pharmacokinetics of AZT.

7.2 Effect-site Concentration

Free (unbound) AZT from the plasma compartment is exchanged with the peripheral mononuclear cells (PBMCs), where it becomes phosphorylated to form AZT-MP$^{\text{e}}$, AZT-DP$^{\text{e}}$ and finally AZT-TP$^{\text{e}}$, which exerts the effect (superscript e= effect compartment).

AZT and AZT-MP. The membrane permeation in PBMCs was assumed to be fast and linear, in line with the experimental data in [639,643,646]. From [644], an unbound plasma AZT-to-intracellular AZT partition coefficient $K^{\text{up:e}} = 1$ was derived. In [145] (supplementary material), we have shown that the kinetics underlying the phosphorylation from AZT$^{\text{e}}$ to AZT-MP$^{\text{e}}$ and the de-phosphorylation from AZT-MP$^{\text{e}}$ to AZT$^{\text{e}}$ are linear and fast, represented by $K^{\text{e}}_{\text{MP:AZT}} = 6.14$ [145], so that the intracellular concentrations of AZT-MP are proportional to the plasma concentrations of AZT by the proportionality factor $K^{\text{e:p}}_{\text{MP:AZT}} = K^{\text{e}}_{\text{MP:AZT}} \cdot {f_{\text{u}}}^{\text{p}} / K^{\text{up:e}} = 4.6$ (utilizing ${f_{\text{u}}}^{\text{p}} = 0.75$ [646]).

AZT-MP and AZT-DP. AZT-MP phosphorylation to AZT-DP by thymidylate kinase has been identified as the rate limiting step in zidovudine activation [651, 652]. The authors of [651, 652] report a substrate inhibition due to AZT-MP binding to the ATP binding site. This has two important

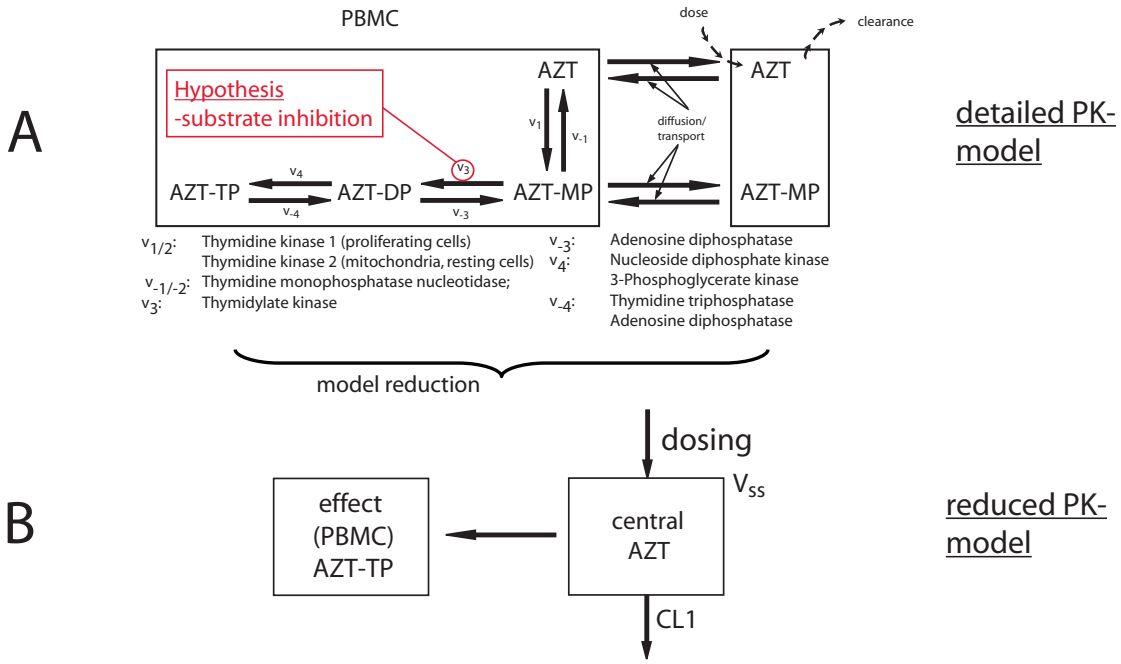

Figure 7.2: A) Detailed model of the intracellular phosphorylation cascade of AZT. B) Simplified kinetic model.

consequences: First, substrate inhibition of the thymidylate kinase by AZT-MP also reduces the phosphorylation of the natural substrate thymidine monophosphate, see section 7.3.1. Second, regarding the zidovudine phosphorylation cascade, non-competitive substrate inhibition and competitive inhibition by deoxythymidine monophosphate (dTMP) are taken into account. The phosphorylation and de-phosphorylation velocities $v_{\mathrm{MP}\to\mathrm{DP}}$ and $v_{\mathrm{DP}\to\mathrm{MP}}$ of AZT-MP (MP) and AZT-DP (DP) are given by

$$v_{\mathrm{MP}\to\mathrm{DP}} = \frac{V_{\max}\cdot \mathrm{MP}}{\mathrm{MP}\left(1+\frac{\mathrm{MP}}{K_{\mathrm{i}}^{\mathrm{MP}}}\right)+K_{\mathrm{M}}^{\mathrm{MP}}\left(1+\frac{\mathrm{dTMP}}{K_{\mathrm{i}}^{\mathrm{dTMP}}}\right)} \tag{7.3}$$

$$v_{\mathrm{DP}\to\mathrm{MP}} = v_{-3}\cdot \mathrm{DP} \tag{7.4}$$

with kinetic constants $K_{\mathrm{M}}^{\mathrm{MP}} = 6[\mu\mathrm{M}]$, $K_{\mathrm{i}}^{\mathrm{MP}} = 30[\mu\mathrm{M}]$ and $K_{\mathrm{i}}^{\mathrm{dTMP}} = 9[\mu\mathrm{M}]$ have been measured experimentally [652]. For our simulations, we assumed constant dTMP levels of $\mathrm{dTMP} = 4.1[\mu\mathrm{M}]$ due to homeostatic effects [653]. The maximal phosphorylation velocity $V_{\max} = 135$ [pmol/h] depends on the thymidylate kinase concentration. Due to the lack of knowledge about the thymidylate kinase concentration in PBMCs we estimated $V_{\max}$ from the *in vivo* data in [145]. We infer, in agreement with *in vivo* data, that the derived value of $V_{\max}$ causes a rate limiting behavior. The velocity v_{-3} [ml/h], by which AZT-DP is de-phosphorylated, is also unknown and was estimated from *in vivo* data resulting in $v_{-3} = 0.07$[ml/h]. The dephosphorylation of AZT-DP is subsequently identified as the rate limiting step, which increases the cellular half life of AZT-TP in comparison to plasma AZT (see fig. 5.17).

AZT-DP and AZT-TP. Experimental data [629,641,642] indicate that the kinetics between AZT-DP and AZT-TP are linear and fast in comparison to the time scale of interests here. Consequently, we describe the relation between AZT-DP and AZT-TP by the AZT-DP-to-AZT-TP ratio $K_{\mathrm{DP:TP}}$, as above in the case of AZT and AZT-MP. We derived an average ratio $K_{\mathrm{DP:TP}}$ of ≈ 1.1 in caucasians [642].

Summary: pharmacokinetics at the effect site. The kinetic steps in PBMCs between all AZT anabolites, except AZT-MP and AZT-DP are fast and linear. The phosphorylation from AZT-MP to

param.	value	ref.	param.	value	ref.
$f_u{}^p$	0.75	[646]	K_i^{MP}	30 [μM]	[652]
$K_{MP:AZT}^{e:p}$	4.6	see text	$K_i^{dTMP} = K_M^{dTMP}$	9 [μM]	[652]
V_{max}	135 [pmol/h]	see text	v_{-3}	0.07	see text
$K_{DP:TP}$	1.1	[642]	K_M^{MP}	6 [μM]	[652]

Table 7.2: Parameters for the intracellular pharmacokinetics of AZT.

AZT-DP is non-linear and the dephosphorylation of AZT-DP is rate limiting, causing the difference between the half life of AZT in the plasma and halflife of AZT-TP in the cells (see e.g. fig. 5.17). Therefore, we can derive the following system of equations that couples the concentrations of all anabolites in the PBMCs to the pharmacokinetics of the plasma AZT:

$$\begin{aligned} AZT^e(t) &= AZT^p(t)/f_u{}^p && (7.5)\\ MP^e(t) &= AZT^p(t)\cdot K_{MP:AZT}^{e:p} && (7.6)\\ V^e\frac{d}{dt}DP^e &= \frac{V_{max}\cdot MP^e}{MP^e\left(1+\frac{MP^e}{K_i^{MP}}\right)+K_M^{MP}\left(1+\frac{dTMP}{K_i^{dTMP}}\right)} - v_{-3}\cdot DP^e && (7.7)\\ TP^e(t) &= DP^e/K_{DP:TP}, && (7.8) \end{aligned}$$

where V^e is the volume of the PBMC compartment, which consists of $\approx$ 800 $CD4^-$ [10^6cells/L] [599] and a variable $CD4^+$ cell count in HIV-infected patients (healthy reference: 800 [10^6cells/L] [599]), with an average volume of 140 [fL/cell] [654]. The variables AZT^e, MP^e, DP^e and TP^e denote the concentration of AZT, AZT-MP, AZT-DP and AZT-TP at the effect site (PBMCs). Here, we have neglected the impact of intracellular AZT-DP and AZT-TP on the plasma pharmacokinetics of AZT ($v_{-3} = 0$). The model can further be reduced by lumping the pool of AZT-DP and AZT-TP [145] (e.g. fig. 7.2, B).

7.2.1 Validation with Clinical Data

The simulated plasma- and intracellular pharmacokinetics of AZT and its anabolites are shown in fig. 7.3 (left) together with experimental data from various clinical studies. In fig. 7.3 (right), we show the pharmacokinetic profiles of plasma AZT, intracellular AZT-MP, -DP and -TP, following a 600mg dose of AZT. The nonlinear relation between extracellular AZT and intracellular AZT-TP is illustrated in the inset.

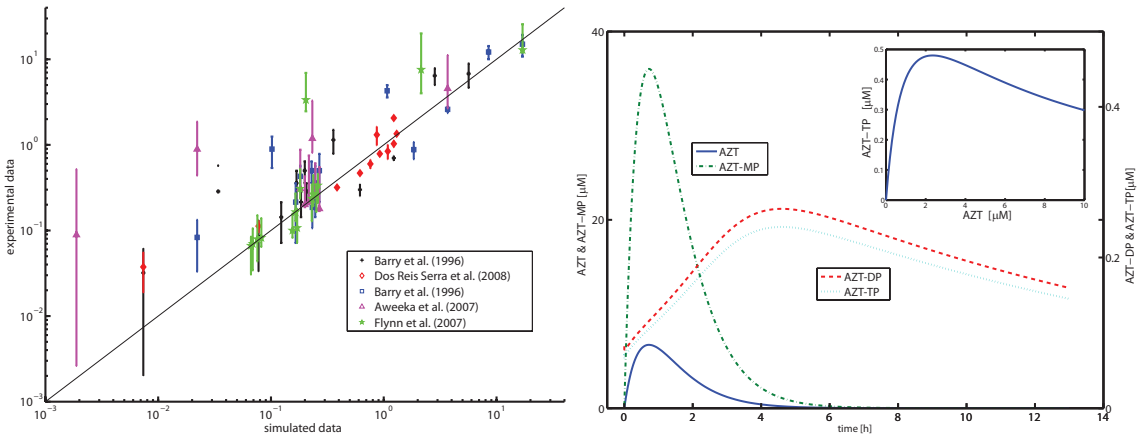

Figure 7.3: Left panel: Simulated versus measured clinical data from [632, 633, 642, 650]. Clinical data comprises AZT (plasma) and AZT-MP, AZT-DP and AZT-TP in the PBMCs following oral doses of 100, 300 and 600 [mg] zidovudine. Right panel: Sample profile for an oral dose of 600 [mg] zidovudine at steady state. The inset illustrates the saturable relation of AZT to AZT-TP.

param.	value	ref.	param.	value	ref.
$K^{\mathrm{RT}}_{\mathrm{m,TP}}$	2.42	[616]	$K^{\mathrm{RT}}_{\mathrm{m,dTTP}}$	0.32	[616]

Table 7.3: Pharmacodynamic parameters for AZT.

The intracellular kinetics have the following major implications:

1. Increasing the dose of AZT does not necessarily increase the amount of AZT-TP, which exerts the effect. This is due to the saturability of AZT-MP phosphorylation (see eq. (7.7), fig. 7.3, inset).
2. The maximum intracellular AZT-TP concentration (= maximum effect) does not coincide with the maximal AZT plasma concentration.
3. The dephosphorylation of AZT-DP determines the intracellular half life of AZT. From our model, we estimate an intracellular halflife of $\approx$ 6h. However, depending on the abundance of the dephosphorylating enzyme (adenosine diphosphatase) in some target cells, this half life might be sufficiently faster (equal to the plasma half life of $\approx$ 1.3h in the worst case).

The combination of saturated AZT phosphorylation kinetics and the relatively short intracellular half life might create windows of insufficient suppression for dose-intense, less-frequent dosing schemes. We will analyze this relation in the next section.

7.3 Temporally resolved Effects of AZT

The major effect of zidovudine is related to termination of the nascent viral DNA by AZT-TP. The propensity a_+ of prolongation of the DNA chain by a single dTTP in the presence of TP is given by

$$a_+ = \frac{k_{\mathrm{cat}} \cdot \mathrm{RT} \cdot \mathrm{dTTP}(t)/\alpha}{K^{\mathrm{RT}}_{\mathrm{m,dTTP}} \left(1 + \frac{\mathrm{TP}(t)}{K^{\mathrm{RT}}_{\mathrm{m,TP}}}\right) + \mathrm{dTTP}(t)/\alpha}, \tag{7.9}$$

where k_{cat} [1/s] is the rate of insertion, and RT denotes the number of reverse transcriptases. The parameters $K^{\mathrm{RT}}_{\mathrm{m,dTTP}}$ and $K^{\mathrm{RT}}_{\mathrm{m,TP}}$ denote the Michaelis-Menten constants for insertion of dTTP and TP, respectively. The parameter α denotes the depletion of dTTP due to a secondary effect of AZT-MP (discussed below). Analogously, the propensity a_0 of termination of the DNA chain by insertion of a single TP in the presence of dTTP is given by

$$a_0 = \frac{k_{\mathrm{cat}} \cdot \mathrm{RT} \cdot \mathrm{TP}(t)}{K^{\mathrm{RT}}_{\mathrm{m,TP}} \left(1 + \frac{\mathrm{dTTP}(t)/\alpha}{K^{\mathrm{RT}}_{\mathrm{m,dTTP}}}\right) + \mathrm{TP}(t)}. \tag{7.10}$$

Based on the above two propensities, we can compute the probability q of dTTP insertion (under the condition that either AZT-TP or dTTP is inserted) according to

$$q = \frac{a_+}{a_0 + a_+} = \frac{1}{1 + \frac{\mathrm{TP}(t)\cdot\alpha}{\mathrm{dTTP}(t)} \cdot \frac{K^{\mathrm{RT}}_{\mathrm{m,dTTP}}}{K^{\mathrm{RT}}_{\mathrm{m,TP}}}}. \tag{7.11}$$

where we have utilized the fact, that the catalytic rate constants of AZT-TP and dTTP are identical [616].

7.3.1 Secondary Effect.

Deoxythymidine monophosphate is phosphorylated by the same enzyme (thymidylate kinase) as AZT-MP. The levels of dTDP, the predecessor of the natural RT substrate, dTTP, are reduced through

competitive and non-competitive inhibition of the phosphorylating enzyme by AZT-MP [652].

The velocity of dTMP-phosphorylation in the presence of AZT-MP can be expressed as:

$$v_{\mathrm{dTMP}\to\mathrm{dTDP}}(\mathrm{MP}) = \frac{V_{\max}^{\mathrm{dTMP}} \cdot \mathrm{dTMP}}{K_{\mathrm{M}}^{\mathrm{dTMP}}\left(1+\frac{\mathrm{MP}}{K_{\mathrm{M}}^{\mathrm{MP}}}\right)+\mathrm{dTMP}\left(1+\frac{\mathrm{MP}}{K_{\mathrm{i}}^{\mathrm{MP}}}\right)}, \tag{7.12}$$

where dTMP, dTDP and MP denote the concentrations of deoxythymidine mono- and di-phosphate, and zidovudine monophosphate, respectively. The parameters $K_{\mathrm{M}}^{\mathrm{MP}}$, $K_{\mathrm{M}}^{\mathrm{dTMP}}$ and $K_{\mathrm{i}}^{\mathrm{MP}}$ denote the Michaelis Menten constants of AZT-MP and dTMP to thymidylate kinase and the inhibitory constant, respectively. The maximum velocity of dTMP phosphorylation is denoted by $V_{\max}^{\mathrm{dTMP}}$. The relative extent of dTDP reduction by AZT-MP is estimated by the quotient of the phosphorylation velocities in the absence and presence of AZT-MP

$$\frac{\mathrm{dTDP}(\phi)}{\mathrm{dTDP}(\mathrm{MP})} = \frac{v_{\mathrm{dTMP}\to\mathrm{dTDP}}(\phi)}{v_{\mathrm{dTMP}\to\mathrm{dTDP}}(\mathrm{MP})} =: \alpha. \tag{7.13}$$

Assuming a one-to-one relation between dTDP depletion and dTTP depletion, we propose to model the impact of AZT-MP on dTTP levels according to

$$\mathrm{dTTP}(\mathrm{MP}) = \mathrm{dTTP}(\phi)/\alpha, \tag{7.14}$$

where $\mathrm{dTTP}(\phi) = 4.1$ [μM] [653] denotes the level of dTTP in the absence of an inhibitor.

7.3.2 Reverse Transcription under AZT Treatment.

We can use either of the models in eq. (6.20) or eq. (6.12), depending the assumption of enzyme-limitation or template-limitation (see section 6.2). However, the template-limited model cannot take the major- and secondary effect of AZT into account separately, because it dose not consider the time that the reverse transcriptase needs in order to produce DNA. Let us assume here, that the amount of enzyme is limiting for reverse transcription. We derive

$$(1-\varepsilon(t)) = \frac{a_+}{a_+(\phi)} \cdot N q^{N-1} \frac{1-q}{1-q^N}, \tag{7.15}$$

wity N denoting the total number of thymidine bases to be incorporated. We couple this model to the pharmacodynamic model (eq. (7.1), (7.8)) to derive the pharmacokinetic-pharmacodynamic relationship for AZT.

The percent of successful viral DNA reverse transcription under AZT treatment $(1-\varepsilon)$ is shown in Figure 7.4 (left) for different dosing schemes; (a) 100mg six times a day (b) 100mg three times a day, (c) 300mg two times a day; and (d) 600mg once daily. The impact of low AZT-TP concentrations at the end of each dosing interval is most pronounced in the 600mg once daily dosing scheme. For the latter, the active drug concentration is insufficient for almost the entire second half of the dosing interval, leading to ineffective inhibition of the reverse transcription process. This lack of effect coincides with the time at which levels of AZT-TP drop below approximately 0.05 [μM], and at which almost no dTDP depletion remains (see [145], supplementary material). This implies that the chance of mutational viral escape is rising at the time before the next dosing in case of less frequent dosing. We evaluated the % of residual RT activity (relative to the absence of AZT) in Table 7.4 for a 24h interval $(1-\varepsilon)_{24\mathrm{h}}$ after reaching steady state (day 3-4). It can be seen that for the 600mg dosing scheme insufficient inhibition (approx. 80 %) is reached in PBMCs.

We have provided a quantitative assessment of the effect of pharmacokinetic profiles of AZT-MP and AZT-TP on suppression of reverse transcription. We used the proposed pharmacokinetic-

dosing scheme	AUC_{0-24} (AZT-MP)	$100 \cdot (1-\varepsilon)_{24h}$
100mg every 4h	70.4 [h·μM]	$3.6 \cdot 10^{-8}$
100mg every 8h	35.4 [h·μM]	$5.9 \cdot 10^{-2}$
300mg every 12h	70.8[h·μM]	0.26
600mg every 24h	70.8 [h·μM]	18.9

Table 7.4: Exposure to AZT-MP and the efficacy of the treatment during 24h after pharmacokinetic steady state (day 3-4). The efficacy is expressed in % of residual RT activity during the 24h interval.

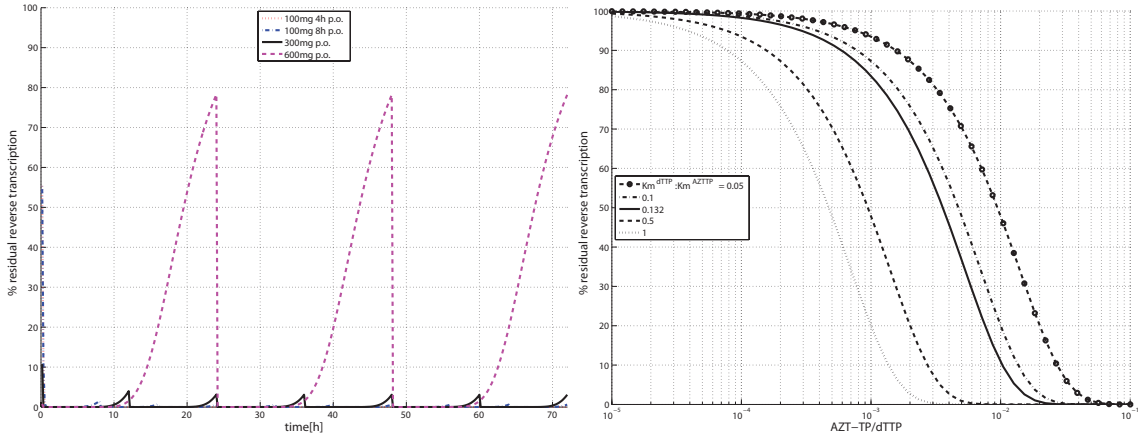

Figure 7.4: Left panel: Residual virus DNA production for different dosing schemes after the initiation of AZT therapy. The curves show the % residual reverse transcription $(1-\varepsilon)$ after a once daily dose of 600 [mg] (dashed magenta line), a twice daily oral dose of 300 [mg] (solid black line), an oral dose of 100 [mg] every 8 hours (dash-dotted blue line) and an oral dose of 100 [mg] every 4 hours (dotted red line). Right panel: Influence of the dTTP:AZT-TP ratio on the suppression of reverse transcription for different $K^{RT}_{m,dTTP} : K^{RT}_{m,TP}$ ratios. The solid line corresponds to the literature $K^{RT}_{m,dTTP} : K^{RT}_{m,TP}$ ratio, while the other values are chosen to illustrate the impact of resistance mutation (rightmost lines) or hypersensitivity (leftmost lines) on % residual reverse transcription.

(eq. (7.1), eq. (7.5)-(7.8)) and effect model (eq. (6.20)) to analyze four different dosing schemes *in silico*: 100 mg every 4 hours, 100 mg every 8 hours, 300 mg every 12 hours and 600 mg every 24 hours. From our simulations, we conclude that the 100mg (every 8 hours) dosing scheme has the best properties regarding (maximal) efficacy and (minimal) exposure to AZT-MP (which is connected to toxicity [327, 328, 655]), when taking the kinetics in PBMCs as a reference for other target cells (see Table 7.4). In the case of the 600mg once daily dosing scheme, incomplete suppression can be seen in the time before the next dosing (Fig. 7.4, left). This apparent lack of efficacy could explain the observed weaker viral suppression for this dosing scheme in comparison with the 300mg twice daily scheme [638]. It is suspected to leave enough opportunities for viral escape in PBMCs. The other dosing schemes provide very good suppression of reverse transcription in PBMCs. When comparing the 300mg twice daily with the 100mg every 4 hours dosing scheme, similar exposure to AZT-MP is found and potent suppression of viral RT in both cases is observed (Table 7.4). The results are in agreement with clinical trials [637], in which similar antiviral effects for both dosing schemes were observed. Also, the associated toxicity of both dosing strategies was comparable [637].
AZT-TP levels in $CD4^+$ cells are sufficiently lower than AZT-TP levels in other cells of the PBMC compartment [631, 656]. The exact relation has not fully been resolved yet, however in [656], concentrations of AZT-TP in $CD4^+$ cells were related to the concentrations of AZT-TP in $CD4^+$ depleted PBMC. For the analyzed extent of $CD4^+$ depletion (14 % $CD4^+$ cells in the $CD3^+$ gate) [656] found that the levels in purified $CD4^+$ cells are approximately 25% of those in PBMCs (see fig. 7.5). We might utilize this conversion factor to predict the levels of AZT-TP in $CD4^+$ cells based on AZT-TP concentration in PBMCs. An analysis of the efficacy based on this assumption is presented in Table 7.5. We infer that all dosing schemes, except for the 100mg (every 4h) would insufficiently suppress viral replication in $CD4^+$ cells. However, this assumption remains speculative until further data is available.

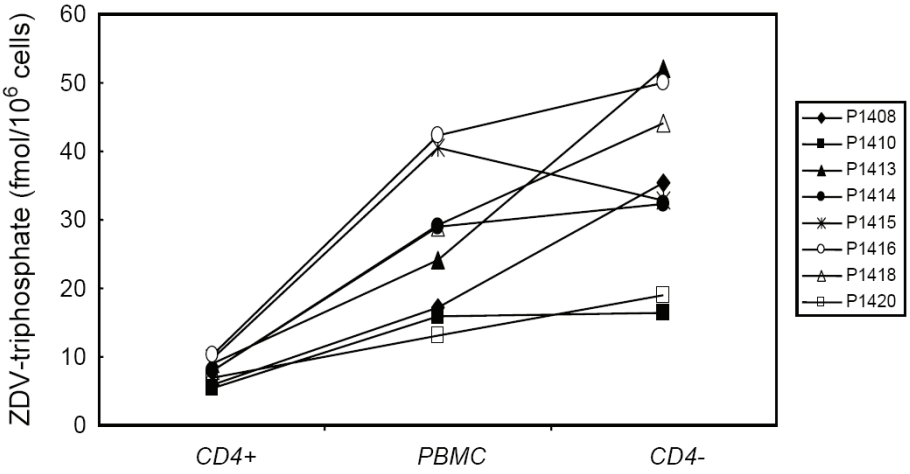

Figure 7.5: Correlation between intracellular levels of AZT-TP in $CD4^+$ cells, PBMCs and $CD4^-$ cells. Illustration from [656].

dosing scheme [mg]	100 (/4h)	100 (/8h)	300 (/12h)	600 (/24h)
$100 \cdot (1-\varepsilon)_{24h}$	0.3	10	12	42

Table 7.5: Efficacy expressed in % of residual RT activity during the whole interval if the AZT-TP concentrations in $CD4^+$ cells are 25% of those in PBMCs, as suggested by [656].

7.4 Summary

We used a novel mechanistic effect model to predict the impact of zidovudine and its anabolites on the reverse transcription process. The pharmacodynamic model (eq. (6.20)) considers the competitive mode of RT binding and the resultant chain termination mechanistically rather than empirically, utilizing experimental data from single nucleotide extension assays [616]. The effect is described by the deceleration of successful viral DNA chain completion in the presence of zidovudine compared to the situation without drug treatment. The two potential mechanisms, by which zidovudine acts, can be analyzed separately. The primary effect is attributed to the insertion of AZT-TP into the growing DNA chain. Once inserted, the reverse transcription process is stopped, resulting in a degradation of the uncompleted DNA chain. As a net result this process increases the time to successful completion of the DNA chain. It has been shown in [634, 657] that the AZT-TP:dTTP ratio is a major determinant of antiviral efficacy. Based on our proposed effect model, we can give a mechanistic justification of this determinant. The parameter with most influence on the overall effect is the probability of successful dTTP incorporation q. The relation between q, AZT-TP, dTTP and the K_{M} values is described by the very simple relation (7.11). It states that the larger the quotient AZT-TP:dTTP, the smaller q, as observed experimentally [634, 657]. The second factor involved in eq. (7.11) is the ratio $K^{\mathrm{RT}}_{\mathrm{m,dTTP}} : K^{\mathrm{RT}}_{\mathrm{m,TP}}$. Mechanistically, AZT-TP powerfully inhibits reverse transcription due to the potentiation of a low probability of incorporation by a large number of opportunities for incorporation [652]. Therefore, very small changes in the extent of incorporation q can have a dramatic effect on the degree of inhibition. In the light of our effect model (cf. eq.(6.20)), the probability of successful thymidine incorporation enters the effect model to the $(N\text{-}1)th$ power, where N denotes the number of thymidine bases that have to be inserted. Therefore, the effect through AZT-TP is very sensitive to (a) variations in the AZT-TP:dTTP ratio caused by depletion of dTTP pools, or (b) temporal fluctuations in the AZT-TP concentrations caused by the pharmacokinetics after oral dosing and (c) small modifications in the affinity of AZT-TP to RT, e.g. as a result of mutations in the RT. Because the effect of AZT-TP (and other NRTIs) is highly sensitive to fluctuations in the AZT-TP:dTTP ratio, we speculate that the heterogeneities in the AZT-TP (and most likely other NRTI) levels can create a major window of unsuppressed viral replication as illustrated in fig. 7.4 (left).

Part IV

Discussion, Conclusion & Perspectives

Highly active antiretroviral therapy (HAART) consists of a cocktail of antiviral drugs. This cocktail of drugs is usually changed in the context of treatment failure[1] [517]. However, there is little consensus when a treatment change would be optimal [2]. One major reason for treatment failure is the emergence of drug resistant strains, which leads to the relapse of virus in the patient's blood circulation. In this case, the timing of treatment change might be sub-optimal, because the chances that the virus develops resistance against a potential salvage regimen are higher than during viral suppression, when the viral population is small.

Consequences of viral relapse. When resistance development under HAART is the main cause of viral relapse, the major circulating strains are treatment resistant (see e.g. fig. 4.17). In HIV, the reservoir of latently infected cells serves as an archive of circulating viral strains before the suppression of viremia [658, 659], which can be re-filled in case of viral relapse [660]. Therefore, if viral relapse is driven by treatment resistant strains, it is very likely that those strains become archived in the latent, inducible reservoir [661]. If the previously failing regimen is re-used at a later time, viral relapse might directly originate from induction of latently infected cells, harboring resistant strains. Therefore, once viral relapse has occurred, it might limit the use of the failing regimen for the remaining life-time of the patients. Since drug resistance can be class-wide, this scenario might seriously eliminate treatment options for the affected patient. As a conclusion, viral relapse under therapy should be avoided by all means.

Timing & causes of resistance emergence and viral relapse. The mechanisms and the possible delay by which HIV resistance emergences under effective therapy, are key unsolved problems.

Under monotherapy, resistance usually develops within a few days (see fig. 7.6, left) [395, 662]. The main reasons for resistance development can in this case be attributed to the selection of pre-existing resistant strains [507] (see e.g. fig. 4.10) or incomplete suppression. The rapid emergence of drug resistance can readily be reproduced by mathematical models.

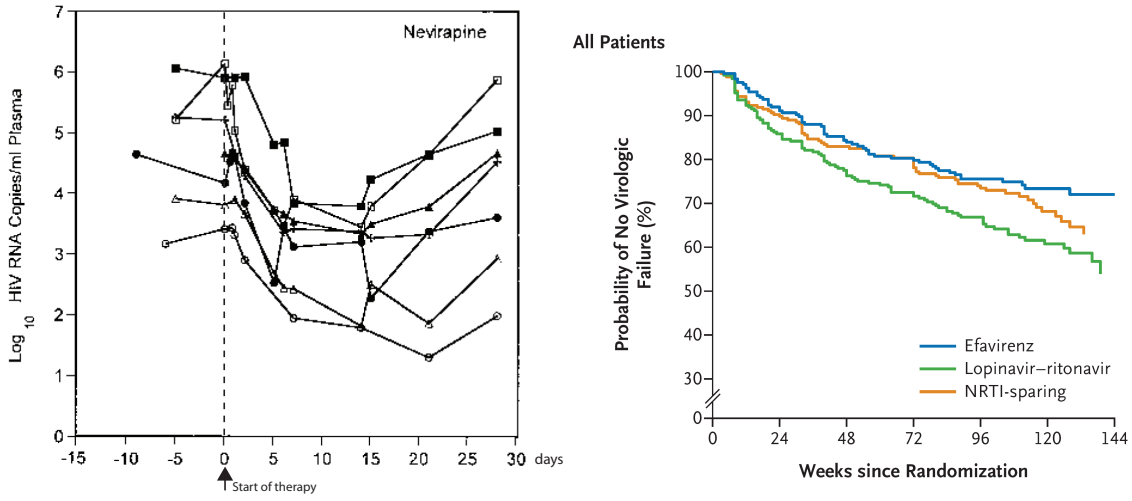

Figure 7.6: Left: Rebound of viral load after nevirapine monotherapy. Illustration from [662]. Right: Virological failure after HAART therapy. Illustration from [663].

Under effective HAART therapy, the occurrence of drug resistance and virological failure is orderly delayed (timescale of months and years) and seems to happen at random times (see fig. 7.6, right).

[1] e.g. viral relapse, drug intolerance. Definition in chapter 3

- Drug resistance in the context of HAART arises *de novo* as a result of ongoing viral replication [664], indicating non-suppressive antiretroviral therapy, which is usually the result of inadequate drug exposure [3].
- However, under non-suppressive antiretroviral therapy, drug resistance would develop within a short time span, since the viral turnover is rapid [488] (see also fig. 7.6, left).
- On the other hand, **if treatment is suppressive**, *de novo* emergence of drug resistance at a progressed stage of effective treatment is somewhat unintuitive: The pool of replicating virus shrinks by several orders of magnitude ($\geq 10^6$) under effective treatment (see fig. 1.4). Thus, it is far more likely that resistance develops at some earlier time point, compared to a later time point (schematically illustrated in fig. 7.7, left). Resistance development should, therefore, predominantly occur shortly after treatment initiation, in contradiction to the observation from clinical trials (see fig. 7.6, right).

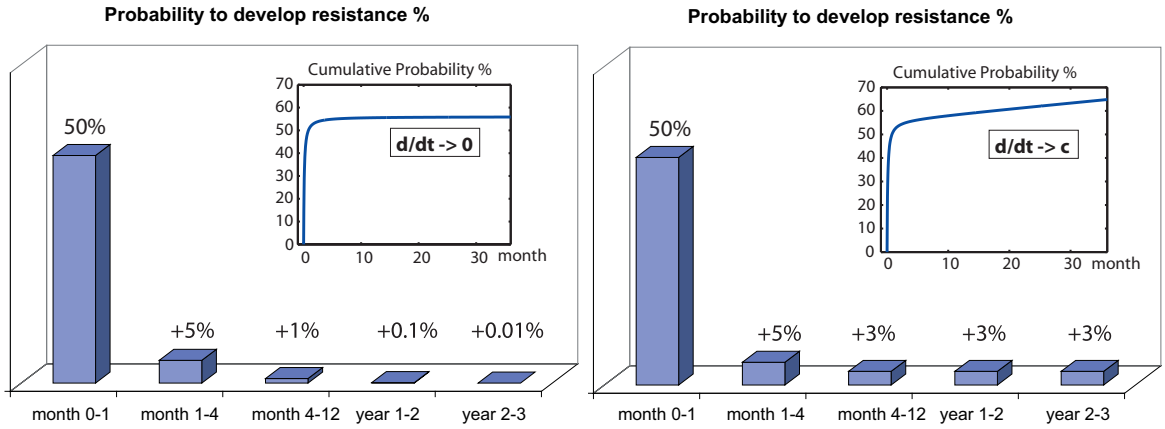

Figure 7.7: Left: Probability to develop resistance within a certain time-frame, in the case where the amount of replicating virus is decreasing. Inset: Cumulative probability to develop resistance. Right: Probability to develop resistance within a certain time-frame, in the case where the the virus continues to proliferate within a small, stable anatomical sanctuary, while it is decreasing in the bulk of infected compartments. Inset: Cumulative probability to develop resistance.

One explanation for the delayed emergence of drug resistance under HAART is poor adherence at some random time after treatment initiation. If the pool of replicating virus has not been entirely eradicated, non-adherence might allow replication, which in turn can produce drug resistant viral mutants at the time of non-adherence. Therefore, poor adherence can explain the random distribution and the delay of resistance development, as observed in clinical trials (see e.g. fig. 7.6, right).

In fact, poor adherence is the main cause of resistance development under HAART [664]. However, even in 100 % adherent patients, resistance can develop (see fig. 7.8) and thus adherence cannot be the only factor leading to virological failure. Interestingly, protease mutations were more frequent in highly adherent individuals on protease inhibitor-based HAART, compared to patients with low treatment adherence [665]. Although these associations appear paradoxical, they were substantiated in subsequent studies that utilized different means of adherence and resistance assessment [666, 667]. Mathematical models and longitudinal analysis of the association between adherence and resistance development verified that the greatest risk of protease inhibitor resistance occurs at moderate-to-high levels of adherence [668–670] (see fig. 7.8). Resistance development declines modestly with perfect levels of adherence [670], however, it does not vanish (see fig. 7.8).

One possible explanation for the delayed emergence of drug resistance, despite 100% adherence could be the ongoing replication in a pharmacological sanctuary that is in poor exchange with the plasma virus (which is typically measured) [671–678]. In this case, treatment **appears to be fully suppressive**, because plasma virus is declining below the levels of detection. However, treatment is

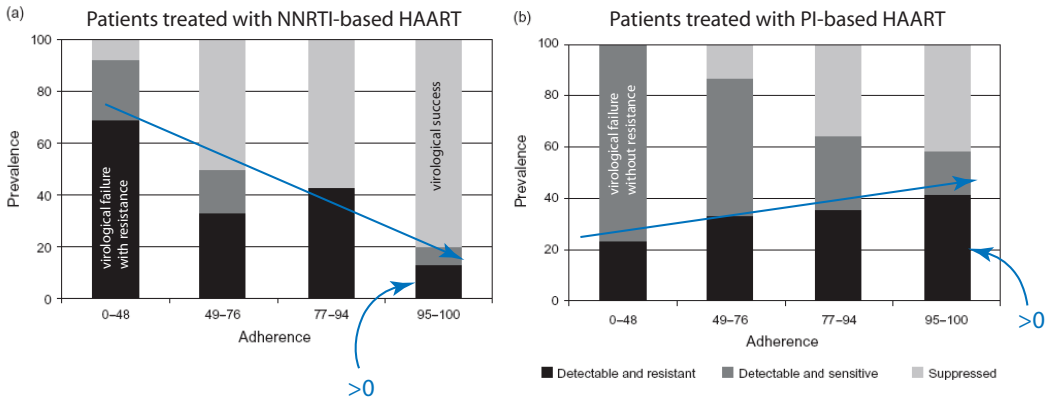

Figure 7.8: Correlation between adherence and virological success (light gray), virological failure without resistance development (dark grey) and virological failure with resistance development (black). Illustration modified from [664].

not suppressive within a small, but stable, anatomical sanctuary. Over time, replication (= mutation) within this small, unsuppressed viral population constantly increases the probability that resistance emerges (see fig. 7.7, right).

There are various lines of evidence, that most drugs poorly penetrate the brain and the testis (see chapter 3). Furthermore, the penetration of PIs, for example, can be highly restricted by efflux transporters. In the case of NRTIs, some target cells might produce insufficient amounts of intracellular NRTI-triphosphate. The penetration of antivirals into different infected compartments might therefore be highly heterogeneous, effectively leading to sub-optimal suppression, or mono-therapy in some compartments, which lowers the barrier to resistance and facilitates the emergence of drug resistance [679]. Ongoing replication in anatomical sanctuaries might occur in conjunction with the necessity to develop multiple mutations sequentially to obtain resistance [680], which generally requires more time than single point-mutations [664].

Strategy to avoid viral relapse. There are two major obstacles to the clinical implementation of strategies that aim at avoiding resistance emergence and virological rebound under whatever cause (e.g. adherence, compartmentalization):

- Resistance emergence and viral relapse occurs at random times.
- Viral relapse occurs within an extremely short time (days–weeks), which leaves a very small time-frame between the detection of resistance emergence and viral relapse.

Because of the random distribution of virological failure over time, constant monitoring would be required in order to detect virological failure. Since virological failure can manifest within such a short time-scale, monitoring would have to be very frequent.

Let us assume for the moment that frequent patient monitoring is feasible. The proposed strategy for the optimal sequencing of drugs (see section 4.6) utilizes the reproductive capacity, for which we have shown, that it can detect virological failure prior to e.g. the (total) virus load (see e.g. fig. 4.13, 4.14), thus expanding the time-frame between the detection of resistance and viral relapse. However, R_{cap} requires a detailed knowledge about the viral quasi-species composition in the patient, which necessitates the use of genotypic- or phenotypic assays. Already, the FDA recommends to perform drug resistance testing during antiretroviral therapy, in the case of virological failure [2]. However, there are certain limitations to these assays that currently limit the use of the proposed strategy in a clinical setting.

- The sensitivity to detect minor variants in standard assays is usually low (20–50%). However pyro-sequencing might increase the sensitivity of genotypic assays. Recent phenotypic assays have been reported to be sensitive enough to reveal $< 1\%$ mutants in mixed samples [681].

- The turnover of genotypic- or phenotypic assays is usually a few weeks, although results might be available within 8 days [681].
- When viremia is below the limit of detection, there might be no way of assessing the viral quasi-species distribution.

Besides these methodological issues, there are certain issues that have not been considered in this work. Drug penetration is usually heterogeneous, as previously discussed. More frequent therapy change, which might be a result of the proposed treatment switching strategy (section 4.6), might help to purge anatomical sanctuaries that could exist and manifest under a single drug combination. In this respect, the proposed strategy might create an extra benefit over traditional HAART. However, one serious concern is multi-integration of provirus in infected cells. Actively infected T-cells have a relatively short half-life and only about four integrated pro-viruses [621]. However, latently infected $CD4^+$ cells might harbor as many as 100 copies of integrated provirus [682]. Multi-integration can be a problem, because during the lifetime of these cells, they might be exposed to many different treatment regimen in the context of the switching strategy. As a result, a single cell might harbor many resistant proviruses, that together confer multi-regimen resistance. The impact of this phenomenon and the likelihood of its appearance has not yet been investigated.

7.5 Acknowledgements

I want to thank my supervisor Wilhelm Huisinga for giving me the freedom to follow my own ideas and to self-organize my work. I think it was an excellent idea to choose pharmacometrics as a research topic and I am optimistic that we fruitfully continue this research. I have always been fascinated in virus research and am truly grateful, that I had the chance to contribute and share some of this fascination. I would also like to thank you for your patience and sometimes fatherly support. I think I have really learned a lot from you and hope that I could also give something back.
I want to especially emphasize my gratitude to Stephan Menz (HIV-bro) for our joint work on optimizing the treatment of HIV. Without Stephan parts of the project would not have been executable. I think we are very good at triggering each others motivation and this fact has made the work very enjoyable and motivating. I am sure we will find some more interesting projects in the future (my head is full of them).
I would like to thank my girlfriend for all support, backup, love and trust. It is not easy to live a relationship like we did, with 3.5 years of distance and only the fewest people make it work out well. However, we did it, there was not even a millisecond of doubt, –possibly the greatest achievement of all.
Finally, I want to thank modern medicine, without which I would be dead already 10 years ago. I cannot name a particular person, that did the key inventions, but I believe that all the methods, treatments and trained professionals are an outcome of countless efforts by many motivated researchers. Just in the very same way I want to give something back to modern medicine and possibly contribute to saving somebodies else's life. Deep down this was my motivation for studying bio-informatics in the first place.

Bibliography

[1] UNAIDS. *2008 Report on the global AIDS epidemic* (2008).

[2] Current HIV treatment guidelines: (`http://www.aidsinfo.nih.gov/guidelines/`). Tech. Rep., National Institute of Health (accessed 25-May-2009).

[3] Clavel, F. & Hance, A. J. HIV drug resistance. *N Engl J Med* **350**, 1023–1035 (2004).

[4] Mansky, L. M. & Temin, H. M. Lower in vivo mutation rate of human immunodeficiency virus type 1 than that predicted from the fidelity of purified reverse transcriptase. *J Virol* **69**, 5087–5094 (1995).

[5] Nijhuis, M., van Maarseveen, N. M. & Boucher, C. A. B. Antiviral resistance and impact on viral replication capacity: evolution of viruses under antiviral pressure occurs in three phases. *Handb Exp Pharmacol* 299–320 (2009).

[6] Lambotte, O. *et al.* The lymphocyte HIV reservoir in patients on long-term HAART is a memory of virus evolution. *AIDS* **18**, 1147–1158 (2004).

[7] Beerenwinkel, N., Eriksson, N. & Sturmfels, B. Evolution on distributive lattices. *J Theor Biol* **242**, 409–420 (2006).

[8] Beerenwinkel, N. *et al.* Geno2pheno: Estimating phenotypic drug resistance from HIV-1 genotypes. *Nucleic Acids Res* **31**, 3850–3855 (2003).

[9] Rabinowitz, M. *et al.* Accurate prediction of HIV-1 drug response from the reverse transcriptase and protease amino acid sequences using sparse models created by convex optimization. *Bioinformatics* **22**, 541–549 (2006).

[10] Deforche, K. *et al.* Estimation of an in vivo fitness landscape experienced by HIV-1 under drug selective pressure useful for prediction of drug resistance evolution during treatment. *Bioinformatics* **24**, 34–41 (2008).

[11] Perelson, A. S., Neumann, A. U., Markowitz, M., Leonard, J. M. & Ho, D. D. HIV-1 dynamics in vivo: virion clearance rate, infected cell life-span, and viral generation time. *Science* **271**, 1582–1586 (1996).

[12] Perelson, A. S. *et al.* Decay characteristics of HIV-1-infected compartments during combination therapy. *Nature* **387**, 188–191 (1997).

[13] Ho, D. D. *et al.* Rapid turnover of plasma virions and CD4 lymphocytes in HIV-1 infection. *Nature* **373**, 123–126 (1995).

[14] Bonhoeffer, S., May, R. M., Shaw, G. M. & Nowak, M. A. Virus dynamics and drug therapy. *Proc Natl Acad Sci U S A* **94**, 6971–6976 (1997).

[15] Huang, Y., Rosenkranz, S. L. & Wu, H. Modeling HIV dynamics and antiviral response with consideration of time-varying drug exposures, adherence and phenotypic sensitivity. *Math Biosci* **184**, 165–186 (2003).

[16] Wu, H. *et al.* Modeling long-term HIV dynamics and antiretroviral response: effects of drug potency, pharmacokinetics, adherence, and drug resistance. *J Acquir Immune Defic Syndr* **39**, 272–283 (2005).

[17] Wu, H. *et al.* Pharmacodynamics of antiretroviral agents in HIV-1 infected patients: using viral dynamic models that incorporate drug susceptibility and adherence. *J Pharmacokinet Pharmacodyn* **33**, 399–419 (2006).

[18] Dixit, N. M. & Perelson, A. S. Complex patterns of viral load decay under antiretroviral therapy: influence of pharmacokinetics and intracellular delay. *J Theor Biol* **226**, 95–109 (2004).

[19] Dixit, N. M., Markowitz, M., Ho, D. D. & Perelson, A. S. Estimates of intracellular delay and average drug efficacy from viral load data of HIV-infected individuals under antiretroviral therapy. *Antivir Ther* **9**, 237–246 (2004).

[20] Rosario, M. C., Poland, B., Sullivan, J., Westby, M. & van der Ryst, E. A pharmacokinetic-pharmacodynamic model to optimize the phase iia development program of maraviroc. *J Acquir Immune Defic Syndr* **42**, 183–191 (2006).

[21] Jacqmin, P., McFadyen, L. & Wade, J. R. A receptor theory-based semimechanistic PD model for the CCR5 noncompetitive antagonist maraviroc. *Br J Clin Pharmacol* **65 Suppl 1**, 95–106 (2008).

[22] Marx, J. L. New disease baffles medical community. *Science* **217**, 618–621 (1982).

[23] Barré-Sinoussi, F. *et al.* Isolation of a T-lymphotropic retrovirus from a patient at risk for acquired immune deficiency syndrome (AIDS). *Science* **220**, 868–871 (1983).

[24] Gallo, R. C. *et al.* Isolation of human T-cell leukemia virus in acquired immune deficiency syndrome (AIDS). *Science* **220**, 865–867 (1983).

[25] Broder, S. & Gallo, R. C. A pathogenic retrovirus (HTLV-III) linked to AIDS. *N Engl J Med* **311**, 1292–1297 (1984).

[26] Castro, K. G. *et al. 1993 Revised Classification System for HIV Infection and Expanded Surveillance Case Definition for AIDS Among Adolescents and Adults* (CDC, 1993).

[27] Simon, V. & Ho, D. D. HIV-1 dynamics in vivo: implications for therapy. *Nat Rev Microbiol* **1**, 181–190 (2003).

[28] McMichael, A. J. HIV vaccines. *Annu Rev Immunol* **24**, 227–255 (2006).

[29] Li, Q. *et al.* Peak SIV replication in resting memory CD4+ T cells depletes gut lamina propria CD4+ T cells. *Nature* **434**, 1148–1152 (2005).

[30] Pope, M. & Haase, A. T. Transmission, acute HIV-1 infection and the quest for strategies to prevent infection. *Nat Med* **9**, 847–852 (2003).

[31] Brenchley, J. M. *et al.* CD4+ T cell depletion during all stages of HIV disease occurs predominantly in the gastrointestinal tract. *J Exp Med* **200**, 749–759 (2004).

[32] Mattapallil, J. J. *et al.* Massive infection and loss of memory CD4+ T cells in multiple tissues during acute SIV infection. *Nature* **434**, 1093–1097 (2005).

[33] Mehandru, S. *et al.* Primary HIV-1 infection is associated with preferential depletion of CD4+ T lymphocytes from effector sites in the gastrointestinal tract. *J Exp Med* **200**, 761–770 (2004).

[34] Phillips, A. N. Reduction of HIV concentration during acute infection: independence from a specific immune response. *Science* **271**, 497–499 (1996).

[35] Borrow, P., Lewicki, H., Hahn, B. H., Shaw, G. M. & Oldstone, M. B. Virus-specific CD8+ cytotoxic T-lymphocyte activity associated with control of viremia in primary human immunodeficiency virus type 1 infection. *J Virol* **68**, 6103–6110 (1994).

[36] Safrit, J. T., Andrews, C. A., Zhu, T., Ho, D. D. & Koup, R. A. Characterization of human immunodeficiency virus type 1-specific cytotoxic T lymphocyte clones isolated during acute seroconversion: recognition of autologous virus sequences within a conserved immunodominant epitope. *J Exp Med* **179**, 463–472 (1994).

[37] Silvestri, G. *et al.* Nonpathogenic SIV infection of sooty mangabeys is characterized by limited bystander immunopathology despite chronic high-level viremia. *Immunity* **18**, 441–452 (2003).

[38] Grossman, Z., Meier-Schellersheim, M., Paul, W. E. & Picker, L. J. Pathogenesis of HIV infection: what the virus spares is as important as what it destroys. *Nat Med* **12**, 289–295 (2006).

[39] Brenchley, J. M. *et al.* Microbial translocation is a cause of systemic immune activation in chronic HIV infection. *Nat Med* **12**, 1365–1371 (2006).

[40] McCune, J. M. The dynamics of CD4+ T-cell depletion in HIV disease. *Nature* **410**, 974–979 (2001).

[41] Dion, M.-L. *et al.* HIV infection rapidly induces and maintains a substantial suppression of thymocyte proliferation. *Immunity* **21**, 757–768 (2004).

[42] Dalgleish, A. G. *et al.* The CD4 (T4) antigen is an essential component of the receptor for the AIDS retrovirus. *Nature* **312**, 763–767 (1984).

[43] Klatzmann, D. *et al.* T-lymphocyte T4 molecule behaves as the receptor for human retrovirus LAV. *Nature* **312**, 767–768 (1984).

[44] Alkhatib, G. *et al.* Cc ckr5: a rantes, mip-1alpha, mip-1beta receptor as a fusion cofactor for macrophage-tropic HIV-1. *Science* **272**, 1955–1958 (1996).

[45] Feng, Y., Broder, C. C., Kennedy, P. E. & Berger, E. A. HIV-1 entry cofactor: functional cDNA cloning of a seven-transmembrane, G protein-coupled receptor. *Science* **272**, 872–877 (1996).

[46] Choe, H. *et al.* The beta-chemokine receptors CCR3 and CCR5 facilitate infection by primary HIV-1 isolates. *Cell* **85**, 1135–1148 (1996).

[47] Deng, H. *et al.* Identification of a major co-receptor for primary isolates of HIV-1. *Nature* **381**, 661–666 (1996).

[48] Dragic, T. *et al.* HIV-1 entry into CD4+ cells is mediated by the chemokine receptor CC-CKR-5. *Nature* **381**, 667–673 (1996).

[49] Moore, J. P., Trkola, A. & Dragic, T. Co-receptors for HIV-1 entry. *Curr Opin Immunol* **9**, 551–562 (1997).

[50] Cheng-Mayer, C., Seto, D., Tateno, M. & Levy, J. A. Biologic features of HIV-1 that correlate with virulence in the host. *Science* **240**, 80–82 (1988).

[51] Grivel, J. C. & Margolis, L. B. CCR5- and CXCR4-tropic HIV-1 are equally cytopathic for their T-cell targets in human lymphoid tissue. *Nat Med* **5**, 344–346 (1999).

[52] Hsu, M. *et al.* Increased mucosal transmission but not enhanced pathogenicity of the CCR5-tropic, simian AIDS-inducing simian/human immunodeficiency virus SHIV(sf162p3) maps to envelope gp120. *J Virol* **77**, 989–998 (2003).

[53] Symatlas. Tech. Rep., Genomics Institute of the Novartis Research Foundation (`http://symatlas.gnf.org/SymAtlas/`) (07-Mar-2009).

[54] Berger, E. A. *et al.* A new classification for HIV-1. *Nature* **391**, 240 (1998).

[55] Connor, R. I., Sheridan, K. E., Ceradini, D., Choe, S. & Landau, N. R. Change in coreceptor use correlates with disease progression in HIV-1–infected individuals. *J Exp Med* **185**, 621–628 (1997).

[56] Stevenson, M. HIV-1 pathogenesis. *Nat Med* **9**, 853–860 (2003).

[57] Stebbing, J., Gazzard, B. & Douek, D. C. Where does HIV live? *N Engl J Med* **350**, 1872–1880 (2004).

[58] Klatzmann, D. *et al.* Selective tropism of lymphadenopathy associated virus (LAV) for helper-inducer T lymphocytes. *Science* **225**, 59–63 (1984).

[59] Brenchley, J. M. *et al.* T-cell subsets that harbor human immunodeficiency virus (HIV) in vivo: implications for HIV pathogenesis. *J Virol* **78**, 1160–1168 (2004).

[60] Koenig, S. *et al.* Detection of AIDS virus in macrophages in brain tissue from AIDS patients with encephalopathy. *Science* **233**, 1089–1093 (1986).

[61] Sharkey, M. E. *et al.* Persistence of episomal HIV-1 infection intermediates in patients on highly active antiretroviral therapy. *Nat Med* **6**, 76–81 (2000).

[62] Patterson, S., Rae, A., Hockey, N., Gilmour, J. & Gotch, F. Plasmacytoid dendritic cells are highly susceptible to human immunodeficiency virus type 1 infection and release infectious virus. *J Virol* **75**, 6710–6713 (2001).

[63] Sol-Foulon, N. *et al.* HIV-1 Nef-induced upregulation of DC-SIGN in dendritic cells promotes lymphocyte clustering and viral spread. *Immunity* **16**, 145–155 (2002).

[64] Cameron, P. U. *et al.* Dendritic cells exposed to human immunodeficiency virus type-1 transmit a vigorous cytopathic infection to CD4+ T cells. *Science* **257**, 383–387 (1992).

[65] Motsinger, A. *et al.* CD1d-restricted human natural killer T cells are highly susceptible to human immunodeficiency virus 1 infection. *J Exp Med* **195**, 869–879 (2002).

[66] Valentin, A. *et al.* Persistent HIV-1 infection of natural killer cells in patients receiving highly active antiretroviral therapy. *Proc Natl Acad Sci U S A* **99**, 7015–7020 (2002).

[67] Price, R. W. *et al.* The brain in AIDS: central nervous system HIV-1 infection and AIDS dementia complex. *Science* **239**, 586–592 (1988).

[68] Eilbott, D. J. *et al.* Human immunodeficiency virus type 1 in spinal cords of acquired immunodeficiency syndrome patients with myelopathy: expression and replication in macrophages. *Proc Natl Acad Sci U S A* **86**, 3337–3341 (1989).

[69] Lipton, S. A. & Gendelman, H. E. Seminars in medicine of the beth israel hospital, boston. dementia associated with the acquired immunodeficiency syndrome. *N Engl J Med* **332**, 934–940 (1995).

[70] Glass, J. D. & Johnson, R. T. Human immunodeficiency virus and the brain. *Annu Rev Neurosci* **19**, 1–26 (1996).

[71] Takahashi, K. *et al.* Localization of HIV-1 in human brain using polymerase chain reaction/in situ hybridization and immunocytochemistry. *Ann Neurol* **39**, 705–711 (1996).

[72] Taxonomy of viruses. Tech. Rep., International Committee on Taxonomy of Viruses (ICTV) (`http://www.ictvonline.org`) (accessed 05-Mar-2009).

[73] Sanchez-Pescador, R. *et al.* Nucleotide sequence and expression of an AIDS-associated retrovirus (arv-2). *Science* **227**, 484–492 (1985).

[74] Wain-Hobson, S., Sonigo, P., Danos, O., Cole, S. & Alizon, M. Nucleotide sequence of the AIDS virus, LAV. *Cell* **40**, 9–17 (1985).

[75] Ratner, L. *et al.* Complete nucleotide sequence of the AIDS virus, HTLV-III. *Nature* **313**, 277–284 (1985).

[76] Wong-Staal, F. *et al.* Genomic diversity of human T-lymphotropic virus type III (HTLV-III). *Science* **229**, 759–762 (1985).

[77] Wei, X. *et al.* Antibody neutralization and escape by HIV-1. *Nature* **422**, 307–312 (2003).

[78] Richman, D. D., Wrin, T., Little, S. J. & Petropoulos, C. J. Rapid evolution of the neutralizing antibody response to HIV type 1 infection. *Proc Natl Acad Sci U S A* **100**, 4144–4149 (2003).

[79] Kwong, P. D. *et al.* Structure of an HIV gp120 envelope glycoprotein in complex with the CD4 receptor and a neutralizing human antibody. *Nature* **393**, 648–659 (1998).

[80] Wyatt, R. *et al.* The antigenic structure of the HIV gp120 envelope glycoprotein. *Nature* **393**, 705–711 (1998).

[81] Li, Y. *et al.* Broad HIV-1 neutralization mediated by CD4-binding site antibodies. *Nat Med* **13**, 1032–1034 (2007).

[82] Frey, G. *et al.* A fusion-intermediate state of HIV-1 gp41 targeted by broadly neutralizing antibodies. *Proc Natl Acad Sci U S A* **105**, 3739–3744 (2008).

[83] Tsubota, H., Lord, C. I., Watkins, D. I., Morimoto, C. & Letvin, N. L. A cytotoxic T lymphocyte inhibits acquired immunodeficiency syndrome virus replication in peripheral blood lymphocytes. *J Exp Med* **169**, 1421–1434 (1989).

[84] Walker, C. M., Moody, D. J., Stites, D. P. & Levy, J. A. CD8+ lymphocytes can control HIV infection in vitro by suppressing virus replication. *Science* **234**, 1563–1566 (1986).

[85] Yang, O. O. *et al.* Suppression of human immunodeficiency virus type 1 replication by CD8+ cells: evidence for hla class I-restricted triggering of cytolytic and noncytolytic mechanisms. *J Virol* **71**, 3120–3128 (1997).

[86] Phillips, R. E. *et al.* Human immunodeficiency virus genetic variation that can escape cytotoxic T cell recognition. *Nature* **354**, 453–459 (1991).

[87] Allen, T. M. *et al.* Tat-specific cytotoxic T lymphocytes select for SIV escape variants during resolution of primary viraemia. *Nature* **407**, 386–390 (2000).

[88] Barouch, D. H. *et al.* Eventual AIDS vaccine failure in a rhesus monkey by viral escape from cytotoxic T lymphocytes. *Nature* **415**, 335–339 (2002).

[89] Pantaleo, G. *et al.* Major expansion of CD8+ T cells with a predominant v beta usage during the primary immune response to HIV. *Nature* **370**, 463–467 (1994).

[90] Koup, R. A. *et al.* Temporal association of cellular immune responses with the initial control of viremia in primary human immunodeficiency virus type 1 syndrome. *J Virol* **68**, 4650–4655 (1994).

[91] Letvin, N. L. & Walker, B. D. Immunopathogenesis and immunotherapy in AIDS virus infections. *Nat Med* **9**, 861–866 (2003).

[92] Mattapallil, J. J. *et al.* Vaccination preserves CD4 memory T cells during acute simian immunodeficiency virus challenge. *J Exp Med* **203**, 1533–1541 (2006).

[93] Sawyer, S. L., Emerman, M. & Malik, H. S. Ancient adaptive evolution of the primate antiviral DNA-editing enzyme APOBEC3G. *PLoS Biol* **2**, E275 (2004).

[94] Singh, S. K. RNA interference and its therapeutic potential against HIV infection. *Expert Opin Biol Ther* **8**, 449–461 (2008).

[95] Lee, N. S. & Rossi, J. J. Control of HIV-1 replication by RNA interference. *Virus Res* **102**, 53–58 (2004).

[96] Zhou, Y., Zhang, H., Siliciano, J. D. & Siliciano, R. F. Kinetics of human immunodeficiency virus type 1 decay following entry into resting CD4+ T cells. *J Virol* **79**, 2199–2210 (2005).

[97] Wahl, S. M., Greenwell-Wild, T. & Vzquez, N. HIV accomplices and adversaries in macrophage infection. *J Leukoc Biol* **80**, 973–983 (2006).

[98] Barouch, D. H. Challenges in the development of an HIV-1 vaccine. *Nature* **455**, 613–619 (2008).

[99] Clercq, E. D. The design of drugs for HIV and HCV. *Nat Rev Drug Discov* **6**, 1001–1018 (2007).

[100] Richman, D. D. HIV chemotherapy. *Nature* **410**, 995–1001 (2001).

[101] Hessell, A. J. *et al.* Effective, low-titer antibody protection against low-dose repeated mucosal SHIV challenge in macaques. *Nat Med* **15**, 951–954 (2009).

[102] Johnson, P. R. *et al.* Vector-mediated gene transfer engenders long-lived neutralizing activity and protection against SIV infection in monkeys. *Nat Med* **15**, 901–906 (2009).

[103] Vogels, R. *et al.* Replication-deficient human adenovirus type 35 vectors for gene transfer and vaccination: efficient human cell infection and bypass of preexisting adenovirus immunity. *J Virol* **77**, 8263–8271 (2003).

[104] Abbink, P. *et al.* Comparative seroprevalence and immunogenicity of six rare serotype recombinant adenovirus vaccine vectors from subgroups b and d. *J Virol* **81**, 4654–4663 (2007).

[105] Thorner, A. R. *et al.* Age dependence of adenovirus-specific neutralizing antibody titers in individuals from sub-saharan africa. *J Clin Microbiol* **44**, 3781–3783 (2006).

[106] Kostense, S. *et al.* Adenovirus types 5 and 35 seroprevalence in AIDS risk groups supports type 35 as a vaccine vector. *AIDS* **18**, 1213–1216 (2004).

[107] Immunizations are discontinued in two HIV vaccine trials (`http://www3.niaid.nih.gov/news/newsreleases/2007/step_statement.htm`). Tech. Rep., National Institute of Allergy and Infectious Diseases (NIAID) (accessed 12-August-2009).

[108] Licensed anti-HIV drugs: (`http://www.fda.gov/oashi/aids/virals.html`). Tech. Rep., National Institute of Health (accessed 05-Mar-2009).

[109] Carr, A. Toxicity of antiretroviral therapy and implications for drug development. *Nat Rev Drug Discov* **2**, 624–634 (2003).

[110] Lewis, W., Day, B. J. & Copeland, W. C. Mitochondrial toxicity of NRTI antiviral drugs: an integrated cellular perspective. *Nat Rev Drug Discov* **2**, 812–822 (2003).

[111] Bagasra, O. A unified concept of HIV latency. *Expert Opin Biol Ther* **6**, 1135–1149 (2006).

[112] Pomerantz, R. J. Reservoirs, sanctuaries, and residual disease: the hiding spots of HIV-1. *HIV Clin Trials* **4**, 137–143 (2003).

[113] Pierson, T., McArthur, J. & Siliciano, R. F. Reservoirs for HIV-1: mechanisms for viral persistence in the presence of antiviral immune responses and antiretroviral therapy. *Annu Rev Immunol* **18**, 665–708 (2000).

[114] Monie, D. *et al.* A novel assay allows genotyping of the latent reservoir for human immunodeficiency virus type 1 in the resting CD4+ T cells of viremic patients. *J Virol* **79**, 5185–5202 (2005).

[115] Chun, T. W. *et al.* Quantification of latent tissue reservoirs and total body viral load in HIV-1 infection. *Nature* **387**, 183–188 (1997).

[116] Coombs, R. W. *et al.* Association between culturable human immunodeficiency virus type 1 (HIV-1) in semen and HIV-1 RNA levels in semen and blood: evidence for compartmentalization of HIV-1 between semen and blood. *J Infect Dis* **177**, 320–330 (1998).

[117] Eron, J. J. *et al.* Resistance of HIV-1 to antiretroviral agents in blood and seminal plasma: implications for transmission. *AIDS* **12**, F181–F189 (1998).

[118] Ellis, R. J. *et al.* Cerebrospinal fluid HIV RNA originates from both local CNS and systemic sources. *Neurology* **54**, 927–936 (2000).

[119] Gnthard, H. F. *et al.* Residual human immunodeficiency virus (HIV) type 1 RNA and DNA in lymph nodes and HIV RNA in genital secretions and in cerebrospinal fluid after suppression of viremia for 2 years. *J Infect Dis* **183**, 1318–1327 (2001).

[120] Fulcher, J. A. *et al.* Compartmentalization of human immunodeficiency virus type 1 between blood monocytes and CD4+ T cells during infection. *J Virol* **78**, 7883–7893 (2004).

[121] Alexaki, A., Liu, Y. & Wigdahl, B. Cellular reservoirs of HIV-1 and their role in viral persistence. *Curr HIV Res* **6**, 388–400 (2008).

[122] Swanson, P. *et al.* Evaluation of performance across the dynamic range of the abbott realtime HIV-1 assay as compared to versant HIV-1 RNA 3.0 and amplicor HIV-1 monitor v1.5 using serial dilutions of 39 group m and o viruses. *J Virol Methods* **141**, 49–57 (2007).

[123] Berger, A. *et al.* Comparative evaluation of the cobas amplicor HIV-1 monitor ultrasensitive test, the new cobas ampliprep/cobas amplicor HIV-1 monitor ultrasensitive test and the versant HIV RNA 3.0 assays for quantitation of HIV-1 RNA in plasma samples. *J Clin Virol* **33**, 43–51 (2005).

[124] Galli, R., Merrick, L., Friesenhahn, M. & Ziermann, R. Comprehensive comparison of the versant HIV-1 RNA 3.0 (bDNA) and cobas amplicor HIV-1 monitor 1.5 assays on 1,000 clinical specimens. *J Clin Virol* **34**, 245–252 (2005).

[125] Richman, D. D. Principles of HIV resistance testing and overview of assay performance characteristics. *Antivir Ther* **5**, 27–31 (2000).

[126] Gnthard, H. F., Wong, J. K., Ignacio, C. C., Havlir, D. V. & Richman, D. D. Comparative performance of high-density oligonucleotide sequencing and dideoxynucleotide sequencing of HIV type 1 pol from clinical samples. *AIDS Res Hum Retroviruses* **14**, 869–876 (1998).

[127] Havlir, D. V., Eastman, S., Gamst, A. & Richman, D. D. Nevirapine-resistant human immunodeficiency virus: kinetics of replication and estimated prevalence in untreated patients. *J Virol* **70**, 7894–7899 (1996).

[128] Stuyver, L. *et al.* Line probe assay for rapid detection of drug-selected mutations in the human immunodeficiency virus type 1 reverse transcriptase gene. *Antimicrob Agents Chemother* **41**, 284–291 (1997).

[129] Eriksson, N. *et al.* Viral population estimation using pyrosequencing. *PLoS Comput Biol* **4**, e1000074 (2008).

[130] Zhang, H. *et al.* Novel single-cell-level phenotypic assay for residual drug susceptibility and reduced replication capacity of drug-resistant human immunodeficiency virus type 1. *J Virol* **78**, 1718–1729 (2004).

[131] Shen, L. *et al.* Dose-response curve slope sets class-specific limits on inhibitory potential of anti-HIV drugs. *Nat Med* **14**, 762–766 (2008).

[132] Beerenwinkel, N. *et al.* Diversity and complexity of HIV-1 drug resistance: a bioinformatics approach to predicting phenotype from genotype. *Proc Natl Acad Sci U S A* **99**, 8271–8276 (2002).

[133] Vercauteren, J. & Vandamme, A.-M. Algorithms for the interpretation of HIV-1 genotypic drug resistance information. *Antiviral Res* **71**, 335–342 (2006).

[134] HIV drug resistance mutations. Tech. Rep., International AIDS Society-USA (`http://www.iasusa.org/resistance_mutations/`) (accessed 12-August-2009).

[135] Frankel, A. D. & Young, J. A. HIV-1: fifteen proteins and an RNA. *Annu Rev Biochem* **67**, 1–25 (1998).

[136] Westby, M. & van der Ryst, E. CCR5 antagonists: host-targeted antivirals for the treatment of HIV infection. *Antivir Chem Chemother* **16**, 339–354 (2005).

[137] Luban, J. Absconding with the chaperone: essential cyclophilin-Gag interaction in HIV-1 virions. *Cell* **87**, 1157–1159 (1996).

[138] Fassati, A. & Goff, S. P. Characterization of intracellular reverse transcription complexes of human immunodeficiency virus type 1. *J Virol* **75**, 3626–3635 (2001).

[139] Miller, M. D., Farnet, C. M. & Bushman, F. D. Human immunodeficiency virus type 1 preintegration complexes: studies of organization and composition. *J Virol* **71**, 5382–5390 (1997).

[140] Nermut, M. V. & Fassati, A. Structural analyses of purified human immunodeficiency virus type 1 intracellular reverse transcription complexes. *J Virol* **77**, 8196–8206 (2003).

[141] Bukrinsky, M. I. *et al.* A nuclear localization signal within HIV-1 matrix protein that governs infection of non-dividing cells. *Nature* **365**, 666–669 (1993).

[142] Zhang, H., Zhang, Y., Spicer, T., Henrard, D. & Poiesz, B. J. Nascent human immunodeficiency virus type 1 reverse transcription occurs within an enveloped particle. *J Virol* **69**, 3675–3682 (1995).

[143] Trono, D. Partial reverse transcripts in virions from human immunodeficiency and murine leukemia viruses. *J Virol* **66**, 4893–4900 (1992).

[144] Zhang, H., Dornadula, G., Orenstein, J. & Pomerantz, R. J. Morphologic changes in human immunodeficiency virus type 1 virions secondary to intravirion reverse transcription: evidence indicating that reverse transcription may not take place within the intact viral core. *J Hum Virol* **3**, 165–172 (2000).

[145] von Kleist, M. & Huisinga, W. Pharmacokinetic-pharmacodynamic relationship of NRTIs and its connection to viral escape: an example based on zidovudine. *Eur J Pharm Sci* **36**, 532–543 (2009).

[146] Harrich, D. & Hooker, B. Mechanistic aspects of HIV-1 reverse transcription initiation. *Rev Med Virol* **12**, 31–45 (2002).

[147] Isel, C., Keith, G., Ehresmann, B., Ehresmann, C. & Marquet, R. Mutational analysis of the tRNA3lys/HIV-1 RNA (primer/template) complex. *Nucleic Acids Res* **26**, 1198–1204 (1998).

[148] Vandegraaff, N. & Engelman, A. Molecular mechanisms of HIV integration and therapeutic intervention. *Expert Rev Mol Med* **9**, 1–19 (2007).

[149] Greber, U. F. & Fassati, A. Nuclear import of viral DNA genomes. *Traffic* **4**, 136–143 (2003).

[150] McDonald, D. *et al.* Visualization of the intracellular behavior of HIV in living cells. *J Cell Biol* **159**, 441–452 (2002).

[151] Heinzinger, N. K. *et al.* The Vpr protein of human immunodeficiency virus type 1 influences nuclear localization of viral nucleic acids in nondividing host cells. *Proc Natl Acad Sci U S A* **91**, 7311–7315 (1994).

[152] Popov, S. *et al.* Viral protein r regulates nuclear import of the HIV-1 pre-integration complex. *EMBO J* **17**, 909–917 (1998).

[153] Maele, B. V. & Debyser, Z. HIV-1 integration: an interplay between HIV-1 integrase, cellular and viral proteins. *AIDS Rev* **7**, 26–43 (2005).

[154] Delelis, O., Carayon, K., Sab, A., Deprez, E. & Mouscadet, J.-F. Integrase and integration: biochemical activities of HIV-1 integrase. *Retrovirology* **5**, 114 (2008).

[155] Wang, G. P., Ciuffi, A., Leipzig, J., Berry, C. C. & Bushman, F. D. HIV integration site selection: analysis by massively parallel pyrosequencing reveals association with epigenetic modifications. *Genome Res* **17**, 1186–1194 (2007).

[156] Koelsch, K. K. *et al.* Dynamics of total, linear nonintegrated, and integrated HIV-1 DNA in vivo and in vitro. *J Infect Dis* **197**, 411–419 (2008).

[157] Karn, J. Tackling Tat. *J Mol Biol* **293**, 235–254 (1999).

[158] Dayton, A. I., Sodroski, J. G., Rosen, C. A., Goh, W. C. & Haseltine, W. A. The trans-activator gene of the human T cell lymphotropic virus type III is required for replication. *Cell* **44**, 941–947 (1986).

[159] Fisher, A. G. *et al.* The trans-activator gene of HTLV-III is essential for virus replication. *Nature* **320**, 367–371 (1986).

[160] Molle, D. *et al.* A real-time view of the tar:Tat:p-tefb complex at HIV-1 transcription sites. *Retrovirology* **4**, 36 (2007).

[161] Weinberger, L. S. & Shenk, T. An HIV feedback resistor: auto-regulatory circuit deactivator and noise buffer. *PLoS Biol* **5**, e9 (2007).

[162] Gupta, S. & Mitra, D. Human immunodeficiency virus-1 Tat protein: immunological facets of a transcriptional activator. *Indian J Biochem Biophys* **44**, 269–275 (2007).

[163] Huigen, M. C. D. G., Kamp, W. & Nottet, H. S. L. M. Multiple effects of HIV-1 trans-activator protein on the pathogenesis of HIV-1 infection. *Eur J Clin Invest* **34**, 57–66 (2004).

[164] Nekhai, S. & Jeang, K.-T. Transcriptional and post-transcriptional regulation of HIV-1 gene expression: role of cellular factors for Tat and Rev. *Future Microbiol* **1**, 417–426 (2006).

[165] Arold, S. T. & Baur, A. S. Dynamic Nef and Nef dynamics: how structure could explain the complex activities of this small HIV protein. *Trends Biochem Sci* **26**, 356–363 (2001).

[166] Aiken, C., Konner, J., Landau, N. R., Lenburg, M. E. & Trono, D. Nef induces CD4 endocytosis: requirement for a critical dileucine motif in the membrane-proximal CD4 cytoplasmic domain. *Cell* **76**, 853–864 (1994).

[167] Luria, S., Chambers, I. & Berg, P. Expression of the type 1 human immunodeficiency virus Nef protein in T cells prevents antigen receptor-mediated induction of interleukin 2 mRNA. *Proc Natl Acad Sci U S A* **88**, 5326–5330 (1991).

[168] Geleziunas, R., Xu, W., Takeda, K., Ichijo, H. & Greene, W. C. HIV-1 Nef inhibits ask1-dependent death signalling providing a potential mechanism for protecting the infected host cell. *Nature* **410**, 834–838 (2001).

[169] Schwartz, O., Marchal, V., Gall, S. L., Lemonnier, F. & Heard, J. M. Endocytosis of major histocompatibility complex class I molecules is induced by the HIV-1 Nef protein. *Nat Med* **2**, 338–342 (1996).

[170] Day, C. L. *et al.* Pd-1 expression on HIV-specific T cells is associated with T-cell exhaustion and disease progression. *Nature* **443**, 350–354 (2006).

[171] Trautmann, L. *et al.* Upregulation of pd-1 expression on HIV-specific CD8+ T cells leads to reversible immune dysfunction. *Nat Med* **12**, 1198–1202 (2006).

[172] Muthumani, K. *et al.* Human immunodeficiency virus type 1 Nef induces programmed death 1 expression through a p38 mitogen-activated protein kinase-dependent mechanism. *J Virol* **82**, 11536–11544 (2008).

[173] Kestler, H. W. *et al.* Importance of the nef gene for maintenance of high virus loads and for development of AIDS. *Cell* **65**, 651–662 (1991).

[174] Marin, M., Rose, K. M., Kozak, S. L. & Kabat, D. HIV-1 Vif protein binds the editing enzyme APOBEC3G and induces its degradation. *Nat Med* **9**, 1398–1403 (2003).

[175] He, J. *et al.* Human immunodeficiency virus type 1 viral protein r (Vpr) arrests cells in the G2 phase of the cell cycle by inhibiting p34cdc2 activity. *J Virol* **69**, 6705–6711 (1995).

[176] Jowett, J. B. *et al.* The human immunodeficiency virus type 1 vpr gene arrests infected T cells in the G2 + M phase of the cell cycle. *J Virol* **69**, 6304–6313 (1995).

[177] Re, F., Braaten, D., Franke, E. K. & Luban, J. Human immunodeficiency virus type 1 Vpr arrests the cell cycle in G2 by inhibiting the activation of p34cdc2-cyclin B. *J Virol* **69**, 6859–6864 (1995).

[178] Rogel, M. E., Wu, L. I. & Emerman, M. The human immunodeficiency virus type 1 vpr gene prevents cell proliferation during chronic infection. *J Virol* **69**, 882–888 (1995).

[179] Goh, W. C. *et al.* HIV-1 Vpr increases viral expression by manipulation of the cell cycle: a mechanism for selection of Vpr in vivo. *Nat Med* **4**, 65–71 (1998).

[180] Zhu, Y. *et al.* Comparison of cell cycle arrest, transactivation, and apoptosis induced by the simian immunodeficiency virus SIVagm and human immunodeficiency virus type 1 vpr genes. *J Virol* **75**, 3791–3801 (2001).

[181] Bolton, D. L. & Lenardo, M. J. Vpr cytopathicity independent of G2/M cell cycle arrest in human immunodeficiency virus type 1-infected CD4+ T cells. *J Virol* **81**, 8878–8890 (2007).

[182] Andersen, J. L., Rouzic, E. L. & Planelles, V. HIV-1 Vpr: mechanisms of G2 arrest and apoptosis. *Exp Mol Pathol* **85**, 2–10 (2008).

[183] Hout, D. R. *et al.* Vpu: a multifunctional protein that enhances the pathogenesis of human immunodeficiency virus type 1. *Curr HIV Res* **2**, 255–270 (2004).

[184] Strebel, K., Klimkait, T., Maldarelli, F. & Martin, M. A. Molecular and biochemical analyses of human immunodeficiency virus type 1 vpu protein. *J Virol* **63**, 3784–3791 (1989).

[185] Willey, R. L., Maldarelli, F., Martin, M. A. & Strebel, K. Human immunodeficiency virus type 1 Vpu protein induces rapid degradation of CD4. *J Virol* **66**, 7193–7200 (1992).

[186] Weinberger, L. S., Burnett, J. C., Toettcher, J. E., Arkin, A. P. & Schaffer, D. V. Stochastic gene expression in a lentiviral positive-feedback loop: HIV-1 Tat fluctuations drive phenotypic diversity. *Cell* **122**, 169–182 (2005).

[187] Lassen, K. G., Ramyar, K. X., Bailey, J. R., Zhou, Y. & Siliciano, R. F. Nuclear retention of multiply spliced HIV-1 RNA in resting CD4+ T cells. *PLoS Pathog* **2**, e68 (2006).

[188] Burnett, J. C., Miller-Jensen, K., Shah, P. S., Arkin, A. P. & Schaffer, D. V. Control of stochastic gene expression by host factors at the HIV promoter. *PLoS Pathog* **5**, e1000260 (2009).

[189] Richman, D. D. *et al.* The challenge of finding a cure for HIV infection. *Science* **323**, 1304–1307 (2009).

[190] Pearson, R. *et al.* Epigenetic silencing of human immunodeficiency virus (HIV) transcription by formation of restrictive chromatin structures at the viral long terminal repeat drives the progressive entry of HIV into latency. *J Virol* **82**, 12291–12303 (2008).

[191] Lehrman, G. *et al.* Depletion of latent HIV-1 infection in vivo: a proof-of-concept study. *Lancet* **366**, 549–555 (2005).

[192] Siliciano, J. D. *et al.* Stability of the latent reservoir for HIV-1 in patients receiving valproic acid. *J Infect Dis* **195**, 833–836 (2007).

[193] Morita, E. & Sundquist, W. I. Retrovirus budding. *Annu Rev Cell Dev Biol* **20**, 395–425 (2004).

[194] Moulard, M. & Decroly, E. Maturation of HIV envelope glycoprotein precursors by cellular endoproteases. *Biochim Biophys Acta* **1469**, 121–132 (2000).

[195] D'Souza, V. & Summers, M. F. How retroviruses select their genomes. *Nat Rev Microbiol* **3**, 643–655 (2005).

[196] Gttlinger, H. G., Dorfman, T., Sodroski, J. G. & Haseltine, W. A. Effect of mutations affecting the p6 gag protein on human immunodeficiency virus particle release. *Proc Natl Acad Sci U S A* **88**, 3195–3199 (1991).

[197] Briggs, J. A. G. *et al.* The stoichiometry of Gag protein in HIV-1. *Nat Struct Mol Biol* **11**, 672–675 (2004).

[198] Bukrinskaya, A. HIV-1 matrix protein: a mysterious regulator of the viral life cycle. *Virus Res* **124**, 1–11 (2007).

[199] Freed, E. O. HIV-1 gag proteins: diverse functions in the virus life cycle. *Virology* **251**, 1–15 (1998).

[200] Davis, M. R., Jiang, J., Zhou, J., Freed, E. O. & Aiken, C. A mutation in the human immunodeficiency virus type 1 Gag protein destabilizes the interaction of the envelope protein subunits gp120 and gp41. *J Virol* **80**, 2405–2417 (2006).

[201] Dupont, S. *et al.* A novel nuclear export activity in HIV-1 matrix protein required for viral replication. *Nature* **402**, 681–685 (1999).

[202] Gamble, T. R. *et al.* Structure of the carboxyl-terminal dimerization domain of the HIV-1 capsid protein. *Science* **278**, 849–853 (1997).

[203] Klein, K. C., Reed, J. C. & Lingappa, J. R. Intracellular destinies: degradation, targeting, assembly, and endocytosis of HIV Gag. *AIDS Rev* **9**, 150–161 (2007).

[204] Li, J., Tang, S., Hewlett, I. & Yang, M. HIV-1 capsid protein and cyclophilin a as new targets for anti-AIDS therapeutic agents. *Infect Disord Drug Targets* **7**, 238–244 (2007).

[205] Jewell, N. A. & Mansky, L. M. In the beginning: genome recognition, RNA encapsidation and the initiation of complex retrovirus assembly. *J Gen Virol* **81**, 1889–1899 (2000).

[206] Amarasinghe, G. K. *et al.* NMR structure of the HIV-1 nucleocapsid protein bound to stem-loop SL2 of the psi-RNA packaging signal. implications for genome recognition. *J Mol Biol* **301**, 491–511 (2000).

[207] Russell, R. S., Liang, C. & Wainberg, M. A. Is HIV-1 RNA dimerization a prerequisite for packaging? yes, no, probably? *Retrovirology* **1**, 23 (2004).

[208] Chertova, E. *et al.* Proteomic and biochemical analysis of purified human immunodeficiency virus type 1 produced from infected monocyte-derived macrophages. *J Virol* **80**, 9039–9052 (2006).

[209] Roda, R. H. *et al.* Role of the reverse transcriptase, nucleocapsid protein, and template structure in the two-step transfer mechanism in retroviral recombination. *J Biol Chem* **278**, 31536–31546 (2003).

[210] Houzet, L. *et al.* Nucleocapsid mutations turn HIV-1 into a DNA-containing virus. *Nucleic Acids Res* **36**, 2311–2319 (2008).

[211] Didierlaurent, L., Houzet, L., Morichaud, Z., Darlix, J.-L. & Mougel, M. The conserved n-terminal basic residues and zinc-finger motifs of HIV-1 nucleocapsid restrict the viral cDNA synthesis during virus formation and maturation. *Nucleic Acids Res* **36**, 4745–4753 (2008).

[212] Thomas, J. A., Bosche, W. J., Shatzer, T. L., Johnson, D. G. & Gorelick, R. J. Mutations in human immunodeficiency virus type 1 nucleocapsid protein zinc fingers cause premature reverse transcription. *J Virol* **82**, 9318–9328 (2008).

[213] Mougel, M., Houzet, L. & Darlix, J.-L. When is it time for reverse transcription to start and go? *Retrovirology* **6**, 24 (2009).

[214] Salzwedel, K., Martin, D. E. & Sakalian, M. Maturation inhibitors: a new therapeutic class targets the virus structure. *AIDS Rev* **9**, 162–172 (2007).

[215] Mazz, F. M. & Degrve, L. The role of viral and cellular proteins in the budding of human immunodeficiency virus. *Acta Virol* **50**, 75–85 (2006).

[216] Fujii, K., Hurley, J. H. & Freed, E. O. Beyond tsg101: the role of alix in 'ESCRTing' HIV-1. *Nat Rev Microbiol* **5**, 912–916 (2007).

[217] Klimkait, T., Strebel, K., Hoggan, M. D., Martin, M. A. & Orenstein, J. M. The human immunodeficiency virus type 1-specific protein vpu is required for efficient virus maturation and release. *J Virol* **64**, 621–629 (1990).

[218] Terwilliger, E. F., Cohen, E. A., Lu, Y. C., Sodroski, J. G. & Haseltine, W. A. Functional role of human immunodeficiency virus type 1 vpu. *Proc Natl Acad Sci U S A* **86**, 5163–5167 (1989).

[219] Ewart, G. D., Mills, K., Cox, G. B. & Gage, P. W. Amiloride derivatives block ion channel activity and enhancement of virus-like particle budding caused by HIV-1 protein Vpu. *Eur Biophys J* **31**, 26–35 (2002).

[220] Gonzlez, M. E. & Carrasco, L. The human immunodeficiency virus type 1 Vpu protein enhances membrane permeability. *Biochemistry* **37**, 13710–13719 (1998).

[221] Pettit, S. C., Everitt, L. E., Choudhury, S., Dunn, B. M. & Kaplan, A. H. Initial cleavage of the human immunodeficiency virus type 1 GagPol precursor by its activated protease occurs by an intramolecular mechanism. *J Virol* **78**, 8477–8485 (2004).

[222] Pettit, S. C., Lindquist, J. N., Kaplan, A. H. & Swanstrom, R. Processing sites in the human immunodeficiency virus type 1 (HIV-1) Gag-Pro-Pol precursor are cleaved by the viral protease at different rates. *Retrovirology* **2**, 66 (2005).

[223] Pettit, S. C., Clemente, J. C., Jeung, J. A., Dunn, B. M. & Kaplan, A. H. Ordered processing of the human immunodeficiency virus type 1 GagPol precursor is influenced by the context of the embedded viral protease. *J Virol* **79**, 10601–10607 (2005).

[224] Krusslich, H. G., Fcke, M., Heuser, A. M., Konvalinka, J. & Zentgraf, H. The spacer peptide between human immunodeficiency virus capsid and nucleocapsid proteins is essential for ordered assembly and viral infectivity. *J Virol* **69**, 3407–3419 (1995).

[225] Katz, R. A. & Skalka, A. M. The retroviral enzymes. *Annu Rev Biochem* **63**, 133–173 (1994).

[226] Tzsr, J. & Oroszlan, S. Proteolytic events of HIV-1 replication as targets for therapeutic intervention. *Curr Pharm Des* **9**, 1803–1815 (2003).

[227] Davis, D. A. *et al.* Regulation of HIV-1 protease activity through cysteine modification. *Biochemistry* **35**, 2482–2488 (1996).

[228] Louis, J. M., Wondrak, E. M., Kimmel, A. R., Wingfield, P. T. & Nashed, N. T. Proteolytic processing of HIV-1 protease precursor, kinetics and mechanism. *J Biol Chem* **274**, 23437–23442 (1999).

[229] Szeltner, Z. & Polgr, L. Rate-determining steps in HIV-1 protease catalysis. the hydrolysis of the most specific substrate. *J Biol Chem* **271**, 32180–32184 (1996).

[230] Kaplan, A. H., Manchester, M. & Swanstrom, R. The activity of the protease of human immunodeficiency virus type 1 is initiated at the membrane of infected cells before the release of viral proteins and is required for release to occur with maximum efficiency. *J Virol* **68**, 6782–6786 (1994).

[231] Krusslich, H. G. Human immunodeficiency virus proteinase dimer as component of the viral polyprotein prevents particle assembly and viral infectivity. *Proc Natl Acad Sci U S A* **88**, 3213–3217 (1991).

[232] Poorman, R. A., Tomasselli, A. G., Heinrikson, R. L. & Kzdy, F. J. A cumulative specificity model for proteases from human immunodeficiency virus types 1 and 2, inferred from statistical analysis of an extended substrate data base. *J Biol Chem* **266**, 14554–14561 (1991).

[233] Pomerantz, R. J. & Horn, D. L. Twenty years of therapy for HIV-1 infection. *Nat Med* **9**, 867–873 (2003).

[234] Rachlis, A. R. Zidovudine (retrovir) update. *CMAJ* **143**, 1177–1185 (1990).

[235] Larder, B. A. & Kemp, S. D. Multiple mutations in HIV-1 reverse transcriptase confer high-level resistance to zidovudine (AZT). *Science* **246**, 1155–1158 (1989).

[236] Hammer, S. M. *et al.* A controlled trial of two nucleoside analogues plus indinavir in persons with human immunodeficiency virus infection and CD4 cell counts of 200 per cubic millimeter or less. AIDS clinical trials group 320 study team. *N Engl J Med* **337**, 725–733 (1997).

[237] Hirsch, M. *et al.* A randomized, controlled trial of indinavir, zidovudine, and lamivudine in adults with advanced human immunodeficiency virus type 1 infection and prior antiretroviral therapy. *J Infect Dis* **180**, 659–665 (1999).

[238] Detels, R. *et al.* Effectiveness of potent antiretroviral therapy on time to AIDS and death in men with known HIV infection duration. multicenter AIDS cohort study investigators. *JAMA* **280**, 1497–1503 (1998).

[239] Palella, F. J. *et al.* Declining morbidity and mortality among patients with advanced human immunodeficiency virus infection. HIV outpatient study investigators. *N Engl J Med* **338**, 853–860 (1998).

[240] Kulkosky, J. & Pomerantz, R. J. Approaching eradication of highly active antiretroviral therapy-persistent human immunodeficiency virus type 1 reservoirs with immune activation therapy. *Clin Infect Dis* **35**, 1520–1526 (2002).

[241] Kulkosky, J. *et al.* Intensification and stimulation therapy for human immunodeficiency virus type 1 reservoirs in infected persons receiving virally suppressive highly active antiretroviral therapy. *J Infect Dis* **186**, 1403–1411 (2002).

[242] Pomerantz, R. J. Reservoirs of human immunodeficiency virus type 1: the main obstacles to viral eradication. *Clin Infect Dis* **34**, 91–97 (2002).

[243] Investigational drugs. (`http://www.aidsinfo.nih.gov/DrugsNew/SearchResults.aspx?MenuItem=Drugs&DrugName=&DrugClass=All&DrugType=Investigational+Drugs`). Tech. Rep., National Institute of Health (accessed 05-Mar-2009).

[244] Greene, W. C. *et al.* Novel targets for HIV therapy. *Antiviral Res* **80**, 251–265 (2008).

[245] Deeks, S. G. *et al.* HIV RNA and CD4 cell count response to protease inhibitor therapy in an urban AIDS clinic: response to both initial and salvage therapy. *AIDS* **13**, F35–F43 (1999).

[246] Fätkenheuer, G. *et al.* Virological treatment failure of protease inhibitor therapy in an unselected cohort of HIV-infected patients. *AIDS* **11**, F113–F116 (1997).

[247] Palella, F. J., Chmiel, J. S., Moorman, A. C., Holmberg, S. D. & Investigators, H. I. V. O. S. Durability and predictors of success of highly active antiretroviral therapy for ambulatory HIV-infected patients. *AIDS* **16**, 1617–1626 (2002).

[248] Lucas, G. M., Chaisson, R. E. & Moore, R. D. Highly active antiretroviral therapy in a large urban clinic: risk factors for virologic failure and adverse drug reactions. *Ann Intern Med* **131**, 81–87 (1999).

[249] Temesgen, Z., Cainelli, F., Poeschla, E. M., Vlahakis, S. A. R. & Vento, S. Approach to salvage antiretroviral therapy in heavily antiretroviral-experienced HIV-positive adults. *Lancet Infect Dis* **6**, 496–507 (2006).

[250] Mansky, L. M. HIV mutagenesis and the evolution of antiretroviral drug resistance. *Drug Resist Updat* **5**, 219–223 (2002).

[251] Johnson, V. A. *et al.* Update of the drug resistance mutations in HIV-1. *Top HIV Med* **16**, 138–145 (2008).

[252] Halvas, E. K. *et al.* Blinded, multicenter comparison of methods to detect a drug-resistant mutant of human immunodeficiency virus type 1 at low frequency. *J Clin Microbiol* **44**, 2612–2614 (2006).

[253] Bailey, J. R. *et al.* Residual human immunodeficiency virus type 1 viremia in some patients on antiretroviral therapy is dominated by a small number of invariant clones rarely found in circulating CD4+ T cells. *J Virol* **80**, 6441–6457 (2006).

[254] Chun, T. W. *et al.* Presence of an inducible HIV-1 latent reservoir during highly active antiretroviral therapy. *Proc Natl Acad Sci U S A* **94**, 13193–13197 (1997).

[255] Finzi, D. *et al.* Identification of a reservoir for HIV-1 in patients on highly active antiretroviral therapy. *Science* **278**, 1295–1300 (1997).

[256] Wong, J. K. *et al.* Recovery of replication-competent HIV despite prolonged suppression of plasma viremia. *Science* **278**, 1291–1295 (1997).

[257] Finzi, D. *et al.* Latent infection of CD4+ T cells provides a mechanism for lifelong persistence of HIV-1, even in patients on effective combination therapy. *Nat Med* **5**, 512–517 (1999).

[258] Gnthard, H. F. *et al.* Evolution of envelope sequences of human immunodeficiency virus type 1 in cellular reservoirs in the setting of potent antiviral therapy. *J Virol* **73**, 9404–9412 (1999).

[259] Saksena, N. K., Rodes, B., Wang, B. & Soriano, V. Elite HIV controllers: myth or reality? *AIDS Rev* **9**, 195–207 (2007).

[260] Haynes, B. F., Pantaleo, G. & Fauci, A. S. Toward an understanding of the correlates of protective immunity to HIV infection. *Science* **271**, 324–328 (1996).

[261] Clercq, E. D. Strategies in the design of antiviral drugs. *Nat Rev Drug Discov* **1**, 13–25 (2002).

[262] Coffin, J. M. HIV population dynamics in vivo: implications for genetic variation, pathogenesis, and therapy. *Science* **267**, 483–489 (1995).

[263] Sorin, M. & Kalpana, G. V. Dynamics of virus-host interplay in HIV-1 replication. *Curr HIV Res* **4**, 117–130 (2006).

[264] Kellam, P. Attacking pathogens through their hosts. *Genome Biol* **7**, 201 (2006).

[265] Kenakin, T. New concepts in drug discovery: collateral efficacy and permissive antagonism. *Nat Rev Drug Discov* **4**, 919–927 (2005).

[266] Moore, J. P. & Stevenson, M. New targets for inhibitors of HIV-1 replication. *Nat Rev Mol Cell Biol* **1**, 40–49 (2000).

[267] Flexner, C. HIV drug development: the next 25 years. *Nat Rev Drug Discov* **6**, 959–966 (2007).

[268] Ptak, R. G. HIV-1 regulatory proteins: targets for novel drug development. *Expert Opin Investig Drugs* **11**, 1099–1115 (2002).

[269] Harrich, D., McMillan, N., Munoz, L., Apolloni, A. & Meredith, L. Will diverse Tat interactions lead to novel antiretroviral drug targets? *Curr Drug Targets* **7**, 1595–1606 (2006).

[270] Richter, S. N. & Pal, G. Inhibitors of HIV-1 Tat-mediated transactivation. *Curr Med Chem* **13**, 1305–1315 (2006).

[271] Haubrich, R. H. *et al.* A randomized trial of the activity and safety of ro 24-7429 (Tat antagonist) versus nucleoside for human immunodeficiency virus infection. the AIDS clinical trials group 213 team. *J Infect Dis* **172**, 1246–1252 (1995).

[272] Ishaq, M. *et al.* Knockdown of cellular RNA helicase DDX3 by short hairpin RNAs suppresses HIV-1 viral replication without inducing apoptosis. *Mol Biotechnol* **39**, 231–238 (2008).

[273] Cochrane, A. Controlling HIV-1 Rev function. *Curr Drug Targets Immune Endocr Metabol Disord* **4**, 287–295 (2004).

[274] Richter, S. N., Frasson, I. & Pal, G. Strategies for inhibiting function of HIV-1 accessory proteins: a necessary route to AIDS therapy? *Curr Med Chem* **16**, 267–286 (2009).

[275] Dean, M. *et al.* Genetic restriction of HIV-1 infection and progression to AIDS by a deletion allele of the CKR5 structural gene. hemophilia growth and development study, multicenter AIDS cohort study, multicenter hemophilia cohort study, san francisco city cohort, alive study. *Science* **273**, 1856–1862 (1996).

[276] Liu, R. *et al.* Homozygous defect in HIV-1 coreceptor accounts for resistance of some multiply-exposed individuals to HIV-1 infection. *Cell* **86**, 367–377 (1996).

[277] Samson, M. *et al.* Resistance to HIV-1 infection in caucasian individuals bearing mutant alleles of the CCR-5 chemokine receptor gene. *Nature* **382**, 722–725 (1996).

[278] Palani, A. & Tagat, J. R. Discovery and development of small-molecule chemokine coreceptor CCR5 antagonists. *J Med Chem* **49**, 2851–2857 (2006).

[279] Wood, A. & Armour, D. The discovery of the CCR5 receptor antagonist, uk-427,857, a new agent for the treatment of HIV infection and AIDS. *Prog Med Chem* **43**, 239–271 (2005).

[280] Carter, N. J. & Keating, G. M. Maraviroc. *Drugs* **67**, 2277–88; discussion 2289–90 (2007).

[281] Briz, V., Poveda, E. & Soriano, V. HIV entry inhibitors: mechanisms of action and resistance pathways. *J Antimicrob Chemother* **57**, 619–627 (2006).

[282] Dorr, P. *et al.* Maraviroc (uk-427,857), a potent, orally bioavailable, and selective small-molecule inhibitor of chemokine receptor CCR5 with broad-spectrum anti-human immunodeficiency virus type 1 activity. *Antimicrob Agents Chemother* **49**, 4721–4732 (2005).

[283] Rosario, M. C. *et al.* Population pharmacokinetic/pharmacodynamic analysis of CCR5 receptor occupancy by maraviroc in healthy subjects and HIV-positive patients. *Br J Clin Pharmacol* **65 Suppl 1**, 86–94 (2008).

[284] Westby, M. *et al.* Reduced maximal inhibition in phenotypic susceptibility assays indicates that viral strains resistant to the CCR5 antagonist maraviroc utilize inhibitor-bound receptor for entry. *J Virol* **81**, 2359–2371 (2007).

[285] Daar, E. S. Emerging resistance profiles of newly approved antiretroviral drugs. *Top HIV Med* **16**, 110–116 (2008).

[286] Walker, D. K. *et al.* Preclinical assessment of the distribution of maraviroc to potential human immunodeficiency virus (HIV) sanctuary sites in the central nervous system (CNS) and gut-associated lymphoid tissue (GALT). *Xenobiotica* **38**, 1330–1339 (2008).

[287] Berger, E. A. HIV entry and tropism: the chemokine receptor connection. *AIDS* **11 Suppl A**, S3–16 (1997).

[288] Michael, N. L. *et al.* Exclusive and persistent use of the entry coreceptor CXCR4 by human immunodeficiency virus type 1 from a subject homozygous for CCR5 delta32. *J Virol* **72**, 6040–6047 (1998).

[289] Zhang, Y. J. & Moore, J. P. Will multiple coreceptors need to be targeted by inhibitors of human immunodeficiency virus type 1 entry? *J Virol* **73**, 3443–3448 (1999).

[290] Glushakova, S. *et al.* Preferential coreceptor utilization and cytopathicity by dual-tropic HIV-1 in human lymphoid tissue ex vivo. *J Clin Invest* **104**, R7–R11 (1999).

[291] Weiss, C. D. HIV-1 gp41: mediator of fusion and target for inhibition. *AIDS Rev* **5**, 214–221 (2003).

[292] Dando, T. M. & Perry, C. M. Enfuvirtide. *Drugs* **63**, 2755–66 (2003).

[293] Beausjour, Y. & Tremblay, M. J. Susceptibility of HIV type 1 to the fusion inhibitor T-20 is reduced on insertion of host intercellular adhesion molecule 1 in the virus membrane. *J Infect Dis* **190**, 894–902 (2004).

[294] Miyauchi, K., Kim, Y., Latinovic, O., Morozov, V. & Melikyan, G. B. HIV enters cells via endocytosis and dynamin-dependent fusion with endosomes. *Cell* **137**, 433–444 (2009).

[295] Uchil, P. D. & Mothes, W. HIV entry revisited. *Cell* **137**, 402–404 (2009).

[296] Wild, C. T., Shugars, D. C., Greenwell, T. K., McDanal, C. B. & Matthews, T. J. Peptides corresponding to a predictive alpha-helical domain of human immunodeficiency virus type 1 gp41 are potent inhibitors of virus infection. *Proc Natl Acad Sci U S A* **91**, 9770–9774 (1994).

[297] Oldfield, V., Keating, G. M. & Plosker, G. Enfuvirtide: a review of its use in the management of HIV infection. *Drugs* **65**, 1139–1160 (2005).

[298] Mitsuya, H. *et al.* 3'-azido-3'-deoxythymidine (bw a509u): an antiviral agent that inhibits the infectivity and cytopathic effect of human T-lymphotropic virus type III/lymphadenopathy-associated virus in vitro. *Proc Natl Acad Sci U S A* **82**, 7096–7100 (1985).

[299] Furman, P. A. *et al.* Phosphorylation of 3'-azido-3'-deoxythymidine and selective interaction of the 5'-triphosphate with human immunodeficiency virus reverse transcriptase. *Proc Natl Acad Sci U S A* **83**, 8333–8337 (1986).

[300] Kong, W., Engel, K. & Wang, J. Mammalian nucleoside transporters. *Curr Drug Metab* **5**, 63–84 (2004).

[301] Menndez-Arias, L. Mechanisms of resistance to nucleoside analogue inhibitors of HIV-1 reverse transcriptase. *Virus Res* **134**, 124–146 (2008).

[302] Holland, J. *et al.* Rapid evolution of RNA genomes. *Science* **215**, 1577–1585 (1982).

[303] Back, D. J., Burger, D. M., Flexner, C. W. & Gerber, J. G. The pharmacology of antiretroviral nucleoside and nucleotide reverse transcriptase inhibitors: implications for once-daily dosing. *J Acquir Immune Defic Syndr* **39 Suppl 1**, S1–23 (2005).

[304] Pastor-Anglada, M. *et al.* Cell entry and export of nucleoside analogues. *Virus Res* **107**, 151–164 (2005).

[305] Schuetz, J. D. *et al.* Mrp4: A previously unidentified factor in resistance to nucleoside-based antiviral drugs. *Nat Med* **5**, 1048–1051 (1999).

[306] Waqar, M. A., Evans, M. J., Manly, K. F., Hughes, R. G. & Huberman, J. A. Effects of 2',3'-dideoxynucleosides on mammalian cells and viruses. *J Cell Physiol* **121**, 402–408 (1984).

[307] Sharma, P. L., Nurpeisov, V., Hernandez-Santiago, B., Beltran, T. & Schinazi, R. F. Nucleoside inhibitors of human immunodeficiency virus type 1 reverse transcriptase. *Curr Top Med Chem* **4**, 895–919 (2004).

[308] Stretcher, B. N., Pesce, A. J., Frame, P. T., Greenberg, K. A. & Stein, D. S. Correlates of zidovudine phosphorylation with markers of HIV disease progression and drug toxicity. *AIDS* **8**, 763–769 (1994).

[309] Fletcher, C. V. *et al.* Concentration-controlled zidovudine therapy. *Clin Pharmacol Ther* **64**, 331–338 (1998).

[310] Nav, J. F., Eschbach, A., Wolff-Kugel, D., Halazy, S. & Balzarini, J. Enzymatic phosphorylation and pyrophosphorylation of 2',3'-dideoxyadenosine-5'-monophosphate, a key metabolite in the pathway for activation of the anti-HIV (human immunodeficiency virus) agent 2',3'-dideoxyinosine. *Biochem Pharmacol* **48**, 1105–1112 (1994).

[311] Faletto, M. B. *et al.* Unique intracellular activation of the potent anti-human immunodeficiency virus agent 1592u89. *Antimicrob Agents Chemother* **41**, 1099–1107 (1997).

[312] Ahluwalia, G. S., Gao, W. Y., Mitsuya, H. & Johns, D. G. 2',3'-didehydro-3'-deoxythymidine: regulation of its metabolic activation by modulators of thymidine-5'-triphosphate biosynthesis. *Mol Pharmacol* **50**, 160–165 (1996).

[313] Kewn, S., Veal, G. J., Hoggard, P. G., Barry, M. G. & Back, D. J. Lamivudine (3TC) phosphorylation and drug interactions in vitro. *Biochem Pharmacol* **54**, 589–595 (1997).

[314] Gao, W. Y., Shirasaka, T., Johns, D. G., Broder, S. & Mitsuya, H. Differential phosphorylation of azidothymidine, dideoxycytidine, and dideoxyinosine in resting and activated peripheral blood mononuclear cells. *J Clin Invest* **91**, 2326–2333 (1993).

[315] Gao, W. Y., Agbaria, R., Driscoll, J. S. & Mitsuya, H. Divergent anti-human immunodeficiency virus activity and anabolic phosphorylation of 2',3'-dideoxynucleoside analogs in resting and activated human cells. *J Biol Chem* **269**, 12633–12638 (1994).

[316] Perno, C. F. *et al.* Inhibition of human immunodeficiency virus (HIV-1/HTLV-IIIBa-L) replication in fresh and cultured human peripheral blood monocytes/macrophages by azidothymidine and related 2',3'-dideoxynucleosides. *J Exp Med* **168**, 1111–1125 (1988).

[317] Ray, A. S. Intracellular interactions between nucleos(t)ide inhibitors of HIV reverse transcriptase. *AIDS Rev* **7**, 113–125 (2005).

[318] Kakuda, T. N. Pharmacology of nucleoside and nucleotide reverse transcriptase inhibitor-induced mitochondrial toxicity. *Clin Ther* **22**, 685–708 (2000).

[319] Huang, P., Farquhar, D. & Plunkett, W. Selective action of 3'-azido-3'-deoxythymidine 5'-triphosphate on viral reverse transcriptases and human DNA polymerases. *J Biol Chem* **265**, 11914–11918 (1990).

[320] Goody, R. S., Mller, B. & Restle, T. Factors contributing to the inhibition of HIV reverse transcriptase by chain-terminating nucleotides in vitro and in vivo. *FEBS Lett* **291**, 1–5 (1991).

[321] Balzarini, J. *et al.* 2',3'-dideoxycytidine: regulation of its metabolism and anti-retroviral potency by natural pyrimidine nucleosides and by inhibitors of pyrimidine nucleotide synthesis. *Mol Pharmacol* **32**, 798–806 (1987).

[322] Ahluwalia, G. *et al.* Inhibitors of imp dehydrogenase stimulate the phosphorylation of the antiviral nucleoside 2' ,3'-dideoxyguanosine. *Biochem Biophys Res Commun* **171**, 1297–1303 (1990).

[323] Balzarini, J. Effect of antimetabolite drugs of nucleotide metabolism on the anti-human immunodeficiency virus activity of nucleoside reverse transcriptase inhibitors. *Pharmacol Ther* **87**, 175–187 (2000).

[324] Hoggard, P. G., Veal, G. J., Wild, M. J., Barry, M. G. & Back, D. J. Drug interactions with zidovudine phosphorylation in vitro. *Antimicrob Agents Chemother* **39**, 1376–1378 (1995).

[325] Arnér, E. S. & Eriksson, S. Deoxycytidine and 2',3'-dideoxycytidine metabolism in human monocyte-derived macrophages. a study of both anabolic and catabolic pathways. *Biochem Biophys Res Commun* **197**, 1499–1504 (1993).

[326] Bradshaw, P. C., Li, J. & Samuels, D. C. A computational model of mitochondrial AZT metabolism. *Biochem J* **392**, 363–373 (2005).

[327] Susan-Resiga, D., Bentley, A. T., Lynx, M. D., LaClair, D. D. & McKee, E. E. Zidovudine inhibits thymidine phosphorylation in the isolated perfused rat heart. *Antimicrob Agents Chemother* **51**, 1142–1149 (2007).

[328] Lynx, M. D., Bentley, A. T. & McKee, E. E. 3'-azido-3'-deoxythymidine (AZT) inhibits thymidine phosphorylation in isolated rat liver mitochondria: a possible mechanism of AZT hepatotoxicity. *Biochem Pharmacol* **71**, 1342–1348 (2006).

[329] Jochmans, D. Novel HIV-1 reverse transcriptase inhibitors. *Virus Res* **134**, 171–185 (2008).

[330] Wilson, J. E. *et al.* Human immunodeficiency virus type-1 reverse transcriptase. contribution of met-184 to binding of nucleoside 5'-triphosphate. *J Biol Chem* **271**, 13656–13662 (1996).

[331] Krebs, R., Immendörfer, U., Thrall, S. H., Wöhrl, B. M. & Goody, R. S. Single-step kinetics of HIV-1 reverse transcriptase mutants responsible for virus resistance to nucleoside inhibitors zidovudine and 3-tc. *Biochemistry* **36**, 10292–10300 (1997).

[332] Gu, Z., Arts, E. J., Parniak, M. A. & Wainberg, M. A. Mutated K65R recombinant reverse transcriptase of human immunodeficiency virus type 1 shows diminished chain termination in the presence of 2',3'-dideoxycytidine 5'-triphosphate and other drugs. *Proc Natl Acad Sci U S A* **92**, 2760–2764 (1995).

[333] Martin, J. L., Wilson, J. E., Haynes, R. L. & Furman, P. A. Mechanism of resistance of human immunodeficiency virus type 1 to 2',3'-dideoxyinosine. *Proc Natl Acad Sci U S A* **90**, 6135–6139 (1993).

[334] Roberts, J. D., Bebenek, K. & Kunkel, T. A. The accuracy of reverse transcriptase from HIV-1. *Science* **242**, 1171–1173 (1988).

[335] Arion, D., Kaushik, N., McCormick, S., Borkow, G. & Parniak, M. A. Phenotypic mechanism of HIV-1 resistance to 3'-azido-3'-deoxythymidine (AZT): increased polymerization processivity and enhanced sensitivity to pyrophosphate of the mutant viral reverse transcriptase. *Biochemistry* **37**, 15908–15917 (1998).

[336] Meyer, P. R., Matsuura, S. E., So, A. G. & Scott, W. A. Unblocking of chain-terminated primer by HIV-1 reverse transcriptase through a nucleotide-dependent mechanism. *Proc Natl Acad Sci U S A* **95**, 13471–13476 (1998).

[337] Gtte, M., Arion, D., Parniak, M. A. & Wainberg, M. A. The m184v mutation in the reverse transcriptase of human immunodeficiency virus type 1 impairs rescue of chain-terminated DNA synthesis. *J Virol* **74**, 3579–3585 (2000).

[338] Brinkman, K., Smeitink, J. A., Romijn, J. A. & Reiss, P. Mitochondrial toxicity induced by nucleoside-analogue reverse-transcriptase inhibitors is a key factor in the pathogenesis of antiretroviral-therapy-related lipodystrophy. *Lancet* **354**, 1112–1115 (1999).

[339] Wendelsdorf, K. V., Song, Z., Cao, Y. & Samuels, D. C. An analysis of enzyme kinetics data for mitochondrial DNA strand termination by nucleoside reverse transcription inhibitors. *PLoS Comput Biol* **5**, e1000261 (2009).

[340] McKee, E. E., Bentley, A. T., Hatch, M., Gingerich, J. & Susan-Resiga, D. Phosphorylation of thymidine and AZT in heart mitochondria: elucidation of a novel mechanism of AZT cardiotoxicity. *Cardiovasc Toxicol* **4**, 155–167 (2004).

[341] Frick, L. W., Nelson, D. J., Clair, M. H. S., Furman, P. A. & Krenitsky, T. A. Effects of 3'-azido-3'-deoxythymidine on the deoxynucleotide triphosphate pools of cultured human cells. *Biochem Biophys Res Commun* **154**, 124–129 (1988).

[342] de la Asuncin, J. G., del Olmo, M. L., Sastre, J., Pallard, F. V. & Via, J. Zidovudine (AZT) causes an oxidation of mitochondrial DNA in mouse liver. *Hepatology* **29**, 985–987 (1999).

[343] Lim, S. E. & Copeland, W. C. Differential incorporation and removal of antiviral deoxynucleotides by human DNA polymerase gamma. *J Biol Chem* **276**, 23616–23623 (2001).

[344] Johnson, A. A. *et al.* Toxicity of antiviral nucleoside analogs and the human mitochondrial DNA polymerase. *J Biol Chem* **276**, 40847–40857 (2001).

[345] Clercq, E. D. The role of non-nucleoside reverse transcriptase inhibitors (NNRTIs) in the therapy of HIV-1 infection. *Antiviral Res* **38**, 153–179 (1998).

[346] Sluis-Cremer, N., Temiz, N. A. & Bahar, I. Conformational changes in HIV-1 reverse transcriptase induced by nonnucleoside reverse transcriptase inhibitor binding. *Curr HIV Res* **2**, 323–332 (2004).

[347] Hang, J. Q. *et al.* Substrate-dependent inhibition or stimulation of HIV RNase H activity by non-nucleoside reverse transcriptase inhibitors (NNRTIs). *Biochem Biophys Res Commun* **352**, 341–350 (2007).

[348] Miyasaka, T. *et al.* A novel lead for specific anti-HIV-1 agents: 1-[(2-hydroxyethoxy)methyl]-6-(phenylthio)thymine. *J Med Chem* **32**, 2507–2509 (1989).

[349] Pauwels, R. *et al.* Potent and selective inhibition of HIV-1 replication in vitro by a novel series of tibo derivatives. *Nature* **343**, 470–474 (1990).

[350] Merluzzi, V. J. *et al.* Inhibition of HIV-1 replication by a nonnucleoside reverse transcriptase inhibitor. *Science* **250**, 1411–1413 (1990).

[351] Richman, D. D. *et al.* Nevirapine resistance mutations of human immunodeficiency virus type 1 selected during therapy. *J Virol* **68**, 1660–1666 (1994).

[352] Clercq, E. D. New developments in anti-HIV chemotherapy. *Curr Med Chem* **8**, 1543–1572 (2001).

[353] Ma, Q. *et al.* Pharmacokinetic drug interactions with non-nucleoside reverse transcriptase inhibitors. *Expert Opin Drug Metab Toxicol* **1**, 473–485 (2005).

[354] Clercq, E. D. Non-nucleoside reverse transcriptase inhibitors (NNRTIs): past, present, and future. *Chem Biodivers* **1**, 44–64 (2004).

[355] Geretti, A. M. Shifting paradigms: the resistance profile of etravirine. *J Antimicrob Chemother* **62**, 643–647 (2008).

[356] Kohlstaedt, L. A., Wang, J., Friedman, J. M., Rice, P. A. & Steitz, T. A. Crystal structure at 3.5 a resolution of HIV-1 reverse transcriptase complexed with an inhibitor. *Science* **256**, 1783–1790 (1992).

[357] Abbondanzieri, E. A. *et al.* Dynamic binding orientations direct activity of HIV reverse transcriptase. *Nature* **453**, 184–189 (2008).

[358] Liu, S., Abbondanzieri, E. A., Rausch, J. W., Grice, S. F. J. L. & Zhuang, X. Slide into action: dynamic shuttling of HIV reverse transcriptase on nucleic acid substrates. *Science* **322**, 1092–1097 (2008).

[359] Rittinger, K., Divita, G. & Goody, R. S. Human immunodeficiency virus reverse transcriptase substrate-induced conformational changes and the mechanism of inhibition by nonnucleoside inhibitors. *Proc Natl Acad Sci U S A* **92**, 8046–8049 (1995).

[360] Grobler, J. A. *et al.* HIV-1 reverse transcriptase plus-strand initiation exhibits preferential sensitivity to non-nucleoside reverse transcriptase inhibitors in vitro. *J Biol Chem* **282**, 8005–8010 (2007).

[361] Sluis-Cremer, N. & Tachedjian, G. Mechanisms of inhibition of HIV replication by non-nucleoside reverse transcriptase inhibitors. *Virus Res* **134**, 147–156 (2008).

[362] Xia, Q., Radzio, J., Anderson, K. S. & Sluis-Cremer, N. Probing nonnucleoside inhibitor-induced active-site distortion in HIV-1 reverse transcriptase by transient kinetic analyses. *Protein Sci* **16**, 1728–1737 (2007).

[363] Ivetac, A. & McCammon, J. A. Elucidating the inhibition mechanism of HIV-1 non-nucleoside reverse transcriptase inhibitors through multicopy molecular dynamics simulations. *J Mol Biol* **388**, 644–658 (2009).

[364] Tachedjian, G., Orlova, M., Sarafianos, S. G., Arnold, E. & Goff, S. P. Nonnucleoside reverse transcriptase inhibitors are chemical enhancers of dimerization of the HIV type 1 reverse transcriptase. *Proc Natl Acad Sci U S A* **98**, 7188–7193 (2001).

[365] Figueiredo, A. *et al.* Potent nonnucleoside reverse transcriptase inhibitors target HIV-1 Gag-Pol. *PLoS Pathog* **2**, e119 (2006).

[366] Ren, J. & Stammers, D. K. Structural basis for drug resistance mechanisms for non-nucleoside inhibitors of HIV reverse transcriptase. *Virus Res* **134**, 157–170 (2008).

[367] Condra, J. H. *et al.* Identification of the human immunodeficiency virus reverse transcriptase residues that contribute to the activity of diverse nonnucleoside inhibitors. *Antimicrob Agents Chemother* **36**, 1441–1446 (1992).

[368] Hazuda, D. J. Inhibitors of human immunodeficiency virus type I integration. *Curr Opin HIV AIDS* **1**, 212–217 (2006).

[369] Goldgur, Y. *et al.* Structure of the HIV-1 integrase catalytic domain complexed with an inhibitor: a platform for antiviral drug design. *Proc Natl Acad Sci U S A* **96**, 13040–13043 (1999).

[370] Hazuda, D. J. *et al.* Inhibitors of strand transfer that prevent integration and inhibit HIV-1 replication in cells. *Science* **287**, 646–650 (2000).

[371] Hazuda, D. J., Iwamoto, M. & Wenning, L. Emerging pharmacology: Inhibitors of human immunodeficiency virus integration. *Annu Rev Pharmacol Toxicol* (2008).

[372] Jegede, O. *et al.* HIV type 1 integrase inhibitors: from basic research to clinical implications. *AIDS Rev* **10**, 172–189 (2008).

[373] Mekouar, K. *et al.* Styrylquinoline derivatives: a new class of potent HIV-1 integrase inhibitors that block HIV-1 replication in cem cells. *J Med Chem* **41**, 2846–2857 (1998).

[374] Hong, H. *et al.* Discovery of HIV-1 integrase inhibitors by pharmacophore searching. *J Med Chem* **40**, 930–936 (1997).

[375] Zhao, H. *et al.* Hydrazide-containing inhibitors of HIV-1 integrase. *J Med Chem* **40**, 937–941 (1997).

[376] Neamati, N. *et al.* Salicylhydrazine-containing inhibitors of HIV-1 integrase: implication for a selective chelation in the integrase active site. *J Med Chem* **41**, 3202–3209 (1998).

[377] Grobler, J. A. *et al.* Diketo acid inhibitor mechanism and HIV-1 integrase: implications for metal binding in the active site of phosphotransferase enzymes. *Proc Natl Acad Sci U S A* **99**, 6661–6666 (2002).

[378] Marchand, C. *et al.* Metal-dependent inhibition of HIV-1 integrase by beta-diketo acids and resistance of the soluble double-mutant (f185k/c280s). *Mol Pharmacol* **64**, 600–609 (2003).

[379] Espeseth, A. S. *et al.* HIV-1 integrase inhibitors that compete with the target DNA substrate define a unique strand transfer conformation for integrase. *Proc Natl Acad Sci U S A* **97**, 11244–11249 (2000).

[380] Wiskerchen, M. & Muesing, M. A. Human immunodeficiency virus type 1 integrase: effects of mutations on viral ability to integrate, direct viral gene expression from unintegrated viral DNA templates, and sustain viral propagation in primary cells. *J Virol* **69**, 376–386 (1995).

[381] Stevenson, M., Stanwick, T. L., Dempsey, M. P. & Lamonica, C. A. HIV-1 replication is controlled at the level of T cell activation and proviral integration. *EMBO J* **9**, 1551–1560 (1990).

[382] Hicks, C. & Gulick, R. M. Raltegravir: the first HIV type 1 integrase inhibitor. *Clin Infect Dis* **48**, 931–939 (2009).

[383] Cocohoba, J. & Dong, B. J. Raltegravir: the first HIV integrase inhibitor. *Clin Ther* **30**, 1747–1765 (2008).

[384] Kohl, N. E. *et al.* Active human immunodeficiency virus protease is required for viral infectivity. *Proc Natl Acad Sci U S A* **85**, 4686–4690 (1988).

[385] Peng, C., Ho, B. K., Chang, T. W. & Chang, N. T. Role of human immunodeficiency virus type 1-specific protease in core protein maturation and viral infectivity. *J Virol* **63**, 2550–2556 (1989).

[386] Vacca, J. P. *et al.* L-735,524: an orally bioavailable human immunodeficiency virus type 1 protease inhibitor. *Proc Natl Acad Sci U S A* **91**, 4096–4100 (1994).

[387] Overton, H. A. *et al.* Effect of two novel inhibitors of the human immunodeficiency virus protease on the maturation of the HIV gag and gag-pol polyproteins. *Virology* **179**, 508–511 (1990).

[388] Anderson, J., Schiffer, C., Lee, S.-K. & Swanstrom, R. Viral protease inhibitors. *Handb Exp Pharmacol* 85–110 (2009).

[389] Debouck, C. The HIV-1 protease as a therapeutic target for AIDS. *AIDS Res Hum Retroviruses* **8**, 153–164 (1992).

[390] Wlodawer, A. & Erickson, J. W. Structure-based inhibitors of HIV-1 protease. *Annu Rev Biochem* **62**, 543–585 (1993).

[391] Roberts, N. A. *et al.* Rational design of peptide-based HIV proteinase inhibitors. *Science* **248**, 358–361 (1990).

[392] Randolph, J. T. & DeGoey, D. A. Peptidomimetic inhibitors of HIV protease. *Curr Top Med Chem* **4**, 1079–1095 (2004).

[393] Flexner, C. HIV-protease inhibitors. *N Engl J Med* **338**, 1281–1292 (1998).

[394] Imamichi, T. Action of anti-HIV drugs and resistance: reverse transcriptase inhibitors and protease inhibitors. *Curr Pharm Des* **10**, 4039–4053 (2004).

[395] Nijhuis, M. *et al.* Increased fitness of drug resistant HIV-1 protease as a result of acquisition of compensatory mutations during suboptimal therapy. *AIDS* **13**, 2349–2359 (1999).

[396] Condra, J. H. *et al.* Genetic correlates of in vivo viral resistance to indinavir, a human immunodeficiency virus type 1 protease inhibitor. *J Virol* **70**, 8270–8276 (1996).

[397] Molla, A. *et al.* Ordered accumulation of mutations in HIV protease confers resistance to ritonavir. *Nat Med* **2**, 760–766 (1996).

[398] Schapiro, J. M., Winters, M. A., Vierra, M., Crawford, S. & Merigan, T. C. Lymph node human immunodeficiency virus RNA levels and resistance mutations in patients receiving high-dose saquinavir. *J Infect Dis* **177**, 477–480 (1998).

[399] Colonno, R. *et al.* Identification of I50L as the signature atazanavir (ATV)-resistance mutation in treatment-naive HIV-1-infected patients receiving atv-containing regimens. *J Infect Dis* **189**, 1802–1810 (2004).

[400] Plosker, G. L. & Figgitt, D. P. Tipranavir. *Drugs* **63**, 1611–1618 (2003).

[401] Rusconi, S. *et al.* Susceptibility to pnu-140690 (tipranavir) of human immunodeficiency virus type 1 isolates derived from patients with multidrug resistance to other protease inhibitors. *Antimicrob Agents Chemother* **44**, 1328–1332 (2000).

[402] Koh, Y. *et al.* Novel bis-tetrahydrofuranylurethane-containing nonpeptidic protease inhibitor (PI) uic-94017 (tmc114) with potent activity against multi-PI-resistant human immunodeficiency virus in vitro. *Antimicrob Agents Chemother* **47**, 3123–3129 (2003).

[403] Lefebvre, E. & Schiffer, C. A. Resilience to resistance of HIV-1 protease inhibitors: profile of darunavir. *AIDS Rev* **10**, 131–142 (2008).

[404] Dierynck, I. *et al.* Binding kinetics of darunavir to human immunodeficiency virus type 1 protease explain the potent antiviral activity and high genetic barrier. *J Virol* **81**, 13845–13851 (2007).

[405] Justesen, U. S. Protease inhibitor plasma concentrations in HIV antiretroviral therapy. *Dan Med Bull* **55**, 165–185 (2008).

[406] Varatharajan, L. & Thomas, S. A. The transport of anti-HIV drugs across blood-CNS interfaces: summary of current knowledge and recommendations for further research. *Antiviral Res* **82**, A99–109 (2009).

[407] Denissen, J. F. *et al.* Metabolism and disposition of the HIV-1 protease inhibitor ritonavir (abt-538) in rats, dogs, and humans. *Drug Metab Dispos* **25**, 489–501 (1997).

[408] Martin, C., Sönnerborg, A., Svensson, J. O. & Stahle, L. Indinavir-based treatment of HIV-1 infected patients: efficacy in the central nervous system. *AIDS* **13**, 1227–1232 (1999).

[409] Solas, C. *et al.* Discrepancies between protease inhibitor concentrations and viral load in reservoirs and sanctuary sites in human immunodeficiency virus-infected patients. *Antimicrob Agents Chemother* **47**, 238–243 (2003).

[410] Antinori, A. *et al.* Efficacy of cerebrospinal fluid (CSF)-penetrating antiretroviral drugs against HIV in the neurological compartment: different patterns of phenotypic resistance in CSF and plasma. *Clin Infect Dis* **41**, 1787–1793 (2005).

[411] Taylor, S. *et al.* Antiretroviral drug concentrations in semen of HIV-infected men: differential penetration of indinavir, ritonavir and saquinavir. *J Antimicrob Chemother* **48**, 351–354 (2001).

[412] Fitzsimmons, M. E. & Collins, J. M. Selective biotransformation of the human immunodeficiency virus protease inhibitor saquinavir by human small-intestinal cytochrome p4503a4: potential contribution to high first-pass metabolism. *Drug Metab Dispos* **25**, 256–266 (1997).

[413] Kumar, G. N., Rodrigues, A. D., Buko, A. M. & Denissen, J. F. Cytochrome p450-mediated metabolism of the HIV-1 protease inhibitor ritonavir (abt-538) in human liver microsomes. *J Pharmacol Exp Ther* **277**, 423–431 (1996).

[414] Chiba, M., Hensleigh, M., Nishime, J. A., Balani, S. K. & Lin, J. H. Role of cytochrome p450 3a4 in human metabolism of mk-639, a potent human immunodeficiency virus protease inhibitor. *Drug Metab Dispos* **24**, 307–314 (1996).

[415] Kim, R. B. *et al.* The drug transporter p-glycoprotein limits oral absorption and brain entry of HIV-1 protease inhibitors. *J Clin Invest* **101**, 289–294 (1998).

[416] Polli, J. W. *et al.* Role of p-glycoprotein on the CNS disposition of amprenavir (141w94), an HIV protease inhibitor. *Pharm Res* **16**, 1206–1212 (1999).

[417] Choo, E. F. *et al.* Pharmacological inhibition of p-glycoprotein transport enhances the distribution of HIV-1 protease inhibitors into brain and testes. *Drug Metab Dispos* **28**, 655–660 (2000).

[418] Park, S. & Sinko, P. J. P-glycoprotein and mutlidrug resistance-associated proteins limit the brain uptake of saquinavir in mice. *J Pharmacol Exp Ther* **312**, 1249–1256 (2005).

[419] Bachmeier, C. J., Spitzenberger, T. J., Elmquist, W. F. & Miller, D. W. Quantitative assessment of HIV-1 protease inhibitor interactions with drug efflux transporters in the blood-brain barrier. *Pharm Res* **22**, 1259–1268 (2005).

[420] Huang, L. *et al.* Induction of p-glycoprotein and cytochrome p450 3a by HIV protease inhibitors. *Drug Metab Dispos* **29**, 754–760 (2001).

[421] Bossi, P. *et al.* P-glycoprotein in blood CD4 cells of HIV-1-infected patients treated with protease inhibitors. *HIV Med* **4**, 67–71 (2003).

[422] Huisman, M. T. *et al.* P-glycoprotein limits oral availability, brain, and fetal penetration of saquinavir even with high doses of ritonavir. *Mol Pharmacol* **59**, 806–813 (2001).

[423] Mouly, S. J., Paine, M. F. & Watkins, P. B. Contributions of CYP3A4, p-glycoprotein, and serum protein binding to the intestinal first-pass extraction of saquinavir. *J Pharmacol Exp Ther* **308**, 941–948 (2004).

[424] Zhang, Y. & Benet, L. Z. The gut as a barrier to drug absorption: combined role of cytochrome p450 3a and p-glycoprotein. *Clin Pharmacokinet* **40**, 159–168 (2001).

[425] Hochman, J. H., Chiba, M., Nishime, J., Yamazaki, M. & Lin, J. H. Influence of p-glycoprotein on the transport and metabolism of indinavir in caco-2 cells expressing cytochrome p-450 3a4. *J Pharmacol Exp Ther* **292**, 310–318 (2000).

[426] Boffito, M. *et al.* Alpha 1-acid glycoprotein levels in human immunodeficiency virus-infected subjects on antiretroviral regimens. *Drug Metab Dispos* **30**, 859–860 (2002).

[427] Eagling, V. A., Back, D. J. & Barry, M. G. Differential inhibition of cytochrome p450 isoforms by the protease inhibitors, ritonavir, saquinavir and indinavir. *Br J Clin Pharmacol* **44**, 190–194 (1997).

[428] von Moltke, L. L. *et al.* Protease inhibitors as inhibitors of human cytochromes p450: high risk associated with ritonavir. *J Clin Pharmacol* **38**, 106–111 (1998).

[429] Lillibridge, J. H. *et al.* Characterization of the selectivity and mechanism of human cytochrome p450 inhibition by the human immunodeficiency virus-protease inhibitor nelfinavir mesylate. *Drug Metab Dispos* **26**, 609–616 (1998).

[430] Weemhoff, J. L. *et al.* Apparent mechanism-based inhibition of human Cyp3A in-vitro by lopinavir. *J Pharm Pharmacol* **55**, 381–386 (2003).

[431] Ernest, C. S., Hall, S. D. & Jones, D. R. Mechanism-based inactivation of Cyp3A by HIV protease inhibitors. *J Pharmacol Exp Ther* **312**, 583–591 (2005).

[432] Hsu, A. *et al.* Multiple-dose pharmacokinetics of ritonavir in human immunodeficiency virus-infected subjects. *Antimicrob Agents Chemother* **41**, 898–905 (1997).

[433] Justesen, U. S., Klitgaard, N. A., Brosen, K. & Pedersen, C. Pharmacokinetic interaction between amprenavir and delavirdine after multiple-dose administration in healthy volunteers. *Br J Clin Pharmacol* **55**, 100–106 (2003).

[434] Washington, C. B., Duran, G. E., Man, M. C., Sikic, B. I. & Blaschke, T. F. Interaction of anti-HIV protease inhibitors with the multidrug transporter p-glycoprotein (p-gp) in human cultured cells. *J Acquir Immune Defic Syndr Hum Retrovirol* **19**, 203–209 (1998).

[435] Vishnuvardhan, D., Moltke, L. L., Richert, C. & Greenblatt, D. J. Lopinavir: acute exposure inhibits p-glycoprotein; extended exposure induces p-glycoprotein. *AIDS* **17**, 1092–1094 (2003).

[436] Perloff, M. D., von Moltke, L. L., Fahey, J. M., Daily, J. P. & Greenblatt, D. J. Induction of p-glycoprotein expression by HIV protease inhibitors in cell culture. *AIDS* **14**, 1287–1289 (2000).

[437] Perloff, M. D., Moltke, L. L. V., Marchand, J. E. & Greenblatt, D. J. Ritonavir induces p-glycoprotein expression, multidrug resistance-associated protein (mrp1) expression, and drug transporter-mediated activity in a human intestinal cell line. *J Pharm Sci* **90**, 1829–1837 (2001).

[438] Gutmann, H., Fricker, G., Drewe, J., Toeroek, M. & Miller, D. S. Interactions of HIV protease inhibitors with atp-dependent drug export proteins. *Mol Pharmacol* **56**, 383–389 (1999).

[439] Drewe, J. *et al.* HIV protease inhibitor ritonavir: a more potent inhibitor of p-glycoprotein than the cyclosporine analog sdz psc 833. *Biochem Pharmacol* **57**, 1147–1152 (1999).

[440] van der Sandt, I. C. *et al.* Assessment of active transport of HIV protease inhibitors in various cell lines and the in vitro blood–brain barrier. *AIDS* **15**, 483–491 (2001).

[441] Olson, D. P., Scadden, D. T., D'Aquila, R. T. & Pasquale, M. P. D. The protease inhibitor ritonavir inhibits the functional activity of the multidrug resistance related-protein 1 (mrp-1). *AIDS* **16**, 1743–1747 (2002).

[442] Patel, J. & Mitra, A. K. Strategies to overcome simultaneous p-glycoprotein mediated efflux and Cyp3A4 mediated metabolism of drugs. *Pharmacogenomics* **2**, 401–415 (2001).

[443] Kempf, D. J. *et al.* Pharmacokinetic enhancement of inhibitors of the human immunodeficiency virus protease by coadministration with ritonavir. *Antimicrob Agents Chemother* **41**, 654–660 (1997).

[444] Justesen, U. S. *et al.* The long-term pharmacokinetics and safety of adding low-dose ritonavir to a nelfinavir 1,250 mg twice-daily regimen in HIV-infected patients. *HIV Med* **6**, 334–340 (2005).

[445] Justesen, U. S. *et al.* Pharmacokinetics of two randomized trials evaluating the safety and efficacy of indinavir, saquinavir and lopinavir in combination with low-dose ritonavir: the maxcmin1 and 2 trials. *Basic Clin Pharmacol Toxicol* **101**, 339–344 (2007).

[446] Fichtenbaum, C. J. & Gerber, J. G. Interactions between antiretroviral drugs and drugs used for the therapy of the metabolic complications encountered during HIV infection. *Clin Pharmacokinet* **41**, 1195–1211 (2002).

[447] Hoffman, N. G., Schiffer, C. A. & Swanstrom, R. Covariation of amino acid positions in HIV-1 protease. *Virology* **314**, 536–548 (2003).

[448] Johnston, E. *et al.* Association of a novel human immunodeficiency virus type 1 protease substrate cleft mutation, l23i, with protease inhibitor therapy and in vitro drug resistance. *Antimicrob Agents Chemother* **48**, 4864–4868 (2004).

[449] Rhee, S.-Y. *et al.* HIV-1 protease and reverse-transcriptase mutations: correlations with antiretroviral therapy in subtype b isolates and implications for drug-resistance surveillance. *J Infect Dis* **192**, 456–465 (2005).

[450] Wu, T. D. *et al.* Mutation patterns and structural correlates in human immunodeficiency virus type 1 protease following different protease inhibitor treatments. *J Virol* **77**, 4836–4847 (2003).

[451] King, N. M. *et al.* Structural and thermodynamic basis for the binding of tmc114, a next-generation human immunodeficiency virus type 1 protease inhibitor. *J Virol* **78**, 12012–12021 (2004).

[452] Prabu-Jeyabalan, M., Nalivaika, E. & Schiffer, C. A. Substrate shape determines specificity of recognition for HIV-1 protease: analysis of crystal structures of six substrate complexes. *Structure* **10**, 369–381 (2002).

[453] Patick, A. K. *et al.* Antiviral and resistance studies of ag1343, an orally bioavailable inhibitor of human immunodeficiency virus protease. *Antimicrob Agents Chemother* **40**, 292–297 (1996).

[454] Ho, D. D. *et al.* Characterization of human immunodeficiency virus type 1 variants with increased resistance to a c2-symmetric protease inhibitor. *J Virol* **68**, 2016–2020 (1994).

[455] el Farrash, M. A. *et al.* Generation and characterization of a human immunodeficiency virus type 1 (HIV-1) mutant resistant to an HIV-1 protease inhibitor. *J Virol* **68**, 233–239 (1994).

[456] Otto, M. J. *et al.* In vitro isolation and identification of human immunodeficiency virus (HIV) variants with reduced sensitivity to c-2 symmetrical inhibitors of HIV type 1 protease. *Proc Natl Acad Sci U S A* **90**, 7543–7547 (1993).

[457] Condra, J. H. *et al.* In vivo emergence of HIV-1 variants resistant to multiple protease inhibitors. *Nature* **374**, 569–571 (1995).

[458] Wynn, G. H. *et al.* Antiretrovirals, part 1: overview, history, and focus on protease inhibitors. *Psychosomatics* **45**, 262–270 (2004).

[459] Perez, E. E. *et al.* Establishment of HIV-1 resistance in CD4+ T cells by genome editing using zinc-finger nucleases. *Nat Biotechnol* **26**, 808–816 (2008).

[460] Alper, J. One-off therapy for HIV. *Nature Biotechnology* **27**, 300 (2009).

[461] Htter, G. *et al.* Long-term control of HIV by CCR5 delta32/delta32 stem-cell transplantation. *N Engl J Med* **360**, 692–698 (2009).

[462] Nagasawa, T. *et al.* Defects of B-cell lymphopoiesis and bone-marrow myelopoiesis in mice lacking the cxc chemokine pbsf/sdf-1. *Nature* **382**, 635–638 (1996).

[463] Tachibana, K. *et al.* The chemokine receptor CXCR4 is essential for vascularization of the gastrointestinal tract. *Nature* **393**, 591–594 (1998).

[464] Zou, Y. R., Kottmann, A. H., Kuroda, M., Taniuchi, I. & Littman, D. R. Function of the chemokine receptor CXCR4 in haematopoiesis and in cerebellar development. *Nature* **393**, 595–599 (1998).

[465] Fransen, S. *et al.* Suppression of dualtropic human immunodeficiency virus type 1 by the CXCR4 antagonist amd3100 is associated with efficiency of CXCR4 use and baseline virus composition. *Antimicrob Agents Chemother* **52**, 2608–2615 (2008).

[466] Hendrix, C. W. *et al.* Safety, pharmacokinetics, and antiviral activity of amd3100, a selective CXCR4 receptor inhibitor, in HIV-1 infection. *J Acquir Immune Defic Syndr* **37**, 1253–1262 (2004).

[467] Loeb, L. A. *et al.* Lethal mutagenesis of HIV with mutagenic nucleoside analogs. *Proc Natl Acad Sci U S A* **96**, 1492–1497 (1999).

[468] Anderson, J. P., Daifuku, R. & Loeb, L. A. Viral error catastrophe by mutagenic nucleosides. *Annu Rev Microbiol* **58**, 183–205 (2004).

[469] Jonsson, C. B., Milligan, B. G. & Arterburn, J. B. Potential importance of error catastrophe to the development of antiviral strategies for hantaviruses. *Virus Res* **107**, 195–205 (2005).

[470] Harris, K. S., Brabant, W., Styrchak, S., Gall, A. & Daifuku, R. Kp-1212/1461, a nucleoside designed for the treatment of HIV by viral mutagenesis. *Antiviral Res* **67**, 1–9 (2005).

[471] Wiegers, K. *et al.* Sequential steps in human immunodeficiency virus particle maturation revealed by alterations of individual Gag polyprotein cleavage sites. *J Virol* **72**, 2846–2854 (1998).

[472] Pettit, S. C. *et al.* The p2 domain of human immunodeficiency virus type 1 Gag regulates sequential proteolytic processing and is required to produce fully infectious virions. *J Virol* **68**, 8017–8027 (1994).

[473] Chun, T.-W. *et al.* Decay of the HIV reservoir in patients receiving antiretroviral therapy for extended periods: implications for eradication of virus. *J Infect Dis* **195**, 1762–1764 (2007).

[474] Margolis, D. M. Confronting proviral HIV infection. *Curr HIV/AIDS Rep* **4**, 60–64 (2007).

[475] Margolis, D. M. & Archin, N. M. Eliminating persistent HIV infection: getting to the end of the rainbow. *J Infect Dis* **195**, 1734–1736 (2007).

[476] Margolis, D. M. & Archin, N. M. Attacking HIV provirus: therapeutic strategies to disrupt persistent infection. *Infect Disord Drug Targets* **6**, 369–376 (2006).

[477] Williams, S. A. & Greene, W. C. Regulation of HIV-1 latency by T-cell activation. *Cytokine* **39**, 63–74 (2007).

[478] Archin, N. M. *et al.* Valproic acid without intensified antiviral therapy has limited impact on persistent HIV infection of resting CD4+ T cells. *AIDS* **22**, 1131–1135 (2008).

[479] Fraser, C. *et al.* Reduction of the HIV-1-infected T-cell reservoir by immune activation treatment is dose-dependent and restricted by the potency of antiretroviral drugs. *AIDS* **14**, 659–669 (2000).

[480] Wang, F.-X. *et al.* IL-7 is a potent and proviral strain-specific inducer of latent HIV-1 cellular reservoirs of infected individuals on virally suppressive HAART. *J Clin Invest* **115**, 128–137 (2005).

[481] Sagot-Lerolle, N. *et al.* Prolonged valproic acid treatment does not reduce the size of latent HIV reservoir. *AIDS* **22**, 1125–1129 (2008).

[482] Gowen, B. B. *et al.* Tlr3 is essential for the induction of protective immunity against punta toro virus infection by the double-stranded RNA (dsRNA), poly(i:c12u), but not poly(i:c): differential recognition of synthetic dsRNA molecules. *J Immunol* **178**, 5200–5208 (2007).

[483] Essey, R. J., McDougall, B. R. & Robinson, W. E. Mismatched double-stranded RNA (polyi-polyc(12)u) is synergistic with multiple anti-HIV drugs and is active against drug-sensitive and drug-resistant HIV-1 in vitro. *Antiviral Res* **51**, 189–202 (2001).

[484] Murray, J. M. *et al.* Antiretroviral therapy with the integrase inhibitor raltegravir alters decay kinetics of HIV, significantly reducing the second phase. *AIDS* **21**, 2315–2321 (2007).

[485] Dalmau, D., Klimkait, T. & Telenti, A. Opinion paper. resistance to new anti-HIV agents: problems in the pathway of drug registration. *Antivir Ther* **10**, 867–872 (2005).

[486] Wei, X. *et al.* Viral dynamics in human immunodeficiency virus type 1 infection. *Nature* **373**, 117–122 (1995).

[487] Ho, D. D. Viral counts count in HIV infection. *Science* **272**, 1124–1125 (1996).

[488] Perelson, A. S. Modelling viral and immune system dynamics. *Nat Rev Immunol* **2**, 28–36 (2002).

[489] Perelson, A. S., Kirschner, D. E. & Boer, R. D. Dynamics of HIV infection of CD4+ T cells. *Math Biosci* **114**, 81–125 (1993).

[490] Ramratnam, B. *et al.* Rapid production and clearance of HIV-1 and hepatitis C virus assessed by large volume plasma apheresis. *Lancet* **354**, 1782–1785 (1999).

[491] Wu, H., Zhu, H., Miao, H. & Perelson, A. S. Parameter identifiability and estimation of HIV/AIDS dynamic models. *Bull Math Biol* **70**, 785–799 (2008).

[492] Zhang, L. *et al.* Quantifying residual HIV-1 replication in patients receiving combination antiretroviral therapy. *N Engl J Med* **340**, 1605–1613 (1999).

[493] Furtado, M. R. *et al.* Persistence of HIV-1 transcription in peripheral-blood mononuclear cells in patients receiving potent antiretroviral therapy. *N Engl J Med* **340**, 1614–1622 (1999).

[494] Dornadula, G. *et al.* Residual HIV-1 RNA in blood plasma of patients taking suppressive highly active antiretroviral therapy. *JAMA* **282**, 1627–1632 (1999).

[495] Siliciano, J. D. & Siliciano, R. F. Latency and viral persistence in HIV-1 infection. *J Clin Invest* **106**, 823–825 (2000).

[496] Novak, M. A. & May, R. M. *Virus Dynamics: Mathematical Principles of Immunology and Virology* (Oxford University Press, 2000).

[497] Murray, J. M. HIV dynamics and integrase inhibitors. *Antivir Chem Chemother* **19**, 157–164 (2009).

[498] Sedaghat, A. R., Dinoso, J. B., Shen, L., Wilke, C. O. & Siliciano, R. F. Decay dynamics of HIV-1 depend on the inhibited stages of the viral life cycle. *Proc Natl Acad Sci U S A* **105**, 4832–4837 (2008).

[499] Sedaghat, A. R., Siliciano, R. F. & Wilke, C. O. Constraints on the dominant mechanism for HIV viral dynamics in patients on raltegravir. *Antivir Ther* **14**, 263–271 (2009).

[500] Ross, J. mRNA stability in mammalian cells. *Microbiol Rev* **59**, 423–450 (1995).

[501] Houseley, J. & Tollervey, D. The many pathways of RNA degradation. *Cell* **136**, 763–776 (2009).

[502] Pierson, T. C. *et al.* Molecular characterization of preintegration latency in human immunodeficiency virus type 1 infection. *J Virol* **76**, 8518–8531 (2002).

[503] Perelson, A. S. & Nelson, P. W. Mathematical analysis of HIV-1 dynamics in vivo. *SIAM Review* **41**, 3–44 (1999).

[504] Bonhoeffer, S., Chappey, C., Parkin, N. T., Whitcomb, J. M. & Petropoulos, C. J. Evidence for positive epistasis in HIV-1. *Science* **306**, 1547–1550 (2004).

[505] Bonhoeffer, S., Barbour, A. D. & Boer, R. J. D. Procedures for reliable estimation of viral fitness from time-series data. *Proc Biol Sci* **269**, 1887–1893 (2002).

[506] Alfonsi, A., Cancès, E., Turinici, G., Ventura, B. & Huisinga, W. Exact simulation of hybrid stochastic and deterministic models for biochemical systems. *ESAIM Proc* **14**, 1–23 (2005).

[507] Ribeiro, R. M., Bonhoeffer, S. & Nowak, M. A. The frequency of resistant mutant virus before antiviral therapy. *AIDS* **12**, 461–465 (1998).

[508] Heesterbeek, J. A. P. A brief history of r0 and a recipe for its calculation. *Acta Biotheor* **50**, 189–204 (2002).

[509] Heffernan, J. M., Smith, R. J. & Wahl, L. M. Perspectives on the basic reproductive ratio. *J R Soc Interface* **2**, 281–293 (2005).

[510] Gulnik, S. V. *et al.* Kinetic characterization and cross-resistance patterns of HIV-1 protease mutants selected under drug pressure. *Biochemistry* **34**, 9282–9287 (1995).

[511] Kuiken, T. *et al.* Host species barriers to influenza virus infections. *Science* **312**, 394–397 (2006).

[512] Rodrigo, A. G. *et al.* Coalescent estimates of HIV-1 generation time in vivo. *Proc Natl Acad Sci U S A* **96**, 2187–2191 (1999).

[513] von Kleist, M., Menz, S. & Huisinga, W. Drug-class specific impact of antivirals on the reproductive capacity of HIV. *PLoS Comput Biol (submitted)* .

[514] Petropoulos, C. J. *et al.* A novel phenotypic drug susceptibility assay for human immunodeficiency virus type 1. *Antimicrob Agents Chemother* **44**, 920–928 (2000).

[515] Struble, K. *et al.* Antiretroviral therapies for treatment-experienced patients: current status and research challenges. *AIDS* **19**, 747–756 (2005).

[516] Tozzi, V. *et al.* Drug-class-wide resistance to antiretrovirals in HIV-infected patients failing therapy: prevalence, risk factors and virological outcome. *Antivir Ther* **11**, 553–560 (2006).

[517] Anderson, A. M. L. & Bartlett, J. A. Changing antiretroviral therapy in the setting of virologic relapse: review of the current literature. *Current HIV/AIDS report* **3**, 79–85 (2006).

[518] Gazzard, B. G. & Group, B. H. I. V. A. T. G. W. British HIV association guidelines for the treatment of HIV-1-infected adults with antiretroviral therapy 2008. *HIV Med* **9**, 563–608 (2008).

[519] Gillespie, D. T. Stochastic simulation of chemical kinetics. *Annu Rev Phys Chem* **58**, 35–55 (2007).

[520] daniel T Gillespie. Exact stochastic simulation of coupled chemical reactions. *Journal of Physical Chemistry* **81**, 2340–2361 (1977).

[521] Gillespie, D. T. A general method for numerically simulating the stochastic time evolution of coupled chemical reactions. *Journal of Computational Physics* **22**, 403–434 (1976).

[522] Bushman, F. D. *et al.* Massively parallel pyrosequencing in HIV research. *AIDS* **22**, 1411–1415 (2008).

[523] Rozera, G. *et al.* Massively parallel pyrosequencing highlights minority variants in the HIV-1 Env quasispecies deriving from lymphomonocyte sub-populations. *Retrovirology* **6**, 15 (2009).

[524] Le, T. *et al.* Low-abundance HIV drug-resistant viral variants in treatment-experienced persons correlate with historical antiretroviral use. *PLoS One* **4**, e6079 (2009).

[525] Nowak, M. A. & Bangham, C. R. Population dynamics of immune responses to persistent viruses. *Science* **272**, 74–79 (1996).

[526] Kuritzkes, D. R. *et al.* Plasma HIV-1 RNA dynamics in antiretroviral-naive subjects receiving either triple-nucleoside or efavirenz-containing regimens: Actg a5166s. *J Infect Dis* **195**, 1169–1176 (2007).

[527] Louie, M. *et al.* Determining the relative efficacy of highly active antiretroviral therapy. *J Infect Dis* **187**, 896–900 (2003).

[528] Polis, M. A. *et al.* Correlation between reduction in plasma HIV-1 RNA concentration 1 week after start of antiretroviral treatment and longer-term efficacy. *Lancet* **358**, 1760–1765 (2001).

[529] Markowitz, M. *et al.* Antiretroviral activity, pharmacokinetics, and tolerability of mk-0518, a novel inhibitor of HIV-1 integrase, dosed as monotherapy for 10 days in treatment-naive HIV-1-infected individuals. *J Acquir Immune Defic Syndr* **43**, 509–515 (2006).

[530] Grinsztejn, B. *et al.* Safety and efficacy of the HIV-1 integrase inhibitor raltegravir (mk-0518) in treatment-experienced patients with multidrug-resistant virus: a phase II randomised controlled trial. *Lancet* **369**, 1261–1269 (2007).

[531] Markowitz, M. *et al.* Rapid and durable antiretroviral effect of the HIV-1 integrase inhibitor raltegravir as part of combination therapy in treatment-naive patients with HIV-1 infection: results of a 48-week controlled study. *J Acquir Immune Defic Syndr* **46**, 125–133 (2007).

[532] Steigbigel, R. T. *et al.* Raltegravir with optimized background therapy for resistant HIV-1 infection. *N Engl J Med* **359**, 339–354 (2008).

[533] Dayam, R., Al-Mawsawi, L. Q. & Neamati, N. HIV-1 integrase inhibitors: an emerging clinical reality. *Drugs R D* **8**, 155–168 (2007).

[534] DeJesus, E. *et al.* Antiviral activity, pharmacokinetics, and dose response of the HIV-1 integrase inhibitor gs-9137 (jtk-303) in treatment-naive and treatment-experienced patients. *J Acquir Immune Defic Syndr* **43**, 1–5 (2006).

[535] Goffinet, C. *et al.* Pharmacovirological impact of an integrase inhibitor on human immunodeficiency virus type 1 cDNA species in vivo. *J Virol* **83**, 7706–7717 (2009).

[536] Eron, J. J. Managing antiretroviral therapy: changing regimens, resistance testing, and the risks from structured treatment interruptions. *J Infect Dis* **197 Suppl 3**, S261–S271 (2008).

[537] Tozer, T. N. & Rowland, M. *Introduction to Pharmacokinetics and Pharmacodynamics: The quantitative basis of drug therapy* (Lippincott Williams and Wilkins, 2006).

[538] Kwon, Y. *Handbook of Essential Pharmacokinetics, Pharmacodynamics, and Drug Metabolism for Industrial Scientists* (Kluwer Academic/Plenum Publishers, New York, 2001).

[539] Schoenwald, R. D. *Pharmacokinetics in Drug Discovery and Development* (CRC, 2002).

[540] Birkett, D. *Pharmacokinetics Made Easy* (McGraw-Hill Book Company Australia, 2002).

[541] Smith, D. A., van de Waterbeemd, H. & Walker, D. K. *Pharmacokinetics and Metabolism in Drug Design* (Wiley-VCH, 2006).

[542] Nestorov, I. Whole body pharmacokinetic models. *Clin Pharmacokinet* **42**, 883–908 (2003).

[543] Grass, G. M. & Sinko, P. J. Physiologically-based pharmacokinetic simulation modelling. *Adv Drug Deliv Rev* **54**, 433–451 (2002).

[544] Edginton, A. N., Theil, F.-P., Schmitt, W. & Willmann, S. Whole body physiologically-based pharmacokinetic models: their use in clinical drug development. *Expert Opin Drug Metab Toxicol* **4**, 1143–1152 (2008).

[545] Lüpfert, C. & Reichel, A. Development and application of physiologically based pharmacokinetic-modeling tools to support drug discovery. *Chem Biodivers* **2**, 1462–1486 (2005).

[546] Poulin, P. & Theil, F.-P. Prediction of pharmacokinetics prior to in vivo studies. II. generic physiologically based pharmacokinetic models of drug disposition. *J Pharm Sci* **91**, 1358–1370 (2002).

[547] Jones, H. M., Parrott, N., Jorga, K. & Lav, T. A novel strategy for physiologically based predictions of human pharmacokinetics. *Clin Pharmacokinet* **45**, 511–542 (2006).

[548] Rowland, M., Balant, L. & Peck, C. Physiologically based pharmacokinetics in drug development and regulatory science: a workshop report (georgetown university, washington, dc, may 29-30, 2002). *AAPS J* **6**, 56–67 (2004).

[549] Björkman, S. Reduction and lumping of physiologically based pharmacokinetic models: prediction of the disposition of fentanyl and pethidine in humans by successively simplified models. *J Pharmacokinet Pharmacodyn* **30**, 285–307 (2003).

[550] Brochot, C., Tth, J. & Bois, F. Y. Lumping in pharmacokinetics. *J Pharmacokinet Pharmacodyn* **32**, 719–736 (2005).

[551] Nestorov, I. A., Aarons, L. J., Arundel, P. A. & Rowland, M. Lumping of whole-body physiologically based pharmacokinetic models. *J Pharmacokinet Biopharm* **26**, 21–46 (1998).

[552] Mohanty, U. & Dixit, N. M. Mechanism-based model of the pharmacokinetics of enfuvirtide, an HIV fusion inhibitor. *J Theor Biol* **251**, 541–551 (2008).

[553] Skowron, G. & Ogden, R. *Reverse transcriptase inhibitors in HIV/AIDS therapy* (Humana Press, Totowa, New Jersey, 2006).

[554] Abel, S. *et al.* Assessment of the absorption, metabolism and absolute bioavailability of maraviroc in healthy male subjects. *Br J Clin Pharmacol* **65 Suppl 1**, 60–67 (2008).

[555] McKeage, K., Perry, C. M. & Keam, S. J. Darunavir: a review of its use in the management of HIV infection in adults. *Drugs* **69**, 477–503 (2009).

[556] Flexner, C. Dual protease inhibitor therapy in HIV-infected patients: pharmacologic rationale and clinical benefits. *Annu Rev Pharmacol Toxicol* **40**, 649–674 (2000).

[557] Kappelhoff, B. S. *et al.* Population pharmacokinetics of efavirenz in an unselected cohort of HIV-1-infected individuals. *Clin Pharmacokinet* **44**, 849–861 (2005).

[558] Smith, P. F., DiCenzo, R. & Morse, G. D. Clinical pharmacokinetics of non-nucleoside reverse transcriptase inhibitors. *Clin Pharmacokinet* **40**, 893–905 (2001).

[559] Willmann, S., Schmitt, W., Keldenich, J., Lippert, J. & Dressman, J. B. A physiological model for the estimation of the fraction dose absorbed in humans. *J Med Chem* **47**, 4022–4031 (2004).

[560] Yu, L. X., Crison, J. R. & Amidon, G. L. Compartmental transit and dispersion model analysis of small intestinal transit flow in humans. *International Journal of Pharmaceutics* **140**, 111–118 (1996).

[561] Weiss, M. A novel extravascular input function for the assessment of drug absorption in bioavailability studies. *Pharm Res* **13**, 1547–1553 (1996).

[562] Yu, L. X., Lipka, E., Crison, J. R. & Amidon, G. L. Transport approaches to the biopharmaceutical design of oral drug delivery systems: prediction of intestinal absorption. *Adv Drug Deliv Rev* **19**, 359–376 (1996).

[563] Yu, L. X. & Amidon, G. L. Saturable small intestinal drug absorption in humans: modeling and interpretation of cefatrizine data. *Eur J Pharm Biopharm* **45**, 199–203 (1998).

[564] Yu, L. X. & Amidon, G. L. A compartmental absorption and transit model for estimating oral drug absorption. *Int J Pharm* **186**, 119–125 (1999).

[565] Agoram, B., Woltosz, W. S. & Bolger, M. B. Predicting the impact of physiological and biochemical processes on oral drug bioavailability. *Adv Drug Deliv Rev* **50 Suppl 1**, S41–S67 (2001).

[566] Kadono, K., Yokoe, J., Ogawara, Higaki, K. & Kimura, T. Analysis and prediction of absorption behavior for theophylline orally administered as powders based on gastrointestinal-transit-absorption (gita) model. *Drug Metab Pharmacokinet* **17**, 307–315 (2002).

[567] Kimura, T. & Higaki, K. Gastrointestinal transit and drug absorption. *Biol Pharm Bull* **25**, 149–164 (2002).

[568] Sawamoto, T., Haruta, S., Kurosaki, Y., Higaki, K. & Kimura, T. Prediction of the plasma concentration profiles of orally administered drugs in rats on the basis of gastrointestinal transit kinetics and absorbability. *J Pharm Pharmacol* **49**, 450–457 (1997).

[569] Willmann, S., Schmitt, W., Keldenich, J. & Dressman, J. B. A physiologic model for simulating gastrointestinal flow and drug absorption in rats. *Pharm Res* **20**, 1766–1771 (2003).

[570] Willmann, S., Edginton, A. N. & Dressman, J. B. Development and validation of a physiology-based model for the prediction of oral absorption in monkeys. *Pharm Res* **24**, 1275–1282 (2007).

[571] Park, G. B. & Mitra, A. K. Mechanism and site dependency of intestinal mucosal transport and metabolism of thymidine analogues. *Pharm Res* **9**, 326–331 (1992).

[572] Yu, L. X. An integrated model for determining causes of poor oral drug absorption. *Pharm Res* **16**, 1883–1887 (1999).

[573] Rodgers, T., Leahy, D. & Rowland, M. Physiologically based pharmacokinetic modeling 1: predicting the tissue distribution of moderate-to-strong bases. *J Pharm Sci* **94**, 1259–1276 (2005).

[574] Rodgers, T. & Rowland, M. Physiologically based pharmacokinetic modelling 2: predicting the tissue distribution of acids, very weak bases, neutrals and zwitterions. *J Pharm Sci* **95**, 1238–1257 (2006).

[575] Berezhkovskiy, L. M. Volume of distribution at steady state for a linear pharmacokinetic system with peripheral elimination. *J Pharm Sci* **93**, 1628–1640 (2004).

[576] Poulin, P. & Theil, F. P. A priori prediction of tissue:plasma partition coefficients of drugs to facilitate the use of physiologically-based pharmacokinetic models in drug discovery. *J Pharm Sci* **89**, 16–35 (2000).

[577] Poulin, P., Schoenlein, K. & Theil, F. P. Prediction of adipose tissue: plasma partition coefficients for structurally unrelated drugs. *J Pharm Sci* **90**, 436–447 (2001).

[578] Boffito, M. *et al.* Protein binding in antiretroviral therapies. *AIDS Res Hum Retroviruses* **19**, 825–835 (2003).

[579] Schmitt, W. General approach for the calculation of tissue to plasma partition coefficients. *Toxicol In Vitro* **22**, 457–467 (2008).

[580] Espié, P., Tytgat, D., Sargentini-Maier, M.-L., Poggesi, I. & Watelet, J.-B. Physiologically based pharmacokinetics (PBPK). *Drug Metab Rev* **41**, 391–407 (2009).

[581] Willmann, S., Lippert, J. & Schmitt, W. From physicochemistry to absorption and distribution: predictive mechanistic modelling and computational tools. *Expert Opin Drug Metab Toxicol* **1**, 159–168 (2005).

[582] Kawai, R., Mathew, D., Tanaka, C. & Rowland, M. Physiologically based pharmacokinetics of cyclosporine a: extension to tissue distribution kinetics in rats and scale-up to human. *J Pharmacol Exp Ther* **287**, 457–468 (1998).

[583] Rodgers, T. & Rowland, M. Mechanistic approaches to volume of distribution predictions: understanding the processes. *Pharm Res* **24**, 918–933 (2007).

[584] von Kleist, M. & Huisinga, W. Physiologically based pharmacokinetic modelling: a sub-compartmentalized model of tissue distribution. *J Pharmacokinet Pharmacodyn* **34**, 789–806 (2007).

[585] Poulin, P. & Theil, F.-P. Prediction of pharmacokinetics prior to in vivo studies. I. mechanism-based prediction of volume of distribution. *J Pharm Sci* **91**, 129–156 (2002).

[586] Keldenich, J. A physiological/mechanistic model for predicting organ/plasma partitioning and volume of distribution. Tech. Rep., LogP2004 The 3rd Lipophilicity Symposium (2004).

[587] Ito, K., Iwatsubo, T., Kanamitsu, S., Nakajima, Y. & Sugiyama, Y. Quantitative prediction of in vivo drug clearance and drug interactions from in vitro data on metabolism, together with binding and transport. *Annu Rev Pharmacol Toxicol* **38**, 461–499 (1998).

[588] Keener, J. & Sneyd, J. *Mathematical Physiology* (Springer, 2001).

[589] Hakooz, N. *et al.* Determination of a human hepatic microsomal scaling factor for predicting in vivo drug clearance. *Pharm Res* **23**, 533–539 (2006).

[590] Houston, J. B. Utility of in vitro drug metabolism data in predicting in vivo metabolic clearance. *Biochem Pharmacol* **47**, 1469–1479 (1994).

[591] Komura, H. & Iwaki, M. Nonlinear pharmacokinetics of propafenone in rats and humans: application of a substrate depletion assay using hepatocytes for assessment of nonlinearity. *Drug Metab Dispos* **33**, 726–732 (2005).

[592] Pang, K. S. & Rowland, M. Hepatic clearance of drugs. I. theoretical considerations of a "well-stirred" model and a "parallel tube" model. influence of hepatic blood flow, plasma and blood cell binding, and the hepatocellular enzymatic activity on hepatic drug clearance. *J Pharmacokinet Biopharm* **5**, 625–653 (1977).

[593] Bonate, P. L., Reith, K. & Weir, S. Drug interactions at the renal level. implications for drug development. *Clin Pharmacokinet* **34**, 375–404 (1998).

[594] Stevens, L. A., Coresh, J., Greene, T. & Levey, A. S. Assessing kidney function–measured and estimated glomerular filtration rate. *N Engl J Med* **354**, 2473–2483 (2006).

[595] Stevens, L. A., Coresh, J., Greene, T. & Levey, A. S. Assessing kidney function–measured and estimated glomerular filtration rate. *N Engl J Med* **354**, 2473–2483 (2006).

[596] Aktories, K., F/"orstermann, U., Hofmann, F. & Forth, W. *Allgemeine und spezielle Pharmakologie und Toxikologie* (Urban and Fischer, 2001).

[597] Dobson, P. D., Lanthaler, K., Oliver, S. G. & Kell, D. B. Implications of the dominant role of transporters in drug uptake by cells. *Curr Top Med Chem* **9**, 163–181 (2009).

[598] Dobson, P. D. & Kell, D. B. Carrier-mediated cellular uptake of pharmaceutical drugs: an exception or the rule? *Nat Rev Drug Discov* **7**, 205–220 (2008).

[599] Bisset, L. R., Lung, T. L., Kaelin, M., Ludwig, E. & Dubs, R. W. Reference values for peripheral blood lymphocyte phenotypes applicable to the healthy adult population in switzerland. *Eur J Haematol* **72**, 203–212 (2004).

[600] Rabel, S. R., Patel, M., Sun, S. & Maurin, M. B. Electronic and resonance effects on the ionization of structural analogues of efavirenz. *AAPS PharmSci* **3**, E28 (2001).

[601] Tanaka, R. *et al.* Intracellular efavirenz levels in peripheral blood mononuclear cells from human immunodeficiency virus-infected individuals. *Antimicrob Agents Chemother* **52**, 782–785 (2008).

[602] Eilers, M., Roy, U. & Mondal, D. Mrp (abcc) transporters-mediated efflux of anti-HIV drugs, saquinavir and zidovudine, from human endothelial cells. *Exp Biol Med (Maywood)* **233**, 1149–1160 (2008).

[603] Janneh, O., Jones, E., Chandler, B., Owen, A. & Khoo, S. H. Inhibition of p-glycoprotein and multidrug resistance-associated proteins modulates the intracellular concentration of lopinavir in cultured CD4 T cells and primary human lymphocytes. *J Antimicrob Chemother* **60**, 987–993 (2007).

[604] Janneh, O. *et al.* Modulation of the intracellular accumulation of saquinavir in peripheral blood mononuclear cells by inhibitors of mrp1, mrp2, p-gp and bcrp. *AIDS* **19**, 2097–2102 (2005).

[605] Weiss, J. *et al.* Modulation of human bcrp (abcg2) activity by anti-HIV drugs. *J Antimicrob Chemother* **59**, 238–245 (2007).

[606] Gray, J. H., Owen, R. P. & Giacomini, K. M. The concentrative nucleoside transporter family, SLC28. *Pflugers Arch* **447**, 728–734 (2004).

[607] Baldwin, S. A. *et al.* The equilibrative nucleoside transporter family, SLC29. *Pflugers Arch* **447**, 735–743 (2004).

[608] Csajka, C. & Verotta, D. Pharmacokinetic-pharmacodynamic modelling: history and perspectives. *J Pharmacokinet Pharmacodyn* **33**, 227–279 (2006).

[609] Levy, G. Relationship between elimination rate of drugs and rate of decline of their pharmacologic effects. *J Pharm Sci* **53**, 342–343 (1964).

[610] Levy, G. Kinetics of pharmacologic effects. *Clin Pharmacol Ther* **7**, 362–372 (1966).

[611] Wagner, J. G. Kinetics of pharmacologic response. i. proposed relationships between response and drug concentration in the intact animal and man. *J Theor Biol* **20**, 173–201 (1968).

[612] Cheng, Y. & Prusoff, W. H. Relationship between the inhibition constant (K1) and the concentration of inhibitor which causes 50 per cent inhibition (I50) of an enzymatic reaction. *Biochem Pharmacol* **22**, 3099–3108 (1973).

[613] Cheng, H. C. The influence of cooperativity on the determination of dissociation constants: examination of the cheng-prusoff equation, the scatchard analysis, the schild analysis and related power equations. *Pharmacol Res* **50**, 21–40 (2004).

[614] Ette, E. I. & Williams, P. J. *Pharmacometrics. The Science of Quantitative Pharmacology* (Wiley, 2006).

[615] Turner, T. E., Schnell, S. & Burrage, K. Stochastic approaches for modelling in vivo reactions. *Computational Biology and Chemistry* **28**, 165–178 (2004).

[616] Cases-Gonzlez, C. E. & Menndez-Arias, L. Nucleotide specificity of HIV-1 reverse transcriptases with amino acid substitutions affecting Ala-114. *Biochem J* **387**, 221–229 (2005).

[617] Langtry, H. D. & Campoli-Richards, D. M. Zidovudine. A review of its pharmacodynamic and pharmacokinetic properties, and therapeutic efficacy. *Drugs* **37**, 408–450 (1989).

[618] Gussin, G. N. Kinetic analysis of RNA polymerase-promoter interactions. *Methods Enzymol* **273**, 45–59 (1996).

[619] Crespan, E. *et al.* Drug resistance mutations in the nucleotide binding pocket of human immunodeficiency virus type 1 reverse transcriptase differentially affect the phosphorolysis-dependent primer unblocking activity in the presence of stavudine and zidovudine and its inhibition by efavirenz. *Antimicrob Agents Chemother* **49**, 342–349 (2005).

[620] Dixit, N. M. & Perelson, A. S. Multiplicity of human immunodeficiency virus infections in lymphoid tissue. *J Virol* **78**, 8942–8945 (2004).

[621] Dixit, N. M. & Perelson, A. S. HIV dynamics with multiple infections of target cells. *Proc Natl Acad Sci U S A* **102**, 8198–8203 (2005).

[622] Dutta, S., Matsumoto, Y. & Ebling, W. F. Is it possible to estimate the parameters of the sigmoid emax model with truncated data typical of clinical studies? *J Pharm Sci* **85**, 232–239 (1996).

[623] Sharma, P. L. & Crumpacker, C. S. Attenuated replication of human immunodeficiency virus type 1 with a didanosine-selected reverse transcriptase mutation. *J Virol* **71**, 8846–8851 (1997).

[624] Sharma, P. L. & Crumpacker, C. S. Decreased processivity of human immunodeficiency virus type 1 reverse transcriptase (RT) containing didanosine-selected mutation Leu74Val: a comparative analysis of RT variants Leu74Val and lamivudine-selected Met184Val. *J Virol* **73**, 8448–8456 (1999).

[625] Deval, J. *et al.* A loss of viral replicative capacity correlates with altered DNA polymerization kinetics by the human immunodeficiency virus reverse transcriptase bearing the k65r and l74v dideoxynucleoside resistance substitutions. *J Biol Chem* **279**, 25489–25496 (2004).

[626] Feng, J. Y. & Anderson, K. S. Mechanistic studies examining the efficiency and fidelity of DNA synthesis by the 3TC-resistant mutant (184v) of HIV-1 reverse transcriptase. *Biochemistry* **38**, 9440–9448 (1999).

[627] Panhard, X. *et al.* Population pharmacokinetic analysisof lamivudine, stavudine and zidovudine in controlled HIV-infected patients on HAART. *Eur J Clin Pharmacol* (2007).

[628] Capparelli, E. V. *et al.* Population pharmacokinetics and pharmacodynamics of zidovudine in HIV-infected infants and children. *J Clin Pharmacol* **43**, 133–140 (2003).

[629] Wattanagoon, Y. *et al.* Pharmacokinetics of zidovudine phosphorylation in human immunodeficiency virus-positive thai patients and healthy volunteers. *Antimicrob Agents Chemother* **44**, 1986–1989 (2000).

[630] Stretcher, B. N. *et al.* Concentrations of phosphorylated zidovudine (ZDV) in patient leukocytes do not correlate with ZDV dose or plasma concentrations. *Ther Drug Monit* **13**, 325–331 (1991).

[631] Anderson, P. L., Kakuda, T. N., Kawle, S. & Fletcher, C. V. Antiviral dynamics and sex differences of zidovudine and lamivudine triphosphate concentrations in HIV-infected individuals. *AIDS* **17**, 2159–2168 (2003).

[632] Barry, M. G. *et al.* The effect of zidovudine dose on the formation of intracellular phosphorylated metabolites. *AIDS* **10**, 1361–1367 (1996).

[633] Aweeka, F. T. *et al.* Pharmacokinetic evaluation of the effects of ribavirin on zidovudine triphosphate formation: Actg 5092s study team. *HIV Med* **8**, 288–294 (2007).

[634] Arts, E. J., Marois, J. P., Gu, Z., Grice, S. F. L. & Wainberg, M. A. Effects of 3'-deoxynucleoside 5'-triphosphate concentrations on chain termination by nucleoside analogs during human immunodeficiency virus type 1 reverse transcription of minus-strand strong-stop DNA. *J Virol* **70**, 712–720 (1996).

[635] Fridland, A., Connelly, M. C. & Ashmun, R. Relationship of deoxynucleotide changes to inhibition of DNA synthesis induced by the antiretroviral agent 3'-azido-3'-deoxythymidine and release of its monophosphate by human lymphoid cells (CCRF-CEM). *Mol Pharmacol* **37**, 665–670 (1990).

[636] Rodman, J. H., Robbins, B., Flynn, P. M. & Fridland, A. A systemic and cellular model for zidovudine plasma concentrations and intracellular phosphorylation in patients. *J Infect Dis* **174**, 490–499 (1996).

[637] Shepp, D. H. *et al.* A comparative trial of zidovudine administered every four versus every twelve hours for the treatment of advanced HIV disease. *J Acquir Immune Defic Syndr Hum Retrovirol* **15**, 283–288 (1997).

[638] Ruane, P. J. *et al.* Pharmacodynamic effects of zidovudine 600 mg once/day versus 300 mg twice/day in therapy-nave patients infected with human immunodeficiency virus. *Pharmacotherapy* **24**, 307–312 (2004).

[639] Chow, H. H., Li, P., Brookshier, G. & Tang, Y. In vivo tissue disposition of 3'-azido-3'-deoxythymidine and its anabolites in control and retrovirus-infected mice. *Drug Metab Dispos* **25**, 412–422 (1997).

[640] Arnér, E. S., Valentin, A. & Eriksson, S. Thymidine and 3'-azido-3'-deoxythymidine metabolism in human peripheral blood lymphocytes and monocyte-derived macrophages. A study of both anabolic and catabolic pathways. *J Biol Chem* **267**, 10968–10975 (1992).

[641] Toyoshima, T., Kimura, S., Muramatsu, S., Takahagi, H. & Shimada, K. A sensitive nonisotopic method for the determination of intracellular azidothymidine 5'-mono-, 5'-di-, and 5'-triphosphate. *Anal Biochem* **196**, 302–307 (1991).

[642] Flynn, P. M. *et al.* Intracellular pharmacokinetics of once versus twice daily zidovudine and lamivudine in adolescents. *Antimicrob Agents Chemother* **51**, 3516–3522 (2007).

[643] Domin, B. A. *et al.* Membrane permeation characteristics of 5'-modified thymidine analogs. *Mol Pharmacol* **41**, 950–956 (1992).

[644] Zimmerman, T. P., Mahony, W. B. & Prus, K. L. 3'-azido-3'-deoxythymidine. An unusual nucleoside analogue that permeates the membrane of human erythrocytes and lymphocytes by nonfacilitated diffusion. *J Biol Chem* **262**, 5748–5754 (1987).

[645] Purcet, S. *et al.* 3'-azido-2',3'-dideoxythymidine (zidovudine) uptake mechanisms in T lymphocytes. *Antivir Ther* **11**, 803–811 (2006).

[646] Luzier, A. & Morse, G. D. Intravascular distribution of zidovudine: role of plasma proteins and whole blood components. *Antiviral Res* **21**, 267–280 (1993).

[647] Brown, R. P., Delp, M. D., Lindstedt, S. L., Rhomberg, L. R. & Beliles, R. P. Physiological parameter values for physiologically based pharmacokinetic models. *Toxicol Ind Health* **13**, 407–484 (1997).

[648] Acosta, E. P., Page, L. M. & Fletcher, C. V. Clinical pharmacokinetics of zidovudine. An update. *Clin Pharmacokinet* **30**, 251–262 (1996).

[649] Wilde, M. I. & Langtry, H. D. Zidovudine. An update of its pharmacodynamic and pharmacokinetic properties, and therapeutic efficacy. *Drugs* **46**, 515–578 (1993).

[650] Serra, C. H. D. R. *et al.* Bioequivalence and pharmacokinetics of two zidovudine formulations in healthy brazilian volunteers: An open-label, randomized, single-dose, two-way crossover study. *Clin Ther* **30**, 902–908 (2008).

[651] Lavie, A. *et al.* Structure of thymidylate kinase reveals the cause behind the limiting step in AZT activation. *Nat Struct Biol* **4**, 601–604 (1997).

[652] Lavie, A. *et al.* The bottleneck in AZT activation. *Nat Med* **3**, 922–924 (1997).

[653] Traut, T. W. Physiological concentrations of purines and pyrimidines. *Mol Cell Biochem* **140**, 1–22 (1994).

[654] Begenisich, T. *et al.* Physiological roles of the intermediate conductance, Ca2+-activated potassium channel KCNN4. *J Biol Chem* **279**, 47681–47687 (2004).

[655] Törnevik, Y., Ullman, B., Balzarini, J., Wahren, B. & Eriksson, S. Cytotoxicity of 3'-azido-3'-deoxythymidine correlates with 3'-azidothymidine-5'-monophosphate (AZTMP) levels, whereas anti-human immunodeficiency virus (HIV) activity correlates with 3'-azidothymidine-5'-triphosphate (AZTTP) levels in cultured cem T-lymphoblastoid cells. *Biochem Pharmacol* **49**, 829–837 (1995).

[656] Anderson, P. L. *et al.* Concentrations of zidovudine- and lamivudine-triphosphate according to cell type in HIV-seronegative adults. *AIDS* **21**, 1849–1854 (2007).

[657] Gao, W. Y., Johns, D. G., Tanaka, M. & Mitsuya, H. Suppression of replication of multidrug-resistant HIV type 1 variants by combinations of thymidylate synthase inhibitors with zidovudine or stavudine. *Mol Pharmacol* **55**, 535–540 (1999).

[658] Sedaghat, A. R., Siliciano, J. D., Brennan, T. P., Wilke, C. O. & Siliciano, R. F. Limits on replenishment of the resting CD4+ T cell reservoir for HIV in patients on HAART. *PLoS Pathog* **3**, e122 (2007).

[659] Ruff, C. T. *et al.* Persistence of wild-type virus and lack of temporal structure in the latent reservoir for human immunodeficiency virus type 1 in pediatric patients with extensive antiretroviral exposure. *J Virol* **76**, 9481–9492 (2002).

[660] Karlsson, A. C., Lindkvist, A., Lindbck, S., Gaines, H. & Snnerborg, A. Recent origin of human immunodeficiency virus type 1 variants in resting CD4+ T lymphocytes in untreated and suboptimally treated subjects. *J Infect Dis* **184**, 1392–1401 (2001).

[661] Chun, T. W. *et al.* Presence of an inducible HIV-1 latent reservoir during highly active antiretroviral therapy. *Proc Natl Acad Sci U S A* **94**, 13193–13197 (1997).

[662] Havlir, D. V., Eastman, S., Gamst, A. & Richman, D. D. Nevirapine-resistant human immunodeficiency virus: kinetics of replication and estimated prevalence in untreated patients. *J Virol* **70**, 7894–7899 (1996).

[663] Riddler, S. A. *et al.* Class-sparing regimens for initial treatment of HIV-1 infection. *N Engl J Med* **358**, 2095–2106 (2008).

[664] Gardner, E. M., Burman, W. J., Steiner, J. F., Anderson, P. L. & Bangsberg, D. R. Antiretroviral medication adherence and the development of class-specific antiretroviral resistance. *AIDS* **23**, 1035–1046 (2009).

[665] Bangsberg, D. R. *et al.* Adherence to protease inhibitors, HIV-1 viral load, and development of drug resistance in an indigent population. *AIDS* **14**, 357–366 (2000).

[666] Gallego, O. *et al.* Drug resistance in patients experiencing early virological failure under a triple combination including indinavir. *AIDS* **15**, 1701–1706 (2001).

[667] Walsh, J. C., Pozniak, A. L., Nelson, M. R., Mandalia, S. & Gazzard, B. G. Virologic rebound on HAART in the context of low treatment adherence is associated with a low prevalence of antiretroviral drug resistance. *J Acquir Immune Defic Syndr* **30**, 278–287 (2002).

[668] Bangsberg, D. R. *et al.* High levels of adherence do not prevent accumulation of HIV drug resistance mutations. *AIDS* **17**, 1925–1932 (2003).

[669] Bangsberg, D. R. *et al.* Modeling the HIV protease inhibitor adherence-resistance curve by use of empirically derived estimates. *J Infect Dis* **190**, 162–165 (2004).

[670] King, M. S., Brun, S. C. & Kempf, D. J. Relationship between adherence and the development of resistance in antiretroviral-naive, HIV-1-infected patients receiving lopinavir/ritonavir or nelfinavir. *J Infect Dis* **191**, 2046–2052 (2005).

[671] Ellis, R. J. *et al.* Cerebrospinal fluid HIV RNA originates from both local CNS and systemic sources. *Neurology* **54**, 927–936 (2000).

[672] Sei, S. *et al.* Evaluation of human immunodeficiency virus (HIV) type 1 RNA levels in cerebrospinal fluid and viral resistance to zidovudine in children with HIV encephalopathy. *J Infect Dis* **174**, 1200–1206 (1996).

[673] Pialoux, G. *et al.* Central nervous system as a sanctuary for HIV-1 infection despite treatment with zidovudine, lamivudine and indinavir. *AIDS* **11**, 1302–1303 (1997).

[674] McCrossan, M. *et al.* An immune control model for viral replication in the CNS during presymptomatic HIV infection. *Brain* **129**, 503–516 (2006).

[675] Gnthard, H. F. *et al.* Residual human immunodeficiency virus (HIV) type 1 RNA and DNA in lymph nodes and HIV RNA in genital secretions and in cerebrospinal fluid after suppression of viremia for 2 years. *J Infect Dis* **183**, 1318–1327 (2001).

[676] Chun, T.-W. *et al.* HIV-infected individuals receiving effective antiviral therapy for extended periods of time continually replenish their viral reservoir. *J Clin Invest* **115**, 3250–3255 (2005).

[677] Chun, T.-W. *et al.* Persistence of HIV in gut-associated lymphoid tissue despite long-term antiretroviral therapy. *J Infect Dis* **197**, 714–720 (2008).

[678] Zrate, S., Pond, S. L. K., Shapshak, P. & Frost, S. D. W. Comparative study of methods for detecting sequence compartmentalization in human immunodeficiency virus type 1. *J Virol* **81**, 6643–6651 (2007).

[679] Kepler, T. B. & Perelson, A. S. Drug concentration heterogeneity facilitates the evolution of drug resistance. *Proc Natl Acad Sci U S A* **95**, 11514–11519 (1998).

[680] Braithwaite, R. S., Shechter, S., Chang, C.-C. H., Schaefer, A. & Roberts, M. S. Estimating the rate of accumulating drug resistance mutations in the HIV genome. *Value Health* **10**, 204–213 (2007).

[681] Louvel, S. *et al.* Detection of drug-resistant HIV minorities in clinical specimens and therapy failure. *HIV Med* **9**, 133–141 (2008).

[682] Han, Y., Wind-Rotolo, M., Yang, H.-C., Siliciano, J. D. & Siliciano, R. F. Experimental approaches to the study of HIV-1 latency. *Nat Rev Microbiol* **5**, 95–106 (2007).

[683] Alan D McNaught, A. W. *Compendium of chemical terminology: IUPAC recommendations* (IUPAC, 1997).

[684] Voet, D. & Voet, J. G. *Biochemistry* (Wiley, 1995).

[685] Zumdahl, S. S. *Chemical Principles* (Houghton Mifflin Company, 1998).

Part V

Appendix

Appendix A

Ionization

Consider the dynamics of proton dissociation for mono-protonic acids and mono-protonic bases respectively

$$\begin{aligned} \mathbf{A}:\mathbf{H} &\rightleftharpoons \mathbf{H}^+ + \mathbf{A}^- \quad \text{(mono-protonic acids)} \\ \mathbf{B}:\mathbf{H}^+ &\rightleftharpoons \mathbf{H}^+ + \mathbf{B} \quad \text{(mono-protonic bases)} \end{aligned}$$

where $\mathbf{A}:\mathbf{H}$ and $\mathbf{B}\mathbf{H}^+$ denote the acid, respectively, the protonated base (conjugate acid), while $\mathbf{A}^-$ and $\mathbf{B}$ refer to the deprotonated acid (conjugate base), respectively, base. In the case of acids, the fully protonated compound ($\mathbf{A}:\mathbf{H}$) is considered as 'neutral', whereas it is the fully deprotonated compound for bases ($\mathbf{B}$). The other forms are considered as 'ionized'. Analogous formula hold for di-protonic acids, di-protonic bases, i.e. molecules with two acidic, respectively, basic groups. In the case of di-protonic acids, di-protonic bases we generally assume that $\mathrm{pK_{a,2}} > \mathrm{pK_{a,1}}$. For zwitterionic compounds, i.e., neutral compounds having formal unit electrical charge of opposite sign [683], it is

$$\mathbf{H}:\mathbf{A}\mathbf{B}:\mathbf{H}^+ \rightleftharpoons \mathbf{H}^+ + \mathbf{A}^-\mathbf{B}:\mathbf{H}^+ \rightleftharpoons \mathbf{2}\mathbf{H}^+ + \mathbf{A}^-\mathbf{B} \quad \text{(zwitterions)}$$

In the case of zwitterions we will refer to the zwitterionic form ($\mathbf{A}^-\mathbf{B}:\mathbf{H}^+$) as 'neutral', and the acidic and basic forms ($\mathbf{A}^-\mathbf{B}$ and $\mathbf{H}:\mathbf{A}\mathbf{B}:\mathbf{H}^+$) will be referred as 'ionized'. For equilibrium conditions, the relationship between the acidity of a medium, expressed by the pH value, and the degree of compound ionization within the medium has been formalized by Henderson and Hasselbalch.[1] [684, 685] For the mono-protonic case, it is

$$\log_{10}\left(\frac{\text{Ionized}}{\text{Neutral}}\right) = \begin{cases} +(\mathrm{pH}-\mathrm{pK_a}); & \text{mono-protonic acids} \\ -(\mathrm{pH}-\mathrm{pK_a}); & \text{mono-protonic bases} \end{cases} \tag{A.1}$$

For zwitterionic compounds, the ionized form consists of the acidic and basic species. At pH=pKa the concentrations of ionized and non-ionized species are equal (see fig. A.1).

In order to abstract from the particular ionization properties of a drug, we introduce the **neutral fraction** fn, defined by

$$\mathrm{fn} = \frac{\text{Neutral}}{\text{Neutral} + \text{Ionized}}.$$

Exploiting Eq. (A.1) yields for the neutral fraction fn

$$\frac{1}{\mathrm{fn}} = \begin{cases} 1 + 10^{+(\mathrm{pH}-\mathrm{pK_a})}; & \text{mono-protonic acids} \\ 1 + 10^{-(\mathrm{pH}-\mathrm{pK_a})}; & \text{mono-protonic bases} \\ 1 + 10^{+(\mathrm{pH}-\mathrm{pK_{a,1}})} + 10^{+(2\mathrm{pH}-\mathrm{pK_{a,1}}-\mathrm{pK_{a,2}})}; & \text{di-protonic acids} \\ 1 + 10^{-(\mathrm{pH}-\mathrm{pK_{a,2}})} + 10^{-(2\mathrm{pH}-\mathrm{pK_{a,1}}-\mathrm{pK_{a,2}})}; & \text{di-protonic bases} \\ 1 + 10^{+(\mathrm{pH}-\mathrm{pK_a(base)})} + 10^{-(\mathrm{pH}-\mathrm{pK_a(acid)})}; & \text{zwitterions} \\ 1; & \text{neutrals.} \end{cases} \tag{A.2}$$

[1] Note, that this equation only applies for ionizable compounds. Some compounds ('neutrals') cannot be ionized.

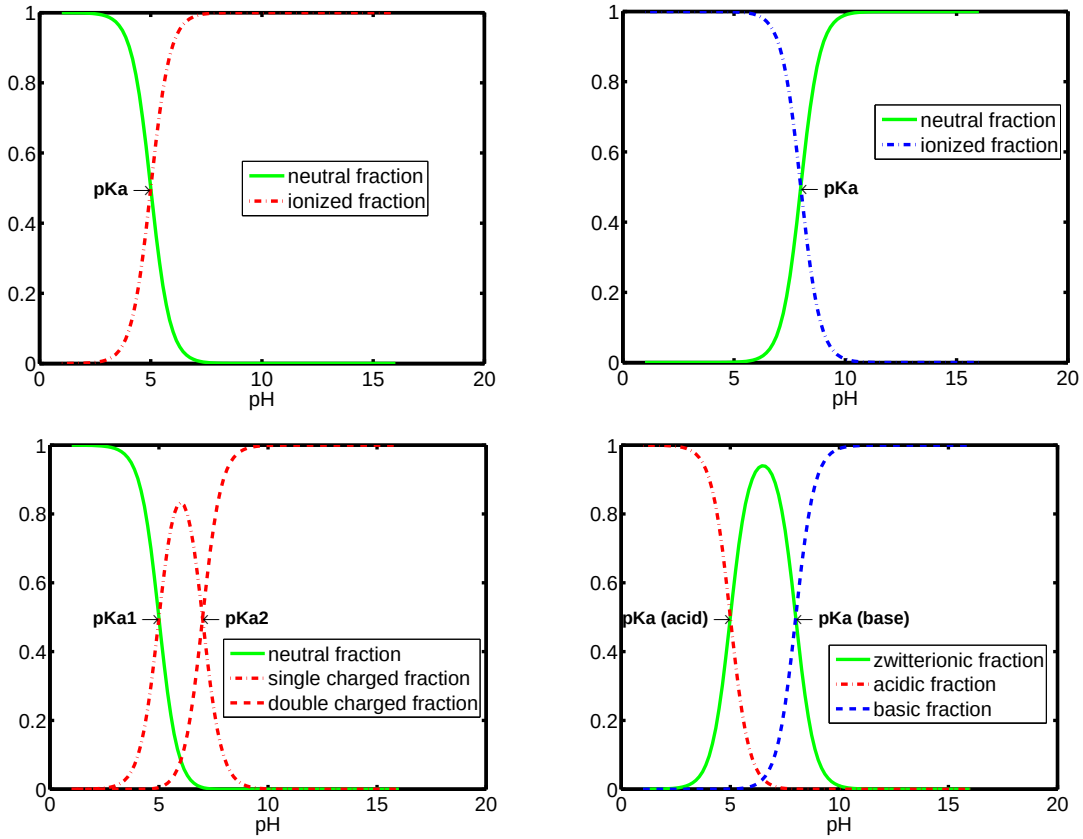

Figure A.1: Ionization profiles of a mono-protonic acid with $pK_a = 5$ (upper left panel); a mono-protonic base with $pK_a = 8$ (upper right panel); a di-protonic acid with $pK_{a,1} = 5$ and $pK_{a,2} = 7$ (lower left panel); and a zwitterionic compound with $pK_{a,1} = 5$ and $pK_{a,2} = 8$ (lower right panel). For details, see the text.

In the case of di-protonic acids or bases we assume that $pK_{a,2} > pK_{a,1}$.